Project THEMIS
Technical Report No. 9

NUMERICAL AND WIND TUNNEL SIMULATION OF RESPONSE OF STRATIFIED SHEAR LAYERS TO NONHOMOGENEOUS SURFACE FEATURES

by

Tetsuji Yamada

and

Robert N. Meroney

FLUID MECHANICS PROGRAM
ENGINEERING RESEARCH CENTER
COLLEGE OF ENGINEERING

COLORADO STATE UNIVERSITY

FORT COLLINS, COLORADO

Project THEMIS
Technical Report No.

NUMERICAL AND WIND TUNNEL SIMULATI
OF STRATIFIED SHEAR LAYEF
NONHOMOGENEOUS SURFACE FEA

by

Tetsuji Yamada

and

Robert N. Meroney

Prepared under

Office of Naval Research

Contract No. N00014-68-A-0493-0001

Project No. NR 062-414/6-6-68(Code 438)

U. S. Department of Defense

Washington, D. C.

Fluid Dynamics and Diffusion Laboratory
College of Engineering
Colorado State University
Fort Collins, Colorado

June 1971

CER70-71TY-RNM62

ABSTRACT

NUMERICAL AND WIND TUNNEL SIMULATION OF RESPONSE OF
STRATIFIED SHEAR LAYERS TO NONHOMOGENEOUS SURFACE FEATURES

Two-dimensional airflows over various nonuniform surfaces in a stratified atmosphere are studied both numerically and experimentally. Three problems are investigated, classified by the effect of the external forcing functions upon the basic airflow. They are: 1) mountain lee waves, 2) heat islands (sea breezes are included here), and 3) heated mountain phenomena in a stratified airflow. Both experiments and numerical analyses are conducted for each case. A wind tunnel was designed and constructed for these particular problems, since they require very small velocities and a strong temperature stratification.

Both numerical and wind tunnel experiments succeed in producing clear lee waves behind the square obstacle. The amplitude of the first wave is about the same order of magnitude as the obstacle height, and wave length closely agrees with that predicted by the linear theory.

Perturbations of a stratified shear flow by a heated boundary, which may represent a heated island or an urban region, are investigated experimentally and numerically. These experiments are apparently the first attempt to simulate the urban heat island effect in a wind tunnel facility. The results obtained by both numerical and experimental methods agree quantitatively. Several modifications of meteorological factors by urbanization are reproduced: a downward wind and acceleration of a horizontal velocity in the surface layer of an approach flow

to a city, temperature cross over, and frequent elevated inversion but less frequent surface inversion over the city during the night.

If the obstacle is heated, then the flow combines the features of the airflow over an obstacle and that over a heated island.

A detailed examination of the results reveals a strong nonlinearity which does not allow one to utilize conventional linearization techniques as a first approximation of the phenomenon.

Tetsuji Yamada
Fluid Mechanics Program
Department of Civil Engineering
Colorado State University
Fort Collins, Colorado 80521
June 1971

TABLE OF CONTENTS

TABLE OF CONTENTS (Continued)

TABLE OF CONTENTS (Continued)

TABLE OF CONTENTS (Continued)

TABLE OF CONTENTS (Continued)

LIST OF TABLES

LIST OF FIGURES

LIST OF FIGURES (Continued)

LIST OF FIGURES (Continued)

LIST OF FIGURES (Continued)

LIST OF FIGURES (Continued)

LIST OF FIGURES (Continued)

LIST OF SYMBOLS

Symbol	Definition	Dimensions
A	An amplitude of an equivalent mountain	L
a	A height of a ridge	L
b	Dimensionless half width of an obstacle, an obstacle half width/a water channel height	-
b	A half width parameter	L
C	Speed of sound	LT^{-1}
$\overline{c}$	Mean speed of sound	LT^{-1}
c'	Fluctuation of a speed of sound	LT^{-1}
c_p	Specific heat at constant pressure	$L^2T^{-1}\theta^{-2}$
C_1, C_2, C_3,	Constants	-
D	Half width of a heated island	L
d	Dimensionless half width of a heated island, (U/K)D	-
e	Exponential function	-
$(Fr)_L$	Froude number, $\frac{U}{\sqrt{gs}\ L}$	-
$(\overline{Fr})_H$	Arithmetic averaged Froude number of those in lower and upper surface regions	-
g	Acceleration of gravity	LT^{-2}
H	A wind tunnel or a water channel height	L
j	j^{th} grid point in x direction in a finite difference expression	-
K	Total viscosity (kinematic viscosity plus eddy viscosity)	L^2T^{-1}

Symbols used to indicate dimension are M - Mass, L - Length, T - Time, θ - Temperature

Symbol	Definition	Dimensions
K'	Total diffusivity of heat	L^2T^{-1}
K	Constant	-
k	Stability factor used in Long's model; $\nabla^2\delta + k^2\delta = 0$. k is the inverse of the Froude number based on H/π , $\frac{1}{(Fr)_{\frac{H}{\pi}}}$	-
k	Thermal conductivity	$MLT\theta^{-3}$
L	Characteristic length	L
L_1, L_2	Upstream and downstream lateral boundaries of the numerical scheme	L
ℓ	ℓ^{th} grid point in a finite-difference expression	-
ℓ^2	Scorer's stability parameter, $\frac{g\overline{\beta}}{\overline{U}^2} - \frac{\frac{\partial^2\overline{U}}{\partial z^2}}{\overline{U}}$	L^2
M	Mach number	-
M	Physical or an equivalent thermal mountain height	L
MJ, ML	Maximum grid numbers in x and z directions, respectively, in a numerical computational region	-
MST, MEND	Grid numbers along the lower boundary to specify the beginning and the end positions of an obstacle or a heated island in a numerical computation	-
MHEI	Grid number to specify the height of an obstacle in a numerical computation	-

LIST OF SYMBOLS (Continued)

Symbol	Definition	Dimensions
N_h	Non-homogeneity parameter to characterize a heating intensity of a heated island, $\frac{-(\frac{\partial T}{\partial z})_{z=0}}{\frac{T_{island} - T_o}{L}}$	-
n	n^{th} time step in a numerical computation	-
p	Pressure	$ML^{-1}T^{-2}$
p'	Pressure fluctuation	$ML^{-1}T^{-2}$
P_r	Prandtl number, $\frac{\rho \nu C_p}{k}$	-
R	Gas constant	$L^2T^{-2}\theta^{-1}$
R_e	Reynolds number, $\frac{UL}{\nu}$	-
R_i	Global Richardson number, $\frac{gsL^2}{U^2}$	-
s	Stability, $\frac{1}{\overline{T}} \frac{\partial T}{\partial z}$	L^{-1}
Sc	Scorer's function, $M^2 (\frac{sg}{\overline{u}^2} - \frac{\frac{\partial^2 \overline{u}}{\partial z^2}}{\overline{u}})$	-
T	Temperature	θ
$\overline{T}$	Mean temperature	θ
T_{island}	Temperature over a heated island	θ
T_o	Surrounding surface temperature	θ
t	Time coordinate	T
$\overline{U}$	Mean longitudinal velocity component	LT^{-1}
u, v, w	Velocity components in x, y, and z direction, respectively	LT^{-1}

LIST OF SYMBOLS (Continued)

Symbol	Definition	Dimensions
u', w'	Velocity fluctuations in x, and z direction, respectively	LT^{-1}
x,y,z	Space coordinate in longitudinal, lateral, and vertical direction, respectively	L
x_o	Shape parameter of an equivalent thermal mountain, $\frac{U^3}{gsk}$	L
α	Specific volume, $\frac{1}{\rho}$	$M^{-1}L^3$
α	Vertical temperature gradient, $\frac{-\partial T}{\partial z}$	θL^{-1}
β	Dimensionless obstacle height $\frac{M}{H}$	-
β	Coefficient of expansion of gas, $\frac{1}{T}$ for a perfect gas	θ^{-1}
$\overline{\beta}$	Stability factor, $s - \frac{g}{\overline{C}^2}$	L^{-1}
Γ	Adiabatic lapse rate	θL^{-1}
$\delta(z)$	Displacement of streamlines from the undisturbed level far upstream	L
δx, δz	Space grid increments in x and z directions respectively in a finite-difference expression	L
δt	Time grid increment in a finite-difference expression	T
ΔT	Temperature excess over a heated island, $T_{island} - T_o$.	θ

LIST OF SYMBOLS (Continued)

Symbol	Definition	Dimensions
ζ	Vorticity component in y direction $\frac{\partial w}{\partial x} - \frac{\partial u}{\partial z}$	T^{-1}
λ	Wave length	L
ν	Kinematic viscosity	L^2T^{-1}
ν_p	Pseudo-viscosity introduced in the upstream finite-difference approximation scheme	L^2T^{-1}
ξ	Dimensionless coordinates in x direction, (U/K)x	-
ρ	Density	ML^{-3}
σ^2	Stability factor in Long's original work $\frac{g}{U^2} \left\vert \frac{1}{\rho} \frac{\partial \rho}{\partial z} \right\vert_o$	L^{-2}
ψ	Stream function	L^2T^{-1}
$\overline{\ }$	Statistical average	-
'	Fluctuation in a quantity	-
1,2	Subscripts to indicate the quantities in a lower and an upper surface layer when different stabilities are used in the layers	-

CHAPTER I

INTRODUCTION

The major effort of this research is a direct attack by laboratory studies and numerical analysis on two-and three-dimensional shear flows produced by non-uniform boundary conditions. The following non-uniformities were chosen for detailed study of the perturbations they produce on an approaching two-dimensional shear flow:

1. Non-uniform surface temperature on a plane;
2. Mountain-like surface irregularities;
3. Mountain-like surface irregularities associated with non-uniform temperature distributions.

All of these boundary conditions produce flows and cross-flows, which in turn result in turbulence interactions about which very little is known.

The aerodynamic research reported here focuses on fluid mechanics problems related to environmental winds within the lower layer of the atmosphere, and is primarily experimental in nature. The objectives of this program, complemented by analysis and experiments on mathematical models achieved through use of a digital computer and correlation with available field data, are:

1. To develop a body of fundamental knowledge of the physical nature of shear flows with complex boundary conditions which lead to two- or three-dimensional mean motion.

2. To establish similarity criteria relating laboratory shear flows to corresponding flows (winds) in the lower layer of the atmosphere.

3. To further develop the potential use of low-speed thermal wind tunnels for the purpose of predicting local winds at specific sites and for specific purposes.

1.1 Non-uniform Surface Temperature on a Plane

Some of the most dramatic atmospheric phenomena occur as a result of sudden changes in the earth's surface temperature. In fact the driving mechanisms for the atmospheric circulation can be visualized as a complex extension on the global scale of the cellular motions of Benard's problem. On the smaller mesoscale the vagrancies of sea-land breezes, the effects of inversions on pollution in cities, or the flow over a heated island or a city represent examples of two- and three-dimensional interaction of a thermal boundary with the lower atmospheric shear flow. Specifically, the interaction of a metropolitan area as a heat source of finite extent with wind patterns, and the potential penetration of heat plumes through inversion layers resulting in fumigation, are relevant research topics which have received little or no attention. It has been postulated that convection motions and diffusion patterns recently encountered in the extensive study of Ft. Wayne, Indiana, (Hilst and Bowne, 1966) may be a result of the heat island phenomenon; however, some individuals argue that these motions may be more directly related to non-uniformity of the surface roughness.

A review of the literature reveals that past attention to the effects of thermal convection on the atmosphere has been limited to three areas. First are those mathematical studies related to the idealized case of free convection cell origin between parallel infinite flat plates -- i.e., the Rayleigh-Jeffreys or Benard problem (Saltzman,

1962; Segel and Stuart, 1961). Second are those studies of the effect of stratification upon wind profiles, turbulence, and transport phenomena when the flow is developed and the boundary conditions are laterally and longitudinally homogeneous (Plate and Lin, 1966; Lumley and Panofsky, 1964; Monin and Obukhov, 1954). The third group includes the effect of non-homogeneities in the surface boundary condition of the atmospheric boundary layer.

The response of a two-dimensional turbulent boundary layer to abrupt changes in surface conditions has received extensive recent attention (Townsend, 1965a, 1965b; Chanda, 1958; Meroney and Cermak, 1967). The growth of the inner boundary layer due to a step change in roughness or temperature has been studied with respect to the sea-land breeze, evaporation, forest and agricultural crop meteorology, and for wind break design (Cermak and Koloseus, 1953; Plate, 1964). The implications of the effects of finite non-homogeneous temperature distribution on the atmospheric boundary layer have not received such attention.

Numerical analysis of the problem of airflow over a mountain barrier has been discussed at considerable length in the literature and is well documented. It was found some years ago by Malkus and Stern (1953) that from a theoretical point of view, the introduction of a heating function at the surface of a stratified fluid could be interpreted as a heat mountain. Thus, alternately, the mountain problem could be considered from a thermodynamic point of view (with certain modifications for energy consideration). The heating problem has been studied numerically by Tanouye (1966), Estoque (1968, 1969, 1970), Spelman (1969), Myrup (1968), Tag (1969), and Delage and Taylor (1970).

The last three papers study specifically the urban heat island phenomena. Olfe and Lee (1971), and Vukovich (1971) provide two of the very few analytical treatments of urban heat island convection.

Malkus and Stern studied the effects of the flow of a stable atmosphere over the heated islands of Puerto Rico and Nantucket, (Malkus and Stern, 1953; Malkus and Bunker, 1952; Malkus, 1955). Simple numerical models have been developed for their case, (Stern, 1955; Smith, 1955). These suggested that the rising air above the island may result in an upsurging in the stabilized layer followed by a wave propagating outward much like a stone thrown into the water. The possible case of complete penetration of the stable layers above a heated island was apparently not considered.

1.2 Mountain-like Surface Irregularities

As a density-stratified flow passes over obstacles, such as mountains or hills, the air current tends to be wavy in the lee of the obstacles. This lee-wave phenomenon greatly affects aerodynamics since associated with the formation of mountain lee-waves, strong downslope wind occurs in the lee of the mountain and high turbulence exists in the rotor region underneath the wave crest.

Since Lyra first studied lee-waves in 1943, a number of analyses and experiments have been conducted to explain the physics of the phenomenon (see Queney, 1960, for a historical review). A few laboratory experiments were conducted by Long (1955), Davis (1969), and Lin and Binder (1967). Several field observations are well documented by Queney (1960). Foldvik and Wurtele (1967) presented the first attempt to numerically integrate the governing equations. Both laboratory and field observations revealed that the lee-wave phenomenon has nonlinear

characteristics; hence, it is desirable to retain nonlinear terms in a numerical approach. Long (1955) cleverly avoided the necessity of solving the nonlinear equations by introducing special upstream boundary conditions. Nevertheless, in order to simulate the general problem under less restricted situations, laboratory and numerical experiments are necessary.

1.2.1 Laboratory experiment - Geometric and dynamic similitude with matched boundary conditions must be satisfied to reproduce prototype atmospheric phenomena by model experiments (Cermak et al., 1966). It is extremely difficult to satisfy all similitude requirements simultaneously in the laboratory. For example, although Long (1955) generated wavy motions downwind of a moving obstacle towed in a water channel, exact similarity to atmospheric lee-wave motions was not obtained due to the absence of Prandtl number similarity and incorrect upper boundary conditions.

Lin and Binder (1967) improved laboratory simulation by utilizing the meteorological wind tunnel at Colorado State University. In a wind tunnel experiment it is possible to measure directly dependent variables such as velocity, temperature, and turbulence. A typical wind tunnel experiment conducted by Lin and Binder (1967) is reproduced in Fig. 1-1. The second lee wave crest is apparent in the isotherm results. The velocity downslope of the bell-shaped obstacle has a large magnitude which coincides with field observations.

Similarity in a wind tunnel experiment requires a very small velocity ($\sim$ 10 cm/sec) and strong stratification ($\sim 1^{o}C/cm$). In practice it is not easy to change temperature and velocity profiles independently because of their mutual interactions.

The effect of viscosity in a wind tunnel experiment is not yet fully understood. It is commonly accepted that in the prototype lee-wave phenomenon, viscosity does not affect the nature of the phenomenon since the Reynolds number is large. It may be adequate for Reynolds number similarity to use an eddy viscosity in the prototype and a molecular viscosity in the model experiment (Scorer, 1953, p. 72).

1.2.2 Numerical approach - Ideally, numerical simulation can avoid all the difficulties encountered in a laboratory experiment. Since the former is a direct one-to-one simulation there is no need to consider scaling effects. The accuracy of a numerical experiment, however, depends on many factors, such as the particular differencing scheme used, the magnitude of grid and time increments, the boundary conditions imposed, the size of the computational area, etc. Therefore it is necessary to investigate the reliability of numerical results by other means. If the problem is simple enough, a comparison with a known analytical solution might be possible. This is not normally the case, however, for such nonlinear problems as are described here. A wind tunnel is extremely useful in determining the reliability of numerical results. Once confidence is established in numerical procedures through a wind tunnel simulation, then the direct application of the numerical program to the atmosphere is reasonable. Another advantage to a numerical approach is that it is possible to extend or change meteorological variables easily. For example, the effect of varying viscosity in a wind tunnel experiment may be examined by a numerical experiment.

In this manner, theoretical, experimental, and numerical simulation improve the understanding of complicated fluid motions.

1.3 Cross Flow Effects Associated with Non-homogeneous Surface Irregularities

Probably the strongest statement regarding the three dimensional aspects of such flows has been made by Bradshaw (1966) in his review of turbulent boundary layers.

> When the crossflow is small, the same simplifications can be made as in laminar flow -- although one feels intuitively that the interactions between streamwise flow and crossflow will be more important in turbulent flow.

Accordingly, this research was designed to help reach an understanding of the fundamental behavior of mildly three-dimensional turbulent shear flows.

But in addition, this research specifically hopes to provide a working knowledge of some commonly occurring atmospheric flows near the earth's surface. Lettau (1955) emphasizes the dependence of aerodynamic processes on the horizontal variability of conditions at the earth-air interface and the need for systematic studies to determine the resulting flow interactions. In spite of this recognition that three-dimensional shear flows represent a common natural aerodynamic state, the bulk of analytical and field studies have been restricted to two-dimensional situations. The research discussed here, although difficult and tedious, represents an attempt to provide needed basic information of practical importance.

1.4 Objectives of Research

To put the forcing problem into proper perspective, therefore, it seems that both the heating and topographically forced flows should be studied independently; then, the results should be compared and precise analogies discussed. If the physical and kinematic parameters are

properly selected, the results of the experiments should be applicable also to the atmosphere -- for scales small enough so that rotation can be ignored. It should then be possible to state the atmospheric conditions necessary for instability due to surface heating and to explore the possibility of establishing those required conditions. Among the practical problems to which these results could be applied are the initiation of convection and resulting precipitation, and the dispersion of pollution, fog, dust and other stable but undesirable atmospheric contaminants.

Investigations are specifically conducted in a stably stratified atmosphere (temperature increases with height), since effects of urban heat islands are more significant during the night (Mitchell, 1961) when the atmosphere is frequently in an inversion configuration. Moreover some interesting phenomena in the atmosphere, such as gravity waves behind a mountain, or a heated island, or an atmospheric jet flow, are the results of the interaction of inertia and buoyancy forces caused by stratification.

CHAPTER II

LITERATURE REVIEW

2.1 Review of Mountain Lee-Wave Phenomena

2.1.1 Introduction - The subject of a fluid motion over obstacles has been of continuing interest to fluid dynamicists and meteorologists because it relates to such important phenomena as separation, wakes (rotors), hydraulic jumps, and mountain lee-waves.

At least four recent reviews are available for airflows over mountainous terrains (Corby, 1954; Queney, 1960; Krishnamurti, 1964; Lin and Cermak, 1969). In this report we shall describe in detail only more recent efforts, especially those which approach time dependent problems by a numerical integration. In order to provide continuity to the present work, a brief review of its historical context follows.

2.1.2 Observational evidences - Discontinuous clouds over mountainous regions have been observed; this indicates the existence of pairs of ascending and descending motions. The fluid motion associated with these cloud rows is commonly known as a "mountain lee-wave" phenomenon. The formation of clouds corresponds to the wave crest position. Cloud spacing, which corresponds to wave length, ranges from 5 to 25 km but is primarily between 8 and 10 km (Queney, 1960). As many as eleven waves have been counted while five or six waves are commonly observed (Scorer, 1951).

Glider pilots commonly testify to the presence of strong wave motions near the mountains. They are able to glide to a very high altitude riding on the ascending motion of a mountain lee-wave. Many

ascents are recorded to well above 12,000 m, and vertical components of velocity of 10 m/sec are common. It is believed that the vertical velocity may exceed 25 m/sec occasionally (Corby, 1954, p. 494). Queney (1960, p. 35) reports from the results obtained by the Sierra Wave Project that the double wave amplitude exceeded 2,100 m at mean altitude 4,100 m and vertical components in the wave motion were 12.5 m/sec and -9.5 m/sec.

Observations suggest that the occurrence of wave phenomena is limited to certain favorable physical and meteorological situations. Förchtgott suggests, for example, "that for a ridge of 900 m high, a wind of 12 m/sec was necessary for wave streaming. If the obstacle is a solitary hill, rather than a very long ridge, a much stronger wind speed is necessary for a given type of flow than in the case of a long ridge of a similar height" (Corby, 1954, p. 516). Observations have shown that wave motions exist when the atmosphere is appreciably stable. Commonly the distribution of the lapse rate was more stable at lower levels, 1 to 4 km, and less stable above 4 km (Queney, 1960, p. 32).

2.1.3 Theoretical studies - Analytical models for airflow over mountains were all based on a linear perturbation method until Long developed his nonlinear model in 1953. Queney, Lyra, Scorer and others made important contributions to develop the linear theory. Primary contributions to Long's model are found, in addition to Long's own works (Long, 1953, 1954, 1955), in Yih (1960), Drazin and Moore (1967), Miles (1968a, 1968b), Davis (1969), and Pao (1969).

Common characteristics of both linearized and nonlinear models are the assumptions that they are two-dimensional and stationary. The latter assumption introduces the incorrect mathematical possibility of

an infinite set of upstream waves associated with solution singularities (see Queney, 1960, pp. 53, 54). In order to assure uniqueness with statements, Rayleigh introduced Rayleigh friction terms in his system of equations. Further, an alternative way to establish uniqueness is to treat the problem as an initial value problem rather than a stationary one (Krishnamurti, 1964, p. 594). However, if the problem is treated as an initial value problem, then the convenient transformation of variables which Yih introduced is no longer possible (Yih, 1965). This limitation explains why research programs since the 1950's are primarily based on numerical integrations utilizing a digital computer (Foldvik and Wurtele, 1967; Lin and Apelt, 1970).

The complete meteorological description of the mountain lee-wave phenomenon is, of course, extremely complex. A total description must include thermal energy balance, humidity, condensation and evaporation, insolation, etc. A few authors have attempted to include some secondary variables; however, they could not include all of the factors mentioned above (Magata and Ogura, 1967; Orville, 1965, 1968a, 1969).

In order to include lateral effects of an obstacle, a horizontally two-dimensional model may in some cases be constructed utilizing shallow water theory (Spelman, 1969; Oobayashi, 1970). This theory recognizes that "the trade-wind atmosphere has a relatively simple structure for modeling purposes, namely a well-mixed layer below about 2 km having nearly homogeneous potential temperature and wind fields in the vertical, capped by an inversion" (Spelman, 1969, p. 73).

If one combines the above approaches, then a complete three-dimensional picture is obtained. Several papers based on linear

perturbation theory (Sawyer, 1967; Onishi, 1969), are available for such a three-dimensional treatment.

2.1.3.1 Linearized theory - The following derivation of the basic equation for the airflows over mountains is taken from the work by Lin and Cermak (1969).

The basic system of the equations consists of the equation of motion along the longitudinal x and vertical z axes, the equation of continuity, the statement of adiabatic motion, and an equation of state for air. No heating and an inviscid fluid are assumed. The list of the symbols used below is presented at the beginning of this report.

Equations of Motion

$$u\frac{\partial u}{\partial x} + w\frac{\partial u}{\partial z} = -\frac{1}{\rho}\frac{\partial p}{\partial x} \qquad (2.1.3.1\text{-}1)$$

$$u\frac{\partial w}{\partial x} + w\frac{\partial w}{\partial z} = -\frac{1}{\rho}\frac{\partial p}{\partial z} - g \qquad (2.1.3.1\text{-}2)$$

Equation of Continuity

$$u\frac{\partial \rho}{\partial x} + w\frac{\partial \rho}{\partial z} = -\left(\frac{\partial u}{\partial x} + \frac{\partial w}{\partial z}\right) \qquad (2.1.3.1\text{-}3)$$

Adiabatic Equation

$$u\frac{\partial p}{\partial x} + w\frac{\partial p}{\partial z} = c^2\left(u\frac{\partial \rho}{\partial x} + w\frac{\partial \rho}{\partial z}\right)$$

All dependent variables are replaced by

$u = \bar{u}(z) + u'(x,z)$,

$w = 0 + w'(x,z)$,

$$\rho = \bar{\rho}(z) + \rho'(x,z),$$

$$p = \bar{p}(z) + p'(x,z),$$

and

$$c = \bar{c} + c'(x,z)$$

where bared quantities are mean values and primed ones are the perturbations.

The mean quantities are governed by the relations:

$$\bar{p} = \bar{\rho} R \bar{T}; \qquad \text{Equation of State}$$

$$\frac{1}{\bar{\rho}} \frac{\partial \bar{p}}{\partial z} = - g; \qquad \text{Hydrostatic Balance.}$$

The perturbations, their derivatives, and their products are neglected in comparison with those containing mean quantities because the linearizing assumption requires that the perturbed quantities be at least one order of magnitude less than their mean values.

In the following expressions the primes are eliminated from the perturbation quantities. Table 2-1 shows both retained and neglected terms.

Linearized equations are

$$\bar{\rho} \left(\bar{U} \frac{\partial u}{\partial x} + w \frac{\partial \bar{U}}{\partial z}\right) = - \frac{\partial p}{\partial x}, \qquad (2.1.3.1\text{-}4)$$

$$\bar{\rho}\, \bar{U} \frac{\partial w}{\partial x} = - \frac{\partial p}{\partial z} - \rho g, \qquad (2.1.3.1\text{-}5)$$

$$\bar{U} \frac{\partial \rho}{\partial x} + w \frac{\partial \bar{\rho}}{\partial z} + \bar{\rho} \left(\frac{\partial u}{\partial x} + \frac{\partial w}{\partial z}\right) = 0, \qquad (2.1.3.1\text{-}6)$$

and

$$\overline{U}\,\frac{\partial p}{\partial x} + w\,\frac{\partial \overline{p}}{\partial z} - \overline{c}^2\,\left(\overline{U}\,\frac{\partial \rho}{\partial x} + w\,\frac{\partial \overline{\rho}}{\partial z}\right) = 0. \qquad (2.1.3.1\text{-}7)$$

Through lengthy algebraic manipulations, and incorporating the assumptions that $\overline{U}^2 << \overline{c}^2$, $\overline{U}\,\frac{\partial \overline{U}}{\partial z} << g$, and $\overline{U}\,\frac{\partial \overline{U}}{\partial z} << \overline{c}^2$, a simple wave equation with respect to the vertical velocity component, w, is obtained

$$\frac{\partial^2 w}{\partial x^2} + \frac{\partial^2 w}{\partial z^2} - \overline{s}\,\frac{\partial w}{\partial z} + \left(\frac{\beta g}{\overline{U}} - \frac{\frac{\partial^2 \overline{U}}{\partial z^2}}{\overline{U}}\right) w = 0, \qquad (2.1.3.1\text{-}8)$$

where $\overline{s} = -\frac{\partial \overline{\rho}}{\partial z} / \overline{\rho}$ and $\overline{\beta} = \overline{s} - g/\overline{c}^2$. The various steps to obtain Eq. (2.1.3-8) from Eqs. (2.1.3.1-4) to (2.1.3.1-7) are described in Lin and Cermak (1969, p. 20) or in Krishnamurti (1964, p. 596). The final expression is slightly different from those shown in Queney (1960, p. 51) or in Krishnamurti (1964, p. 597). In their expressions the first term is multiplied by $\overline{M} = 1 - \overline{U}^2/\overline{c}^2$ and a term $\overline{s}\,\frac{\partial u}{\partial z} / \overline{U}$ is included in the parenthesis of the fourth term. As long as the assumptions above are justified, both expressions coincide.

2.1.3.2 Necessary conditions for lee-waves and the factors influencing their amplitudes - Scorer (1949) developed necessary conditions for the occurrence of lee-waves. His parameter ℓ must normally decrease upwards, where

$$\ell^2 = \frac{g\overline{\beta}}{\overline{U}^2} - \frac{\frac{\partial^2 \overline{U}}{\partial z^2}}{\overline{U}} \; . \qquad (2.1.3.2\text{-}1)$$

With two layers, the lower of depth h, waves can occur if

$$\ell_1^2 - \ell_2^2 > \frac{\pi^2}{4h^2} , \qquad (2.1.3.2\text{-}2)$$

where subscripts 1 and 2 refer to lower and upper layers, respectively.

Corby and Wallington (1956) investigated the factors which influence the lee-wave amplitude. They investigated the influence in the special case of an idealized two-dimensional ridge described by the bell-shaped equation

$$M(x) = \frac{a^2 b}{b^2 + x^2}$$

where a is the height of the ridge and b is the "half-width" parameter. The flow pattern by such a ridge is indicated by the term

$$\delta(z) = - 2\pi a\, b\, e^{-kb}\, (\bar{U}_1/\bar{U})\quad \psi_{z,k}\, \left(\frac{\partial \psi_{1,k}}{\partial k}\right)^{-1} \sin kx$$

where $\delta(z)$; displacement of a streamline from its undisturbed level at height z,

k; the lee wave number,

$\bar{U}$; horizontal wind speed,

ψ; satisfies the equation

$$\frac{\partial^2 \psi}{\partial z^2} + (\ell^2 - k^2)\psi = 0$$

and the suffix 1 refers to ground level.

If the height of a ridge is kept constant, then the factor abe^{-kb} takes a maximum value at $b = k^{-1}$. If the shape of a ridge is changed keeping the ratio $a : b$ constant, then the maximum occurs at $b = 2k^{-1}$. On first glance a wind speed decreasing with height apparently increases the wave amplitude. Velocity, however, is also included in the expression for ℓ^2 by Eq. (2.1.3.2-1). Since a decrease of ℓ^2 is the necessary condition for waves, a combination of wind and stability distributions should be considered. Hence if two airstreams have the same ℓ^2 profiles with different combinations of wind and stability, then the airstream for which $\overline{U}_1/\overline{U}$ is larger will have the greater amplitude waves.

The last factor $\psi_k(\frac{\partial \psi_{1,k}}{\partial k})^{-1}$ is directly related to the ℓ^2 profile. But ℓ^2 is interrelated with the lee-wave number k and the factor abe^{-kb}. If the effect ℓ^2 alone is investigated, then there exists an optimum value of ℓ^2 which provides for the maximum value of the factor $\psi_k (\frac{\partial \psi_{1,k}}{\partial k})^{-1}$. However, if ℓ^2 conditions are made more favorable for waves to occur, the amplitude falls off sharply.

Lee-wave amplitudes were interpreted to be very sensitive to optimum meteorological conditions. Apart from this sensitive region, Corby and Wallington (1956, p. 274) concluded that "larger amplitude waves were theoretically more likely in airstreams containing a shallow layer of great stability than in conditions of slight stability through a deep layer."

2.1.3.3 The validity and limitations of the results of perturbation theory - The linear theory results obtained by Queney and Lyra showed apparent violations of the assumptions used to derive the linearized wave equation. The mountain involved was always a finite

amplitude perturbuation. The solutions exhibited very large vertical velocities at great heights above the grcunds; thus, the neglect of the nonlinear terms is not justified. The results obtained by Lyra and Queney are shown in Queney (1960, p. 57 and p. 61). These unrealistic results may be a result of the fact that both Queney's and Lyra's mean atmosphere was characterized by a constant temperature and wind.

Scorer (1949) was the first to examine a two layer model, i.e., the atmosphere was characterized by two layers which have different wind and temperature distributions, but stability parameters are constants in each layer. This innovaticn eliminated the second deficiency obtained by Lyra and Queney. Stability and velocity profiles were chosen so that they satisfied the necessary conditions for occurrence of lee-waves as given by relation (2.1.3.2-2). The result is shown in Fig. 2-1.

Meteorological measurements of the lee-wave phenomenon are not complete enough to provide a critique of Scorer's model. However, it is appropriate to examine the credibility of Scorer's underlying assumptions. Corby (1954) examined the assumptions involved in Scorer's model in detail: a) inviscid fluid, b) isentropic, c) steady flow, d) small perturbation, and e) neglect of the earth's rotation. Corby justified assumptions b), and e). He concluded that the restriction to steady laminar flow was serious since there was ample evidence that the flow over mountains was commonly unsteady. The effect of the viscosity would be expected to exert a damping effect on the disturbances. Janowitz (1968) examined the effect of viscosity on wave length and wave amplitude. When the Reynolds number, defined by the cubic root of the square of the product of the internal Froude number and the internal

Reynolds number of the shear wave, is small (<7), then viscosity lengthens the wave and alternates its amplitude.

This Reynolds number becomes very large under meteorological conditions typical of mountain lee-wave phenomena. For this very large Reynolds number (order of 10^2) there are no viscosity effects either on the wave length or on the attenuation constant.

A small displacement is a fundamental requirement of the perturbation theory. It is reasonable to accept the results, at least qualitatively, provided the mountain height is no more than about ten percent of the width. (Queney claims rough validity if the ratio 'height to width' is up to 1/4 or even 1/2 in special cases (Corby, 1954, p. 510)).

Scorer (1953) himself noted that the disturbance could be as large as the mean quantity. Strictly speaking, the second-order terms in the equations of motion were thus neglected unjustifiably; however, the solutions are still qualitatively correct, and the neglected terms would have only a 'modifying influence.

Anticipating the results obtained by the nonlinear model proposed by Long, we may explain the unusually good agreement between the linear theory and mountain lee-wave observations. If the vertical gradients of the density and the kinetic energy of the basic flow are constant far upstream, then the nonlinear terms vanish exactly in the wave equation; thus the finite amplitude flow is given by the linear dynamics (Krishnamurti, 1964, p. 622; Queney, 1960, p. 109).

2.1.3.4 Long's model and its solutions - Long (1953) obtained a linear wave equation which was applicable even for finite amplitude waves, provided that special boundary conditions were

satisfied far upstream. Motion was assumed to be steady, incompressible, inviscid and two-dimensional in the vertical plane normal to the obstacle.

The complete governing stream function equation under these circumstances is

$$\nabla^2\psi + \frac{1}{\rho}\frac{d\rho}{d\psi}\frac{(\nabla\psi)^2}{\nu} = \zeta(\psi) + \frac{1}{\rho}\left(\frac{d\rho}{d\psi}\right)\left[\frac{U^2}{\nu} + g(z_o - z)\right] \qquad (2.1.3.4\text{-}1)$$

where ψ is a stream function, $\rho(\psi)$, and $\zeta(\psi)$ are the density and the vorticity upstream, respectively. $z_o(\psi)$ and $z(\psi)$ are the height of the streamlines, ψ = constant, far upstream and downstream, respectively. U is a horizontal velocity component upstream which is a known function of z_o or ψ.

Equation (2.1.3.4-1) is an exact expression for an arbitrary density and velocity distribution upstream. It is, however, a nonlinear equation; therefore, it is very difficult to solve the equation analytically. Long sought a model which is linear and mathematically tractable. Long first introduced the notation

$$\frac{d}{d\psi} = -\frac{1}{U}\frac{d}{dz_o}$$

provided that U does not vanish anywhere and

$$\delta = z_o - z.$$

Equation (2.1.3.4-1) transforms to

$$\nabla^2\delta + \frac{1}{2}\left[(\nabla\delta)^2 + \nu\frac{\partial\delta}{\partial z}\right]\frac{d}{dz_o}(\ell n\, U^2\rho) = \frac{g}{U^2\rho}\frac{d\rho}{dz_o}\delta\ ,$$

(2.1.2.4-2)

If $U^2\rho$ = constant and the density is linear in z_o, the above equation reduces to

$$\nabla^2\delta + \sigma^2\delta = 0, \qquad (2.1.3.4\text{-}3)$$

where

$$\sigma^2 = \frac{g\left|\frac{1}{\rho}\frac{d\rho}{dz_o}\right|}{U^2}\ .$$

σ^2 is a stability factor which is related to a global Richardson number Ri and the internal Froude number Fr by

$$Ri = \sigma^2 H^2$$

and

$$Fr = \frac{1}{\sigma H}$$

where H is the channel height.

In a subsequent paper Long (1955) discussed solutions of the flow over an obstacle of finite length and height. He also conducted experiments with a stratified fluid in a water channel. Agreement between theory and experiment was excellent. Some of Long's figures are reproduced here (see Fig. 2-2). Long also analytically obtained criteria for overturning instability (density increases with height) for a given stability and obstacle height. Fig. 2-3 displays the result; it suggests that if $Fi < \frac{1}{\pi}$, there is a critical obstacle

height for overturning instability. Higher obstacles will produce a negative density gradient at some point in the flow field. Figure 2-3 indicates that there are singularity points in the flow fields corresponding to the Froude number $= (p\pi)^{-1}$ where p is an integer number. When the Froude number is decreased and the obstacle is large, a stable steady-state solution cannot be obtained theoretically. Experiments showed that impulses are sent upstream by the obstacle; this leads to alternate jets and stagnation regions in the vertical. Simultaneously turbulence is produced over the obstacle and in its lee; this result is obviously not a steady state.

Since Long published his original papers many authors, utilizing Long's model, have contributed to the study of fluid motion over various obstacles. Different mathematical approaches were attempted to obtain more realistic solutions and to simplify computational procedures.

Lin and Cermak (1969) discussed all mathematical aspects of these works, hence we shall only review their conclusions and the interesting contradiction which arises.

Yih (1960) generalized Long's equations (Eq. (2.1.3.4-2)) through transformations of variables. He could obtain three different classes of flow which provide linearization, one of which was obtained by Long earlier (1953). A detailed discussion of the solutions for these three classes of flow are given in Yih (1965, pp. 78-113). Both Long and Yih employed an inverse calculation method; that is, the exact obstacle shape is obtained after the flow field has been calculated. Therefore, a flow pattern cannot be conveniently investigated for a pre-prescribed obstacle shape.

Drazin and Moore (1967) developed a mathematical model which was applicable for arbitrary obstacle shapes. Two examples were given: one was for a dipole, and another was for a vertical wall. They found an interesting but contradictory result of Long's theory (1955). Long (1955) suggested that a sufficiently large obstacle in a strong stability fluid exerts a blocking effect. Waves may be propagated upstream boundary to disturb the prescribed upstream boundary conditions. Dazin and Moor concluded that there is no critical internal Froude number to destroy the existence of a steady flow solutions if no restrictions are placed on the amount of energy available to drive the flow. Pao (1969) came to a similar conclusion.

The wave drag associated with stratified flow past various obstacles was investigated by Miles (1968a, b). He computed wave drag utilizing Long's model and found that there is a region where wave drag increases with decreasing wind velocity. Experiments conducted by Davis (1969) showed that the wave drag coefficient was not, for a thin barrier, the dominant function of stratification. Both Miles and Davis pointed out that these anormalous predictions are subject to two serious objections: those solutions which are associated with large drag are not consistent with the derivation of Long's equation and, even if they are interpreted as legitimate steady-state flows, these solutions probably represent unstable motions (Davis, 1969, p. 141).

Indirectly speaking Miles and Davis support Long's contension that there are physical limitations to the application of Long's equation. Davis' measurements of wave drag demonstrated that for a larger value of $k(1 < k < 4)$, the results predicted phenomena which were not described by Long's equation.

Davis (1969) conducted numerical and water channel experiments over a triangular and a thin barrier. Figure 2-4 shows some of his results. The agreement of the results is at least qualitatively correct when k is small. The first wave crest in the experiments is, however, always located further downstream than predicted by the theory. With increasing stability k, the experimental results exhibit strong turbulent, or at least very unstable, regions next to the boundary. In this range of stratification, Long's solution could not predict the flow, because non-stationary cases can not be included in Long's final equation.

Pao (1969) investigated a stratified flow over a single obstacle and a series of semi-circular obstacles constructed from vortex pairs and doublets. His boundary conditions were somewhat unique. He required not only that all the disturbances generated by the obstacle vanish far upstream, but also that far upstream the disturbance pressure force, the total disturbance kinetic energy, and the total disturbance potential energy vanish. These additional restrictions were added to obtain a unique solution of an inviscid stratified flow. His results over a single barrier could simulate a rotor phenomenon. The effect of the second barrier placed in line with the first weakened or strengthened the waves depending on the stability.

2.1.3.5 Some concluding remarks on Long's model - As we have seen, Long's model is a remarkable mathematical simplification for two-dimensional, steady, incompressible, and inviscid stratified flows involving finite amplitude waves. However, if stratification is increased and a larger obstacle is used, then the predictability of the theory is doubtful, since the flow tends to become unstable. Since

experiments often show evidence of turbulent motion, Long's assumption of stationary flow is no longer valid. Solutions obtained from Long's model often indicate regions of closed streamline flow. This violates the initial model derivation, since it was assumed that all fluid particles were connected to upstream origins. The model's prediction of upstream blockage is also controversial (Long, 1955; Drazin and Moore, 1967; Pao, 1969).

2.1.4 Time dependent treatment - A time dependent treatment is an alternative way to assure the uniqueness of a mountain lee-wave analytical solution. If the problem is treated as an initial value problem, then the main deficiencies of Long's model can be eliminated. For example, negative density gradients which may lead to unstable motion are acceptable, closed streamlines do not violate the equation, and the blocking effect propagating to the upstream boundary may be eliminated.

Time dependent solutions can also be applied to more realistic cases where the meteorological factors such as wind, temperature, and pressure are varying.

Some simple time dependent cases are described in Krishnamurti (1964), i.e., the works by Wurtele (1953), Palm (1953), and Queney (1954). We shall not discuss their works here, because their search for a closed form analytical time dependent solution has resulted in overly restrictive geometries and initial conditions.

2.1.5 Numerical research - The many complicated, interacting, nonlinear, diffusive effects such as velocity, temperature, topography and surface heating make numerical modeling an attractive method. Stationary, two-dimensional linear or nonlinear mountain lee-wave

problems were solved numerically by Sokhov and Gutman (1968), Kozhevnikov (1968), and Pekelis (1969). Since we are primarily interested in a non-stationary treatment, those papers which have a time dependent nature will be discussed.

Foldvik and Wurtele (1967) constructed a numerical model of an airflow over a rectangular-shaped mountain. They used the Boussinesq approximation to derive the vorticity equation, but friction terms were not included.*

Foldvick and Wurtele used periodic (cyclic) boundary conditions for the two streamwise boundaries. Their solution developed a computational instability from the boundary when the number of integrations was large.** A nonlinear instability (see section 4.27) was also evident in the Foldvick-Wurtele scheme. It developed upwind from the obstacle, yet its magnitude was small so that the majority of the field was apparently not affected. They claimed that the numerical results provided a good qualitative agreement with some observations.

Lin and Apelt (1970) conducted numerical experiments of fluid motion over a thin barrier. The Boussenesq approximation, including friction terms, was used. The numerical method was a combination of the

---

*We also utilized a similar basic equation which was obtained from physical consideration of the phenomena. The majority of the papers were characterized by the Boussinesq approximation. Therefore the significance of the approximation will be described later in sections 4.6 and 4.7.

** Since inflow and outflow boundary conditions cannot be specified in advance for a specific problem, the least restrictive conditions should ordinarily be used. These will depend upon the characteristics of the individual problems. A numerical investigation of different boundary conditions will be discussed in sections 4.25 and 4.26.

Crank-Nicolson method (see Smith, 1965, p. 17) with a strongly implicit iterative method developed by Stone (1968). They used the Milne predictor formula at lateral boudaries. This also introduced boundary perturbations at the upstream boundary for increasing integration times. Two cases were computed - one for $Re = 397$, $Pr = 10$ and $Ri = 1.58$ and another for $Re = 5000$, $Pr = 1$ and $Ri = 1.58$. The two results did not display considerable differences primarily because the amplitude of the lee-waves generated was so small. Strong damping or diffusing effects were evident due to the finite difference scheme used. Their upstream difference scheme has a very large pseudo-viscosity (see section 4.11.2) which can eliminate otherwise wavy motion behind an obstacle.

Magata and Ogura (1967) investigated the effect of heating and cooling on the airflow over a mountain. The governing equations were the same as used in his sea breeze modeling (Magata, 1965). Hydrostatic balance was assumed; therefore, the vertical velocity component and the pressure term were obtained from the diagnostic equations. The results obtained could explain qualitatively the local phenomenon observed in Japan. Local strong wind appeared under the lee of the mountain when air passing over the mountain was cooled by the earth's surface.

Orville (1965, 1967, 1968a, 1969, 1970) has been investigating air flow over mountains, including moisture effects. His model assumed two-dimensionality, incompressibility, and constancy and equality of eddy coefficients for heat, moisture and momentum. Since it is beyond the scope of the present study to include the moisture budget, Orville's results will be referred to in the later discussion of the heated mountain. Very important observational data over a mountain ridge have

been supplied by Fosberg (1967, 1969). Data were taken in the San Jacinto Mountains about 130 km east of Los Angeles, California (1967), and across the Santa Ana mountains of Southern California (1969). Finer detail data points were obtained by a numerical integration of the basic fluid equation incorporating field data. Results obtained by Magata, Orville, and Fosberg will be compared with results obtained here in Chapter V.

2.1.6 Application of shallow water theory - It is natural to seek a more realistic mathematical model to simulate the actual three-dimensional airflow over mountains. Infinitely long mountains are not realistic. Two papers (Oobayashi, 1970 and Spelman, 1969) are available which utilize the shallow layer theory, to include the lateral effects of discontinuities. Since Spelman included the effects of surface heating, roughness and topography, the results will be discussed in detail during comparison with the results of this research.

2.1.7 Further applications and some concluding remarks on numerical works - Three-dimensional models have been presented for mountain waves. Such examples are discussed by Sawyer (1962) and Onishi (1969). Their equations were linearized by the perturbation method. Since we do not yet know the effect of nonlinearity of convection terms even for two-dimensional flows, it seems inappropriate to discuss here the justification of the perturbation method used for a three-dimensional problem.

In principle, a numerical integration by finite difference approximation is a very powerful approach to apply to the complicated nonlinear problems. The validity of results so obtained is not clear, however, because there are very few observational data available. In

addition there are many important unresolved problems in the finite difference approximation itself, such as criteria of stability, convergence, proper assignment of boundary conditions, etc.

Another limitation, of course, is the finite capacity of a digital computer. In order to simulate turbulent phenomena accurately, we need a very small grid size if energy-containing eddies are also small. This generally requires a large number of grid points. An expanded grid system is sometimes an alternative way to reduce the number of grid points; but unfortunately finite lee-wave motions are expected even far downstream from the initial forcing perturbation, therefore an expanded grid may lose wave characteristics.

Consequently, in the future, if the capacity of a computer is not grossly expanded, a combination of analytical and numerical approaches may be required rather than a strictly computational one, especially for three-dimensional, turbulent flow.

2.1.8 Model experiments - Very few experimental results are available on stratified flow over obstacles. Long (1955) and Davis (1969) obtained results in a water channel. Lin and Binder's (1967) results are the only ones available from wind tunnel experiments. Model experiments in wind tunnels are very difficult, as pointed out by Scorer (1953), since similarity law requires a very strong temperature gradient and a very small velocity. Fortunately it is not impossible to have a vertical temperature gradient of 1^{o}c/cm and a horizontal velocity of 10 cm/sec (see Chapter III on wind tunnel design). The experimental results discussed here were specifically generated to verify any numerical scheme proposed.

2.2 Review of Heat Island Phenomena

2.2.1 Introduction - The climate over cities is quite different from that over the surrounding rural areas. Figure 2-5 shows diurnal variation of temperature in Vienna, Austria (Mitchell, 1961) and in Frankfurt, Germany (Georgii, 1968). As one can see, the urban station remained warmer most of the time ("urban heat island"). The largest temperature differences were observed at night both in summer and in winter. Maximum and minimum temperatures in the cities occurred one or two hours after those in the suburbs. Many other climatic elements such as wind, radiation, humidity, cloudiness, and pollution are also changed by urbanization. Landsberg (1968) organized such climatic data into a table (see Table 2-2) to provide a quick understanding of average differences in climatic factors of urban and non-urban regions. The rest of this chapter will discuss how those differences developed, and how recent observations are correlated with meteorological factors.

Only a few attempts to explain the phenomena above are recorded (Myrup, 1969; Tag, 1969; Olfe and Lee, 1971; Vukovich, 1971). However, similar phenomena to those of urban heat islands have been observed in oceanographic fields. Malkus and Bunker (1952) observed periodically-spaced rows of small cumuli leeward of small islands on sunny summer days. This occurrence is now known as a "heated island" phenomenon (Malkus and Stern, 1953). Wavy air motion at the lee side of an island in a strongly stable stratified airflow is the result of unbalanced buoyancy forces which have been produced by the temperature difference between the island and the surrounding ocean. Since this is a "lee-wave" phenomenon as described previously in Section 2.1, Malkus and

Stern (1953) looked for the similarity between the heated island convection and airflow over a physical mountain. The heated island was replaced by an "equivalent mountain" whose shape is a function of the difference in temperature between the island and the ocean, stability of the air, wind speed, and eddy diffusivity. This theory will be described in detail in a later section.

2.2.2 Urban heat island - That certain cities have warmer temperatures than their surroundings has been known since the beginning of the eighteenth century, "but it was not until the relationships between the cities' heat island and the pathogenic and pernicious effects of air pollution were made evident that the study of this urban phenomenon was stimulated and accelerated" (Kopec, 1970, p. 602). Comprehensive reviews of recent works on the matter are available in Peterson (1969) and in a W.M.O. technical note (1968).

2.2.2.1 Basic causes of an urban heat island - Many authors have contributed to the discovery of the various physical and meteorological factors responsible for the formation of urban heat islands (Landsberg, 1956; Mitchell, 1961; Bornstein, 1968). Their conclusions are somewhat similar. The following description is primarily from Landsberg's work (1956, p. 585). The first effect of urbanization is an alteration in surface texture and roughness. Relatively smooth or hilly grass-covered regions are replaced by a formation of rocklike substances, such as stone, brick, concrete and asphalt. Naturally moist areas are drained and the reduced surface moisture decreases the need for energy for evaporation, thus increasing the energy available for transfer to the atmosphere and to the urban surfaces (Bornstein, 1968). Aerodynamic roughness is increased by building

structures of varying size which reduce surface wind velocity and introduce a more turbulent motion. The fluid motions are also favorable to the formation of an urban heat island. In addition, these urban structures absorb large amounts of solar radiation during the day. Most building and structural materials have a large heat capacity and a high heat conductivity; these thermal properties prevent rapid cooling after sunset and rapid warming after sunrise (Bornstein, 1968).

The second cause for climatic change is artificial heat generation through combustion processes in industry, homes, automobile engines, and human and animal metabolisms. Garnett and Bach (1965) computed the ratio of artificial heat generation to natural radiation heating in Sheffield, England. Their conclusion was that the artificial heat represented nearly one-third of the net radiation balance. This is comparable with results reported for several other cities -- 1/3 for Berlin, Germany, and 1/6 to 1/4 for Vienna, Austria (Peterson, 1969, p. 16). Bornstein (1968) obtained for Manhattan, New York, values of 5/2 in winter and 1/6 in summer.

The third major factor in urbanization is the change produced in atmospheric composition. More pollutants are emitted into the atmosphere with growing population and increased industrialization. Georgii (1968) presents an excellent discussion of the effects of air pollution on the various climatic elements in Frankfurt, Germany, such as the intensity of solar radiation, the range of visibility, the temperature distribution, the relative humidity, the local wind distribution, and the distribution of precipitation. We are primarily interested here in temperature and local velocity distributions; therefore, only a brief discussion of the remaining factors will be

given here. Georgii provided a comparison of the concentration of trace constituents in both pure and polluted atmospheres, and he showed a reduction of incoming solar radiation due to the haze dome above cities (see Table 2-3). The greatest loss of sunshine is commonly observed during the winter months, when pollutants emitted from domestic heating are at a maximum. In addition to the "blanketing effect" of pollutants on incoming solar radiation during the day, at night the pollutants absorb heat energy transmitted from a city surface and reradiate it downward to intensify the nocturnal heat island. An elevated inversion layer may be generated over the city when the pollution upper surface is cooled by long wave radiation to the sky. This, in turn, promotes the further increase of pollution concentration in the city, until morning when the sun's heat may finally destroy the inversion (Mitchell, 1961).

A very interesting explanation concerning the formation of fog in a city is given in Georgii (1968, p. 221). "The frequency of fog formation in urban environment is higher in spite of the fact that the air temperature in cities is higher and the relative humidity is lower within the cities compared to the countryside. The explanation for this contradiction must be seen in the mechanism of fog formation. High concentration of sulfur dioxide, the formation of sulfuric acid by catalytic oxidation on the surface of particulate matter in a humid environment leads to the formation of small fog droplets under conditions when in a pure atmosphere fog would not yet form."

Five to ten percent precipitation increase over cities is commonly accepted. But a quantitative verification of the relation between precipitation and urbanization is not available. Several possible

reasons for an increase of precipitation over an urban complex are: increased convection by added heat, added updraft motions from friction-barrier effects, added water vapor, and added condensation nuclei and freezing nuclei (Changnon, 1968; Peterson, 1969). Oke and Hannel (1968) noted a formation of small cumulus clouds at about 300 m over steelmills.

Three major causes of urban heat islands have been discussed. The following sections describe recent observational evidences of urban heat islands over several major cities, show their common characteristics, and seek to correlate meteorological factors with the formation of a heat island.

2.2.2.2 Observations of urban heat islands (temperature and local wind distributions) - Since urban heat island effects are most pronounced at night, almost all past observers described the nocturnal heat island. Daytime temperature differences have also been observed (Ludwig and Kealoha, 1968; Preston-Whyte, 1970), but their magnitudes are generally small. Furthermore, measurement difficulties arise since "daytime attempts to record temperature patterns were frustrated by constant sun-shade changes along the roads traveled, caused by trees, buildings and other roadside obstructions" (Kopec, 1970).

a) Duckworth and Sandberg's work (California)

Duckworth and Sandberg (1954) measured horizontal and vertical temperature gradients over three California cities, San Francisco, San Jose, and Palo Alto, by intensive traverse with automobile-mounted thermistors and by release of a wire sonde simultaneously at urban centers and peripheral open areas.

Most surveys were made in the evening, between 2000 and 2400 hours, when urban differentials appear to be most pronounced; no correction for change of temperature with time appeared necessary. The maximum temperature was almost always located in the most densely built-up area, defining the center of an urban heat island; the minimum temperature almost always appeared at some point on peripheral open lands. To characterize the scale of urban effects, three different measures were developed: urban differential D_T, which was defined as the difference between the maximum and minimum observed temperatures in the traversed area; $R/\Delta T$, which was defined as the least distance in miles along which a $1^{o}F$ temperature change might be obtained; and area A, which was defined as the area continguous to the urban center, with a temperature more than $2^{o}F$ greater than the mean of the chart, as based upon the maximum and minimum temperatures.

The urban differential D_T increases with increasing city size but at a relatively slow rate. Representative values of D_T are $4\text{-}6^{o}F$ for Palo Alto, $7\text{-}9^{o}F$ for San Jose, and $10\text{-}12^{o}F$ for San Francisco, even though the population of San Francisco is 24 times greater than that of Palo Alto. On two consecutive nights with nearly identically favorable meteorological conditions the observed D_T values were $12^{o}F$ for Palo Alto and $20^{o}F$ for San Francisco, indicating the difference in city size.

The quantity $R/\Delta T$ shows values increasing somewhat more rapidly with city size, i.e., from 0.05 - 0.15 $mi/^{o}F$ for Palo Alto to 0.30 - 0.40 $mi/^{o}F$ for San Francisco. This relation follows from the fact that the total differential varies slowly with increase in city size; hence a slight increase in differential must spread over a

greater distance in the city. Consequently, the larger city has a flatter temperature gradient near its center. The heat island area A in square miles is 0.1 - 0.3 for Palo Alto, 1.5 - 2.0 for San Jose, and 4.0 - 6.0 for San Francisco.

For times between 2000 and 0100 PST, 32 pairs of comparable soundings resulted; 30 of the 32 showed a radiation type inversion over open land while in built-up areas there was inversion in only 7 cases, isothermal conditions in 7, and lapse conditions in 18.

At some point between 100 and 300 feet the soundings over built-up and undeveloped areas usually coincided, indicating a possible limit to the direct effect of heating from the urban surface. Temperatures above this point were significantly cooler over the built-up area than over the open area ("cross over") in 6 out of the 12 surveys for which simultaneous vertical soundings were made.

An example of pronounced "cross over" effect was observed at San Francisco on March 26, 1952. The two-meter temperature at the built-up site was over 11^{o}F greater than that at the undeveloped. At 70 feet, however, the two temperatures coincided, and between 70 and 320 feet the observed temperatures remained about 2^{o}F colder over the business district than over the open park.

On the other hand, a temperature survey of Palo Alto March 25, 1952, under very similar meteorological conditions, showed no appreciable "cross over" effect.

b) DeMarrais' work (Louisville, Kentucky)

Similar observations were reported by DeMarrais (1961) at the 60, 170, and 524 ft. levels on the WHAS-TV tower in Louisville, Kentucky. The data indicated that the heat island of an urban area

had considerable effects on the vertical temperature differences observed at night, so that the normal diurnal range of stability conditions over an urban area is much smaller than that over open country.

Temperature-difference records from flat, unpopulated areas showed that surface inversions formed almost every night and superadiabatic conditions existed during most of the daylight hours; weak lapse conditions (between isothermal and adiabatic) prevailed during the transitional hours. The times of occurrence of the various temperature-difference categories were so regular that they could be predicted with a fair degree of accuracy.

The 60 to 524 ft. layer at Louisville (urban area), however, did not show the daily temperature pattern demonstrated at non-urban sites. Even though the average hourly temperature differences for alternate hours for each half-month showed prevailing superadiabatic conditions during the day light hours, no generalizations could be made for the other hours. Inversions were observed during approximately 10 percent of the nocturnal hours from mid-November to mid-April (winter months) and during about 30 percent of the night-time hours in the remaining part of the year.

One of the outstanding features of the bi-hourly, semi-monthly plot of average temperature differences for the 60 to 170 ft. stratum was that only two of these averages showed an inversion condition. During the night hours in June, July, and September the averages were often greater than adiabatic, indicating that the 60 to 170 ft. stratum was thermally unstable most of the time during those periods.

DeMarrais' conclusions were (1) that, during the day, Louisville experienced lapse rates which differed only slightly from those observed in a non-urban area, and (2) that, during the night, Louisville experienced temperature differences unlike those observed in non-urban areas. Nocturnal inversions through the 60 to 524 ft height existed infrequently.

c) Bornstein's work (New York City)

Bornstein (1968) observed the differences in the temperature fields through the lowest 700 m of the atmosphere in and around New York City during the period from 2 hours before to 2 hours after sunrise.

In summary, he pointed out that the main features of the temperature distribution in the hours around sunrise are the following: 1) intense surface inversions at non-urban sites, 2) absence of surface inversions over the city, 3) one or more relatively weak elevated inversion layers over the city, and 4) an urban temperature excess which decreases rapidly with height.

Twenty-nine out of forty mornings studied exhibited surface inversions at rural sites, while on only four out of forty-two mornings were surface inversions observed at the city.

Two of the characteristics of an urban heat island effect are the existence of one or more weak elevated inversion layers over the city and the presence of "cross over", which means that the temperature over the city is lower than that over the rural region. Thirty-seven out of forty-two mornings showed one or more elevated inversion layers which had mean depths over the city of 95 m, while elevated inversions were observed over the rural area 5 out of 34 mornings.

The height variation of the mean urban-rural temperature differences between the 50 m averaged temperatures at these sites showed an almost linear decrease in the mean urban temperature excess from 1.7°C at 1.25 m to 0°C at 300 m. Above 300 m the magnitude of the difference is less than 0.2°C, and is negative from 300 to 500 m. During more than two-thirds of the test mornings a reverse heat island effect (cross over) was observed through a layer whose base was always above 150 m.

d) Further observations

Ludwig and Kealoha (1968) conducted very extensive temperature and humidity field observations over the city of Dallas, Texas. They presented a comprehensive coverage of measurements, which were obtained not only at night but also during the day. The daytime temperature differences were, however, very small - about 1°C. One of the very interesting findings of their study is that the magnitude of the urban-rural temperature difference is found to be highly correlated with the stability factor of the upwind rural region. The details will be discussed in a later section.

An urban heat island effect is not limited to very large cities. Kopec (1970) took night measurements of Chapel Hill, N.C., whose population is around 24,900. An urban temperature excess as large as 14°F was observed.

Preston-Whyte (1970) provided some of the very scarce daytime data by motor-traversing the Darban area, South Africa, during the summer of 1968-69. A temperature difference of 1.0°C was observed, and the center of the heat island was displaced away from the central business

district by the sea breeze. It has been commonly observed that the warm-air mass is displaced in the direction of the prevailing wind (Sundborg, 1950).

e) Convergence of airflow into cities

It has been observe that in order to compensate for an upward current in a convection cell induced by a city-rural temperature difference, there exist convergent flows on the ground into a city. Okita (1960) deduced the magnitude of such convergent currents in Japan by estimating the direction of rime formations on trees. Similar figures were prepared by Davidson (1967) for New York City and by Pooler (1963) for Louisville, Kentucky. All of the results showed clear, strong convergent current toward cities.

2.2.2.3 Summary of urban heat island observations - Commonly observed urban heat island characteristics are:

1) Regular variation of daily temperature over flat unpopulated areas, no generalizations of variation over urban regions;
2) Formation of one or more elevated inversion layers over cities, less frequent formation over rural regions;
3) Formation of "cross over" phenomena over cities;
4) Displacement of heat island center windward;
5) Less frequent occurrence of nocturnal inversion over a city;
6) Day time urban heat islands are less intense than their counterparts at night;
7) Stronger nocturnal urban heat islands are observed in a calm, clear atmosphere;
8) The intensity of an urban heat island depends on meteorological (wind, stability) and physical (city size) factors;

9) The upper limit of an urban heat island's direct effect extends occasionally up to 1000 m but the average height ranges 50 ~ 400 m.

2.2.2.4 Empirical formulae to correlate meteorological and physical factors with urban heat island formation - As mentioned above, intensity of urban-rural temperature differences depends on many meteorological and physical factors. Since their contributions are nonlinearly interrelated, a physical explanation of each contribution to the phenomenon is very difficult. Therefore, only empirical regression formulae are possible from observational data. These may be helpful in guiding further study and useful in practical investigations.

a) Sundborg's Formula (1950)

The temperature contrast $\Delta T(^{o}C)$ between a city and its rural area is assumed to be expressed by the linear combination:

$$\Delta T = C_1 + C_2 N + C_3 U + C_4 T + C_5 e$$

where N is cloudiness in the ten-degree scale, U is the wind velocity (m/sec), T is temperature (^{o}C), and e is absolute humidity (g/kg). From his work in Uppsala City, Sandborg computed constants and obtained

$$(\Delta T)_{Day} = 1.4 - 0.01\ N - 0.09\ U - 0.01\ T - 0.04\ e\ ,$$

and

$$(\Delta T)_{Night} = 2.8 - 0.10\ N - 0.38\ U - 0.02\ T + 0.03\ e\ .$$

The last expression was applied by Duckworth and Sandberg (1954) to their measurements in the San Francisco Bay area, and found to be in general agreement with observational data.

b) Ludwig and Kealoha's Formula (1968)

$$\Delta T = C_1 - C_2\gamma$$

where γ is the rate of change of temperature with pressure in degrees centigrade per millibar. In practice γ is obtained from

$$\gamma = \frac{T_o - T_1}{P_o - P_1} ,$$

where subscripts "o" and "1" refer to the values at the surface and at the first level measured above the surface, respectively. Numerical values of constants are found to be a function of city size (population) and are given as

$$\Delta T = 1.3 - 6.78\ \gamma \quad \text{for} \quad P < 500{,}000,$$

$$\Delta T = 1.7 - 7.24\ \gamma \quad \text{for} \quad 500{,}000 < P < 2 \text{ million},$$

and

$$\Delta T = 2.6 - 14.8\ \gamma \quad \text{for} \quad P > 2 \text{ million}$$

where P is the population of a city.

c) Oke and Hannell's Formula (1968)

Calm nights create favorable conditions for the formation of a strong nocturnal urban heat island. On the other hand, strong winds necessarily obliterate the heat island effect. Such a critical wind speed was fitted by the exponential equation:

$$U_{crit} = 3.4 \log P - 11.6$$

where P is population as before. From this relation, a $P \approx 2000$ gives $U_{crit} = 0$ which means that a city with a population of around 2000 does not generate a significant heat island, even under calm conditions.

2.2.2.5 A theoretical model of an urban heat island - Because of the complexity of the urban heat island effect, very few analytical modelings are available. Two numerical models will be presented here - one by Tag (1969) and another by Myrup (1969). In both models, the surface temperatures were pre-specified and the general flows over the surface were very much simplified. Tag utilized the equation of motion in his numerical integration, while an energy balance equation for the surface of the earth was a basic equation in Myrup's treatment.

(a) Tag's work (1969)

Tag utilized a numerical model for the atmosphere which is essentially the same as Estoque's (Estoque, 1962). They divided the atmosphere into two parts: a constant flux layer of 50 m depth and a transition layer where eddy mixing decreased linearly with height. A soil layer with 50 cm depth was also added. Horizontal advection terms were assumed to be zero.

The results obtained showed clearly the effects of certain characteristic parameters on city-rural temperature contrasts. These parameters were soil diffusivity, soil constant, albedo, and soil mositure. City surface temperature remained warmer when the appropriate parameters were chosen separately for the city and the country. If however, the same numerical values for moisture and albedo were used for both city and country, a higher rural temperature was obtained at noon time. Therefore, it was concluded with further

analysis that moisture and albedo parameters are dominant factors in the daytime temperature distribution, whereas correct diffusivity and soil constant are essential in forming a nocturnal heat island.

(b) Myrup's work (1969)

Myrup started with an energy balance equation for the surface of the earth

$$R_N = LE + H + S \qquad (1)$$

where R_N is the net radiation flux; E, the evaporation rate; L, the latent heat of water (so that LE is the latent heat flux); H, the sensible heat flux to the air; and S, the flux of heat into the soil. The net radiation term is a function of albedo, transmission coefficient for the atmosphere, latitude, etc., and an empirical formula was assumed. Turbulent fluxes of heat (H) and latent energy (LE) were related to gradients of potential temperature and specific humidity. A logarithmic profile was assumed for the horizontal velocity component; all eddy diffusivities for heat, mass and water vapor were constants. A set of equations were integrated by a finite difference technique. The results were summarized as follows.

The rural heat budget showed that the majority of the available solar energy was going into evaporating water, while in the city it was consumed to heat the concrete. No energy appeared in the latent heat flux term in the city because only a 10 percent evaporating area was assumed. This model could produce a daytime heat island of $3.9^{o}C$ and a nocturnal heat island of $6.0^{o}C$.

In order to see more clearly how the various competing parameters combined to produce the calculated temperatures, a systematic

sensitivity analysis was made for the leading parameters, such as rural wind speed and temperature, albedo, roughness factor, and evaporation. Results indicated that the urban temperature excess was the net effect of several competing physical processes, each of which, if acting alone, could produce relatively large temperature contrasts. Generally, there was a tendency for a cancellation effect so that ordinarily the temperature contrast between city and country was small. For instance, the decrease in evaporation as the city center was approached was balanced by the increasing size of the buildings, which augments the diffusion of heat upward. In a city park case these two factors work together to produce the largest contrast at the city center.

2.2.2.6 Heat islands on the prairie - Heat island effects are not limited to urbanized regions only. As we saw in Section 2.2.2.1, alteration of the earth's surface character is one of the major causes of a temperature difference. Holmes (1969) made observations to identify thermal discontinuities in the atmospheric boundary layer over the South Alberta Prairie, Canada, mainly during the hours between 1200 and 1500 when the highest surface temperatures were established.

Three different types of "oasis effect", defined as the climatic result (e.g., modification of air temperature, atmospheric moisture, diffusion) of many types of discontinuities in the surface, were reported: 1) the prairie-lake oasis, 2) the irrigation oasis, and 3) the agricultually complex region. In the first case, the cooling effect on the air of two lakes, Lake Pakowki and Lake Murray, was examined. In both oases large variations in surface temperature were

noted, with the lake surface temperature about 30°C lower than the surrounding agricultural land.

The surface temperature variation with time (1200, 1600, and 2100 hours) showed the rapid cooling of the soil surfaces compared with the lake. The effect of the lake on the temperature of the air passing over it was noted at both 15 and 45 m height; the temperature perturbations were 3°C and 2°C, respectively. At 75 m on this particular day, there was no measurable effect. An interesting discovery was that the regions of cool temperature at 15 and 45 m are almost entirely displaced from the lake, while the regions where air temperature at 2 m is influenced by known ground conditions were almost completely restricted to the immediate area. The reason that the cooled air was displaced to the lee was not immediately obvious, but important factors such as radiational heating of the surface (stability), wind speed, and wind direction were suggested.

In both the second and third cases results similar to the first were observed; the surface temperatures had a local character influenced by the ground condition, while those at higher levels had been affected by surface heating, wind speed, and wind direction.

2.2.2.7 Heated island (observations and analytical treatments) - The heat island effect introduced by a physical island in the ocean will be described here. It has been previously mentioned (see 2.2.1) that this phenomenon was produced by mechanisms similar to those which produced an urban heat island. Therefore, only the analytical models will be presented in this section.

Malkus and Stern (1953) and Stern and Malkus (1953) developed an analytical model for a heated island problem assuming that the flow is

stationary, two-dimensional, incompressible, and inviscid. Furthermore, the governing equations were linearized by a perturbation method. The final equation for a perturbed stream function has a formulation similar to that previously used for airflow over mountains. The only additional feature is a "heating function" which is responsive to the surface temperature distribution. The solution, except in the immediate vicinity of the island, has many characteristics of airflows over an "equivalent physical mountain".

If $\frac{k}{U}\left(\frac{gs}{U}\right)^{1/2}$ and $2D$ (width of a heated area) are large, then the mountain function is

$$M(x) = \frac{\Delta T(x,o)}{\Gamma - \alpha} \quad . \qquad (2.2.2.7\text{-}1)$$

If $\frac{k}{U}\left(\frac{gs}{U}\right)^{1/2} << \frac{1}{2}$

$$M(x) = \frac{\Delta T}{\Gamma-\alpha} \begin{cases} 1 - e^{-\frac{gsk}{U^3}x} & \text{for } x \leq 2D \\ e^{-\frac{gsk}{U^3}x}\left(e^{2D\frac{gsk}{U^3}} - 1\right) & \text{for } x > 2D \end{cases} \qquad (2.2.2.7\text{-}2)$$

where Γ is the dry-adiabatic lapse rate, α is the lapse rate for

undisturbed temperature, $s = (\Gamma-\alpha)/\overline{T}$ where $\overline{T}$ is the mean temperature, k is the eddy diffusivity, and e is an exponential function. (The rest of the variables are listed in the table of symbols.) The amplitude of an equivalent mountain is

$$A = \frac{\Delta T}{sTm} = \frac{\Delta T}{\Gamma-\alpha} , \qquad (2.2.2.7\text{-}3)$$

and its shape parameter is

$$x_o = \frac{U^3}{gsk} , \qquad (2.2.2.7\text{-}4)$$

where x_o is the distance where the mountain function takes the height of $A(1 - \frac{1}{e})$. The dimensionless coordination is introduced as

$$\xi = \frac{U}{k} x$$

$$d = \frac{U}{k} D$$

then Eq. (2.2.2.7-2) is reduced to

$$\frac{M(\xi)}{A} = \begin{cases} 1 - e^{-b^4 \xi} & \text{for } \xi \leq 2d, \\ e^{-b^4 \xi} (e^{2db^4} - 1) & \text{for } \xi > 2d , \end{cases} \qquad (2.2.2.7\text{-}5)$$

where

$$b^4 = \frac{gsk^2}{U^4} = \frac{gsH^2}{U^2} \frac{k}{U^2H^2} = \left(\frac{1}{Fr}\right)^2 \left(\frac{1}{Re}\right)^2 \quad .$$

It is interesting to note that $1/b^4$ is the square of the product of the Froude number and the Reynolds number based on the eddy diffusivity. Janowitz (1968) utilized a special Reynolds number which was equivalent to $b^{-4/3}$ but the derivation was different.

Figure 2-6 displays the equivalent mountain shape as given by Eq. (2.2.2.7-2) associated with a shape parameter x_o. In order to compute quickly an equivalent height from a given set of meteorological parameters, several graphs are drawn in Fig. 2-7. By adding observational data points to the figures, they may also be used to predict the appearance of rows of cumulus clouds over the lee side of a heated island. Suppose from meteorological observations following values are obtained: velocity, U(m/sec); eddy diffusivity, K (m^2/sec); width of a heated island 2D(m); surface temperature excess on a heated island, $\Delta T(^oC)$; stability of the atmosphere, $s(m^{-1})$; and characteristic height, L(m) . From Fig. 2-7c, and Fig. 2-7d the Froude number is obtained. The Reynolds number may be determined utilizing Fig. 2-7a and Fig. 2-7e. The equivalent mountain height at $x = 2D$ is obtained with the dimensionless island width 2d from Fig. 2-7b and the non-dimensional parameter b^4 from Fig. 2-7f.

Observed values are also plotted: solid symbols show the variables when rows of cumulus clouds were produced, and an empty

symbol indicates that no convection clouds were observed. A cross represents a typical meteorological condition for a mountain lee-wave phenomenon. The sources of data and numerical values used in plotting are provided in Table 2-4. From these results we can see that a very low velocity (less than 8 m/sec), a small Froude number (less than 0.05), and a large value of the parameter b^4 (~0.1) created favorable conditions for the formation of a lee-wave motion downwind of the heated islands.

In a subsequent paper, Malkus (1955) reported the existence of a fairly symmetrical orographic-convection cell over the island of Puerto Rico. From the numerical values of meteorological factors the equivalent mountain height obtained from Eq. (2.2.2.7-2) was 900 m, 1 1/3 times as high as the actual mountain. The maximum rate of descending motion was computed as 3.3 cm/sec at 900 m and the average value of ascending air over the island was 10 cm/sec at 1,000 m. Calculated streamlines had a maximum amplitude of 800 m, which was close to the equivalent mountain height. These computations were based on the sea-breeze circulation theory developed by Stern and Malkus (1953). The values seem to be reasonable magnitudes for a pure sea breeze motion; however, they are at least one order of magnitude smaller than the commonly observed mountain lee-wave phenomenon with a wave amplitude equivalent to the computed mountain height here.

Black and Tarmy (1963) proposed the deliberate creation of a thermal mountain, in order to reap the benefit of precipitation from orographically produced clouds. Soil temperature under asphalt coatings may be almost 20°F higher than that under nearby uncoated soil (Black, 1963). The temperature excess of an asphalt-coated surface

was safely assumed to be $9^{o}F$. Black and Tarmy concluded that with favorable meteorological conditions the asphalt-coating technique could theoretically produce an economical water supply.

Observations made by Garstang, et al. (1965) reported that the theoretical height from Eq. (2.2.2.7-1) showed overestimations in almost all cases. The results were plotted in Fig. 2-8. The observed trajectories of balloons, however, definitely indicated the existence of thermal mountains over heated islands as predicted by the theory.

Smith (1955) treated the heated island phenomenon as a time dependent problem. His model differs from that proposed by Malkus and Stern (1953) in that 1) convection terms were neglected, 2) no mean large motion was included, and 3) his model was time dependent. The time dependent vertical velocity components calculated had values similar to those obtained by Malkus and Stern. The model produced a reasonable sea breeze circulation.

2.2.2.8 Heated island (numerical treatment) - In order to retain the convection and the diffusion terms in the original governing equations, several numerical models have been examined by Tanouye (1966), Estoque and Bhumralkar (1968), and Spelman (1969).

Tanouye numerically modeled heated island convection, utilizing a slightly modified version of the scheme which Estoque (1961, 1962) used for sea breeze analyses. Large scale fluid motions of 1, 3, and 5 m/sec were used for each of three island surface temperature excesses of 3, 5, and $10^{o}C$. In all of the nine cases strong upshafts over the islands were produced. The maximum vertical velocity increased with larger island temperature excess and/or decreasing synoptic velocity. The variation of the maximum vertical velocity

computed and large scale motion and/or temperature excess over the island are shown in Table 2-5. The place where the maximum velocity occurred was displaced from the center to the lee of the island with increasing synoptic wind. Assumed meteorological factors used in the computation were included in Fig. 2-7a to Fig. 2-7h. Although they were very close to the conditions reported by Malkus (1963) when a well developed cumulus cloud row was observed, Tanouye's model could not produce any ascending and descending motions over the lee of the island. There are two possible reasons for this: his model itself or his numerical technique. Instead of a vertical equation of motion, Tanouye's model utilized a hydrostatic equation which has resulted in elimination of horizontal variation of the vertical velocity component according to the linearized argument by Magata (1968). Therefore, wavy motions are not expected. The second reason lies in the strong damping effects introduced in the upstream difference molecule utilized; they destroy the wave phenomenon, if any. Anticipating the analysis in Chapter IV, we can conclude that Tanouye's model appears to be inappropriate to simulate atmospheric wave motions.

Moisture budget and non-uniform surface roughness were added to the model by Estoque and Bhumralkar (1968). Approach flows were more strongly retarded when larger roughness elements were added over the island. Otherwise, the results obtained were very similar to those given by Tanouye.

Spelman (1968) described a numerical model for heated island effects utilizing a shallow water theory (see Section 2.1.6). Spelman claimed his results were consistent with observations by Malkus (1955). Vertical updrafts of 4.5 cm sec^{-1} and maximum upward displacement

of the inversion layer of nearly 400 m from its undisturbed height were recorded. Spelman obtained larger maximum upward vertical velocities by increasing the speed of the basic current. But Tanouye's results were completely opposite, i.e., the maximum vertical velocities decreased with increasing basic wind speed. Spelman argued that the different results might arise from the differences in the basic modeling techniques.

Malkus' theory (1963) supported Spelman's results, i.e., an averaged upward disturbance at level h is

$$\overline{w} = \frac{MU}{2D} , \qquad (2.2.2.8\text{-}1)$$

and

$$h = \frac{U^3}{gsk} , \qquad (2.2.2.8\text{-}2)$$

where M is the effective height of an equivalent mountain obtained from Eq. (2.2.2.7-2) and expressed as

$$M = A(1 - \frac{1}{e}) . \qquad (2.2.2.8\text{-}3)$$

As we can see from Eq. (2.2.2.8-1), $\overline{w}$ is proportional to the speed of the basic current, U.

2.3 Review of Sea Breeze Problems

2.3.1 Introduction - During the daytime on a sunny day, summer breezes from the sea to the land are often observed near a shoreline. This atmospheric circulation is called a sea breeze and is caused by the temperature difference between the water and the land. After sunset the flow direction is reversed and the phenomenon is called a land breeze.

Similar motions are observed near lakes (lake breeze) or forests (forest breeze).

Although a sea breeze is quite a familiar phenomenon, very few observational data are available. This is partially due to the difficulty of measurements over the sea; moreover, it is not easy to distinguish the breeze from superposed large scale motions.

An extensive effort has been made to work out an analytical explanation of this rather simple convectional motion in the hope that the solution will lead to the explanation for more complicated heat transfer problems in the atmosphere.

2.3.2 Observational evidence - The sea breeze circulation system consists of a landward current near the earth's surface and a much weaker but deeper return flow above it about two orders of magnitude smaller. The horizontal scale of the circulation is about 30 to 50 km from the seashore landward, but it varies with land-sea temperature contrasts, or the prevailing synoptic situation. Magnitude of the horizontal velocity is around 10-20 m/sec, and that of the vertical velocity component is 10-20 cm/sec (Fisher, 1960). Humphrey (1964, pp. 157-159) estimated the scale of a sea breeze by using a simple model assuming hydrostatic equilibrium and a constant temperature distribution. He predicted a horizontal scale of about 30 km and a vertical scale of around 300 m -- somewhat smaller than observations. The scale of a sea breeze is mainly determined by a combination of many factors, such as temperature contrast over the sea and the land, stability conditions in the air, surface roughness of the sea and the land, or insolations by cloud cover. Consequently the magnitude of the velocities is also a function of a combination of the above conditions.

A land breeze has a smaller scale than a sea breeze. It is weaker over the sea because of smaller temperature differences during the night and the dissipation of energy over the land's rougher surface.

Moroz (1967) observed a lake breeze at a site on the eastern shore of Lake Michigan. The depth of onshore flow in a fully developed lake breeze at the lake shoreline was about 750 m, and horizontal onshore velocities exceeding 7 m/sec have been observed. The region of onshore flow extended 25 to 30 km inland but did not reach 53 km inland for any of the cases observed.

2.3.3 Analytical treatment - A sea breeze circulation is a result of a temperature difference over land and sea coupled with a pressure gradient. This may be understood by applying the circulation theorem (for example, Hess, 1959, pp. 244-246). By taking a curl operation over the two-dimensional equation of motion, a vorticity transport equation with a solenoidal term $-\nabla \frac{1}{\rho} \times \nabla P$ is obtained. This forcing function produces a y-direction vorticity component. It always exists unless $-\nabla \frac{1}{\rho}$ and ∇P are parallel. In a sea breeze situation pressure distribution is safely assumed to be hydrostatic, which means ∇P is directed vertically downward. The density over land has a smaller value than that over the sea if height is held constant, because air over land is heated from the surface. Therefore constant density lines decline in the vicinity of a shoreline, which is the physical explanation for the existence of a solenoidal term $-\nabla \frac{1}{\rho} \times \nabla P$. Since the governing equations are non-linear, exact analytical solutions for the sea breeze phenomenon have not yet been obtained. Therefore some simplifications were unavoidable in order to obtain analytical expressions.

Haurwitz (1947) provided one of the earliest efforts in this field by using a circulation theorem. He incorporated a viscosity term in the equations of motion which is assumed to be proportional to, and in opposite direction to the local velocity. His conclusion was that the friction term in his model brings the maximum intensity of a sea breeze earlier in the day while without the friction term it occurs when the temperature difference between land and water decreases to zero.

The intensity of a sea breeze is influenced by many factors besides land-water temperature difference. The important roles of a gradient wind, topography near the coast, and stability of the atmosphere were explained in Wexler (1946).

2.3.4 Numerical treatment - Fisher (1961) designed a numerical model based on his earlier sea breeze observations along a portion of the New England coast near Block Island, Rhode Island (Fisher, 1960). He assumed an infinitely long beach and neglected the variables along it. He generated a vorticity transport equation to describe the motion in a vertical plane perpendicular to the coast line. Evaluating the magnitude of solenoidal terms in the equation under certain pre-specified ideal atmospheric conditions, he finally obtained the same expression as that obtainable from the Boussinesq approximation. In his original equations of motion he assumed that viscous stresses might be neglected for the vertical component of motion, that horizontal variations of the horizontal components of motion may be neglected, and that eddy viscosity coefficients in both horizontal directions may be regarded as the same. The coefficient of eddy diffusivity with height was given based on observations.

Fisher's model simulated not only general features of the wind system but many of its small details as well. Unfortunately a direct comparison with his earlier observations was not possible because in his model the large scale synoptic motions were assumed to be zero. Fisher's study is not the first to solve a sea breeze problem by numerical analysis (Pearce, 1955), but he did suggest many interesting and important aspects of a numerical analysis, even though he could not prove them all. For example, he noted that solutions depend on different finite difference approximations, size of the finite domain of computation, initial and boundary conditions, etc. Since the need to discuss these factors was encountered in the course of the present numerical formulation of the problem, they will be described in Chapter IV.

Estoque (1961) added the hydrostatic equation to those utilized in Fisher (1961). He decomposed the dependent variables into the sum of two components: one is due to a large scale synoptic motion and the other is a perturbation due to the effects of friction, and differential heating. Consequently he had to solve two sets of equations. He solved, however, only the disturbance quantities, assuming that no synoptic motion existed. The region was divided into two horizontal sublayers; a relatively thin layer, $0 \leq x \leq h \simeq 50$ m characterized by constant vertical eddy fluxes of heat and momentum, and an overlying transition layer, $h < x \leq H \simeq 2$ km where the effect of eddy fluxes decreased with elevation.

Estoque (1962), by an extension of his first paper, eventually investigated the effect of the prevailing synoptic motion on the development of a sea breeze circulation. He assumed as initial conditions

that the lapse rate was 7 $^{o}K/km$ and that the geostropic wind had a magnitude of 5 m/sec, with various shoreline approach angles. His results simulated the diurnal development of a sea breeze. At an early time stage the perturbation remained in the vicinity of the shoreline; it grew with time and eventually penetrated further landward. The circulation recorded a maximum development at eight hours after the motion started, then it decreased. The maximum computed velocity components of 10 m sec^{-1} in the horizontal and ± 14 cm/sec in the vertical direction were consistent with earlier observations.

Magata (1965) added the effects of condensation and evaporation in his energy equation. He derived the temperature distribution at the surface of the land and the water by balancing insolation, nocturnal radiation, conduction and eddy transfer of heat. The distribution of the eddy diffusivity coefficient was assumed to be a function of the vertical coordinate only and was obtained by a numerical analysis of an observed inversion layer. He concluded that the magnitude of synoptic motions and the vertical shear they introduce are significant during sea breeze development.

A universal expression for eddy diffusivity which is appropriate for all atmospheric conditions is not yet available. Fisher and Magata used typical profiles based on an evaluation of atmospheric data. Estoque and Bhumralkar (1968) utilized semi-empirical expressions which are a function of stability, shear, and the roughness element in the lowest constant flux layer. In the upper layer eddy diffusivity is assumed to decrease linearly to zero at the upper boundary. The effect of change of surface roughness and mositure budget was included in all of Estoque's sea breeze modeling (1968).

2.3.5 Some concluding remarks on simulation of sea breeze by a numerical experiment - The above review suggests that the following physical factors should be included in any simulation of sea breeze circulation development:

i) Appropriate expressions for eddy diffusivity including the effects of local velocity and temperature.

ii) Temperature distribution at the surface along the land and the water as governed by the heat balance associated with insolation, nocturnal radiation, conduction into a soil layer and eddy transfer to the atmosphere.

iii) Effect of shear of a basic wind;

iv) The release of a latent heat by condensation and evaporation, and

v) The effect of surface roughness change over the land and the sea.

In addition to improvements in numerical modeling techniques, extensive prototype observations are essential in augmenting theoretical results.

CHAPTER III

EXPERIMENTAL FACILITIES AND PROCEDURES

3.1 Introduction (Necessity of a Wind Tunnel Experiment)

The following methods are available to study small scale geophysical flows, such as a lee-wave motion, a sea breeze circulation, or an urban heat island convection:

1) analytical,

2) numerical,

3) field experimental, and

4) laboratory experimental.

Each method has its own merits and demerits. For example, analytical solutions are not yet available for a complete set of nonlinear governing equations. A numerical solution may be inferior to an analytical one in accuracy, but it is an extremely useful approach when analytically rigorous solutions are not available. A field study may be time consuming and expensive compared with a laboratory simulation. A further advantage of wind tunnel simulation is that important variables may be changed systematically. However, difficulties may arise because it is necessary to consider scaling effects which are not yet fully understood for turbulent motion.

Therefore, it is good strategy to utilize the advantages of each, combining the different methods for a better understanding of complicated geophysical problems.

3.2 Basic Requirements

3.2.1 Similarity in mountain lee-wave phenomena - The complete similarity requirement for a mountain lee-wave phenomenon was described in Cermak et al. (1966, pp. 39-51). Here only certain aspects of geometric and dynamic similarity will be discussed.

Following the arguments in Queney (1960, p. 104) the Scorer function is given as

$$S_c = M^2 \left(\frac{sg}{\overline{u}^2} - \frac{\frac{\partial^2 \overline{u}}{\partial z^2}}{\overline{u}}\right) .$$

If the shear term is neglected, then the Scorer function may be interpreted as a global Richardson number based on the mountain height, M. The following values are substituted from a typical mountain lee-wave situation:

$\gamma = 0.006^{o}$ c/m ,

$\overline{T} = 250$ k, and

$\overline{u} = 20$ m/sec ,

then

$s = 1.6 \times 10^{-5}$ m^{-1} and $\frac{sg}{\overline{u}^2} = 0.4$ km^{-2} for the atmosphere.

If a geometric scaling is $1{:}3 \times 10^{-5}$ and the temperature gradient in a wind tunnel can be maintained at 1^{o}C/cm, the velocity in a model experiment must be 8.6 cm/sec for dynamic similarity. These values are extremely difficult to obtain in the ordinary wind tunnel. Moreover, instruments to measure accurately such a low velocity in a strong temperature stratification have not yet been developed.

3.2.2 Similarity in heated island phenomena - According to a linearized theory proposed by Stern and Malkus (1953), it is necessary to satisfy $\frac{\sqrt{gs}\ k}{U^2} > \frac{1}{2}$ in order to simulate an equivalent mountain capable of developing strong gravity waves downwind of a heated boundary. It will be easily seen that the above relation, because it requires an unusually large stability and a small velocity; cannot be satisfied in any existing wind tunnel facility, for example, $s = 3 \times 10^{-3}$ cm^{-1} ($\frac{\partial T}{\partial z} \approx 1^{o}$C) and $k = 0.2$ cm^2/sec requires $u < 0.83$ cm/sec . If $u = 4$ cm/sec and $k = 0.2$ cm^2/sec then a $s > 1.63$ cm^{-1} is required for a simulation, which is equivalent to 500^{o}C/cm. It is impossible to satisfy the relation $\sqrt{gs}\ k/U^2 > \frac{1}{2}$ unless viscosity k is artificially modified by a factor of at least 30. Thus a thermal equivalent mountain in a wind tunnel experiment must take a plateau shape as described by Eq. (2.2.2.7-2): the mountain starts at the leading edge of the island and increases asymptotically to reach its maximum height directly above the end of the island, then decreases exponentially.

To see the shape of a thermal mountain which might possibly be simulated, the following numerical values are substituted into the same equation.

$u = 4$ cm/sec ,

$s = 4.67 \times 10^{-3}$ cm^{-1} ($\frac{\partial T}{\partial z} = 1.4^{o}$C/cm, $\overline{T} = 300$ k).

Molecular viscosity of 0.2 cm^2/sec , an island width of 8 cm, and a temperature excess over the island of 56^{o}C were assumed. The computed mountain increased its height almost linearly to 8.4 cm at the end of the island, then decreased exponentially, taking the values of 6.1,

2.3, and 0.1 cm at $x = 30$, 100, and 350 cm, respectively. It would be simple to compare the maximum mountain height of 8.4 with experimental results for airflow over an obstacle whose height is 8 cm.

Summarizing, it evidently is necessary to obtain a velocity ranging from 4 to 15 cm/sec, and a temperature gradient of $0.5^{o}C/cm$ to $1.5^{o}C/cm$, in order to simulate atmospheric lee-wave phenomena and heated island problems in a wind tunnel facility. The above requirements are equivalent to attaining a Froude number based on the wind tunnel height (60 cm) from 0.030 to 0.196.

3.3 Design and Construction

3.3.1 Existing thermal wind tunnels - Although there are quite a few low speed, small wind tunnels (see Pope and Hooper, 1966, for general information), guidance for the design of a thermal wind tunnel is limited. Several reports are available, including Plate and Cermak (1963), Strom and Kaplin (1968), Charpentier (1967), Scotti (1969), and Hewett et al. (1970). Since their facilities were designed to satisfy special purposes, duplication of their designs was not desirable. The tunnels of Strom and Kaplin, and Charpentier could not produce the strong temperature gradient required here; Scotti was primarily interested in a free shear layer whose thickness was about 1/4 inch, and Hewett treated flows whose duct Froude numbers were greater than $\frac{1}{\pi}$. Thus, it is necessary to develop our own design criteria.

3.3.2 Test section - Dimensions of the test section of the proposed wind tunnel are 2 ft height x 2 ft width x 15 ft length (see Fig. 3-1).

a) Removable Windows

One side of the wind tunnel wall has five removable windows with 3 ft x 3 ft square area for the convenience of measurements. Two of them are made of plexiglas and seven slots are cut over one quarter of the area of each window. Instruments are inserted from the outside of the wind tunnel so that supports do not disturb the flow inside the test section. Two series of slots shown in Fig. 3-2 provide access to the entire test section by rotating the windows.

b) Adjustable Ceiling

Ceilings are adjustable to compensate for acceleration of the free stream as induced by the growth of boundary layers along the floors, ceiling, and both side walls. The ceiling can be raised to a maximum of about 20 cm near the end of the test section while a displacement thickness for a typical flow situation is around 2.5 cm. Fig. 3-1 displays four pairs of adjustment devices, each of which consists of a screw and a crank.

3.3.3 Entrance and ceiling heaters - A simple computation was conducted to estimate the transport of energy supplied by electric heaters to a wind tunnel atmosphere.

a) Entrance Heaters

The dimensions of an electric sheet heater are assumed to be 6 in. x 24 in. The rate of total heat transfer by convection over the heater is (see Kreith, 1968, p. 296)

$$q = 0.664\ k\ R_{e_L}^{1/2}\ P_r^{1/3}\ b(T_s - T_\infty)\ ,$$

where

b: width of the heater,

T_s: heater surface temperature,

T_∞: ambient air temperature,

R_{e_L}: Reynolds number at x = L, and

k: conductivity.

Then numerical values of b = 24 inch, $T_s = 300^oF$, $T_\infty = 75^o$ F, L = 6 inch, u = 0.5 ft/sec, and k = 0.0171 Btu/hr ft F are substituted to obtain

$$q = 155 \text{ Btu/hr} = 45.4 \text{ watts} .$$

Since heat energy may be transferred from both sides of the heater, q is 90.8 watts per heater. If sixteen heaters are used, then a total of 1453 watts would be transferred to the air in the wind tunnel. The final arrangement of heaters is displayed in Fig. 3-2.

b) Ceiling Heaters

A similar calculation was performed assuming that the temperature at the heater surface was 200^oF and the air temperature was 170^oF. Four large heaters 2 ft x 3 ft were selected. Under these conditions, the heat energy convected from the heaters is

$$q = 49.5 \text{ btu/hr} = 14.5 \text{ watts}.$$

Adding this to the previous result, we find that a total of 1500 watts is emitted from the heaters.

c) Energy Transferred from Wind Tunnel to the Atmosphere

Under stationary conditions the rate of energy supply from the heaters will balance energy transferred from a wind tunnel to the atmosphere. The latter energy is expressed as

$$q = A\rho\, C_p\, u\Delta T ,$$

where

A: area of a wind tunnel cross section, and

ΔT: averaged air temperature difference between inside and outside wind tunnel.

The following numerical values were substituted

$A = 4\ ft^2$, $\rho = 0.071\ lbm/ft^3$, $Cp = 0.240\ Btu/lbm\ F$,

$u = 0.5\ ft/sec$, and $\Delta T = 30^oF$.

Then

$$q = 3681\ Btu/hr$$
$$= 1078\ watts,$$

which is approximately the same amount as the energy available if losses of energy from the wall, ceiling, or floor of the wind tunnel are included.

To summarize, heaters should meet the following requirements:

i) maximum surface temperature should be more than 300^oF,

ii) power consumption should be more than 45 watts per heater (= 0.3 watts/in^2) for the entrance heaters and 4 watts per heater (= 0.005 watts/in^2) for the ceiling heaters.

The following characteristics are specified for commercial heaters available from Chromalox Division:

Area (in^2)	Power ($watts/in^2$)
24 x 6	4.5*
24 x 36	2.0**

These apparently satisfy all the requirements derived from the simple calculation.

3.3.4 Cooling device (heat sink) - It is necessary to install a heat sink along the floor to maintain a strong temperature gradient. For this purpose, cooling panels for tap water were constructed; their dimensions were determined from a simplified heat transfer calculation. The results obtained indicate that a 1/2 inch-depth water panel covered with a 1/4 inch thick aluminum plate (see Fig. 3-3) can remove 480 Btu/hr of heat energy over the surface area. A velocity of 4 cm/sec, for the running water in the panel, an air temperature of $90^{o}F$, and a water temperature of $42^{o}F$ were assumed. The average temperature increase over a 12 ft panel length was computed to be $0.9^{o}F$. The measured temperature difference of water between inlet and outlet was about $1^{o}C$.

3.4 Instrumentation

3.4.1 Velocity measurements (smoke wire) - Low speed velocity measurements in a thermally stratified flow field are extremely difficult to make by conventional techniques. For example, a Pitot static tube is suitable for a higher velocity (~100 cm/sec), hot-wire techniques are very sensitive to ambient temperature changes, and a

* P/N 171-881155-002 TYPE SL/PSA Heater
** P/N 171-881155-001 TYPE SL/PSA Heater

laser doppler velocimeter method was not available for immediate application.

A smoke wire method has been utilized to investigate flow field during thermal stratification. It has been perfected for practical use at the Engineering Research Center, Colorado State University. Figure 3-4 shows a smoke wire with attached instruments for velocity measurements. The advantage of the smoke wire method is an instantaneous visualization of the velocity profile.

The principle of the technique is to follow photographically a white smoke emitted from a wire when light oil is vaporized. In Fig. 3-4 A is a nichrome wire which is heated electrically, thus vaporizing an oil coating. Oil is dropped down by gravity through an oil outlet B . B is connected to an oil reservoir C and an air bag D which is kept outside of the wind tunnel. Squeezing the air bag pushes the oil in the reservoir through the outlet. To measure velocity profiles quantitatively, several auxiliary devices are necessary: a strobe, a strobe delay system, an electronic counter, a trigger circuit, and a camera (see Fig. 3-4). A schematic diagram which shows an arrangement for velocity measurements is provided in Fig. 3-5. A trigger circuit is connected to the smoke wire, to a strobe through a delay unit, and to an electronic counter. When a start button on the front panel of the trigger unit is pushed, a high voltage (~700 volts) is applied to the nichrome wire, vaporizing the oil coating. A white smoke is released instantaneously and is carried along by the ambient wind. A typical time-delay photograph is included in Fig. 3-4. The actual velocity profile can be reduced from the picture by use of the

recorded time difference between the moment of firing the wire and the moment of the strobe picture.

3.4.2 Temperature measurements - Copper-constantan thermocouples of 30 gage were utilized to monitor temperature variations. Sixteen thermocouples were mounted on the entrance heaters, four were on the ceiling heaters, and three were on the floor. Nine thermocouples mounted on a rake were used for vertical temperature distribution measurements. A total of thirty-three thermocouples were connected to a thermocouple rotary switch, and voltages generated were read by a digital voltage meter. Figure 3-6 displays the complete set of devices for temperature measurements.

3.5 Characteristics of the Wind Tunnel

3.5.1 Temperature profile - An example of a vertical temperature profile where neither an obstacle nor a heated island was placed on the floor is given in Fig. 5-7. Froude number 0.100 was obtained in the lower layer from the velocity, 6 cm/sec, and the temperature gradient, $1.25^{o}C/cm$. As seen, there are two nearly constant stability layers -- one of strong stability near the surface ($0 \leq z \leq 13$ cm), and another less stable above it ($z > 13$ cm). This feature of two-layer stability is a common characteristic of the temperature profiles throughout the study, although the height of intersection of the two stability lines varies from case to case.

3.5.2 Standing waves - A Froude number less than $\frac{1}{\pi}$ provides a necessary condition for the formation of standing waves if there exists an appropriate disturbance (obstacle) (Long, 1955). Scotti (1969) experienced finite amplitude waves and stagnation regions in

his free shear flow study. Segur (1969) analyzed Scotti's case utilizing Long's model and concluded that his (Scotti's) wind tunnel had a strong contraction at the entrance section which disturbed airflow. Strong standing waves were also observed by Hewett et al. (1970); In order to minimize heat transfer through the wind tunnel side walls, the average temperature inside the tunnel was kept close to that of the room temperature. The authors believed that this temperature distribution arrangement resulted in two natural convection cells which blocked the tunnel stream and induced waves. They argued that in the upper section colder air particles next to the wall moved down along the wall because of gravity. At the mid-point of the wind tunnel where particles experienced an equilibrium state, they flowed toward the center line of the tunnel. On the other hand, in the lower section, warmer particles moved upward along the wall and at the mid-point they also rotated toward the center line as before. These two flows from both side walls collided and formed stagnation regions.

Fortunately, such strong standing waves were not experienced in the test section of the present experiments. Smoke was released to visualize flow six feet downstream from the end of the heater section. Nearly horizontal streamlines were obtained (as seen in Fig. 3-7) when $Fr = 0.0824$; temperature surveys in the same area also indicated parallel flow (see Fig. 3-8). Isotherms in the cross sections upstream and downstream of the heated island are shown in Fig. 3-9.

So far there was no evidence to indicate a strong wave motion in the wind tunnel as found in other wind tunnels. Temperature distributions just downstream of the entrance heaters, however,

indicated that there existed strong disturbances in the airflow which were generated by large temperature differences between the heaters and the ambient stream (see Fig. 3-10). These disturbances fortunately diminished rapidly in the streamwise direction, and no significant variations were experienced after $x = -130$ cm.

3.5.3 A numerical simulation of airflow in a wind tunnel - A numerical computation was performed to test whether the strong disturbances were generated by the heaters at the entrance section. The program used is discussed in detail in Chapter IV. In the first run, no heaters were placed in the computational region. In the second run, however, entrance heater temperatures were specified along the vertical line at $j = 30$. The results are displayed in Fig. 3-11. The upper configuration had no heaters, and the lower one included heaters. A definite effect of the entrance heaters was detected, and isotherm patterns were qualitatively similar to those obtained by measurements (see Fig. 3-10).

3.5.4 A summary of wind tunnel design - We may conclude that:

1) when Froude number is less than $\frac{1}{\pi}$, standing waves may be introduced by one or more of the following factors:
   a) contractions of a wind tunnel section,
   b) natural convections of density differences generated by side walls, and
   c) a temperature difference between the heaters and approaching air.
2) If a wind tunnel is long enough and waves are not strong, fairly horizontal flow will be obtained in the downstream test section.

CHAPTER IV

THEORETICAL ANALYSES BY NUMERICAL METHODS

4.1 Analytical Approach

Since the governing equations of the fluid motion are given by a set of nonlinear partial differential equations no analytical solutions in closed form have been obtained without simplifications based on intuition, experience, prototype observation, or laboratory experiment. Many different methods have been used to simplify the equations. Generally these may be classified as:

1. Perturbation techniques which linearize the equations after neglecting higher order terms of small quantities.

2. Similarity assumptions which develop a set of ordinarily differential equations from those of the original partial differential equations.

3. Boundary layer type assumptions which produce equations of a parabolic type rather than the original elliptic ones.

Meteorologists have also introduced other simplifications such as the assumptions of hydrostatic and geostrophic equilibrium.

One must decide which simplification or simplifications can be utilized for his special problem. This is not always easy because in many cases needed justifications are only possible after solutions are obtained. There are many examples where the simplified governing equations include solutions which are contradictory to the original assumptions. For example, equations linearlized by perturbation techniques may include solutions in which the perturbations are comparable with or larger than a mean quantity.

We also know, however, that such simplified analytical solutions give a very good insight into even very complicated problems. Thus one of the advantage of analytical solutions is that they may correctly develop functional dependence. Therefore analytical methods are usually preferred where possible.

4.2 Limitations to an Analytical Approach

Long (1953) derived exact analytical expressions for a flow over an obstacle when the flow is two dimensional. Yih (1965) extended Long's model for a broader, more general classification to reduce the original nonlinear equations to linear ones which can be solved analytically. This transformation is possible, however, only when the flow is steady and nonviscous.

Restrictions to the type of solution considered also arise from the upstream boundary conditions required in Long's model, i.e., a linear variation of density with height and a constancy of a dynamic head upstream. These restrictions impose a problem of uniqueness and existence of a solution. Long (1955) himself observed a blocking effect of an obstacle when the Froude number was very small, which by means of an upstream wave alters the assumed density and dynamic pressure distribution at the upstream boundary. Thus the problem is overspecified.

Segur (1969) discussed an existence criterion for solutions of a stratified flow into a two dimensional contraction using Long's model. He suggested an existence criterion which is a function of a stability parameter and a contraction ratio of the channel. According to his notations, this is stated as follows.

For any one-sided contraction with $k > 1$, a bounded solution to Long's model exists uniquely if

$$[k] = [k \frac{\Delta\mu}{\pi}]$$

where $[S]$ denotes the integer corresponding to any real number S such that $0 \leq S - [S] \leq 1$. k is an inverse Froude number based on the height H/π and related to a global Richardson number by $R_i = k^2\pi^2$. H is the original channel height. $\Delta\mu$ is the contracted section height nondimensionalized by H/π. Therefore, $\Delta\mu/\pi$ is a contraction ratio of the channel. He included symmetric and asymmetric contractions, but only the statement for the one sided contraction was quoted here which represents a flow over a plateau.

The above criterion was applied to predict the blocking effect of Long's experiments when a barrier was used. The predicted instabilities were verified by Long's experiments (Table 1 in Segur, 1969). Apparently this is one of the very few cases to have been extensively studied analytically and verified by experiments for a criterion of existence of a solution of Long's equation under the assumed boundary conditions.

This test is not always feasible, however, because of its time consuming procedures. In addition, it may not be suitable for more general problems.

One possible way to eliminate the difficult mathematical existence proof is to treat the problem as an initial value problem rather than a boundary value one.

Transformations of variables are, however, no longer possible (Yih, 1965) which means we cannot use the same procedure which Long or Yih used to reduce the nonlinear governing equations to linear ones for steady problems.

4.3 Necessity of Numerical Integration

An alternative solution approach is a numerical integration using a digital computer. This is one of the most powerful methods available at present for nonlinear problems with complicated boundary and initial conditions. Numerical integration had a long history even before digital computers were developed; however, there are still many unsolved problems in the techniques themselves, especially for nonlinear problems. A stability analysis is considered the most important and yet difficult technique for unsteady problems. The finite difference scheme is said to be stable if the difference between the exact solution of the differential equation and that of the finite difference equation is bounded as the integration time goes to infinity for fixed time and space increments. The stability analysis required depends on the particular differencing molecule chosen. Therefore, it will be discussed in detail after a finite difference scheme for the current problem has been developed.

4.4 Formulation of Problem

4.4.1 Two dimensionality - The formulation of the problem is initially based on the assumption of two dimensonality. Variations in dependent variables are limited only to the planes vertical and longitudinal to the source of flow disturbance, i.e., a heat island or an obstacle.

Physically this indicates that a heat island or an obstacle extends to infinitely in the lateral to the flow direction.

The equation of continuity in two dimensional space may be stated as

$$\frac{D\rho}{Dt} + \rho \left(\frac{\partial u}{\partial x} + \frac{\partial w}{\partial z}\right) = 0 \quad . \qquad (4.4.1\text{-}1)$$

The x and z coordinates are to be taken in the direction perpendicular to the discontinuity (heat island or obstacle) and vertical, respectively. The origin is located upwind of the discontinuity where the flow is from left to right.

Velocity components u and w are in the x and z direction, respectively. ρ is density and D/Dt is the Eulerian operator which is expressed as

$$\frac{D}{Dt} = \frac{\partial}{\partial t} + u \frac{\partial}{\partial x} + w \frac{\partial}{\partial z} \quad .$$

4.4.2 Incompressibility - When $D\rho/Dt = 0$ the fluid is incompressible which means a fluid particle does not change its density along the streamline. This situation is true for homogeneous fluids as long as the fluid velocity is small compared to the speed of sound, i.e.,

$$M = \frac{u^2}{c^2} << 1 \quad .$$

For stratified flow, however, one has to evaluate the magnitude of $1/\rho\ (D\rho/Dt)$ for the specified problem. Fisher (1961) evaluated a typical value of $1/\rho(D\rho/Dt)$ as order of 10^{-6} sec^{-1}, where the maximum rates of individual temperature change in the lower layers of the atmosphere was conventionally assumed to average less than 0.5 deg C per hour, pressure p was 1,000 mb, and temperature T was $300^{o}k$. The horizontal divergence term in the equation of continuity in a small-scale circulation such as a sea breeze is approximately 10^{-4} sec^{-1}

(10 m per sec per 50 km). Therefore, the divergence term is two orders of magnitude larger than the compressibility term in the equation.

The heat island problem and gravity wave phenomena are also the same sort of circulation (horizontal scale, 50 ~ 100 km, and vertical scale, 1 ~ 10 km). Therefore, incompressibility may be safely assumed except perhaps in the local vicinity of the surface temperature discontinuity itself.

A similar argument is given to show the approximate validity of an incompressibility assumption for fluids in wind tunnel experiments. The compressibility term $\frac{1}{\rho}\frac{D\rho}{Dt}$ is evaluated anticipating the following variable magnitudes:

$$w \sim 10 \text{ cm/sec}$$

$$\frac{\partial u}{\partial x}, \frac{\partial w}{\partial z} \sim \frac{10 \text{ cm/sec}}{20 \text{ cm}} = 5 \times 10^{-1}$$

$$\frac{\partial T}{\partial z} \sim 1^{\circ}\text{C/cm, and}$$

$$\overline{T} \sim 300^{\circ}\text{K}$$

Since $\frac{1}{\rho}\frac{D\rho}{Dt} \sim \frac{w}{\overline{T}}\frac{\partial T}{\partial z}$ a substitution of the above numerical values gives

$$\frac{1}{\rho}\frac{D\rho}{Dt} \sim \frac{10}{300} \times 1 \sim 3 \times 10^{-2}$$

which is one order of magnitude less than the divergence terms, $\frac{\partial u}{\partial x}$ or $\frac{\partial w}{\partial z}$. Therefore incompressibility of flow is also justified in wind tunnel experiments.

In past studies of mountain lee waves, incompressibility was not commonly assumed, but linearlizing perturbation techniques were used. Here we take a reverse situation, i.e., we retain nonlinearlity but incompressibility is assumed. Thus the equation of continuity (4.4.1-1) is finally written as

$$\frac{\partial u}{\partial x} + \frac{\partial w}{\partial z} = 0 \qquad (4.4.2\text{-}1)$$

4.5 Vorticity Transport Equation

The x and z components of the equation of motion are

$$\frac{Du}{Dt} = -\frac{1}{\rho}\frac{\partial p}{\partial x} + K\nabla^2 u \qquad (4.5\text{-}1)$$

$$\frac{Dw}{Dt} = -\frac{1}{\rho}\frac{\partial p}{\partial z} - g + K\nabla^2 w \quad , \qquad (4.5\text{-}2)$$

where K is a total diffusivity and is taken to be a constant. Better functional forms for K should be taken if atmospheric turbulent motion is simulated. For example Fisher (1961), Estoque (1961, 1962) and Magata (1965) have used variable diffusivity K in their numerical models. However, as summarized in the paper by Zilitinkevich et al. (1967), the variations of K are quite complicated. Therefore, we take K as a constant for simplicity. Since all numerical works presented here simulate wind tunnel results, a constant K is more realistic. It will be assumed here that K is the same in horizontal and vertical directions. g is the acceleration of gravity. Coriolis force due to

the earth's rotation is neglected for this kind of small circulation. (For example, see Cermak et al., 1966).

∇^2 is the Laplacian operator in two dimensional space

$$\nabla^2 = \frac{\partial^2}{\partial x^2} + \frac{\partial^2}{\partial z^2} \quad .$$

In two dimensional homogeneous flow it is often convenient to use a vorticity transport equation rather than the original equations of motion. In the former equation, pressure terms are absent. It is interesting to note that pressure does not appear in the vorticity equation. However, for nonhomogeneous flow it is not necessarily true that a vorticity transport equation is more convenient than the original equation of motion. It again depends on the problems studied.

The vorticity in y direction, which is the only component, which exists in two dimensional flow, is defined as

$$\zeta = \frac{\partial w}{\partial x} - \frac{\partial u}{\partial z} \quad . \tag{4.5-3}$$

Cross differentiations of Eqs. (4.5-1) and (4.5-2) and subtraction gives (utilizing the incompressibility (4.4.2-1)),

$$\frac{D\zeta}{Dt} = \frac{\partial \alpha}{\partial z}\frac{\partial p}{\partial x} - \frac{\partial \alpha}{\partial x}\frac{\partial p}{\partial z} + K\nabla^2\zeta \quad , \tag{4.5-4}$$

where ζ is defined in Eq. (4.5-3) and α is the specific volume, $\alpha = 1/\rho$. If the flow field is homogeneous, then the solenoidal term

$$\frac{\partial \alpha}{\partial z}\frac{\partial p}{\partial x} - \frac{\partial \alpha}{\partial x}\frac{\partial p}{\partial z}$$

is always zero. Fisher (1961) evaluated the numerical value of the

solenoidal term for the sea breeze phenomena and concluded that the first term $(\partial\alpha/\partial z)(\partial p/\partial x)$ was at least one order of magnitude smaller than the second term $(\partial\alpha/\partial x)(\partial p/\partial z)$ and therefore might be neglected.

Since our study includes an attempt to verify a numerical model by wind tunnel simulation experiments, it is necessary to rejustify the simplified solenoidal term in the vorticity transport equation.

α may be eliminated from the solenoidal term by use of the equation of state, $p = \frac{1}{\alpha} RT$, then we obtain

$$\frac{\partial\alpha}{\partial z}\frac{\partial p}{\partial x} - \frac{\partial\alpha}{\partial x}\frac{\partial p}{\partial z} = \frac{R}{p}\left[\frac{\partial T}{\partial z}\frac{\partial p}{\partial x} - \frac{\partial T}{\partial x}\frac{\partial p}{\partial z}\right] \qquad (4.5\text{-}5)$$

where R is the gas constant for dry air.

The following numerical values were obtained by the wind tunnel test experiments:

$$\frac{\partial T}{\partial z} = \frac{1\ ^{o}c}{1\ cm} = 1\ ^{o}c\ cm^{-1}\ ,$$

$\partial p/\partial x$ is estimated as a first approximation through the Bernoulli equation.

$$\frac{\partial p}{\partial x} = -\rho\, u\frac{\partial u}{\partial x} = 10^{-2}\ \text{dynes}\ cm^{-3}$$

where $\rho \approx 10^{-3}$ gr cm^{-3}, $u \approx 20$ cm sec^{-1}, and $\partial u/\partial x = 5$ cm/sec/10 cm are assumed.

Then $(\partial T/\partial z)(\partial p/\partial x) = 10^{-2}\ ^{o}C$ dynes cm^{-4}. Hydrostatic equilibrium is assumed as a first approximation for $\partial p/\partial z$, i.e.,

$$\frac{\partial p}{\partial z} \approx -\rho g = 1\ \text{dyne}\ cm^{-3}$$

$$\frac{\partial T}{\partial x} = \frac{2^{o}C}{20cm} = 10^{-1}\ ^{o}C\ cm^{-1}\ .$$

Therefore,

$$\frac{\partial T}{\partial x}\ \frac{\partial p}{\partial z} = 10^{-1}\ {}^{o}C \text{ dynes } cm^{-4} .$$

The conclusion is thus the same as for the prototype case derived by Fisher. The $(\partial T/\partial z)(\partial p/\partial x)$ term is one order of magnitude smaller than $(\partial T/\partial x)(\partial p/\partial z)$. Hence, the former may be neglected.

4.6 Simplified Vorticity Transport Equation

Further transformation is conducted on the remaining solenoidal term $(\partial T/\partial x)(\partial p/\partial z)$. Hydrostatic equilibrium is assumed as a first approximation, then we obtain,

$$\frac{\partial T}{\partial x}\frac{\partial p}{\partial z} = -\frac{pg}{RT}\ \frac{\partial T}{\partial x} \quad ;$$

where the equation of state is again used to eliminate density ρ. The final simplified expression of the solenoidal term is, from Eq. (4.5-5),

$$\frac{\partial \alpha}{\partial z}\ \frac{\partial p}{\partial x} - \frac{\partial \alpha}{\partial x}\frac{\partial p}{\partial z} \simeq \frac{\partial \alpha}{\partial x}\ \frac{\partial p}{\partial z}$$

$$\simeq \frac{g}{T}\ \frac{\partial T}{\partial x}$$

Therefore the simplified vorticity transport equation is obtained as

$$\frac{D\zeta}{Dt} = K\nabla^2\zeta + \frac{g}{T}\ \frac{\partial T}{\partial x} \ . \qquad (4.6\text{-}1)$$

4.7 Boussinesq Approximation

The simplified vorticity equation can also be obtained from the Bossinesq approximation. This equation states that the density change caused by temperature nonhomogeneity affects only body forces but not inertia terms (Chandrasekhar, 1961). For simplicity of argument one can neglect diffusion terms from the equation of motion, i.e.,

$$\frac{Du}{Dt} = -\frac{1}{\rho_o}\frac{\partial p}{\partial x}$$

$$\frac{Dw}{Dt} = -\frac{1}{\rho_o}\frac{\partial p}{\partial z} - g\{1 - \beta(T-T_\infty)\} ,$$

where β is the coefficient of expansion and $T - T_\infty$ is the temperature difference between a hotter fluid particle and the colder surroundings. Cross differentiating and subtracting the two equations we have

$$\frac{D\zeta}{Dt} = \frac{g}{T}\frac{\partial T}{\partial x} \quad .$$

If the diffusion terms are reinserted, expression (4.6-1) is obtained.

4.8 Stream Function

The continuity equation of incompressible fluid (4.4.2-1) permits the existence of a stream function ψ such that

$$u = -\frac{\partial \psi}{\partial z} \quad \text{and} \quad w = \frac{\partial \psi}{\partial x} \quad . \tag{4.8-1}$$

Introduction of a stream function ψ guarantees that the continuity equation (4.4.2-1) is satisfied. Substituting the stream function into Eq. (4.5-3) we obtain a relation between the vorticity

ζ and the stream function ψ as

$$\zeta = \nabla^2\psi \tag{4.8-2}$$

4.9 Equation of Energy

The equation of energy in this case is given as

$$\frac{DT}{Dt} = K'\nabla^2 T \tag{4.9-1}$$

where K' is a total heat diffusivity.

The set of equations (4.6-1), (4.8-2) and (4.9-1) with the definition of the stream function (4.8-1) are to be integrated numerically with appropriate boundary and initial conditions.

4.10 General Discussion of Finite Difference Approximations

Partial differential equations may be approximated by finite difference analogy. Variables are represented at a finite number of discrete grid points rather than over a continuous field. Therefore, it is necessary to examine how accurately they represent the exact solutions of the equations. Two different but interrelated criteria must be considered. One is a convergence condition and another is a stability criteria. Detailed discussions are given in many textbooks (for example, Forsythe and Wascow, 1960; Smith, 1965; Richtmyer and Morton, 1967; Carnahan et al., 1969).

4.10.1 The concept of convergence - A finite difference equation is said to be convergent when the exact solutions of a difference equation tends to the exact solution of the original partial differential equation as both space and time grid increments tend to zero. Convergent criteria for linear equations with fairly generaly boundary

conditions are established (Smith, 1965). However, they are not known as yet for nonlinear partial differential equations except for a few special cases.

The convergent criteria for the problem studied herein is not apparent; however, stability of the problem may secure convergence as stated by Lax's equivalence theorem developed for linear problems. Lax's equivalence theorem states that: given a properly posed initial-value problem and a finite-difference approximation to it that satisfies the consistency conditions, stability is the necessary and sufficient conditions for convergence (Richtmyer and Morton, 1967, p. 45). This may not be true of course, for nonlinear problems without a rigorous mathematical proof; however, we will assume that even for nonlinear problems Lax's theorem may hold.

4.10.2 The concept of stability - During numerical integration of a finite difference equation computations are carried out with a finite number of decimal places which introduces a "round off" error. If a stability criterion is not satisfied, round off errors may accumulate as integration proceeds and cause solutions to take unreasonably large values. In such a situation a difference equation is said to be unstable.

The mathematical description of stability requires that the difference between the exact solution of a differential equation and that of its difference equation is bounded after an infinite number of integration steps when time and space grid increments are fixed.

The most frequently applied stability analysis is that of Von Neuman. A Fourier series representation for error is introduced into the finite difference equations and behavior of the amplitude of an error is

examined. A stability analysis for the difference equations used here will be presented in the appropriate sections.

4.10.3 Explicit method - For initial value problems there are two different kinds of finite difference schemes depending on the time step at which the space derivatives are approximated. If they are represented completely at a time when all quantities are known, the scheme is called explicit. The scheme is considered implicit if the space derivatives are expressed as a sum of the finite differences at both new and previous time steps. In the explicit system, values at all grid points at each new time step are computed explicitly point by point using the previously calculated or initial values. But in the implicit case, each new value is related to surrounding new values which are not yet known. Thus, all unknown values have to be solved for simultaneously.

Implicit methods have an advantage in computational stability for linear equations (Richtmyer and Morton, 1967), i.e., the scheme is computationally stable for arbitrary size of integration time increments. Therefore, one can save computational time to reach the desired integration time. In general the size of the integration time increments of explicit schemes are limited, and they are considerably smaller than those for implicit schemes which theoretically have no upper limit.

The DuFort-Frankel method (Smith, 1965) is a popular explicit scheme, and it is unconditionally stable for linear parabolic equations. For this reason it has been used frequently to solve even nonlinear equations. However, stability criterion for the entire difference equations including both diffusion and convection terms have not yet been obtained. Fromm (1963) prepared a stability condition for the DuFort-Frankel scheme by separating the equation into two parts; one is without

diffusion terms and the other is without convection terms. Then stability conditions were evaluated for each case and the more severe one was used for the computation. However, the second equation (without convection terms) are unconditionally stable in any event, which means no matter how large a time increment is chosen the finite difference approximation is computationally stable.

Generally speaking, an equation with convection terms produces more stringent stability constraints than one without them. Consider the following order of magnitude argument. Simple analysis shows a stability condition for an explicit approximation of the equation

$$\frac{\partial u}{\partial t} = K \frac{\partial^2 u}{\partial x^2}$$

is

$$\delta t_{diff} \leq \frac{1}{2} \frac{\delta x^2}{K}$$

where δt_{diff} and δx are time and space grid increments. Whereas an upstream difference approximation for the wave equation

$$\frac{\partial u}{\partial t} + u \frac{\partial u}{\partial x} = 0$$

gives a stability condition

$$\delta t_{convec} \leq \frac{\delta x}{u} \quad .$$

The ratio of the maximum allowable increments for each case produces

$$\frac{\delta t_{diff}}{\delta t_{convec}} = \frac{u \delta x}{2k}$$

given the following approximate numerical values for a simulation of wind tunnel experiments

$$u = 20 \text{ cm/sec}$$

$$\delta x = 4 \text{ cm}$$

$$k = 0.2 \text{ cm}^2/\text{sec}$$

then

$$\frac{\delta t_{diff}}{\delta t_{convec}} = 10^2 .$$

For a simulation of atmospheric phenomenon

$$u = 20 \text{ m/sec}$$

$$\delta x = 50 \text{ m}$$

$$k = 10^5 \text{ cm}^2/\text{sec}$$

might be assumed, which gives

$$\frac{\delta t_{diff}}{\delta t_{convec}} = 10^2 .$$

We can see from this simple calculation that for our present problem a two order of magnitude smaller time step may be required for an equation with any convection terms to satisfy stability conditions.

For nonlinear problems, stability depends not only on the structure of the finite difference system but also generally on the solution being obtained; and for a given solution, the system may be stable for some values of t and not for others, (Richtmeyer and Morton, 1967, p. 205). Since δt depends on a local value of velocity u it is desirable to change the size of δt every time step such that all local velocities satisfy the stability condition.

4.11 Difference Approximation for Heat Island Problem

Test computations indicated that it is necessary to use different schemes for heat island and mountain lee wave problems. The arguments are heuristic and based on experimental evidence. An upstream difference approximation is used for the case of the pure heat island and the heated mountain obstacle. An Arakawa scheme (1966) with an upstream difference step inserted every ten times is used for the mountain lee wave problems.

4.11.1 Upstream difference system - The primary difficulty associated with the approximation of a partial differential equation by a finite difference equation is due to the existence of nonlinear inertial terms such as $u\frac{\partial \zeta}{\partial x}$ or $w\frac{\partial \zeta}{\partial z}$. If one uses a forward difference for a time derivative and a central difference for a space derivative then the difference equation for a differential equation $\partial\zeta/\partial t + u\,\partial\zeta/\partial x = 0$ is unconditionally unstable (Richtmyer and Morton, 1967). Hence, no matter how small a time step is chosen, small errors introduced in the computation grow without limit.

A solution to this instability has been provided by a "forward-backward" molecule which replaces convection terms by

$$\left(u\frac{\partial \zeta}{\partial x}\right)^{n}_{j,\ell} = u^{n}_{j,\ell}\,\frac{\zeta^{n}_{j,\ell} - \zeta^{n}_{j-1,\ell}}{\delta x} \quad \text{when} \quad u^{n}_{j,\ell} \geq 0$$

$$= u^{n}_{j,\ell}\,\frac{\zeta^{n}_{j+1,\ell} - \zeta^{n}_{j,\ell}}{\delta x} \quad \text{when} \quad u^{n}_{j,\ell} < 0 \ .$$

This relation states that when the velocity $u^{n}_{j,\ell}$ is positive then the space derivative is approximated by a backward difference, and when

$u^n_{j,\ell}$ is negative a forward difference is used. In this way the direction of the convection is always the same as that of the local velocity components. All variables are transported from the upstream side of the point in a local sense, which is the origin of the name of an "upstream difference" scheme. Where subscript j and ℓ are j^{th} and ℓ^{th} grid points in x and z direction, respectively. In the same manner, the superscript n stands for the n^{th} time step of integration. $n = 1$ is an initial time. Relations with actual coordinates and time are given as

$$x = (j-1) \times \delta k ,$$

$$x = (\ell-1) \times \delta z ,$$

and $$t = (n-1) \times \delta t ,$$

where δx and δz are space grid increments in the x and z directions, respectively. δt is a time grid increment.

The upstream difference scheme has been used in many place, (for example, Estoque, 1961, 1962, 1968; Tonouye, 1966; Orville, 1968; Torrance and Kockett, 1969; Roache and Muller, 1970; Muller and O'Leary, 1970).

4.11.2 Pseudo viscosity - The upstream difference scheme may introduce an "unexpected" numerical damping which may under certain circumstances modify or control the solution for a given problem. The one dimensional, unsteady, and incompressible vorticity transport equation without a diffusion term is expressed as

$$\frac{\partial \zeta}{\partial t} + u \frac{\partial \zeta}{\partial x} = 0 .$$

Its first order approximation in the upstream scheme is given as

$$\frac{\zeta_j^{n+1} - \zeta_j^n}{\delta t} + u \frac{\zeta_j^n - \zeta_{j-1}^n}{\delta x} = 0 , \qquad (4.11.2\text{-}1)$$

when u is not negative and a forward approximation is used for the time derivative. By a Taylor's series expansion (neglecting higher order terms than δx^3 or δt^3)

$$\zeta_{j-1}^n = \zeta_j^n - \delta x \left(\frac{\partial \zeta}{\partial x}\right)_j^n + \frac{\delta x^2}{2} \left(\frac{\partial^2 \zeta}{\partial x^2}\right)_j^n - \cdots$$

and

$$\zeta_j^{n+1} = \zeta_j^n + \delta t \left(\frac{\partial \zeta}{\partial x}\right)_j^n + \frac{\delta t^2}{2} \left(\frac{\partial^2 \zeta}{\partial t^2}\right)_j^n + \cdots$$

The first term represents an expansion with respect to space and the second one is an expansion with respect to time. The first expansion is substituted into the second term in Eq. (4.11.2-1) and the second expression is substituted into the time difference term. Thus we have

$$\frac{\zeta_j^{n+1} - \zeta_j^n}{\delta t} + u \frac{\zeta_j^n - \zeta_{j-1}^n}{\delta x}$$

$$= \frac{\partial \zeta}{\partial t} + u \frac{\partial \zeta}{\partial x} - \frac{u \delta x}{2} \left(1 - \frac{u \delta t}{\delta x}\right) \frac{\partial^2 \zeta}{\partial t^2} + \cdots \qquad (4.11.2\text{-}2)$$

where the relation

$$\frac{\partial^2 \zeta}{\partial t^2} = u^2 \frac{\partial^2 \zeta}{\partial x^2}$$

is used from the original equation assuming u is constant. A similar expression is obtained when u is negative. If the finite difference equation (4.11.2-1) is solved exactly then the differential equation becomes (combine Eq. (4.11.2-2) with Eq. (4.11.2-1)),

$$\frac{\partial \zeta}{\partial t} + u \frac{\partial \zeta}{\partial x} = \frac{|u| \delta x}{2} \left(1 - \frac{|u| \delta t}{\delta x}\right) \frac{\partial^2 \zeta}{\partial x^2} \quad .$$

The term

$$\nu_p = \frac{|u| \delta x}{2} \left(1 - \frac{|u| \delta t}{\delta x}\right) \qquad (4.11.2\text{-}3)$$

has been called the pseudo viscosity or pseudo diffusivity (Molenkamp, 1968). Molenkamp evaluated ν_p for typical thermal convection situations and numerical values were of the order of 35 $m^2 sec^{-1}$, which is comparable with typical measured turbulent viscosities ranging from 0 to 40 $m^2 sec^{-1}$.

Molenkamp (1968) conducted numerical experiments to show how solutions were deformed with integration for seven different finite difference approximations. For example, as we can see from Eq. (4.11.2-3), ν_p will be smaller if δx is chosen to be smaller. The solution was improved greatly when δx was chosen as half of the previous calculation. From his numerical experiments, Molenkamp concluded that only the Roberts-Weiss approximation advected the initial distribution correctly of all eight schemes investigated.

A similar study has been prepared by Crowley (1967) who reduced distortions by two-time-step schemes, i.e., the state vector is known at time t, and with this information and some intermediate calculated information at $t + 1/2\ \delta t$, the system is advanced to time $t + \delta t$ (Crowley, 1967, p. 472). He extended his work from the second order scheme to the fourth order one and showed that the solution by the fourth

order approximation was very accurate compared with that given by the second order scheme (Crowley, 1968).

Both Crowley (1968) and Molenkamp (1968) concluded that a simple first order scheme (upstream difference) is not accurate enough to simulate diffusion problems.

Orville (1968b) commented on the matters discussed above. Even though he accepted the conclusions by Crowley or Molenkamp on the inaccuracy of the upstream difference for pure advection problems, he argued that the inaccuracy of that scheme applied to the broader turbulent-plus-advection problems has not been established by either of the studies mentioned above. He also stated that it must be realized that upstream differencing was most often applied to problems in which diffusion was an important physical consideration.

Continuous efforts have been made for a long time by different authors to seek accurate finite-difference approximation schemes applied to the Navier-Stokes equation. (Recent works include Fromm, 1969; Cheng, 1970, etc.) However, a complete exact analysis is not available at the present stage for full Navier-Stokes equation. Therefore, the only practical way of judgement on the accuracy of the approximation used is by the comparison with prototype observations and/or laboratory experiments if both advection and turbulence are modeled in the numerical computation.

4.11.3 Usefulness of pseudo-diffusivity - The large damping effect introduced automatically in the upstream difference system is sometimes very convenient to filter or smooth out the computational errors developed near a large temperature discontinuity. These disturbances exist in the unstably stratified regions around a model heat island

which magnifies even a small error introduced during computations. These perturbations usually do not represent physically meaningful phenomena; therefore they should be numerically reduced or eliminated. Hino (1965) used an averaging method to disperse the computational errors. All the values computed were averaged with surrounding points every certain number of integration. However, if the upstream difference scheme is used, any additional steps for smoothing are not necessary since the upstream finite-difference approximation itself acts as a smoothing operator.

4.12 Finite Difference Expression for the Vorticity Transport Equation

A finite difference approximation of the vorticity transport equation (4.6-1) is obtained by replacing the diffusion terms by centered differences while the color equation (Substantial Derivative), $\frac{\partial \zeta}{\partial t} + u \frac{\partial \zeta}{\partial x} + w \frac{\partial \zeta}{\partial z} = 0$, is approximated by the upstream numerical system. The final form is, when u and w are positive,

$$\zeta^{n+1}_{j,\ell} = \zeta^{n}_{j,\ell} + \frac{k\delta t}{\delta x^2} (\zeta^{n}_{j+1,\ell} - 2\zeta^{n}_{j,\ell} + \zeta^{n}_{j-1,\ell})$$

$$+ \frac{k\delta t}{\delta z^2} (\zeta^{n}_{j,\ell+1} - 2\zeta^{n}_{j,\ell} + \zeta^{n}_{j,\ell-1})$$

$$+ \frac{g\delta t}{2\delta x} \frac{T^{n}_{j+1} - T^{n}_{j-1,\ell}}{T^{n}_{j,\ell}} - \frac{u^{n}_{j,\ell}\,\delta t}{\delta x} (\zeta^{n}_{j,\ell} - \zeta^{n}_{j-1,\ell})$$

$$\frac{w^{n}_{j,\ell}\,\delta t}{\delta z} (\zeta^{n}_{j,\ell} - \zeta^{n}_{j,\ell-1}) \qquad (4.12\text{-}1)$$

A detailed derivation is given in Appendix A.

4.13 Successive Over Relaxation Method for Stream Function

The stream function is obtained by solving the Poisson equation with known vorticity values. There are many methods available to solve such an elliptic equation numerically (see for example: Smith, 1965; Thom and Apelt, 1961, etc.).

Herein a successive over relaxation method (S.O.R. method) was utilized. Improvements upon this method or developments of other methods such as "Alternating Direction Implicit" (A.D.I) method or "Fast Fourier Transformation" (F.F.T) method are desirable - especially since the most computation time is utilized to solve the Poisson equation. (Reference is made to Peaceman and Rachford (1955) and Douglass (1955) for the A.D.I. method and to Cooley, et al. (1967) for the F.F.T. method).

The finite difference expression for stream function given by the S.O.R. method is

$$\psi_{j,\ell}^{r+1} = (1-\omega)\,\psi_{j,}^{r} + \frac{\omega}{2\left\{1+\left(\frac{\delta x}{\delta z}\right)^2\right\}}\left\{\psi_{j+1,\ell}^{r} + \psi_{j-1,\ell}^{r} + \left(\frac{\delta x}{\delta z}\right)^2\left(\psi_{j,\ell+1}^{r} + \psi_{j,\ell-1}^{r}\right) - \zeta_{j,\ell}\,\delta x^2\right\}, \qquad (4.13\text{-}1)$$

where ω is an over relaxation factor which lies between one and two. The exact value of ω for a general grid system is determined by a test calculation since no analytical expression for such an optimum value is yet available. When a square mesh system is used (i.e., $\delta x = \delta z = h$) then ω is analytically given as

$$\omega = \frac{2}{1 + \pi \sqrt{\frac{1}{2}\left(\frac{1}{k^2} + \frac{1}{L^2} \right)}} \quad . \tag{4.13-2(a)}$$

when the domain of integration has a rectangular area, Kh x Lh. And when the domain is square

$$\omega = \frac{2}{1 + \sin(h)} \tag{4.13-2(b)}$$

(see for example, Apelt, 1969).

The convergence criterion of the iteration procedure given by Eq. (4.13-1) is

$$|\psi^{r+1} - \psi^{r}|_{max} < \delta$$

i.e., if the absolute value of the maximum difference between the (r+1)th iteration and the previous rth iteration is less than δ then the iteration is stopped. δ should be determined by numerical experiments and here we adjusted δ from 0.01 to 0.10 depending on the magnitude of stream function at the top boundary. In other words,

$$\frac{|\psi^{r+1} - \psi^{r}|_{max}}{|\psi_{top}|} < \frac{\delta}{|\psi_{top}|} \simeq 10^{-4}$$

The derivation of Eq. (4.13-1) is given in Appendix A.

4.14 Finite Difference Expression of Energy Equation

The finite difference approximation for the energy equation (4.9-1) has a very similar appearance to that of the vorticity transport equation. The final difference approximation to Eq. (4.9-1) is

$$T^{n+1}_{j,\ell} = T^{n}_{j,\ell} + \frac{k'\delta t}{\delta x^2}\left(T^{n}_{j+1,\ell} - 2T^{n}_{j,\ell} + T^{n}_{j-1,\ell}\right)$$

$$+ \frac{k'\delta t}{\delta z^2}\left(T^{n}_{j,\ell+1} - 2T^{n}_{j,\ell} + T^{n}_{j,\ell-1}\right)$$

$$- \frac{u^{n}_{j,\ell}\,\delta t}{\delta x}\left(T^{n}_{j,\ell} - T^{n}_{j-1,\ell}\right) - \frac{w^{n}_{j,\ell}\,\delta t}{\delta z}\left(T^{n}_{j,\ell} - T^{n}_{j,\ell-1}\right) \quad (4.14\text{-}1)$$

when both $u^{n}_{j,\ell}$ and $w^{n}_{j,\ell}$ are not negative. If they take different signs then the last two terms for convection are changed according to the upstream difference system described in the previous section (see section 4.11.1).

4.15 Stability Condition for the Upstream Difference Scheme

An accurate stability analysis is the most important and fundamental requirement to obtain reasonably approximated solution to the original differential equations. Since the finite difference approximations for both the vorticity transport and the energy equations have similar expressions, a stability analysis is completed only for the former expression. A Von Neuman stability analysis was applied and the details are given in Appendix A. The final condition which should be satisfied in order to maintain stability is

$$\delta t \leq \frac{0.8}{\frac{|u|_{max}}{\delta x} + \frac{|w|_{max}}{\delta z} + \frac{2k}{\delta x^2} + \frac{2k}{\delta z^2}}, \qquad (4.15\text{-}1)$$

where $|u|_{max}$ and $|w|_{max}$ are the magnitudes of the maximum velocity components u and w, respectively, in the entire computation region. The stability criterion is thus a variable depending upon the magnitude of each set of newly calculated velocity components.

In practice $|u|_{max}$ and $|w|_{max}$ were calculated at each time step and δt was selected such that it satisfied the stability condition (4.15-1).

It is desirable to choose δt as large as possible within the computational stability criterion (4.15-1) in order to save computation time. If a larger time step is chosen, more iterations may be required in the solution of the Poisson equation because the source terms (vorticities) vary by larger steps also. Since the associated iteration technique is a time consuming calculation, a larger time increment does not necessarily save computational time as one might expect.

A simple experiment was prepared to compare the computational time for different sizes of time increments. It was found for example that when the time step was chosen as one-half the maximum value suggested by the stability condition the calculation was faster than that for the maximum time step. A similar argument concerning the proper size time increment is found in Fromm (1963).

4.16 Boundary Conditions

Boundary conditions for the vorticity transport equation cannot be given directly. However, they are closely related with interior values of vorticity and stream functions by means of a Taylor's series expansion. For rigid boundaries this relation is very simple and may be derived analytically from the known boundary conditions of velocities and stream functions.

In this study both the upper and the lower boundaries are rigid and a no-slip velocity condition is used. i.e.,

$$u = w = 0 \quad \text{at} \quad z = 0 \quad \text{and} \quad z = H$$

where H is the height of the top boundary. The stream function is assigned to zero value along the bottom boundary and a constant value is maintained along the top boundary.

A detailed derivation is again available in Appendix A. The final expression is

$$(\zeta)_{bound} = \frac{3}{(\delta z)^2} (\psi_{int} - \psi_{bound}) - \frac{1}{2} \zeta_{int} \qquad (4.16\text{-}1)$$

where ζ_{bound} and ψ_{bound} are the boundary values of vorticity and stream function, respectively. Subscript "int" indicates the values at one grid inside from the boundary. Similar expressions have been used previously (Lin and Apelt 1970; Roache and Mueller; 1970).

Boundary conditions at the up-and down-stream boundaries are more difficult and must be determined more or less empirically. If the computational boundaries could be extended infinitely in the horizontal direction simple boundary conditions are possible such as no disturbances

are detected at $x = \pm \infty$. For numerical computations, however, horizontal boundaries are always finite, and the size depends on the capacity of the digital computer available.

Boundary conditions are sought which imposed the least severe restrictions on the solutions in the interior region, i.e., such that no distorted values at the boundaries propagate into the interior area. The following boundary conditions have been determined from experiments to give the least apparent restrictions and the least distortions.

Streamlines are assumed to change linearly i.e., maintain constant slopes at the lateral boundaries. Thus,

$$\frac{\partial^2 \psi}{\partial x^2} = \frac{\partial^3 \psi}{\partial x^3} = \frac{\partial^4 \psi}{\partial x^4} = \ldots\ldots = 0 \quad . \tag{4.16-2}$$

In terms of velocity component w this specifies

$$\frac{\partial w}{\partial x} = 0 \quad .$$

However since this numerical model is formulated in terms of the vorticity equation one needs boundary conditions for vorticities at the lateral boundaries.

With the assumption that the stream function varies linearly at the lateral system boundaries one may conclude from

$$\frac{\partial^2 \zeta}{\partial x^2} = \frac{\partial^4 \psi}{\partial x^4} + \frac{\partial^2}{\partial z^2}\left(\frac{\partial^2 \psi}{\partial x^2}\right)$$

$$\text{that} \quad \frac{\partial^2 \zeta}{\partial x^2} = 0 \quad . \tag{4.16-3}$$

Boundary conditions for the energy equation at $x = -L_1$ and L_2 are similarly

$$\frac{\partial^2 T}{\partial x^2} = 0 \quad . \tag{4.16-4}$$

4.17 Initial Conditions and Grid System

To integrate the set of the equations described above, initial values must be specified to initialize the numerical integration. Hence, initial velocity components u and w are originally given, and the vorticities and stream functions are initialized by their definitions. In terms of the finite difference expressions

$$\zeta_{j,\ell} = \frac{w_{j+1,\ell} - w_{j-1,\ell}}{2\delta x} - \frac{u_{j,\ell+1} - u_{j,\ell-1}}{2\delta z}$$

and

$$\psi_{j,} = -\frac{1}{2} u_{init} \times \delta z \times (2\ell-3)$$

for the interior the region and boundaries along $x = -L_1$ and L_2. $\zeta_{j,\ell}$ and $\psi_{j,\ell}$ are respectively the vorticity and stream function at (j,ℓ) position. u_{init} is the initial value of u which is assumed to be constant. At initial time $t = 0$ all the values of w are assumed to be zero; therefore vorticity is calculated neglecting the first term of the above expression, $\frac{\partial w}{\partial x}$. The trapezoidal rule is used to integrate velocity numerically

$$\psi = -\int_0^z u dz \quad .$$

For the values along the boundaries $z = 0$ and H forward and backward differences are used, respectively.

$$\zeta_{j,1} = \frac{-(u_{j,2} - u_{j,1})}{\delta z} \qquad \text{along} \quad z = 0$$

$$\zeta_{j,ML} = \frac{-(u_{j,ML} - u_{j,ML-1})}{\delta z} \qquad \text{along} \quad z = H ,$$

where $\ell = 1$ and ML represents the locations along $z = 0$ and H, respectively. For the stream functions, constant values are maintained throughout the integration along the boundaries $z = 0$ and $z = H$.

Arbitrary temperature distributions may be assumed in the vertical direction, but kept constant in horizontal direction at initial time $t = 0$

$$T_{j,\ell} = F(z) \quad (j = 1,2,\ldots,MJ;\ \ell = 1,2,\ldots, ML)$$

where $F(z)$ is an arbitrary function of z.

When a heat island is located along $z = 0$ and has a higher temperature ΔT over the surroundings. Then,

$$T_{island} = T_o + \Delta T ,$$

where T_{island} and T_o are temperatures at the heat island and surrounding surface temperature, respectively. T_{island}, T_o and ΔT are kept constant throughout the computation. All the variables, u, w, ζ, ψ and T are now initialized and a numerical integration may start.

Numerical integrations and experiments have been conducted in such a way that they may be directly compared. Therefore, it was convenient to use the same coordinate system in each case since a direct comparison of results was desirable. Wind tunnel test section is 50 cm height x 60 cm width x 450 cm length. Hence, a region of comparable size was utilized in the numerical computation (see Fig. 4-1). The area was divided by a 81 x 16 square mesh whose dimension is 4 x 4 cm. Therefore, a 60 cm height x 320 cm length area is the computational region - about the same size as the effective wind tunnel test section area.

4.18 Procedures of Integration

1) Using the initial values given at $t = 0$ vorticities interior to the region studied, are obtained by Eq. (4.12-1). Boundary values along $x = -L_1$ and L_2 except the corners are calculated by the finite difference expression of Eq. (4.16-3)

$$\zeta_{1,\ell} = 2\,\zeta_{2,\ell} - \zeta_{3,\ell} \qquad \text{along} \quad x = -L_1$$

and

$$\zeta_{MJ,\ell} = 2\,\zeta_{MJ-1,\ell} - \zeta_{MJ-2,\ell} \qquad \text{along} \quad x = L_2 \ ,$$

where $j = 1$, and MJ show the location along the boundary $x = L_1$, and L_2, respectively.

2) Interior values of stream functions are obtained by iterating Eq. (4.13-1) until a given convergence is achieved. Then the boundary values along $x = -L_1$ and L_2 are computed by the equivalent expression for vorticity ζ, i.e.,

$$\psi_{1,\ell} = 2\,\psi_{2,\ell} - \psi_{3,\ell} \qquad \text{along} \quad x = -L_1$$

and

$$\psi_{MJ,\ell} = 2\,\psi_{MJ-1,\ell} - \psi_{MJ-2,\ell} \qquad \text{along} \quad x = L_2$$

Since boundary values along $z = 0$ and H are kept constant, all new values of stream functions are now known.

3) Velocity components u and w are calculated by the finite difference forms of (4.8-1). For the interior region, central difference approximations are used to evaluate u and w, but along boundaries $x = -L_1$ and $x = L_2$, w are computed by the forward and the backward differences, respectively. u and w are zero along boundaries $z = 0$ and H by the boundary condition.

4) Boundary values of vorticities along $z = 0$ and H are obtained by Eq. (4.16-1). Thus, all new values of vorticities are known.

5) The temperature field is calculated by Eq. (4.14-1) for the interior region, and Eq. (4.16-4) gives boundary values along $x = -L_1$ and L_2. Since values along the boundaries $z = 0$ and H are constant, a new temperature field is obtained.

A set of calculations 1) to 5) is repeated until a pre-specified time period has past.

A somewhat unconventional procedure has been utilized to evaluate the boundary values. Boundary values are obtained from the boundary conditions only, whereas a more rigorous approach would be to use the entire governing equation with consideration of boundary conditions. For example in order to calculate boundary values along $x = -L_1$

from Eq. (4.12-1), the values outside the region $T_{o,\ell}$ or $\zeta_{o,\ell}$ should be eliminated through the boundary condition and boundary values may then be obtained just as for those interior to the region. In this manner, boundary values satisfy both the equation and the boundary condition. However, in the technique specified here, only the boundary condition is satisfied. There is no a priori justification to use this simplified procedure, but it is quite convenient in practice because the boundary values are calculated independently from the governing equation. In this study many different boundary conditions such as ψ = const, $\frac{\partial \psi}{\partial x} = 0$, $\frac{\partial^2 \psi}{\partial x^2} = 0$ $\frac{\partial^3 \psi}{\partial x^3} = 0$, a pericdic boundary condition, and an extrapolation method have been examined and it was found very tedious to change equations of boundary values for each trial. Therefore, boundary values are obtained only thrcugh the boundary conditions as discussed. In any event since there is no general way to impose correct boundary conditions at inflow and outflow boundaries a trial and error method might suggest appropriate boundary conditions.

4.19 Modification of the Scheme for Mountain Lee Wave Problems

It is necessary to make some modifications of boundary and initial conditions to apply the previous finite difference scheme to airflow over an obstacle. A rectangular obstacle is adopted for its simplicity and convenience in the numerical programming. The obstacle is placed on the lower surface from grid number MST to MEND, and its top surface corresponds to ℓ = MHEI as shown in Fig 4-1. Therefore, actual dimensions of the obstacle are (MEND-MST) x δx width x (MHEI-1) x δz height. Along the obstacle surface the stream function is kept constant due to the no-slip condition that velocity components

u and w are zero. Stream functions are assigned a constant value along the upper boundary, z = H. The temperature of the obstacle can be varied from that of the surrounding surface temperature if heating or cooling effects of the mountain are to be investigated. For a simple unheated mountain case, the temperature of the obstacle is maintained at the same value as the surrounding air temperature.

Initial velocity profiles over the simulated mountain are calculated to satisfy continuity. Uniform velocity profiles are assumed whose magnitudes are obtained from a uniform upstream initial velocity profile. Vorticities on the obstacle surface are calculated in the same manner as for the rigid boundaries (see Eq. 4.16-1).

4.20 Test Computations of Airflow over an Obstacle

The first computation of airflow over an obstacle was conducted under very simple conditions. The temperature along the bottom surface was taken as $298^{o}K$ and temperature gradient was $1^{o}C/cm$. Therefore, at the top surface (Z = 60 cm) the temperature was $358^{o}K$. The values along the boundaries were kept constant during the computation. A uniform velocity of 8 cm/sec was given at t = 0. Froude number in this case was $(F_r)_H = 0.077$. An obstacle was placed between J = 21 and 30, and its height was 8 cm. Results were printed out every K time steps where K is between 25 to 50. They include velocity components u and w, stream function, vorticity and temperature. A microfilm recorder 280 was used to plot contour lines of the above variables. Figure 4-2 shows the resulting contoured plots of stream function, vorticity and temperature at t = 16.15 sec.

Streamlines in Fig. 4-2 do not show strong waves behind the obstacle. If a comparison, however, is made with a result obtained in a neutral atmosphere (no stratification) which is also included in Fig. 4-2, we can see definite effects of stratification. In the stratified case, streamlines over the obstacle have been displaced downward because of the negative buoyancy forces introduced by the density difference between a particle and its surroundings. This force together with the requirement of continuity bends streamlines downward behind the obstacle. Because of its inertia, a particle drops down beyond its equilibrium position and encounters a positive buoyancy force which again would lift the particle beyond its equilibrium if no dissipation of energy exists. Fig. 4-3 shows the time variations of a horizontal velocity component u at different locations. All had uniform profiles at $t = 0$. Even at $N = 150$ ($T = 16.15$ sec) they have not precisely reached a steady state but differences from $N = 100$ ($t = 11.14$ sec) are very small. The velocity profiles at $N = 150$ clearly show jet phenomena, i.e., there exist maximums and minimums in the velocity profile (Long, 1959; Janowitz, 1968). In this particular case, there are two maximums and two minimums. Very strong velocities are observed downstream of the obstacle whose magnitude is about twice as large as the averaged velocity. In the same manner, Fig. 4-4 shows horizontal velocity components u at different locations in a neutral situation. Jet phenomena or strong winds were not observed. Figure 4-4 shows only a blocking effect of the obstacle, while Fig. 4-3 also includes the effect of stratification.

The initial calculations obtained displayed many interesting aspects of stratified airflow over an obstacle. They did not generate

lee waves downwind of the obstacle. Since a lee wave amplitude is comparable to the obstacle height, it was suggested that a higher obstacle might give visible lee waves. The obstacle height was increased from 8 cm to 20 cm. The Froude number was still $(F_r)_H = 0.077$. Stream function, vorticity, and temperature contour lines at $t =$ 9.45 sec., are shown in Fig. 4-5. Horizontal velocity profiles at the same time are shown in Fig. 4-6. They again display clear effects of stratification.

4.21 Simulation of Davis' Result

In order to investigate the reason why the initial scheme did not produce lee waves, the program was run under the same conditions for which the best lee waves are observed in Davis' paper (1969). In his paper, the characteristic parameter is expressed by k which is the inverse of the Froude number based on the characteristic length H/π, where H is the channel height. The relation between k and a global Richardson number is given by

$$R_i = \pi^2 k^2 \quad .$$

Since $k = 1.5$ gave Davis the strongest lee wave result, we used this value in our computation.

$$F_r = \frac{1}{\sqrt{R_i}} = \frac{1}{\pi k} = 0.2122 \quad .$$

In his paper, dynamic pressure and vertical density gradient at the far upstream boundary are kept constant (Long's model). From these conditions, an upstream temperature distribution was calculated from

$$\frac{T}{T_o} = e^{\frac{k^2\pi^2}{gH^2}\int_o^z u^2\,dz} , \qquad (4.21\text{-}1)$$

where T_o: Temperature at surface (assumed 300^oK)

H : Depth of the wind tunnel = 60 cm

k : = 1.5

g : acceleration of gravity

U : average velocity (assumed 20 cm/sec).

The resulting temperature profile is shown in Fig. 4-7. Temperature varies almost linearly except for the region very close to the surface. The temperature gradient read from the figure was $0.81^oC/cm$. Stability was $2.48466 \times 10^{-3}\ cm^{-1}$, thus the Froude number was 0.2136 which is very close to the exact value 0.2122. Temperatures obtained by Eq. (4.21-1) were used as initial values. Numerical integration was carried out in 150 steps and results were plotted. Figure 4-8 shows the results. They show very weak first wave crests somewhere near x = 80 cm but compared to Davis' result (Fig. 2-4), they are very small.

Several authors have suggested that the upstream finite-difference approximation introduces a strong damping effect (see section 4.11.2). Pseudo viscosity is expressed by Eq. (4.11.2-3), i.e,

$$\nu_p = \frac{|u|\delta x}{2}\left(1 - \frac{|u|\delta t}{\delta x}\right) , \qquad (4.11.2\text{-}3)$$

where ν_p is a parabolic function with respect to $|u|$ and it has a maximum value

$$(\nu_p)_{max} = \frac{\delta x^2}{8\delta t} = \frac{|u|_{(\nu_p)_{max}} \delta x}{4}$$

at

$$|u|_{(\nu_p)_{max}} = \frac{\delta x}{2\delta t} \quad .$$

In order to have an accurate prediction by the upstream finite difference approximation, the physical viscosity ν should be much greater than the pseudo viscosity ν_p (Fromm, 1969), i.e.,

$$(\nu_p)_{max} = \frac{|u|_{(\nu_p)_{max}} \delta x}{4} << \nu$$

or

$$(R_e)_g = \frac{|u|_{(\nu_p)_{max}} \delta x}{\nu} << 4.$$

Therefore, grid Reynolds number, $(R_e)_g$, should be much less than 4. In the previous calculation (Fig. 4-2) $\delta t = 0.09675$ sec and $\delta x = 4$ cm when $t = 8.96$ sec. Therefore pseudo viscosity ν_p has a maximum value

$$(\nu_p)_{max} = \frac{\delta x^2}{8\delta t} = \frac{4^2}{8x0.09675} = 20.67 \text{ cm}^2/\text{sec}$$

when

$$|u|_{(\nu_p)_{max}} = \frac{\delta x}{2\delta t} = \frac{4}{2x0.09675} = 20.67 \text{ cm/sec.}$$

If the actual viscosity is about 0.15 cm^2/sec (20^oC), the grid Reynolds number is

$$(R_e)_g = \frac{|U|_{(\nu_p)_{max}} \delta x}{\nu} = \frac{20.67 \times 4}{0.15} = 551.$$

Equation (4.11.2-3) was plotted under this special condition in Fig. 4-9a which also shows the pseudo viscosity distribution with height at various locations when $t = 8.96$ sec. (Fig. 4-9b).

Pseudo viscosity distributions with height have a very similar profile to those of horizontal velocity components because the relation between the pseudo viscosity, ν_p and absolute velocity $|u|$ is almost linear as seen from Fig. 4-9a. Since the pseudo viscosity appears to be as large as 100 times the actual viscosity, it is inappropriate to simulate the prototype experiment by the upstream difference approximation.

In order to see the effect of the viscosity in the upstream scheme, the calculations were repeated for a viscosity of 20 cm^2/sec which is about 100 times bigger than the previous value. The same obstacle and the same conditions specified for Fig. 4-2 were used except for the magnitude of the viscosity. Figure 4-10 shows streamline, vortex and temperature contour lines, respectively. Comparisons with Fig. 4-2 do not indicate any great difference; however, the velocity profiles (Fig. 4-11) show the clear effect of a viscosity difference. In Fig. 4-11 velocity profiles for $\nu = 0.18$ cm^2/sec are also presented with broken lines for comparisions. A large viscosity definitely smoothes out the maximums or minimums of the profiles. Figure 4-12a and 4-12b show the relation between the pseudo viscosity and the absolute velocity

in this case (δx = 4 cm, δt = 0.05588 sec) and pseudo viscosity profiles at various locations. Magnitudes as large as 20 cm^2/sec are seen at many locations. The grid Reynolds number in this case was

$$(R_e)_g = 7,$$

which is close to the critical value 4.

Thus, even if the magnitude of viscosity is hypothetically increased 100% over the previous calculation, we may not see any significant differences in the solutions, because that change in viscosity is less than 1% of the pseudo viscosity.

We cannot predict how accurately the scheme can predict phenomena when the true viscosity is much greater than the numerical one. Any conclusions must depend on other tests such as prototype observations, or laboratory experiments. We shall not try to examine this here, because we know that a laminar flow in a wind tunnel cannot have such a large value of viscosity (20 cm^2/sec) and wind tunnel (Lin and Binder, 1967) and water channel (Long 1955; Davis 1969) experiments showed the definite existence of lee waves behind the obstacle. Hence, one can at least conclude that the upstream difference approximation is not suitable for the lee wave problem.

One is now led to search for some second order method with a smaller damping effect. Arakawa's (1966) explicit scheme is one of such differencing techniques. Molenkamp (1968) showed that Arakawa's scheme has increased accuracy compared with the upstream difference method just discussed.

4.22 Arakawa's Scheme

Arakawa (1966) developed his finite difference scheme for the vorticity transport equation in such a manner that it conserves the mean vorticity, the mean kinetic energy, and the mean square vorticity in a closed domain. Since we found the upstream difference approximation system is not appropriate to simulate wave motions behind an obstacle and Arakawa's scheme has been proven to often have better accuracy, we reprogrammed using his scheme.

4.23 Arakawa's Scheme for the Vorticity Transport Equation

Arakawa's scheme for the vorticity transport equation is,

$$\frac{\partial \zeta}{\partial t} = -\frac{1}{12h^2}\left[(\psi_{j,\ell-1} + \psi_{j+1,\ell-1} - \psi_{j,\ell+1} - \psi_{j+1,\ell+1})(\zeta_{j+1,\ell} - \zeta_{j,\ell})\right.$$

$$+(\psi_{j-1,\ell-1} + \psi_{j,\ell-1} - \psi_{j-1,\ell+1} - \psi_{j,\ell+1})(\zeta_{j,\ell} - \zeta_{j-1,\ell})$$

$$+(\psi_{j+1,\ell} + \psi_{j+1,\ell+1} - \psi_{j-1,\ell} - \psi_{j-1,\ell+1})(\zeta_{j,\ell+1} - \zeta_{j,\ell})$$

$$+(\psi_{j+1,\ell-1} + \psi_{j+1,\ell} - \psi_{j-1,\ell-1} - \psi_{j-1,\ell})(\zeta_{j,\ell} - \zeta_{j,\ell-1})$$

$$+(\psi_{j+1,\ell} - \psi_{j,\ell+1})(\zeta_{j+1,\ell+1} - \zeta_{j,\ell})$$

$$+(\psi_{j,\ell-1} - \psi_{j-1,\ell})(\zeta_{j,\ell} - \zeta_{j-1,\ell-1})$$

$$\left.+(\psi_{j,\ell+1} - \psi_{j-1,\ell})(\zeta_{j-1,\ell+1} - \zeta_{j,\ell})\right]$$

$$+(\psi_{j+1,\ell} - \psi_{j,\ell-1})(\zeta_{j,\ell} - \zeta_{j+1,\ell-1})]$$

$$+K\left(\frac{\partial^2\zeta}{\partial x^2} + \frac{\partial^2\zeta}{\partial z^2}\right) + \frac{g}{T}\frac{\partial T}{\partial x} ,$$

and here only the advection terms are approximated by the finite differences because they are the most important factor to maintain accuracy and computational stability. The time derivative is approximated by a centered difference as

$$\left(\frac{\partial\zeta}{\partial t}\right)^n_{j,\ell} = \frac{\zeta^{n+1}_{j,\ell} - \zeta^{n-1}_{j,\ell}}{2\delta t} .$$

The diffusion term $K\left(\frac{\partial^2\zeta}{\partial x^2} + \frac{\partial^2\zeta}{\partial z^2}\right)$ and the source term $\frac{g}{T}\frac{\partial T}{\partial x}$ are also approximated by centered difference molecules. This scheme was expected to give a better result, and it is computationally stable if an appropriate integration time step is used.

The subsequent programming efforts provides a good opportunity to examine the appropriate boundary conditions at up and down-stream boundaries. Therefore, the following paragraphs discuss the process in some detail.

4.24 Preliminary Computations and Improvements of the Programming

The first computation in Arakawa's scheme produced unreasonably large velocities at some grid locations after it had been integrated forty-one times. There was no way to trace exactly where the instability occurred in the programming. The boundary values of the vorticities at up and down-stream boundaries were calculated from the definition

$$\zeta = \frac{\partial w}{\partial x} - \frac{\partial u}{\partial z}$$

where all w and u were known from stream functions. Although computational stability is predicted by the linear stability analysis, there is no reason to believe this condition is sufficient for the nonlinear original equations.

One solution would be to reduce the size of time increments to maintain stable computations. However, another route was chosen; it was decided to intermittently utilize the strong damping effects of the upstream difference approximation*.

Hence, as a second computational scheme, it was decided to insert at every ten integration time steps an upstream difference representation for the inertia terms to stabilize the field. The result was not much different from the previous calculation where only Arakawa's scheme was used. Thus the rate of insertion of the upstream scheme was increased. In the third computation an upstream difference scheme was used every other step. At N = 51 (t=2.61 sec), a velocity at one place exceeded 100 cm/sec hence the computation terminated. Figure 4-13a displays the record of stream function at t = 2.61 sec. We can see an obvious error which is confined to both top and bottom corners of the downstream boundary.

Therefore, the boundary values computed from the equation $\zeta = \frac{\partial w}{\partial x} - \frac{\partial u}{\partial z}$ must have introduced errors at the downstream boundary. Another error is observed in the region in front of the obstacle. It is not clear why errors at the upstream boundary and behind the obstacle

---

*Personal suggestion by Dr. E. C. Nickerson who is one of author's Ph.D. program committee.

are not generated. In order to eliminate those unreasonable values, a smaller time step was used. All previous calculations used half of the magnitude of the maximum allowable time step by the stability analysis. This time factor was reduced to 0.10. The results (Fig. 4-13b) show no improvement in the regions where large errors were observed. Several other trials were conducted and the results are given in Fig. 4-14, here maximum absolute values of horizontal and vertical velocity components are plotted with integrated physical time and if either of them reached 100 cm/sec computation was terminated. As is noted from Fig. 4-14, none of the variations tried could eliminate errors introduced both in the front of the obstacle and at the downstream boundary. Moreover the smaller time steps gave worse results, they were stable over less physical time although the number of integrations increased.

4.25 Improvements of Boundary Conditions

4.25.1 Milne prediction formula - Now it was clear that the large errors at the downstream boundary are not caused by either the size of the time step nor the scheme itself. They come from the incorrect expression for the boundary values. Initially an extrapolation method was used, i.e., boundary values were calculated from the inner value or values. Lin and Apelt (1970) used the Milne predictor formula in their computation of airflow over a fence. Stream function contour lines calculated with such a boundary condition are shown in Fig. 4-13c. The distortions at the downstream boundary were removed but we now have unreasonable disturbances at the upstream boundary. Since the physical time is 2.83 sec and velocity is 20 cm/sec and positive it is not possible to conclude that these disturbances were introduced

by waves propagating backward from the obstacle. Lin and Apelt (1970) also experienced a similar distortion at the upstream boundary when numbers of integration was increased.

4.25.2 Periodic (cyclic) boundary condition - The next attempt involved the use of a periodic boundary condition. Foldvik and Wurtele (1967) used this condition in their numerical work for airflow over a rectangular obstacle. The idea is that the flow is supposed to repeat cyclicly. Therefore all variables at the downstream boundary becomes the new boundary values at upstream boundary. The results shown in Fig. 4-13d represent correctly this condition, but as we expected, distortions introduced either at up or downstream boundary are transferred to the other boundary immediately. At this point we halted the search for alternate boundary conditions, and we examined in detail how those disturbances are introduced.

4.26 Conclusion on Boundary Condition Trials

The conclusion was that the best boundary conditions we found at lateral boundaries were

$$\frac{\partial^2 \psi}{\partial x^2} = 0, \qquad \frac{\partial^2 \zeta}{\partial x^2} = 0, \quad \text{and} \quad \frac{\partial^2 T}{\partial x^2} = 0 ,$$

which have also physical meaning as explained in the section (4.16). The conclusion was drawn from the trials of various boundary conditions described in the previous section. The Milne Predictor formula gave a reasonable value at downstream boundaries. At upstream boundaries, however, it introduced unexplained disturbances of the variables. Table 4-1 shows detail output printings of stream function, velocity components u and w and vorticity at upstream boundary and its adjacent locations.

The boundary values in the parentheses were computed from the present proposed boundary conditions. All these values are data at $t = \delta t$, namely the first output from the initial values. As we can see from Table 4-1 the proposed boundary conditions introduced fewer disturbances in all variables. The improvements were significant in velocity component w field.

A computation was conducted utilizing the lateral boundary conditions $\frac{\partial^2 \psi}{\partial x^2} = 0$, $\frac{\partial^2 \zeta}{\partial x^2} = 0$, and $\frac{\partial^2 T}{\partial x^2} = 0$. As a typical result, temperature field is presented in Fig. 15a and 15b. They show evidently complete elimination of errors at boundaries. Therefore we decided to use the proposed boundary conditions as the final ones in this study.

4.27 Nonlinear Instability

Unfortunately the disturbances produced in front of the obstacle still existed. These disturbances appear to propagate backwards against the mean flow with time as seen clearly in Figs. 4-15a and 4-15b. The speed of propagation was roughly 16 cm/sec. It is not clear why these errors did not propagate downstream (a possible explanation may be obtained from Matsuno (1966), Reference should be made to Phillips (1959) for nonlinear computational instability).

These errors are probably generated because the original equation is nonlinear and a finite difference representation has been used. Phillips (1959) described how nonlinear interactions of two waves mispresent variables in the finite difference system. Matsuno (1966) discussed computational modes which are defined as the solutions given only by the difference equations but do not exist in the original differential equations. In either case we have to eliminate physically unreasonable phenomena introduced by the numerical technique.

Hinc (1965) used as averaging technique which spreads the errors to the surrounding points. Here we tried a similar concept

$$\zeta_{j,\ell} = \alpha\zeta_{j,\ell} + \frac{(1-\alpha)}{4} \left(\zeta_{j+1,\ell} + \zeta_{j-1,\ell} + \zeta_{j,\ell+1} + \zeta_{j,\ell-1}\right)$$

where α was taken to be 0.75.

This procedure eliminated the errors in front of the obstacle as seen in Fig. 15c but it introduced new distortions at the upstream boundary. The averaging process takes extra calculation time. Moreover it was not desirable to change boundary conditions further since we found that the boundary conditions $\frac{\partial^2\zeta}{\partial x^2} = 0$, $\frac{\partial^2\psi}{\partial x^2} = 0$ and $\frac{\partial^2 T}{\partial x^2} = 0$ gave a physically reasonable representation (see section 4.16) and better computational results.

4.28 Mixed Scheme with Upstream Difference

Hence, as a result of computational expediency the computational grid was divided into two regions - one in front of the obstacle and another over and behind the obstacle. The latter region was approximated by Arakama's scheme and the upstream difference system was used in the first one. It was expected that the upstream scheme could disperse numerical errors introduced in front of the obstacle by its large numerical damping effect. Since waves are expected only on the lee side not on the upstream side of a obstacle, we should be able to see lee waves if Arakawa's scheme can represent the original differential equations accurately. Boundary conditions were $\frac{\partial^2\psi}{\partial x^2} = \frac{\partial^2\zeta}{\partial x^2} = \frac{\partial^2 T}{\partial x^2} = 0$ at both lateral boundaries.

The result of a test calculation shown in Fig. 4-16 gives pictures which do not show any computationally introduced errors. Therefore, we

continued calculations and contour lines of stream functions, vorticities and temperatures at different time of integration are shown in Fig. 4-17, 4-18 and 4-19, respectively. Here we can clearly perceive the development of lee waves behind the obstacle with time. Two waves are observed at $t = 20.84$ sec and amplitude of the first wave is about the same magnitude of the obstacle height. The wave length measured from the picture is about 76 cm which is close to 80 cm as predicted by the linear theory. Figure 4-20 shows the developments of horizontal velocity profiles at different locations with time. After $t = 15.10$ sec the velocity field does not change significantly.

4.29 Conclusion on Numerical Simulation of Strong Gravity Effects

A simple explicit upstream difference system was found by test computation to satisfactorily simulate airflow over a flat heat island in the thermal wind tunnel

This same scheme, however, failed to produce observed lee waves behind a finite height obstacle placed in the wind tunnel.

The reason is the large pseudo viscosity introduced by the upstream difference scheme which does introduce a large numerical viscosity. Arakawa's scheme was tested and found to give reasonable results.

Trial and error methods were used to find suitable boundary conditions at the up and down-stream boundaries. It was found that when the second derivatives of all dependent variables with respect to x were set zero, physically reasonable results were obtained. Finally it should be mentioned what happened if we used Arakawa's scheme to the heat island problem. The results are shown in Fig. 4-21. Apparently, large nonlinear instabilities were introduced over the heated surface for all variables, ψ, ζ and T.

Therefore, the upstream difference scheme will be utilized for the problems with surface heating (heat island, heated mountain) while Arakawa's scheme with the upstream difference method will be utilized for finite height obstacles.

4.30 Programming

In this section a brief discussion about the program itself is given. A block diagram of the program structure, instead of complicated flow charts of each program, is given in Fig. 4-22. One main and seven subroutines have been written and contour line plotting subroutines were obtained from the C.S.U computer center library. A brief description of each program follows.

Two different programs were completed, one for the flat heat island and another for mountain obstacles. The latter program can be used for the former problem if the mountain height and width were set zero.

4.30.1 Main Program "MTWAVE" - This program reads constants necessary for the calculations such as space grid size, initial time grid size, viscosity, number of grids in x and z directions, etc. All subroutines are called from this program. If any one of the subroutines give unreasonable values then the main program terminates the computation and prints out the reason. For example, if stream functions do not converge in one hundred iterations or if any velocity components exceed 100 cm/sec then the calculation is stopped.

4.30.2 Subroutine "INITIA" - All variables such as velocity components, vorticities, stream functions, and temperatures are initialized and printed out.

If the computation is the continuation from a previous run then the subroutine "INITIA" reads the required variables from punched cards. Usually one run was terminated after 300 seconds of computation time and all variables were punched on cards which become the input for the next time period. In this way complete loss of the computation is prevented although an extra time is used to punch cards. In order to complete one complete computation it requires from 300 to 1000 seconds computer time depending on the problem.

4.30.3 Subroutine "VORTI 1" - The upstream difference system is used to approximate the vorticity transport equation. The interior values and values along the boundaries $x = - L_1$ and $x = L_2$ are calculated.

4.30.4 Subroutine "VORTI 2" - The same calculation in subroutine "VORTI 1" is conducted by Arakawa's scheme combined with the upstream differences. The front region of the obstacle is approximated by the upstream system and Arakawa's scheme is used in the rest of the area. Boundary values at $x = - L_1$ and $+ L_2$ are calculated.

4.30.5 Subroutine "STREAM" - Using the vorticities just obtained from "VORTI 1" or "VORTI 2" together with previous boundary values stream functions are obtained solving the Poisson equation iteratively. When the maximum difference between the repeated iterations becomes less than a certain limit, then the values are considered to be converged. The criterion selected was

$$|\psi^{r+1} - \psi^{r}| < \quad 0.10$$

where ψ^{r+1} and ψ^{r} stands for r+1 th and r th iteration. respectively.

The number of iterations are counted and if it exceeds one hundred times then the computation is terminated. Results are printed out and contour lines are drawn by every K times of integration. At the final integration step all the values are punched on cards, which are used in a continuative run if necessary.

4.30.6 Subroutine "VELOC" - Velocity components are obtained from the finite difference definition of stream function. Interior values are evaluated by centered differences and boundary values are by forward or backward differences. Final data are printed and punched on the cards in the same manner as stream function.

Maximum values of u and w are obtained and used to determine the size of time step in the next calculation to satisfy the computational stability condition (4.15-1).

4.30.7 Subroutine "BOUNDA" - Boundary values of vorticity along the rigid boundaries are computed according to Eq. (4.16-1). Outputs are printed, contour lines are plotted, and the final values are punched on cards as for the other variables.

4.30.8. Subroutine "TEMPE 1" - Energy equation is solved by the upstream finite difference equation. Data are recorded exactly in the same manner as in "BOUNDA". Prandtl number 0.72 was used.

4.30.9. Subroutine "TEMPE 2" - Arkawa's scheme with the upstream difference system is used to solve the energy equation. The same output format is used as in "TEMP 1".

CHAPTER V

DISCUSSION OF NUMERICAL AND WIND TUNNEL RESULTS

5.1 General

In this chapter the results of wind tunnel and numerical experiments of the mountain lee-wave, the heat island, and the heated mountain problems are presented. The data has been organized into the following categories:

Case A: Airflow over a mountain,

Case B: Airflow over a heat island,

Case C: Airflow over a heated mountain.

One experiment in Case A, three in Case B and one in Case C are reported. Where possible, numerical simulation of these wind tunnel experiments was conducted. Table 5-1 shows a complete tabulation of various cases of wind tunnel and numerical simulation. Numbers following the letter, for example, B-3, indicate the number of the run in the specified case.

5.2 Airflow Over an Obstacle

In this section the order of magnitude of nonlinear fluid interactions will be examined, the characteristics of the laboratory experiments will be compared to prototype experience, and Case A-1 will be discussed.

5.2.1 An initial test calculation by the Arakawa's numerical model-

Figure 5-1 displays streamlines obtained by the program discussed in Section 4.28 when $Fr = 0.21$. The original rectangular obstacle is indicated by the double hatched region, and an effective mountain based

on a separation streamline is shown by the single hatched area. A comparison is made with Long's theoretical prediction and his water channel test. A numerical example was conducted to satisfy Long's experimental conditions, i.e., a constant temperature (density) gradient and a uniform dynamic pressure distribution far upstream.

The wave patterns obtained by the present analysis agree with Long's experimental results. The positions of wave crests and troughs have been connected by broken lines. The linearized theory predicts that the location of the first wave crests is 3/4 wave length downwind from the top of the obstacle. Almost all laboratory experiments, however, reported that the first wave crests were very much further displaced downstream (Long, 1955; Lin and Binder, 1967; Davis, 1969).

The wave length, λ may be computed according to linear theory from the relation

$$\lambda = 2\pi(F_r)_H \cdot H .$$

Wave lengths were observed to increase with height. Thus there existed a wave phase shift in the vertical direction. Wind tunnel experiments by Lin and Binder (1967, Fig. 40) noted a functional variation of wave length with height and Froude number. The present numerical model contains both features, increased wave length and phase shift with height. Nonuniformity of wave length thus makes it difficult to compare the computed wave length with that predicted by the linearized theory. In the present example, the wave length at $z = 30$ cm coincides roughly with the theoretical value of 80 cm. The difference between the present numerical model and Long's analysis is that the latter requires

a constancy of ρU^2 with height at the far upstream boundary, but the former does not. Friction terms were neglected in both cases.

5.2.2 Case A-1 - Airflow over a square obstacle (8 cm x 8 cm) is discussed. Figure 5-2 displays streamlines obtained from a smoke visualization picture taken on October 7, 1970. A five-second exposure time indicated that the flow was very steady. The smoke was dispersed very rapidly under the first wave crest by the presence of a turbulent rotor. Such motions were reported by both prototype (Queney, 1960) and previous laboratory observations (Long, 1955; Lin and Binder, 1967; Davis, 1969).

Temperature contour lines have been constructed from the temperature profiles at various locations as shown in Fig. 5-3. Isotherms taken from experiments performed on different days are superimposed to indicate laboratory reproducibility. A streamline from a smoke picture on September 30, 1970, is also shown in the same figure.

Since the measured temperature distributions were not linear with height, (see Fig. 5-7) two different Froude numbers might be computed. The lower region ($0 \leq z \leq 13$ cm) had a greater stability than the region above ($z > 13$ cm). Three different Froude numbers have been computed for each case, one for the lower layer (subscript 1), one for the upper layer (subscript 2), and one for averaged value (see Table 5-1).

A numerical experiment was performed for identical flow conditions. Streamlines and isotherms are shown in Fig. 5-4, which were enlarged from microfilm contours in Fig. 5-5. General agreement with the wind tunnel experiment was obtained. The wave amplitude in the numerical model was not so large.

Temperature profiles at various locations for both wind tunnel and numerical experiments are presented in Fig. 5-6. The location $x = 0$ corresponds to the upwind edge of the obstacle. A dashed line in each profile indicates the initial distribution provided to the numerical integration. Initial profiles can be arbitrary; however, for a faster convergence a reasonable initialization is desirable. An averaged temperature distribution for the clean wind tunnel field was used as an initializing distribution (Fig. 5-7). Data at $x = -60$ and -20 cm in Fig. 5-6 show clear evidence of upstream flow modification by the existence of an obstacle. Numerical temperature distributions at $x = 12$, 16, and 20 cm appear to simulate regions of overturning instability $(\frac{\partial T}{\partial z} < 0)$, where the flow was supposed to be very unstable. According to Long's analysis (1955) this region should correspond to a reversed flow area.

The existence of turbulent motion under the first wave crest can be seen from the temperature profiles at $x = 48$, and 60 cm. Experimental results at these locations show constant values near the ground as a result of strong turbulent mixing. The numerical model failed to simulate the phenomena in this region primarily due to insufficient numbers of grid points near the ground where the temperature varies rapidly.

A detailed examination of the flow field immediately behind the obstacle is shown in Fig. 5-8. The square obstacle is indicated by a double hatched area, and the effective mountain is represented by a single hatched region. A streamline and the observed flow directions are as indicated. Velocity profiles at $x = 12$, 40, and 60 cm were obtained from smoke wire photographs. The velocity distribution

sketched at $x = 12$ cm represents an average from two pictures taken three minutes apart. Both pictures presented similar profiles; therefore, the result shown here seems to be very reliable.

The measured temperature field behind the obstacle shows a very complicated picture (see Fig. 5-9). Temperature data at all points measured in the experiment are available in Table 5-2.

The motion inside the separated region (or core) was quite different from that observed for neutral density flows. Velocity close to the surface was positive, a negative flow was observed above it, and the flow reversed again outside the core (see Fig. 5-8). The temperature distributions at $x = 12$, 16, 20, 24 and 28 cm also exhibit alternative positive and negative gradients.

This peculiar motion may be easily explained. A fluid particle trapped into the core region originates at some high temperature level (Fig. 5-3). The particle is less dense than the surrounding strata, and thus buoyancy forces drive a counterclockwise circulation.

5.3 Results and Discussion of Heated Island Effects

In a heated island phenomenon the surface temperature is a result of the total heat energy balance, including insolation, heat conduction into a soil layer or a building, convection and radiation to the atmosphere, etc. Since the above mechanism is complicated and not yet fully understood, it is convenient, in constructing a model, to specify a priori the surface temperature as a function of space and time. The daily change of the surface temperature is well described by a simple function such as a Fourier series with a small number of terms (Lönnquist, 1962). Since the purpose here was to simulate the basic

fluid phenomenon and not its time-dependent characteristics, a constant value for the temperature of the heated surface was selected in all cases.

Extensive temperature surveys in the wind tunnel were conducted to draw accurate isotherms over a heated area. A thermocouple-mounted rake was set along the centerline of the wind tunnel. Vertical measurements were made utilizing nine thermocouples of fixed heights, mounted on the rake (Fig. 3-6). In the horizontal direction different intervals were selected, depending upon the horizontal temperature gradient; over the approach region to the island a coarse interval of 4 cm was used, while over and in the leeward vicinity of the heated plate, the increment was decreased to 2 cm. For the far downstream fetch ($x > 40$ cm), the 4 cm interval was used.

Less extensive velocity measurements were obtained. The difficulty in measuring such small velocities in a temperature-stratified flow has already been described in Chapter III. The smoke-wire technique gave a very fast and clearly visible result in some regions. However, when the area of interest was located in turbulent flow regions (over the island, under the crest of lee waves, and close to the surface) smoke released from the heated wire dispersed rapidly due to the mixing effect of turbulence; hence the smoke trace on a picture was very poor. Therefore, construction of streamlines from a measured velocity field was not possible.

Flow visualization of streamlines using $TiCl_4$ streamers was attempted; however, results were only partial since, due to the very small basic wind speed, it was not possible to neglect the weight of the smoke.

Three heat islands were studied experimentally and numerically to investigate the effects of the intensity of heating at the island and of stability in the basic current. The Froude numbers shown in the figures are the averaged values of lower and upper regions. It is necessary to characterize the intensity of heating of different urban situations. It appears to be difficult to arrive at a parameter which does not contradict some prior usage or intuition. A non-homogeneity parameter is proposed here whose variations will be discussed when laboratory and numerical results are obtained. One example will be given in section 5.3.4 to evaluate this parameter for a prototype observation of a heated island effect.

The non-homogeneity parameter introduced here is:

$$N_h = \frac{-\left(\frac{\partial T}{\partial z}\right)_{z=0}}{\frac{T_{island} - T_o}{L}} ,$$

where T_{island} and T_o are the temperature at the island and that of the surrounding surface, respectively. Temperature gradient over the island, $-\left(\frac{\partial T}{\partial z}\right)_{z=o}$, was taken from the experimental data at the center of the island. L is the width of a heated region. Additional information about flow conditions, such as basic wind speed, stability, wave length, viscosity, etc., are available in Table 5-1. Cases B-1 and B-2 had the same basic wind speed and stability (thus the same Froude number), but the intensity of heating varied (different N_h number). Case B-3 had a stronger stability but the same current of 6 cm/sec. Case B-3 also had the highest temperature excess of the

three cases, but the N_h number was approximately the same magnitude as in Case B-1. Each numerical computation was conducted under the same flow conditions as in the corresponding experiment. The following sections describe the results of each case separately.

5.3.1 Case B-1 - The Froude number was 0.100 which was averaged from values of 0.065 and 0.134 in the lower ($0 \leq z \leq 9$ cm) and upper ($z > 9$ cm), regions respectively. Isotherms of 295, 300, 302, 303, and 305^{o}K were drawn from the vertical temperature distribution at various locations. The result is shown in Fig. 5-10, together with velocity profiles in the vicinity of the island. The equivalent thermal mountain shape was computed from the linear theory given in Eq. (2.2.2.7-2). The height increased exponentially from 0 at $x = 0$ to the maximum height, 1.15 cm at the downward edge of the island ($x = 8$ cm). The height then decreased exponentially through the values of 1.14 cm, 1.05 cm, and 0.76 cm at $x = 15$, 50, and 200 cm respectively. The theoretical equivalent mountain had a very flat and broad structure more like a plateau than a step change mountain. Computation of the equivalent mountain height was based on the following initial conditions;

$\Delta T = 47.6^{o}K$,

$\overline{T} = 296.8^{o}K$,

$S_1 = 2.422 \times 10^{-3}$ cm^{-1} (stability in the lower region, $z \leq 8.9$ cm),

$U = 6$ cm/sec,

and

$K = 0.2$ cm^2/sec (kinematic viscosity).

The concept of the equivalent mountain can be applied only in the upper regions where the direct effect of heating from the island is negligible. In the present case it appears that the region is above $z = 15$ cm. The displacement of the $303^{o}K$ temperature contour line was about 8 cm. This is too large for the mountain height of 1.15 cm obtained theoretically from linear theory.

Existence of the basic current destroyed the symmetric thermal plume behavior which is seen in the field when there is no prevailing synoptic current (Delage and Taylor, 1971). The thermal plume over the island was swept streamward, and the isotherm structure was also displaced to the wind direction.

The velocity profiles at $x = 3$, 12 and 20 cm, as reduced from smoke wire photographs, are shown in the same figure (Fig. 5-10). The profile at $x = 3$ cm indicates a strong surface wind accelerated by a counterclockwise sea breeze circulation at the windward edge of the island. This sea breeze motion introduced a strong negative velocity at the upper levels. Interaction with the basic current resulted in a weak negative flow as indicated in the figure. The surface currents in the lee side of the island were reversed; this indicates that the negative flow induced by the sea breeze circulation (generated by the temperature difference at the end portion of the heated island) was stronger than the basic wind. Further, the return currents of the sea breeze motion magnified the positive horizontal velocity component.

$TiCl_4$ smoke was introduced at the surface about 50 cm downwind from the heated plate (see the photograph in Fig. 5-10). Smoke was propagated backward against the basic current and rotated upward

at the lee side of the island. Then the smoke trajectory separated into two directions - one traveled upstream and the other downstream.

The flow directions are shown by arrows added to the picture. These coincide with temperature and velocity measurements discussed above.

A numerical simulation under the equivalent flow condition was conducted. The temperature of the island, however, was set at $320^{o}K$, whereas the laboratory measurement indicated $341^{o}K$. The justification for this variation is as follows. The laboratory model developed very strong temperature gradients in the surface region over the heated island, especially between the surface and the first point from the surface ($z = 0.635$ cm). This effect cannot be represented by the numerical model because minimum grid size is 4 cm. Therefore, an effective surface temperature was obtained by linearly extrapolating the first two values from the surface. Justification of this boundary condition approximation depends, of course, on the comparison of the numerical results with the laboratory measurement.

The computed stream function, vorticity, and temperature contour lines at $t = 27.11$ sec. are provided in Fig. 5-11. The streamline shows a closed region behind the island starting at the lee edge of the heated plate; this region corresponds to the shape of the equivalent thermal mountain. (This interpretation of the equivalent mountain from a separated streamline is one similar to that adopted in the field observation by Garstang et al. (1965), where a trajectory of a balloon released at the surface of the island was used to compute the thermal mountain height). Now we can see definite evidence of a thermal mountain induced by a heated island.

Its shape is broad as predicted by the linear theory, but the height is considerably higher (14 cm) than the theoretically predicted value (1.15 cm). In the theoretical evaluation of the thermal height, only the viscosity was an assumed value; the rest of the input values were obtained from the laboratory measurements. It has been mentioned that locally strong turbulent areas were observed over the heated island; thus, the turbulent mixing effect must be included in the numerical analysis.

A calculation was reversed to evaluate effective K values for the numerical model of the laboratory flow conditions and the thermal mountain height which was obtained from a computed separate streamline. In Fig. 5-12 the relation:

$$M(x = 8) = \frac{\Delta T}{s\overline{T}} \left(1 - e^{-\frac{K}{U}\frac{gs}{U^2}x}\right),$$

is plotted, where $M(x = 8)$ is the height of the equivalent mountain at $x = 8$ cm. From the figure K appears to be 2.7 cm^2/sec, which is 14 times larger than the assumed value. This suggests that any numerical analysis which hopes to be exact must incorporate the variations in turbulent mixing introduced by the unstable thermal mechanisms.

Both the laboratory and the numerical heated island models predict rotation of the flow stream upward at the lee edge of the island and a maximum height at $x = 28$ cm, whereas the linearized theory for the heated island suggests that the equivalent mountain rises abruptly from the upstream edge of the island and the maximum height is attained at the lee edge of the island. Thus, the numerically computed mountain

was displaced downstream. Vorticity contour lines indicate a pair of sea breeze circulations at both edges of the island. These cells are also convected downstream by the basic wind.

Isotherms in Fig. 5-11 reproduced many features described previously in the discussion of the experimental temperature measurements. The central region from $x = -20$ to 60 cm and $z = 0$ to 40 cm has been enlarged in Fig. 5-13 for a direct comparison with the wind tunnel result. A strong thermal plume with inclined axis is observed, but the temperature contour lines in the upper region do not show as a strong variation as that seen in the experiment.

To provide a detailed and direct comparison with experimental results, the numerically computed values of temperature have been added to the plottings of experimental vertical temperature distributions (see Fig. 5-14). Measured values are connected by a solid line and solid circles indicate the computed values. A dashed line indicates the initial temperature distribution in the numerical model. Both results are in close agreement, except in the region close to the island where temperature varies so rapidly that the numerical model, being limited to a finite number of discrete points, is incapable of resolving small scale perturbations between adjacent grid points. From $x = 14$ cm downstream numerical and experimental temperatures coincide very well.

Experimental temperature distributions over and just leeward of the island show different characteristics from the rest of the locations: thermal profiles vary taking maximum and minimum values rather than monotonically increasing with height. Let us define the inversion haze as the point at which a minimum temperature first occurs. This haze height increases with distance x to 1.3, 2.4, 2.9,

5.0, 7.7, and 12.7 cm at $x = 0$, 2, 3, 6, 8, and 10 cm, respectively. These results explain part of the mechanism which creates "elevated inversions" observed over urban areas. In the prototype urban heat island phenomenon, a multi-leveled set of elevated inversion layers are observed. These additional layers may result from the radiation balance to urban pollutant haze.

Another interesting phenomenon observed in these measurements is a "thermal cross over". The "cross over" phenomenon occurs when temperatures at some height over a city take smaller values than those over the upstream rural area, i.e., there is a cooler region over the heated island before it matches with upstream temperature at some greater height. Temperature perturbations about the upwind norm, chosen as that at $x = -20$ cm, are plotted in Fig. 5-15; cooler regions are observed above $z = 15$ cm at $x = 12$ and 20 cm. Measured temperature values are tabulated in Table 5-3.

Numerically computed velocity components u and w are displayed in Fig. 5-16, and may be compared with experimental results in Fig. 5-10. Sea breeze effects are again clearly evident in the surface area. Profiles indicate very complicated features: positive and negative values, minimums and maximums. Stern and Malkus (1953) derived from the linearized theory the height at which a sea breeze reversal occurs on the windward side of the island:

$$h = \frac{1}{2}\pi\left(\frac{gs}{U}\right) - \frac{1}{2} .$$

The order of magnitude of sea breeze perturbation was

$$u' = \frac{g\Delta T}{\bar{T}} \frac{2}{\pi} \frac{K}{U^2} \ln \frac{U^2}{K(gs)^{1/2}} \quad .$$

The predicted values for Case B-1 are $h = 7.8$ cm and $u' = 4.7$ cm/sec. The complete numerically solved equation developed $h = 10$ cm and $u' = 3$ cm/sec.

Vertical velocity profiles in Fig. 5-16 indicate that there existed a strong updraft over the heated area, but that the return downward current was very weak with a wide horizontal extent.

5.3.2 Case B-2 - To examine the effect of heating intensity upon the airflow, the surface temperature excess was increased to 84^{o}K. The equivalent mountain height predicted by the linear theory Eq. (2.2.2.7-2) was 2.02 cm, an increase of 76% over the previous case.

Figure 5-17 presents wind tunnel temperature and velocity measurements. General features are similar to the previous results shown in Fig. 5-10. In this case, however, the thermal plume penetrated more deeply into the basic current and larger variations of the isotherms were observed. The amplitude of the 306^{o}K contour line was about 14 cm, while the maximum variation of the previous case was 10 cm. Since the air over the heated island was displaced upward considerably, a formation of cumulus clouds might be seen over its atmospheric equivalent if the air had enough moisture to condense. The cross over effect will be experienced traversing horizontally at height 30 cm from left to right in the figure. At first a high temperature is encountered until directly above the leading edge of the heated island. Next a cooler region exists up to about $x = 25$ cm or directly over the island; then a high temperature region again appears until the environment

finally returns to the original temperature at $x = 60$ cm. Table 5-4 includes all information necessary to construct isotherms in Fig. 5-17.

Velocity profiles in the same figure indicate a deeper sea breeze circulation than in Case B-1. Over the island a strong wind with negative flow above it was again observed. Therefore the wind profile at this location had at least two maximums and one minimum. These were generated by the interactions of stratification of the air, sea breeze circulation induced by the heated plate, and the basic current. Negative flow downstream of the island extended about 20 cm upward and more than 60 cm horizontally.

A numerical simulation of the experiment was conducted with the same flow characteristics, except that the temperature at the island was $341^{o}K$ rather than the measured value of $377^{o}K$. The argument justifying this modification has already been mentioned in the discussion of the previous Case B-1. Stream function, vorticity, and temperature contour lines at $t = 17.42$ sec are plotted in Fig. 5-18. A dividing streamline separated from the lee edge of the island, reached a maximum height of 28 cm at around $x = 40$ cm, and subsequently decreased its height gradually. Inside of this streamline was a closed region, which may correspond to an equivalent thermal mountain, whose height was again very large compared to the linear theory's predicted value of 2.02 cm. Utilizing the evaluated displacement value of 28 cm from the streamline contour, the value of the effective viscosity was computed as before. Figure 5-12 indicates that K was 6.3 cm^2/sec. which is more than 30 times larger than the kinematic viscosity, and about three times as large as the previously obtained value. Thus Case B-2 may have developed greater vertical turbulent mixing than Case B-1.

Computed horizontal velocity profiles are plotted in Fig. 5-16 for comparision with those obtained in Case B-1. The effects of the higher level of heating are seen in the stronger perturbed profiles and deeper sea breeze circulations.

Two large vorticities of opposite sign were again well developed over the island; both vorticities were bent streamward because of the basic current (see Fig. 5-18).

Computed isotherms in the same figure indicate many features similar to those of the wind tunnel experiment. But a quantitative comparison shows that agreement of the vertical temperature distributions (Fig. 5-19) is not as close as in case B-1.

Several reasons might be proposed to explain variations between the numerical and wind tunnel experiments: (1) since the island was heated more intensely in Case B-2, an extended region of turbulent motion developed which prevented the present programming from simulating the phenomenon, (2) the effective island temperature was not properly estimated for the numerical experiment, and (3) the computed flow field was still developing while the wind tunnel results were at quasi-steady state. The most probable explanation seems to be either (1) or (2), since (3) may be eliminated from the result shown in Fig. 5-20, where time variations of the maximum absolute velocity components u and w are shown. They increased rapidly from their initial values and continued to grow until $t = 15$ sec, after which they remained at constant values of $|u|_{max}$ 14 cm and 16 cm of $|w|_{max}$.

Both numerical and wind tunnel experiments simulated the effect of an introduction of an intense energy source. They reproduced the deep penetration of the heat plume, the large variation of isotherms,

the intense development of a sea breeze circulation, the development of turbulent motion, and the complicated velocity profiles.

5.3.3 Case B-3 - In this case both stability and surface temperature were varied from the previous two cases in order to examine the effect of stability. The average Froude number was 0.064 as against 0.100. The same basic wind of 6 cm/sec was retained. Stronger stability effects are seen in Fig. 5-21 where measured isotherms and velocity profiles are plotted. Smaller penetration of the thermal plume in comparison with Case B-2 was due to the much smaller Froude number in spite of the surface temperature increase to 412^{o}K from 377^{o}K. Case B-3 (Fig. 5-21) displays a very similar isotherm pattern to that of Case B-1 (Fig. 5-10). The counteraction of the more intense surface heating was a result of the more stable free stream retarding forces. This result underlines the necessity of using two different parameters to characterize the flow - one for the stability of the basic flow (Froude Number), and another to specify the heat island intensity (non-homogeneity parameter). The N_h numbers in Cases B-1 and B-3 were nearly equivalent; the Froude number in Case B-3, however, is smaller than that in Case B-1, resulting in less plume penetration. In fact, the scale of the sea breeze circulation in Case B-3 is about 40% smaller than that in Case B-1. Table 5-5 includes all the measured values of temperatures from the wind tunnel.

Numerical results are provided in Fig. 5-22. Estimated equivalent mountain height from a separated streamline was 24 cm, about ten times as large as the theoretically predicted value of 2.42 cm. Reverse calculation of K from the evaluated mountain height was

2.30 cm^2/sec from Fig. 5-12. Both numerical and wind tunnel results of vertical temperature distributions are provided in Fig. 5-23. Generally they agreed quite well except in the area close to the heated island where strong turbulent motions were observed.

5.3.4 Comparison with prototype observations and other studies - Agreement of the results presented here with observational data (Stern and Malkus, 1953, Fig. 4, p. 111 and Fig. 6, p. 112; Fosberg, 1967, Fig. 2 on p. 893; Bornstein, 1968, Fig. 3, p. 578; Spelman, 1969, Fig. 9 on p. 116) is strikingly close. In each case the larger the Froude number and the larger the non-homogeneity parameter, the more deeply a heat plume penetrates into the atmosphere. There also exists an unstable region over the island, and isotherms display wavy configurations (see Fig. 5-17). The crest of an isotherm wave is always displaced streamward for larger Froude numbers and/or smaller N_h values (see Figs. 5-10 and 5-21 in the present results and Fig. 9 in Spelman (1969)).

Observational data described in Chapter II include extremely small Froude number flows. In Table 2-4 Malkus' (1955) observations indicate the largest Froude number, 0.06, for which a formation of cumulus cloud was observed. A very crude calculation was conducted to evaluate the N_h number, a heating intensity, for Malkus' observation. An island surface temperature excess of $1.5^{o}C$, an island width of 80 km, and a temperature gradient at the surface of $-0.3 \times 10^{-3}\ m^{-1}$ were utilized to obtain $N_h = 16$. In the present study, Case B-3 has $Fr = 0.064$ and $N_h = 5.65$ which are approximately the same order of magnitude. Both results (Fig. 7 in Malkus and Fig. 5-21 in the present study) display many common features; however, the wave crests of the isotherms in the present study were displaced more

streamward than those observed by Malkus. In the latter case a stronger blocking effect developed because of its larger N_h number.

5.3.5 A direct measurement based on the predicted (linear theory) equivalent mountain in Case B-3 - In the previous sections, both experimental and numerical results in all cases indicated that the linear theory might have underestimated the thermal mountain height. It is not certain, however, that the interpretation of the equivalent mountain from a separated streamline has a sound physical meaning. Therefore a direct examination of the concept of an "equivalent thermal mountain" proposed by Stern and Malkus (1953) has been attempted. Case B-3 provided the highest equivalent mountain in this study. The thermal mountain suggested by linear theory started at the leading edge of the island. The heights increased almost linearly to 2.42 cm at the end of the island, then decreased exponentially; 2.2 cm at $x = 30$ cm, 1.67 cm at $x = 100$ cm, and 0.74 cm at $x = 300$ cm. In the experiment examined here a simpler mountain form with a 4 cm height plateau and a short transition nose was used, as shown in Fig. 5-24. The flow conditions were maintained as in Case B-3. The isotherm plottings are also available in Fig. 5-24. A comparison with Case B-3 (Fig. 5-21) immediately indicates that the linear theory has grossly underestimated the equivalent mountain height. The reason may be the incorrect estimation of K values (viscosity of value 0.2 cm^2/sec was used to evaluate the mountain height). Recall that the numerical simulation predicted the mountain height of 24 cm and an effective $K = 2.3$ cm^2/sec in the vicinity of the island.

On the other hand Garstang et al. (1965) concluded that, according to their observations, the linear theory overestimated the equivalent mountain heights. Thermal mountain boundaries have been determined from the zero lift balloon trajectories released at the upwind leading edge of the island. Theoretical effective mountain shapes were computed from

$$M = \frac{\Delta T}{\Gamma - \gamma} \quad (1 - \frac{1}{e}) \ ,$$

which has a constant height over the island. Here an eddy diffusivity term does not appear because the shape factor x_o is so small, compared with the island width, that the effect of K can be neglected.

The discrepancies between the linear theory and the observations may result from the difficulty of a correct estimation of eddy diffusivity and the uncertainty about whether a balloon trajectory represented the equivalent mountain concept division by Stern and Malkus (1953).

5.3.6 Case B-3 in neutral stratification - As an extreme case, all stable stratification effect was eliminated in Case B-3. A slight surface inversion was introduced by the cooled aluminum ground plate.

The resultant isotherms are shown in Fig. 5-25. The computed N_h number was 10.22 - double that in Case B-3. The plume caused a strong blocking effect and deep sea breeze circulations.

Vertical temperature distributions are given in Fig. 5-26. An elevated inversion as high as 24 cm is seen at $x = 16$ cm. Profiles at $x = 0$, 4, and 8 cm indicate strong mixing by turbulence.

5.4 Airflow Over a Heated Mountain

5.4.1 Joint influence of heating and obstacles - It is interesting to investigate the combined effect of topography and heating. For example, buildings in a city may maintain higher temperatures than the surrounding grounds because the building materials have a higher heat conductivity which enables them to store more heat energy during the day. A mountain in a coastal area may have higher surface temperatures than the ocean during the day (Fosberg, 1969). Islands in the ocean may have topographic effects in addition to those of the temperature differences. The linearized heated island theory was developed to investigate effects of surface temperature excess upon airflow. Stern and Malkus (1953, p. 119), however, suggested that a heated mountain solution might be obtained by superposing solutions for a physical mountain and an equivalent thermal mountain. This superposition procedure is mathematically correct as long as the linear theory holds. Both mountain and heated island phenomena are not, however, linear problems, as proved by both prototype observations and wind tunnel experiments. Spelman (1969, p. 126) concluded in his numerical modeling of a heated mountain phenomenon that the combined effects of surface heating, topography, and roughness produced a greater disturbance in the mixed layer than any of the individual surface features acting alone. Specifically terrain, roughness, and temperature excess, respectively, produced +25, -15, and +400 m displacements at the lee side of the surface nonuniformity. A combination of the above three factors resulted in a 575 m displacement, a much greater effect than the superposed value of 410 m. Similar results in wind tunnel experiments support the actual importance of the nonlinear characteristics.

5.4.2 Case C-1 - An experiment demonstrating airflow over a non-heated obstacle was first conducted. Flow conditions equivalent to those in Case B experiments were used, i.e., a $(\overline{Fr})_H = 0.100$ was obtained from $u = 6$cm/sec, and $\overline{s} = 1.5 \times 10^{-3}$ cm^{-1}. A flow visualization picture by $TiCl_4$ smoke is seen in Fig. 5-27. A streamline sketch was made from the photograph for a better illustration. There existed several characteristic flow regions; at the surface downstream of the obstacle, turbulence was observed where smoke mixed uniformly and propagated upstream. A dark region in the photograph indicates a high velocity layer, thus smoke was convected dowstream in a wavy trajectory. A stagnation area was found between the high speed region and the ambient area. The wave length observed is about 20 cm. The linear theory predicted value of 25 cm.

Isotherms are shown in Fig. 5-28 as constructed from vertical temperature distributions displayed in Fig. 5-29. Table 5-7 incorporates all measured temperature data. The temperature contour line for 300 K exhibits wave-like motion equivalent to that found in Fig. 5-27. Thus isotherms must approximately represent streamlines. Streamlines are displaced upward just above the obstacle; i.e., the maximum displacement occurs directly over the mountain. All experiments for Case B had similar flow patterns and the results showed that the maximum displacement of the isotherms always occurred at $x = 12$ to 22 cm (see Fig. 5-10, 5-17, and 5-21). Therefore a thermal mountain produced by a surface temperature excess does not necessarily remain over the heated area. Both Spelman's (1969, Fig. 9, p. 116) and the present numerical results (Fig. 5-11, 5-18, and 5-22) suggest this behavior, while the linear

theory requires that an equivalent mountain starts at the leading edge of the island and attains a maximum height at the end of the island.

To develop the effect of a heated mountain, an aluminum obstacle was heated by six electric heaters attached inside of the obstacle. Surface temperature was maintained at 310 K, $20^{o}C$ higher than the floor temperature. Streamlines were visualized by smoke (see Fig. 5-30).

An experiment for a heat island with a temperature excess of exactly $20^{o}C$ was not examined. However, results for a similar flow condition at a low level Froude number = 0.070 (here 0.065) and $\Delta T = 18^{o}C$ did not have any appreciable effects on the airflow. No influence of the heating was detected as low as 5 cm above the island. Therefore, it may be reasonably concluded that heating alone did not create any appreciable disturbance of the basic flow.

A comparison of Fig. 5-30 with Fig. 5-27, however, displays an order of magnitude larger streamline displacements because of the coupled influence of an obstacle and heating. The lowest streamline sketched in Fig. 5-27 is displaced upward about 18 cm in Fig. 5-30. Thus, linear superposition to evaluate the combined effect of heating and topography is not permissible. Figure 5-31 and Fig. 5-32 display isotherms and vertical temperature distributions, respectively. Above the heated obstacle unstable areas were observed. All temperature data are available in Table 5-8. Numerically computed isotherms shown in Fig. 5-33 reproduce the experimental features in Fig. 5-31. Other variables computed are plotted in a contour line; they include stream function, vortex, and velocity components u and w (see Fig. 5-34).

5.5 Three Dimensional Airflow Over a Heated Island (Experimental)

5.5.1 Influence of y direction inhomgeneity - Surface inhomogeneities in a longitudinal direction only, as discussed in the previous chapters, are exceptional cases in nature. Fortunately the assumption of two-dimensionality does not remove the possibility of examining many interesting general effects of heating and topographic discontinuities. However, the horizontal convergence of wind into an urban area (Okita, 1960; Pooler, 1963) cannot be explained by a two-dimensional treatment. Horizontal temperature observations in an urban area, as reported elsewhere (Duckworth and Sandberg, 1954; Kopec, 1970; Preston-Whyte, 1970), always display distorted but usually concentric isotherm patterns centered somewhere near the central business district.

Very few theoretical studies are available due to the mathematical difficulty of solving a set of the nonlinear three-dimensional governing equations. Olfe and lee (1971) did utilize a linear perturbation technique and managed to provide analytical expression for temperature perturbation over a circular heated area. The solution was obtained by superimposing the results from two-dimensional airflow over a heated island where the temperature was distributed in a mountain shape. If the cross section of this profile is rotated $\pm 90^{o}$ a three-dimensional heated island will be constructed. Thus the superimposed solution obtained from the integration of the two-dimensional solutions from -90^{o} to $+90^{o}$ represents a three-dimensional flow. Their result suggests that there will be no significant differences from previous two-dimensional solutions, yet slightly larger temperature perturbations were obtained in the three-dimensional case.

Estoque and Bhumralkar (1970) constructed a three-dimensional numerical model which had a grid system of 15 x 5 x 14 in the x, y, z directions respectively. They provided a comparison only of the lateral velocity component for the two-and three-dimensional configurations. Their results indicated that larger magnitudes of lateral velocity components were obtained in the latter case. Here an attempt has been made to reveal differences between the two configurations in a wind tunnel laboratory experiment.

5.5.2 A wind tunnel experiment of airflow over a rectangular heated area - A rectangular area 30 cm x 8 cm was heated as shown in Fig. 5-35. $TiCl_4$ smoke was released at two locations on the floor symmetric with respect to the central axis of the wind tunnel, in order to display the unique effect of lateral convergence.

The observed flow trajectories are as follows (see Fig. 5-35): smoke started from A, followed a curve ABC, and at point C a vertical vortex which lifted smoke upward was observed. The vertical vortex is bent streamward by the background flow field. Another vortex was observed along the lateral boundaries of the heated plate. It was initially generated in a manner similar to the development of a sea breeze when the synoptic flow is along the coastline.

The vertical vortex formation observed here is that often seen in the motion of dust or leaves behind a building on a windy day. Therefore a heated area seems to have acted as a physical obstacle; this supports the concept of a thermal mountain.

The natural occurrence of a vertical vortex motion in the atmosphere, such as a fire whirl is the result of the simultaneous presence of ambient vorticity and rising air (Emmons and Ying, 1966). Here the

three-dimensional heated island has apparently provided the two conditions; i.e., the ambient vorticity was created by the thermal mountain, and heat energy from the island heated the air and raised it. Therefore it might be concluded that the rectangular high temperature region reproduced a mechanism similar to natural whirls in a wind tunnel.

Figure 5-36 displays horizontal temperature isopleths at three different heights. At $z = 1$ cm from the floor, isotherms have shapes symmetric about the heated area, but at $z = 5$ cm their upwind edges are tilted downstream because of the finite extent of the heated area in the y direction. Moreover the center of the distribution was displaced about 5 cm downwind from the center of the heated area. Displacement of the maximum temperature region by the general flow field from the central business district (which had the highest surface temperature) has often been reported (Sundborg, 1950; Preston-Whyte, 1970). A relatively weak temperature gradient in the direction of increasing temperature and a sharp gradient as temperature again declines is observed at $z = 5$ cm. This may correspond to a hydraulic jump phenomenon over an obstacle. At $z = 10$ cm less than a $1^{o}C$ temperature difference is encountered, except over a limited region along the centerline of the island.

Isotherms in vertical planes parallel to the flow direction are constructed at several locations on the y axis. They are constructed from vertical temperature distributions measured at many locations in the x direction (shown in Fig. 5-37) and $y = 0, \pm5, \pm10, \pm13, \pm15, \pm17$ and ±20 cm. Although distributions were symmetric with respect to the $y = 0$ plane, there existed

large differences very close to the center plane where the flow was very unstable. Therefore values averaged from the corresponding two symmetric planes in the positive and negative y direction were utilized to construct isotherms in Fig. 5-37.

Stronger gradients of the approach isotherms are noted for three-dimensional islands; this contrasts with two-dimensional cases where the gradients were almost horizontal (Fig. 5-10, Fig. 5-17, and Fig. 5-21).

One such example in the atmosphere is provided by comparing Fig. 10 with Fig. 19 in Malkus and Bunker (1952). The former figure shows a stronger horizontal gradient in isotherms which was observed in more three-dimensional flow situation than that in the latter figure.

Olfe and Lee (1971) computed from their linearized analytical model temperature perturbations both for two and three-dimensional cases. The same tendency, i.e., higher temperature perturbations in three-dimensional flow, was obtained (see Fig. 5 in Olfe and Lee).

An immediate explanation of the isotherms' behavior is not apparent; however, the following argument might be reasonable: Isotherms removed from the heated island are usually considered to closely represent streamlines. Therefore it might be sufficient to give a physical explanation for a stronger dipping of the approach flow streamlines in the three-dimensional model. The most significant difference between the flow fields in two-and three-dimensional configurations is the existence of the lateral component of a velocity, i.e., air flows not only across the island but also toward either side of the island. Because of the finite extent of the island in the y direction, the cooler surface regions beyond the side boundaries of the heated island

do not have any blocking effects on the flow. They might act as sinks in comparison with the area over the heated island where strong blocking effects are imposed on the flow. Thus when a portion of the approach flow is sucked to the sides, streamlines may abruptly dip. An excellent example of a blocking effect of an obstacle on a two-dimensional flow into a line sink is given in Yih (1965, p. 82-94).

CHAPTER VI

CONCLUSION

In this report four different categories of flow are investigated in a thermal wind tunnel:

1) Airflow over an infinitely wide obstacle,

2) Airflow over an infinitely wide heated island,

3) Airflow over an infinitely wide heated obstacle, and

4) Airflow over a heated island with a finite width.

The first three categories are two dimensional aspects of prototype phenomena: a mountain lee-wave, an urban heat island, and a heated mountain, respectively. The last displays a three dimensional feature of a corresponding urban heat island phenomenon. Numerical models were constructed for the first three cases. However, for the three dimensional problem, only the wind tunnel experiment was conducted since a numerical integration for such a three dimensional problem is not practical yet.

1) Both laboratory and numerical results showed close agreement. They indicated strong nonlinearity; perturbation quantities could not be neglected compared with their mean values especially in the vicinity of the disturbing source (obstacle, heated area), and a linear superposition rule could not be applied to predict the solution of combined effects of heating and topography.

2) The present results were compared with a linearlized theory by Stern and Malkus (1953). Definite evidence that a thermal mountain is generated by a heated island was observed; however, the shape and the position of the maximum height of the observed equivalent mountain were

different from that predicted by linear theory. Both observed and numerically computed thermal mountains were displaced downstream depending on the scale of the basic current, whereas the linear theory predicts that the effective mountain will always start at the leading edge of the island and attain its maximum height directly above the lee end of the island.

3) Some characteristic features of urban heat island effects were simulated qualitatively both in a wind tunnel and by numerical computation. Both results displayed the less frequent surface and the more frequent elevated inversion layers over a city. A heat cap or a heat plume is projected into the atmosphere which introduces a wavy motion over the city. As a result, temperature cross over (cooler temperature over the city) is observed over the heat island. Moreover a downward wind and an acceleration of a horizontal velocity in the surface layer of the approaching flow to a city were also reproduced.

4) An experimental result of a three-dimensional heated island has shown several different features from those observed in two-dimensional cases. Among them the following are significant:

(1) Horizontal convergence of wind, and

(2) Development of longitudinal vortexes along the lateral boundaries.

A simultaneous occurrence of a formation of vertical vortexes behind the heated area and rising air provided a similar mechanism of a generation of a fire whirl in the atmosphere.

5) It is proposed to utilize a non-homogeneity parameter to characterize a heating intensity in heated island problems in addition to a Froude number. A complete justification to use this number as a

similarity parameter, however, cannot be given until more reliable comparisons of prototype and laboratory observations are made.

6) The complexities of analytical solutions introduced by a set of nonlinear partial differential equations are resolved by the use of a direct numerical integration on a digital computer. Additional advantages, over an analytical treatment, of the numerical approach suggested by this research are that:

(1) arbitrary upstream conditions are rather easily given;

(2) more realistic expressions of diffusion terms may be included,

(3) arbitrary expression of time dependent heating and cooling of the surface are possible,

(4) in principle more complicated topography can be programmed, and

(5) uniqueness of the solution is assured by the time dependent treatment.

7) The numerical program as justified through wind tunnel experiments may be applied directly to predict atmospheric phenomena discussed here (a mountain lee-wave, an urban heat island, and a heated mountain phenomena) with minor changes of boundary or initial conditions. If eddy diffusivities, however, take special functional forms rather than the constant values assumed here, then it is necessary to modify the finite-difference expressions for the diffusion terms. Wind tunnel results for urban heat island phenomena may be used for quantitative predictions of the corresponding atmosphere if conclusion (5) is accepted.

BIBLIOGRAPHY

BIBLIOGRAPHY

Angell, J. K., Pack, D. H., Dickson, C. R., and Hoecher, W. H., 1971; "Urban Influence on Nighttime Airflow Estimated from Tetroon Flights," J. Appl. Meteor., 10, pp. 194-204.

Apelt, C. J., 1969; Lecutre notes distributed in summerschool, Colorado State University.

Arakawa, A., 1966; "Computational Design for Long-Term Numerical Integration of the Equation of Fluid Motion: Two-Dimensional Incompressible Flow. Part 1," J. Comp. Phys., 1, No. 1, pp. 119-143.

Black, J. F., 1963; "Weather Control: Use of Asphalt Coatings to Tap Solar Energy," Science, 139, pp. 226-227.

Black, J. F., and Tarmy, B. L., 1963; "The Use of Asphalt Coatings to Increase Rainfall," J. Appl. Meteor., 2, pp. 557-564.

Bornstein, R. D., 1968; "Observations of the Urban Heat Island Effect in New York City," J. Appl. Meteor., 7, pp. 575-582.

Bradshaw, P., 1966; "Boundary-layer Problems of 1966," NPL AERO Report 1203.

Carnahan, B., Luther, H. A., and Wilkes, J. O., 1969; Applied Numerical Methods, John Wiley and Sons, Inc., New York, 604 pp.

Cermak, J. E. and Koloseus, H. J., 1953; "Lake Hefner Model Studies of Wind Structure and Evaporation," Final Report Part I and II, Contract No. bsr-57053, Bureau of Physics, U.S. Navy, Colorado State University Report No. CER54JEC20.

Cermak, J. E., ed., 1966; "Simulation of Atmospheric Motion by Wind Tunnel Flows," Fluid Dynamics and Diffusion Lab., Colorado State University.

Chanda, Benoyendra, 1958; "Turbulent Boundary Layer over Heated and Unheated Plane, Rough Surfaces," Colorado State University Report CER58BC21, AFCRC TN-58-428.

Chandra-sekhar, S., 1961; Hydrodynamic and Hydromagnetic Stability, Oxford University Press.

Changnon, S. A., Jr., 1968; "Recent Studies of Urban Effects on Precipitation in the United States," in Urban Climates, W.M.O. Tech. Note No. 108, pp. 325-341.

Charpentier, C., 1967; "Etude de la Stabilité d'un Gradient Thermique Produit Artificiellement dans un Ecoulement à Basse Vitesse au Moyen d'une Grille d'Eléments Chauffants," Département Méchanique Théorique, Electricite de France 6, Quai Watier-78 Chatou, 12 pp.

Cheng, S. I., 1970; "Numerical Integration of Navier-Stokes Equations," AIAA J., 8, No. 12, pp. 2115-2122.

Cooley, J. W., Lewis, A. W., and Welch, P. D., 1967; "Historical Notes on the Fast Fourier Transform," IEEE Transactions on Audio and Electroacoustics, Vol. Au-15, No. 2, pp. 76-79.

Corby, G. A., 1954; "The Airflow over Mountains," Quart. J. R. Met. Soc., 80, pp. 491-521.

Corby, G. A., and Wallington, C. E., 1956; "Airflow over Mountains: The Lee-Wave Amplitude," Quart. J. R. Met. Soc., 82, pp. 266-274.

Crowley, W. P., 1967; "Second-Order Numerical Advection," J. Comp. Physics, 1, No. 4, pp. 471-484.

Crowley, W. P., 1968; "Numerical Advection Experiments," Monthly Weather Rev., 97, No. 1, pp. 1-11.

Davidson, B., 1967; "A Summary of the New York Urban Air Pollution Dynamics Research Program," J. Air Poll. Contr. Assoc., 17, pp. 154-158.

Davis, R. E., 1969; "Two-Dimensional Flow of a Stratified Fluid Over an Obstacle," J. Fluid Mech., 36, pp. 127-143.

Delage, Y., and Taylor, P. A., 1970; "Numerical Studies of Heat Island Circulation," Boundary Layer Meteorology, 1, pp. 201-226.

DeMarrais, G. A., 1961; "Vertical Temperature Difference Observed over an Urban Area," Bull. Amer. Meteor. Soc., 42, No. 8, pp. 548-554.

Douglas, J., Jr., 1955; "On the Numerical Integration of $\partial^2 u/\partial x^2 + \partial^2 u/\partial y^2 = \partial u/\partial t$ by Implicit Methods," J. Soc. Indust. Appl. Math., 3, No. 1, pp. 42-65.

Drazin, P. G. and Moore, D. W., 1967; "Steady Two-Dimensional Flow of Variable Density Over an Obstacle," J. Fluid Mech., 28, pp. 353-370.

Duckworth, F. S., and Sandberg, J. S., 1954; "The Effect of Cities upon Horizontal and Vertical Temperature Gradients," Bull. Amer. Meteor. Soc., 35, No. 5, pp. 198-207.

Emmons, H. W., and Ying, S., 1966; "The Fire Whirl," 11th International Combustion Symposium, The Combustion Institute.

Estoque, M. A., 1961; "A Theoretical Investigation of the Sea Breeze," Q. J. Roy. Meteor. Soc., 87, pp. 136-346.

Estoque, M. A., 1962; "The Sea Breeze as a Function of the Prevailing Synoptic Situation," J. Atmosp. Science., 19, pp. 245-250.

Estoque, M. A. and Bhumralkar, C. M., 1968; "Theoretical Studies of the Atmospheric Boundary Layer," Final Rep., Grant DA-AMC-28-043-67-G2, Institute of Atmospheric Science, University of Miami, Coral Gables, Florida 33124.

Estoque, M. A., and Bhumralkar, C. M., 1970; "A Method for Solving the Planetary Boundary-Layer Equations," Boundary-Layer Meteorology 1, pp. 169-194.

Fisher, E. C., 1960; "An Observational Study of the Sea Breeze," J. Meteor., 17, pp. 645-660.

Fisher, E. C., 1961; "A Theoretical Study of the Sea Breeze," J. Meteor., 18, pp. 216-233.

Foldvik, A. and Wurtele, M. G., 1967; "The Computation of the Transient Gravity Wave," Geophys. J. R. Astr. Soc., 13, pp. 167-185.

Forsythe, G. E., and Wascow, W. R., 1967; Finite-Difference Methods for Partial Differential Equations, John Wiley and Sons, New York, pp. 494.

Fosberg, M. A., 1967; "Numerical Analysis of Convective Motions over a Mountain Ridge," J. Appl. Met., 6, No. 5, pp. 889-904.

Fosberg, M. A., 1969; "Airflow over a Heated Coastal Mountain," J. Appl. Met., 8, No. 3, pp. 436-442.

Fromm, J. E., 1963; "A Method for Computing Nonsteady, Incompressible Viscous Flows," LA-2910, Los Alamos Scientific Laboratory of the University of California, Los Alamos, New Mexico.

Fromm, J. E., 1969; "Practical Investigation of Convective Difference Approximations of Reduced Dispersion," Phys. Fluids, Supplement II, pp. II-3 - II-12.

Garnett, A., and Bach, W., 1965; "An Estimation of the Ratio of Artificial Heat Generation to Natural Radiation Heat in Sheffield," Mon. Wea. Rev., 93, No. 6, pp. 383-385.

Garstang, M, Boaz, W. J., and La Seur, N. E., 1965; "The Equivalent Heat Mountain, A Preliminary Study," Florida State University Department of Meteor., 26 pp.

Georgii, H. W., 1968; "The Effects of Air Pollution on Urban Climates," in Urban Climates, W.M.O. Tech. Note No. 108, pp. 214-237.

Haurwitz, B., 1947; "Comments on the Sea-Breeze Circulation," J. Meteor., 4, No. 1, pp. 1-8.

Hess, S. L., 1959; Introduction to Theoretical Meteorology, Holt, Rinehart and Winston, New York, 362 pp.

Hewett, T. A., Fay, J. A., and Hoult, D. P., 1970; "Laboratory Experiments of Smokestack Plumes in a Stable Atmosphere," Fluid Mechanics Laboratory, Department of Mechanical Engineering, Massachusetts Institute of Technology, 31 pp.

Hilst, G. R. and Bowne, N. E., 1966; "A Study of the Diffusion of Aerosols Released from Aerial Line Sources Upwind of an Urban Complex," Final Report, Project No. 4V025001A128, Hartford, Conn., The Travelers Research Center, Inc., Vol. I, and Vol. II.

Hino, M., 1965; "Numerical Analysis of Smoke Concentration Profiles, I Finite Difference Method," Rep. No. 65058, Central Research Center of Electric Power Association, 38 pp. (in Japanese).

Holmes, R. M., 1969; "Airborne Measurements of Thermal Discontinuities in the Lowest Layers of Atmosphere," Inland Waters Branch, Department of Energy, Mines and Resources, 3303-33rd Street, N. W., Calgary, Alberta.

Humphreys, W. J., 1964; Physics of the Air, Dover, 676 pp.

Janowitz, G. S., 1968; "On Wakes in Stratified Fluids," J. Fluid Mech., 33, pp. 417-432.

Kopec, R. J., 1970; "Further Observations of the Urban Heat Island in a Small City," Bull. Amer. Meteor. Soc., 51, No. 7, pp. 602-606.

Kozhevnikov, V. N., 1968; "Orographic Perturbations in the Two-Dimensional Stationary Problem," Izv. , Atmospheric and Oceanic Physics, 4, No. 1, pp. 33-52.

Kreith, F., 1968; Principles of Heat Transfer, Second Edition, International Testbook Company, Scranton, Pennsylvania, pp. 620.

Krishnamurti, T. N., 1964; "Theory of Two-Dimensional Mountain Waves," Review of Geophysics, 2, No. 4, pp. 593-624.

Landsberg, H. E., 1956; "The Climate of Towns," in Man's Role in Changing the Face of the Earth, Chicago, Illinois, University of Chicago Press, pp. 584-606.

Landsberg, H. E., 1968, "Climates and Urban Planning," in Urban Climates, W.M.O. Tech. Note No. 108, pp. 364-374.

Lettau, Heinz, 1959; "Research Problems in Micrometeorology," Final Report Contract DA-36-039-SC-80063 Meteorology Department, U.S. Army Electronic Proving Ground, Fort Huachuca, Arizona.

Lin, J. T., and Binder, G. J., 1967; "Simulation of Mountain Lee-Waves in a Wind Tunnel," Fluid Dynamics and Diffusion Lab., U.S. Army Research Grant DA-AMC-28-043-65-G20, Colorado State University.

Lin, J. T. and Cermak, J. E., 1969; "Dynamics of Stably Stratified Flows," Project THEMIS, Tech. Rep. No. 4, CER69-70JTL2, Fluid Dynamics and Diffusion Laboratory, Colorado State University, Fort Collins, Colorado, 167 pp.

Lin, J. T., and Apelt, C. J., 1970; "Stratified Flow over an Obstacle, A Numerical Experiment," Project THEMIS, Tech. Rep. No. 7, CER69-70JTL-CJA25, Fluid Dynamics and Diffusion Laboratory, Colorado State University, Fort Collins, Colorado, 78 pp.

Long, R. R., 1953; "Some Aspects of the Flow of Stratified Fluids, I: A Theoretical Investigation," Tellus, 5, pp. 42-58.

Long, R. R., 1954; "Some Aspects of the Flow of Stratified Fluids, II. Experiments with a Two-Fluid System," Tellus, 6, pp. 97-115.

Long, R. R., 1955; "Some Aspects of the Flow of Stratified Fluids, III: Continuous Density Gradients," Tellus, 7, pp. 241-357.

Long, R. R., 1959; "A Laboratory Model of Air Flow Over the Sierra Nevada Mountains," The Rossby Memorial Vol., pp. 372-380.

Lönnquist, O., 1962; "On the Diurnal Variation of Surface Temperature," Tellus, XIV, 1, pp. 96-101.

Ludwig, F. L. and Kealoha, J. H. S., 1968; "Urban Climatological Studies," Stanford Research Institute, Menlo Park, California.

Lumley, J. L. and Panofsky, H. A., 1964; The Structure of Atmospheric Turbulence, Interscience, New York.

Magata, M., 1965; "A Study of the Sea Breeze by the Numerical Experiment," Meteor. and Geophysics, 16, No. 1, pp. 23-37.

Magata, M., and Ogura, S., 1967; "On the Airflow over Mountains Under the Influence of Heating and Cooling," J. Met. Soc. Japan, 45, No. 1, pp. 83-95.

Malkus, J. S., 1955; "The Effects of a Large Island Upon the Trade-Wind Air Stream," Q. J. Roy. Meteor. Soc., 81, pp. 538-550.

Malkus, J. S., 1963; "Tropical Rain Induced by a Small Natural Heat Source," J. Appl. Meteor., 2, No. 5, pp. 547-556.

Malkus, J. S. and Bunker, A. F., 1952; "Observational Studies of the Air Flow over Nantucket Island During the Summer of 1950,: Pap. Phys. Ocean. Meteor., Mass. Inst. Tech. and Woods Hole Ocean. Inst. 12, No. 2, 50 pp.

Malkus, J. S., and Stern, M. E., 1953; "The Flow of a Stable Atmosphere Over a Heated Island, Part I," J. Meteor., 10, pp. 30-41.

Matsuno, T., 1966; "False Reflection of Waves at the Boundary Due to the Use of Finite Differences," J. Meteor. Soc., Japan, 44, No. 2, pp. 145-157.

Meroney, R. N. and Cermak, J. E., 1967; "Characteristics of Diffusion Within Model Crop Canopies," Symposium on the Theory and Measurement of Atmospheric Turbulence and Diffusion in the Planetary Boundary Layer, Albuquerque, December 5-7, 1967.

Miles, J. W., 1968a; "Lee Waves in a Stratified Flow, Pt. I, Thin Barrier," J. Fluid Mech., 32, pp. 549-567.

Miles, J. W., 1968b; "Lee Waves in a Stratified Flow, Pt. II, Semi-Circular Obstacle," J. Fluid Mech., 33, pp. 803-814.

Mitchell, J. M., Jr., 1961; "The Temperature of Cities," Weatherwise, 14, pp. 224-229.

Molenkamp, C. R., 1968; "Accuracy of Finite-Difference Methods Applied to the Advection Equation," J. Appl. Meteor., 7, pp. 160-167.

Monin, A. S. and Obukhov, A. M., 1954; "Basic Regularity in Turbulent Mixing in the Surface Layer of the Atmosphere," U.S.S.R. Acad. Sci. Geophys. Inst., No. 24.

Moroz, W. J., 1967; "A Lake Breeze on the Eastern Shore of Lake Michigan; Observation and Model," J. Atmosp. Sci., 24, pp. 337-355.

Mueller, T. J., and O'Leary, R. A., 1970; "Physical and Numerical Experiments in Laminar Incompressible Separating and Reattaching Flows," AIAA 3rd Fluid and Plasma Dynamics Conference, Los Angeles, California, June 29- July 1, 1970, 15 pp.

Myrup, L. O.; 1969; "A Numerical Model of the Urban Heat Island," J. Appl. Meteor., 8, No. 6, pp. 908-918.

Oke, T. R., and Hannel, F. G., 1968; "The Form of the Urban Heat Island in Hamilton, Canada," in Urban Climates, W.M.O. Tech. Note No. 108, pp. 113-126.

Okita, T., 1960; "Estimation of Direction of Air Flow from Observations of Rime Ice," J. Meteor. Soc., Japan, 38, No. 4., pp. 207-209.

Olfe, D. B., and Lee, R. L., 1971; "Linearlized Calculations of Urban Heat Island Convection Effects," AIAA Paper No. 71-13, AIAA 9th Aerospace Sciences Meeting, New York, New York, 14 pp.

Onishi, G., 1969; "A Numerical Method for Three-Dimensional Mountain Waves," J. Met. Soc. Japan, 47, No. 5, pp. 352-359.

Oobayashi, T., 1970; "A Numerical Study of Two-Dimensional Airflow Over an Isolated Mountain," J. Met. Soc. Japan, 48, No. 2, pp. 118-127.

Orville, H. D., 1965; "A Numerical Study of the Initiation of Cumulus Clouds Over Mountainous Terrain," J. Atm. Sci., 22, No. 6, pp. 684-699.

Orville, H. D., 1967; "The Numerical Modeling of Mountain Upslope Winds and Cumulus Clouds," Rep. 67-2, Contract No. 14-06-D-5979, Inst. Atmos. Sci., South Dakota School of Mines and Technology, Rapid City, South Dakota.

Orville, H. D., 1968a; "Ambient Wind Effects on the Initiation and Development of Cumulus Clouds Over Mountains," J. Atm. Sci., 25, No. 3, pp. 385-403.

Orville, H. D., 1968b; "Comments on 'Accuracy of Finite-Difference Methods Applied to the Advection Equation,'" J. Appl. Meteor., 7, No. 5, pp. 938.

Orville, H. D., 1969; "Numerical Modeling of Precipitation and Clouds Shadow Effects on Mountain-Induced Cumuli," J. Atm. Sci., 26, pp. 1283-1298.

Orville, H. D., 1970; "A Numerical Simulation of the Life History of a Rainstorm," J. Atm. Sci., 27, No. 8, pp. 1148-1159.

Palm, E., 1953; "On the Formation of Surface Waves in a Fluid Flowing Over a Corrugated Bed and on the Development of Mountain Waves," Astrophysica Norvegica, 5, No. 3.

Pao, Y. H., 1969; "Inviscid Flows of Stably Stratified Fluids Over Barriers," Quart. J. R. Met. Soc., 95, No. 403, pp. 104-118.

Peaceman, D. W., and Rachford, H. H., Jr., 1955; "The Numerical Solution of Parabolic and Elliptic Differential Equations," J. Soc. Indust. Appl. Math., 3, No. 1, pp. 28-41.

Pearce, R. P., 1955; "The Calculation of a Sea-Breeze Circulation in Terms of the Differential Heating Across the Coastline," Q. J. Roy. Meteor. Soc., 81, pp. 351-371.

Pearson, C. E., 1965; "A Computational Method for Viscous Flow Problems," Journal of Fluid Mech., 21, Part 4, pp. 611-622.

Pekelis, E. M., 1969; "A Numerical Method of Calculating Lee Waves with an Arbitrary Distributions of the Basic-Flow Parameters (Two-Dimensional Linear Problem)," Izv., Atmospheric and Oceanic Physics, 5, No. 1, pp. 3-16.

Peterson, J. T., 1969; "The Climate of Cities: A Survey of Recent Literature," U.S. Department of Health, Educ., and Welfare, Pub. Health Service, Consumer Protection and Environmental Health Service, Nat. Air Poll. Contr. Admin., Raleigh, North Carolina, 48 pp.

Phillips, N. A., 1959; "An Example of Non-Linear Computational Instability," in The Atmosphere and the Sea in Motion, pp. 501-504.

Plate, E. J., and Cermak, J. E., 1963; "Micrometeorological Wind Tunnel Facility, Description and Characteristics," Final Report on Contract No. DA36-039-SC-80371 with Meteorology Department, U.S. Army Electronic Research and Development Activity, Fort Huachuca, Arizona, Fluid Dynamics and Diffusion Laboratory, Colorado State University, Fort Collins, Colorado, CER63-EJP-JEC9, 39 pp.

Plate, E. J., 1964; "The Drag on a Smooth Flatplate with a Fence," Paper No. G4FE17 presented at ASME Symposium on Fully Separated Flow, held in Philadelphia, 1964, CER63-EVP66.

Plate, E. J., and Lin, C. W., 1966; "Investigations of the Thermally Stratified Boundary Layer," Fluid Mechanics Paper No. 5, Colorado State University, February 1966.

Pooler, F., Jr., 1963; "Airflow Over a City in Terrain of Moderate Relief," J. Appl. Meteor. 2, pp. 446-456.

Pope, A., and Hooper, J. J., 1966; Low-Speed Wind Tunnel Testing, John Wiley and Sons.

Preston-Whyte, R. A., 1970; "A Spatial Model of an Urban Heat Island," J. Appl. Meteor., 9, pp. 571-573.

Queney, P., 1959; "Initial Value Problem in a Double Couette-Flow," Autobarotropic Flow Project, Scientific Rep. No. 1, Contract No. AF19(604)-728, Air Force Cambridge Research Center, Cambridge, Mass.

Queney, P., ed., 1960; "The Airflow Over Mountains," W.M.O. Tech. Note No. 34, 132 pp.

Richtmyer, R. D. and Morton, K. W., 1967; Difference Methods for Initial-Value Problems, Interscience Publishers, New York, 405 pp.

Roache, P. J. and Muller, T. J., 1970; "Numerical Solutions of Laminar Separated Flows," AIAA J., 8, No. 3, pp. 530-538.

Saltzman, B., 1962; Selected Papers on the Theory of Thermal Convection, Dover Publications, Inc., New York.

Sawyer, J. S., 1962; "Gravity Waves in the Atmosphere as a Three-Dimensional Problem," Quart. J. R. Met. Soc., 88, pp. 412-425.

Scorer, R. S., 1949; "Theory of Waves in the Lee of Mountains," Quart. J. R. Met. Soc., 75, pp. 41-56.

Scorer, R. S., 1951; "Forecasting the Occurrence of Lee Waves," Weather, 6, pp. 99-103.

Scorer, R. S., 1953; "Theory of Airflow Over Mountains, II. The Flow Over a Ridge," Quart. J. R. Met. Soc., 79, pp. 70-83.

Scotti, R., 1969; "An Experimental Study of a Stratified Shear Layer," Rep. No. AS-69-1, Contract No. USCDE-22-129-68(G), College of Engineering, University of California, Berkeley, 154 pp.

Segel, L. A., and Stuart, J. T., 1961; "On the Tendency Toward Hexagonal Cells in Steady Convection," Renselaer Polytechnic Institute, Mat. Dep., No. 47.

Segur, H. L., 1969; "Stratified Flow into a Contraction," Rept. No. AS-69-15, Contract No.: USCDE-22-129-68(G), College of Engineering, University of California, Berkeley, 178 pp.

Smith, G. D., 1965; Numerical Solution of Partial Differential Equations, Oxford University Press, New York, 179 pp.

Smith, R. C., 1955; "Theory of Air Flow Over a Heated Land Mass," Q. J. Roy. Meteor. Soc., 81, pp. 382-395.

Sokhov, T. Z. and Gutman, L. N., 1968; "The Use of the Long-Wave Method in the Nonlinear Problem of the Motion of a Cold Air Mass Over a Mountain Ridge," Izv., Atmospheric and Oceanic Physics, 4, No. 1, pp. 23-32.

Spelman, M. J., 1969; "Atmospheric Modification of Surface Influences, Pt. II. Response of the Atmosphere to the Surface Features of a Tropical Island," Rep. No. 15, Department of Meteorology, The Pennsylvania State University, University Park, Pennsylvania, pp. 73-132.

Stern, M., 1955; "Theory of the Mean Atmospheric Perturbations Produced by Differential Surface Heating," J. of Met., 11, pp. 495-502.

Stern, M. E., and Malkus, J. S., 1953; "The Flow of a Stable Atmosphere Over a Heated Island, Part II," J. of Meteor. 10, pp. 105-120.

Stone, H. L., 1968; "Iterative Solution of Implicit Approximations of Multi-Dimensional Partial Differential Equations," J. Num. Anal. SIAM, 5, pp. 530-558.

Strom, G. H., and Kaplin, E. J., 1968; "Final Report Convective Turbulence Wind Tunnel Project," Rep. No. 504.04, New York University, School of Engineering and Science, University Heights, New York, New York 10453, 38 pp.

Sundborg, A., 1950; "Local Climatological Studies of the Temperature Conditions in an Urban Area," Tellus, 2, pp. 222-232.

Tag, P. M., 1969; "Surface Temperatures in an Urban Environment," in Atmospheric Modification by Surface Influences, Department of Meteor., The Pennsylvania State University, University Park, Penn., 72 pp.

Tanouye, E. T., 1966; "The Response of the Atmosphere to a Localized Heat Source at the Earth's Surface," in Theoretical Studies of the Atmospheric Boundary Layer, Hawaii Institute of Geophysics, University of Hawaii, pp. 123-173.

Thom, A., and Apelt, C. J., 1961; Field Computations in Engineering and Physics, D. Van Nostrand, Princeton.

Torrance, K. E., and Rocket, J. A., 1969; "Numerical Study of Natural Convection in an Enclosure with Localized Heating from Below - Creeping Flow to the Onset of Laminar Instability," J. Fluid Mech., 36, Part 1, pp. 33-54.

Townsend, A. A., 1965a; "Self-Preserving Flow Inside a Turbulent Boundary Layer," J. Fluid Mechanics, 22, pp. 773-797.

Townsend, A. A., 1965b; "The Response of a Turbulent Boundary Layer to Abrupt Changes in Surface Conditions," J. Fluid Mechanics, 22, pp. 799-822.

Vukovich, F. M., 1971; "A Theoretical Analysis of the Effect of Mean Wind and Stability on a Heat Island Circulation Characteristic of an Urban Complex," Month. Weather Review (to be published).

Wexler, R., 1946; "Theory and Observation of Land and Sea Breezes," Bull. Amer. Meteor. Soc., 27, pp. 272-287.

W.M.O. Tech. Note No. 108, 1968; "Urban Climates," Proceedings of the W.M.O. Symposium on Urban Climates and Building Climatology, Brussels, (Vol. I), 390 pp.

Wurtele, M., 1953; "The Initial-Value Lee-Wave Problem for the Isothermal Atmosphere," Scientific Rep. No. 3, Sierra Wave Project, Contract No. AF19(122)-263, Air Force Cambridge Research Center, Cambridge, Mass.

Yih, C. S., 1960; "Exact Solutions for Steady Two-Dimensional Flow of a Stratified Fluid," J. Fluid Mech., 9, pp. 161-174.

Yih, C. S., 1965; Dynamics of Nonhomogeneous Fluids, MacMillan, New York, 306 pp.

Zilitinkevich, S. S., Laikhtman, D. L., and Monin, A. S., 1967; "Dynamics of the Atmospheric Boundary Layer," Izv., Atmospheric and Oceanic Physics, 3, No. 3, pp. 170-191.

APPENDIX

APPENDIX A.

Herein are the detailed derivations of the equations which were used in the previous chapters.

Equation (4.12-1)

The vorticity transport equation is given by Eq. (4.6-1),

$$\frac{\partial \zeta}{\partial t} + u \frac{\partial \zeta}{\partial x} + w \frac{\partial \zeta}{\partial z} = K\left(\frac{\partial^2 \zeta}{\partial x^2} + \frac{\partial^2 \zeta}{\partial z^2}\right) + \frac{g}{T} \frac{\partial T}{\partial x}$$

Let us assume u and w are positive, then we use the backward difference for the convection terms.

$$\frac{\zeta^{n+1}_{j,\ell} - \zeta^{n}_{j,\ell}}{\delta t} + u^{n}_{j,\ell} \frac{\zeta^{n}_{j,\ell} - \zeta^{n}_{j-1,\ell}}{\delta x} + w^{n}_{j,\ell} \frac{\zeta^{n}_{j,\ell} - \zeta^{n}_{j,\ell-1}}{\delta z}$$

$$= K\left(\frac{\zeta^{n}_{j+1,\ell} - 2\zeta^{n}_{j,\ell} + \zeta^{n}_{j-1,}}{\delta x^2} + \frac{\zeta^{n}_{j,\ell+1} - 2\zeta^{n}_{j,\ell} + \zeta^{n}_{j,\ell+1}}{\delta z^2}\right)$$

$$+ \frac{g}{T^{n}_{j,\ell}} \frac{T^{n}_{j+1,\ell} - T^{n}_{j-1,\ell}}{2\delta x}$$

Multiplying δt and rearranging so that $\zeta^{n+1}_{j,\ell}$ is expressed in terms of the known values at time n, equation (4.12-1) is obtained. When both u and w are negative then the forward differences are used instead of the backward ones in the convection terms.

If u and w have different signs then convection terms are approximated according to the rule of the upstream difference, i.e. one is backward and another is forward depending on the signs of u and w. In the programming, four different approximations are given depending on the combinations of signs of u and w.

Equation (4.13-1)

The Poisson equation $\nabla^2\zeta$ was approximated by

$$\frac{\psi_{j+1,\ell} - 2\psi_{j,\ell} + \psi_{j-1,\ell}}{\delta x^2} + \frac{\psi_{j,\ell+1} - 2\psi_{j,\ell} + \psi_{j,\ell-1}}{\delta z^2} = \zeta$$

multiplying δx^2 and rearranging

$$\psi_{j,\ell} = \frac{1}{2(1+\frac{\delta x^2}{\delta z^2})}\{\psi_{j+1,\ell} + \psi_{j-1,\ell} + \frac{\delta x^2}{\delta z^2}(\psi_{j,\ell+1} + \psi_{j,\ell-1})$$

$$-\delta x^2 \zeta_{j,\ell}\}$$

Using the over relaxation factor ω, r+1 st iteration was expressed as

$$\psi^{r+1}_{j,\ell} = \psi^{r}_{j,\ell} + \omega R_{j,\ell} \qquad (A)$$

where $R_{j,\ell}$ is the remainder given by

$$R_{j,\ell} = \frac{1}{2(1+\frac{\delta x^2}{\delta z^2})}\{\psi_{j+1,\ell} + \psi_{j-1,\ell} + \frac{\delta x^2}{\delta z^2}(\psi_{j,\ell+1} + \psi_{j,\ell-1})$$

$$- \delta x^2 \zeta_{j,\ell}\} - \psi_{j,\ell}$$

Substitution of $R_{j,\ell}$ into Equation (A) gives equation (4.13-1).

Equation (4.14-1)

The derivation is exactly the same as equation (10) except for the buoyancy term $\frac{g}{T}\frac{\partial T}{\partial x}$.

Equation (4.15-1)

Let us suppose $u \geq 0$ and $w \geq 0$ then the vorticity transport equation is approximated as

$$\frac{\zeta^{n+1}_{j,\ell} - \zeta^{n}_{j,\ell}}{\delta t} + u^{n}_{j,\ell} \frac{\zeta^{n}_{j,\ell} - \zeta^{n}_{j-1,\ell}}{\delta x} + w^{n}_{j,\ell} \frac{\zeta^{n}_{j,\ell} - \zeta^{n}_{j,\ell-1}}{\delta z}$$

$$= K \left(\frac{\zeta^{n}_{j+1,\ell} - 2\zeta^{n}_{j,\ell} + \zeta^{n}_{j-1,\ell}}{\delta x^2} + \frac{\zeta^{n}_{j,\ell+1} - 2\zeta^{n}_{j,\ell} + \zeta^{n}_{j,\ell-1}}{\delta z^2} \right) \qquad (A)$$

where the source term $\frac{g}{T} \frac{\partial T}{\partial x}$ is omitted.

When the error is given by a Fourier series and satisfies the finite difference equation, then the error is assumed to be given by

$$E^{k}_{j,\ell} = \xi^{k} \, e^{i(\beta_j j \delta x + \beta_\ell \ell \delta z)} \qquad (B)$$

where $i = \sqrt{-1}$, $\beta_j = \frac{P\pi}{P\delta x}$ and $\beta_\ell = \frac{q\pi}{Q\delta z}$. P and Q are the numbers of mesh points in x and z direction. Since the maximum wave lengthes expressed in the region $P\delta x \times Q\delta z$ are $2P\delta x$ and $2Q\delta z$ in x and z direction, respectively, smaller wave lengthes are given by

$\frac{2P\delta x}{p}$ and $\frac{2Q\delta z}{q}$ in each direction, where

$$p = 1, 2, \ldots\ldots P$$

$$q = 1, 2, \ldots\ldots Q.$$

Now wave numbers β_j and β_ℓ are expressed as

$$\beta_j = \frac{2\pi}{\frac{2P\delta x}{p}} = \frac{p\pi}{P\delta x} \quad \text{in} \quad x$$

and

$$\beta_\ell = \frac{2\pi}{\frac{2Q\delta z}{q}} = \frac{q\pi}{Q\delta z} \quad \text{in} \quad z \quad \text{direction.}$$

$\xi = e^{\alpha \delta t}$ and α is a constant either real or complex. Strictly speaking $E^n_{j,\ell}$ should be given by the summation over p and q as

$$E^n_{j,\ell} = \sum_{p=1}^{P} \sum_{q=1}^{Q} A_{pq}\, \xi^k\, e^{i(\beta_j j \delta x + \beta_\ell \ell \delta z)}$$

However, if one of the arbitrary components grows up then the whole system is considered unstable. Therefore, it is sufficient to consider one of the components for the stability analysis.

For the linear equations, if the numerical solution of the finite difference equation N is given by

$$N = u^k_{j,\ell} + E^k_{j,\ell}$$

where $u^k_{j,\ell}$ is the exact solution of the finite difference system and $E^k_{j,\ell}$ is the error, then $E^k_{j,\ell}$ itself satisfies the finite difference equation. For the nonlinear equations above argument is not true, but for simplicity we assume $E^k_{j,\ell}$ also satisfies the equation (A).

As we can see from equation (B), for stability $|\xi| \leq 1$ should be satisfied, otherwise, $E^k_{j,\ell} \to \infty$ as $k \to \infty$, where k is the number of integration ($t = k\, \delta\, t$). Substituting equation (B) into equation (A) and dividing by

$\xi^n\, e^{i(\beta_j j \delta x + \beta_\ell \ell \delta z)}$ gives

$$\xi - 1 + \frac{u \delta t}{\delta x}\left(1 - e^{-i\beta_j \delta x}\right) + \frac{w \delta t}{\delta z}\left(1 - e^{-i\beta_\ell \delta z}\right)$$

$$= \frac{k\delta t}{\delta x^2} \left(e^{i\beta_j \delta x} - 2 + e^{-i\beta_j \delta x}\right)$$

$$+ \frac{k\delta t}{\delta z^2} \left(e^{i\beta_\ell \delta z} - 2 + e^{-i\beta_\ell \delta z}\right)$$

Using the relations

$$e^{-i\beta_j \delta x} = \cos \beta_j \delta x - i \sin \beta_j \delta x$$

$$\cos \beta_j \delta x = \frac{e^{i\beta_j \delta x} + e^{-i\beta_j \delta x}}{2} \quad \text{etc.}$$

we obtain

$$\xi - 1 + \frac{u\delta t}{\delta x} (1 - \cos \beta_j \delta x) + i \frac{u\delta t}{\delta x} \sin \beta_j \delta x$$

$$+ \frac{w\delta t}{\delta z} (1 - \cos \beta_\ell \delta z) + i \frac{w\delta t}{\delta x} \sin \beta_\ell \delta z$$

$$= \frac{2k\delta t}{\delta x^2} (\cos\beta_j \delta x - 1) + \frac{2k\delta t}{\delta z^2} (\cos\beta_\ell \delta z - 1)$$

Using the relation $\sin^2 \frac{\beta_j \delta x}{2} = \frac{1 - \cos \beta_j \delta x}{2}$

$$\xi - 1 + \frac{2u\delta t}{\delta x} \sin^2 \frac{\beta_j \delta x}{2} + i \frac{u\delta t}{\delta x} \sin \beta_j \delta x$$

$$+ \frac{2w\delta t}{\delta z} \sin^2 \frac{\beta_\ell \delta z}{2} + i \frac{w\delta t}{\delta x} \sin \beta_\ell \delta z$$

$$= \frac{-4k\delta t}{\delta x^2} \left(\sin^2 \frac{\beta_j \delta x}{2}\right) - \frac{4k\delta t}{\delta z^2} \sin^2 \frac{\beta_\ell \delta z}{2}$$

Rearranging

$$\xi = 1 - \delta t \left(\frac{2u}{\delta x} \sin^2 \frac{\beta_j \delta x}{2} + \frac{2w}{\delta z} \sin^2 \frac{\beta_\ell \delta z}{2}\right.$$

$$\left. + \frac{4k}{\delta x^2} \sin^2 \frac{\beta_j \delta x}{2} + \frac{4k}{\delta z^2} \sin^2 \frac{\beta_\ell \delta z}{2}\right)$$

$$- i \left(\frac{u}{\delta x} \sin \beta_j \delta x + \frac{w}{\delta z} \sin \beta_\ell \delta z\right) \delta t$$

Let

$$s = \frac{2u}{\delta x} \sin^2 \frac{\beta_j \delta x}{2} + \frac{2w}{\delta z} \sin^2 \frac{\beta_\ell \delta z}{2}$$

$$+ \frac{4k}{\delta x^2} \sin^2 \frac{\beta_j \delta x}{2} + \frac{4k}{\delta z^2} \sin^2 \frac{\beta_\ell \delta z}{2} \quad \text{and}$$

$$s_1 = \frac{u}{\delta x} \sin \beta_j \delta x + \frac{w}{\delta z} \sin \beta_\ell \delta z$$

Then

$$\xi = 1 - s\delta t - i\, s_1\, \delta t \qquad \text{and}$$

$$\bar{\xi} = 1 - s\delta t + i\, s_1\, \delta t$$

where $\bar{\xi}$ is the complex conjugate of ξ . The square of the magnitude of ξ is

$$|\xi|^2 = \xi \bar{\xi} = (1-s\delta t)^2 + s_1^2 \delta t^2$$

$$= 1 - 2s\delta t + s^2 \delta t^2 + s_1^2 \delta t^2 \leq 1$$

for stability

$$-2\, s\delta t + (s^2 + s_1^2)\, \delta t^2 \leq 0$$

divided by $\delta t > 0$

$$- 2 s + (s^2 + s_1^2)\ \delta t \leq 0$$

Since S is always positive

$$\delta t \leq \frac{1}{\frac{s^2 + s_1^2}{2s}}$$

To get the minimum value of δt we need the maximum value of $\frac{s^2 + s_1^2}{2 S}$.

Since

$$(\text{Max } S_1) \leq 1/2\ (\text{Max } S)$$

Max S is

$$\left(\frac{s^2 + s_1^2}{2s}\right)_{max} \leq \left(\frac{s^2 + \frac{1}{4} s^2}{2s}\right)_{max} = \left(\frac{5}{8} s\right)_{max}$$

$$S_{max} = 2 \left\{\frac{|u|_{max}}{\delta x} + \frac{|w|_{max}}{\delta z} + \frac{2k}{\delta x^2} \sin^2 \frac{\beta_j \delta x}{2}\right.$$

$$\left. + \frac{2k}{\delta z^2} \sin^2 \frac{\beta_\ell \delta z}{2} \right\}$$

$$\therefore \delta t \leq \frac{0.8}{\left\{\frac{|u|_{max}}{\delta x} + \frac{|w|_{max}}{\delta z} + \frac{2k}{\delta x^2} \sin^2 \frac{\beta_j \delta x}{2} + \frac{2k}{\delta z^2} \sin^2 \frac{\beta_\ell \delta z}{2}\right\}}$$

Equation (4.16-1)

By Taylor series expansion of the stream function at a boundary

$$\psi_{int} = \psi_{bound} + \left(\frac{\partial \psi}{\partial n}\right)_{bound} \delta n + \frac{1}{2!} \left(\frac{\partial^2 \psi}{\partial n^2}\right)_{bound} (\delta n)^2$$

$$+ \frac{1}{3!} \left(\frac{\partial^3 \psi}{\partial n^3}\right)_{bound} (\delta n)^3 + 0(\delta n^4) \qquad \text{(A)}$$

where $\frac{\partial}{\partial n}$ is a normal derivative with respect to the boundary. Subscript "bound" and "int" means at boundary and at one grid inside the boundary, respectively. δn is the grid size normal to the boundary. $0(\delta n^4)$ represents higher order terms which has multiplication at least δn^4 .

Substituting equation (4.8-2) into (A) we obtain

$$\psi_{int} = \psi_{bound} + \left(\frac{\partial \psi}{\partial n}\right)_{bound} \delta n + \frac{1}{2!} \left(\zeta - \frac{\partial^2 \psi}{\partial s^2}\right)_{bound} (\delta n)^2$$

$$+ \frac{1}{3!} \frac{\partial}{\partial n} \left(\zeta - \frac{\partial^2 \psi}{\partial s^2}\right)_{bound} (\delta n)^3 + 0(\delta n^4) \qquad (B)$$

where $\frac{\partial}{\partial s}$ is the tangential derivatives along the boundary. Suppose we have a rigid boundary along $z = 0$ then no-slip condition is used, i.e. $u = 0$ and $w = 0$.

Equation (B) reduces to

$$\psi_{int} = \psi_{bound} + \left(\frac{\partial \psi}{\partial z}\right)_{bound} (\delta z) + \frac{1}{2} \left(\zeta - \frac{\partial^2 \psi}{\partial x^2}\right)_{bound} (\delta z)^2$$

$$+ \frac{1}{6} \frac{\partial}{\partial z} \left(\zeta - \frac{\partial^2 \psi}{\partial x^2}\right)_{bound} (\delta z)^3 + 0(\delta z^4)$$

$$= \psi_{bound} + (-u)_{bound} (\delta z) + \frac{1}{2} \left(\zeta - \frac{\partial w}{\partial x}\right)_{bound} (\delta z)^2$$

$$+ \frac{1}{6} \left\{\frac{\partial \zeta}{\partial z} + \frac{\partial^2 u}{\partial x^2}\right\}_{bound} (\delta z)^3 + 0(\delta z^4)$$

where we used the definition

$$u = -\frac{\partial \psi}{\partial z} \qquad \text{and}$$

$$w = \frac{\partial \psi}{\partial x} \quad .$$

Moreover from the no-slip condition $(\frac{\partial w}{\partial x})_{bound} = 0$ and $(\frac{\partial^2 u}{\partial x^2})_{bound} = 0$, therefore

$$\psi_{int} = \psi_{bound} + \frac{1}{2}\,\zeta_{bound}\,(\delta z)^2 + \frac{1}{6}\,\frac{\zeta_{int} - \zeta_{bound}}{\delta z}\,(\delta z)^3 + O(\delta z^4)$$

$$= \psi_{bound} + \frac{(\delta z)^2}{3}\,\zeta_{bound} + \frac{(\delta z)^2}{6}\,\zeta_{int} + O(\delta z^4)$$

Rearranging

$$\zeta_{bound} = \frac{3}{(\delta z)^2}\,(\psi_{int} - \psi_{bound}) - \frac{1}{2}\,\zeta_{int} + O(\delta z^2)$$

TABLES

TABLE 2-1

Retained and Neglected Terms in a Linearlized Equation

		Retained Terms	Neglected Terms	
			Hypothesis	Higher Order
Equation of Motion	x	$\bar{\rho}\,\bar{u}\,\frac{\partial u'}{\partial x}$	$\bar{\rho}\,\bar{u}\,\frac{\partial \bar{u}}{\partial x}$	$\bar{\rho}\,u'\,\frac{\partial u'}{\partial x}$
		$\bar{\rho}\,w'\frac{\partial \bar{u}}{\partial z}$	$\bar{\rho}\,u'\,\frac{\partial \bar{u}}{\partial x}$	$\bar{\rho}\,w'\,\frac{\partial u'}{\partial z}$
		$\frac{\partial p'}{\partial x}$	$\rho'\,\bar{u}\,\frac{\partial \bar{u}}{\partial x}$	$\rho'\,\bar{u}\,\frac{\partial u'}{\partial x}$
			$\rho'u'\,\frac{\partial \bar{u}}{\partial x}$	$\rho'u'\,\frac{\partial \bar{u}}{\partial x}$
				$\rho'u'\,\frac{\partial u'}{\partial x}$
		$\frac{\partial \bar{p}}{\partial x}$		$\rho'w'\,\frac{\partial \bar{u}}{\partial z}$
				$\rho'w'\,\frac{\partial u'}{\partial z}$
	z	$\bar{\rho}\,\bar{u}\,\frac{\partial w'}{\partial x}$		$\bar{\rho}\,u'\,\frac{\partial w'}{\partial x}$
				$\bar{\rho}\,w'\,\frac{\partial w'}{\partial z}$
		$\frac{\partial p'}{\partial z}$		$\rho'\bar{u}\,\frac{\partial w'}{\partial x}$
		$\rho'g$		$\rho'u'\frac{\partial w'}{\partial x}$
				$\rho'w'\,\frac{\partial w'}{\partial z}$

	Retained Terms	Neglected Terms	
		Hypothesis	Higher Order
Equation of Continuity	$\bar{u}\,\frac{\partial \rho'}{\partial x}$	$\bar{u}\,\frac{\partial \bar{\rho}}{\partial x}$	$u'\,\frac{\partial \rho'}{\partial x}$
	$w'\,\frac{\partial \bar{\rho}}{\partial z}$	$u'\,\frac{\partial \bar{\rho}}{\partial x}$	$w'\,\frac{\partial \rho'}{\partial z}$
	$\bar{\rho}\,\frac{\partial u'}{\partial x}$	$\bar{\rho}\,\frac{\partial \bar{u}}{\partial x}, \rho'\frac{\partial \bar{u}}{\partial x}$	$\rho'\,\frac{\partial u'}{\partial x}$
	$\bar{\rho}\,\frac{\partial w'}{\partial z}$		$\rho'\,\frac{\partial w'}{\partial z}$
Adiabatic Equation	$\bar{u}\,\frac{\partial p'}{\partial x}, w'\frac{\partial \bar{p}}{\partial z}$	$\bar{u}\,\frac{\partial \bar{p}}{\partial x}, u'\frac{\partial \bar{p}}{\partial x}$	$u'\frac{\partial p'}{\partial x}, w'\frac{\partial p'}{\partial z}, \quad 2\bar{c}\,c'w'\frac{\partial \rho'}{\partial z}$
	$\bar{c}^2\,\bar{u}\,\frac{\partial \rho'}{\partial x}$	$\bar{c}^2\frac{\partial \bar{\rho}}{\partial x}, \bar{c}^2u'\frac{\partial \bar{\rho}}{\partial x}$	$\bar{c}^2u'\,\frac{\partial \rho'}{\partial x}, \quad c'^2\bar{u}\,\frac{\partial \bar{\rho}}{\partial x}$
	$\frac{}{c}^2\,w'\frac{\partial \bar{\rho}}{\partial z}$	$2\bar{c}\bar{c}'\bar{u}\,\frac{\partial \bar{p}}{\partial x}$	$\frac{}{c}^2\,w'\,\frac{\partial \rho'}{\partial z}, \quad c'^2\,\bar{u}\,\frac{\partial \rho'}{\partial x}$
		$2\bar{c}\bar{c}'u'\frac{\partial \bar{\rho}}{\partial x}$	$2\bar{c}\bar{c}'\bar{u}\,\frac{\partial \rho'}{\partial x}, \quad c'^2u'\,\frac{\partial \bar{\rho}}{\partial x}$
		$c'^2\bar{u}\,\frac{\partial \bar{\rho}}{\partial x}$	$2\bar{c}\bar{c}'u'\frac{\partial \bar{\rho}}{\partial x}, \quad c'^2u'\,\frac{\partial \rho'}{\partial x}$
		$c'^2u'\frac{\partial \bar{\rho}}{\partial x}$	$2\bar{c}\bar{c}'u'\,\frac{\partial \rho'}{\partial x}, \quad c'^2w'\frac{\partial \bar{\rho}}{\partial z}$
			$2\bar{c}\bar{c}'w'\,\frac{\partial \bar{\rho}}{\partial z}, \quad c'^2w'\,\frac{\partial \rho'}{\partial z}$

TABLE 2-2

Average Changes in Climatic Elements Caused by Urbanization (Landsberg, 1968)

Element	Comparison with rural environment
Contaminants:	
condensation nuclei and particulates;	10 times more
gaseous admixtures	5 to 25 times more
Cloudiness:	
cover;	5 to 10% more
fog, winter;	100% more
fog, summer	30% more
Precipitation:	
totals;	5 to 10% more
days with less than 5 mm;	10% more
snowfall	5% less
Relative humidity:	
winter;	2% less
summer	8% less
Radiation:	
global;	15 to 20% less
ultra-violet, winter;	30% less
ultra-violet, summer;	5% less
sunshine duration	5 to 15% less
Temperature:	
annual mean;	0.5 to 1.0°C more
winter minima (average);	1 to 2°C more
heating degree days	10% less
Wind speed:	
annual mean;	20 to 30% less
extreme gusts;	10 to 20% less
calms	5 to 20% more

TABLE 2-3

Average of Bright Sunshine,
London 1921-1950 (Georgii, 1968)

	Hours per day		
	January	July	Year
Surrounding Country	1.7	6.6	4.3
Outer Suburbs	1.4	6.5	4.1
Inner High-level Suburbs	1.3	6.3	4.0
Inner Low-level Suburbs	1.3	6.3	4.0
Central London	0.8	6.2	3.6

TABLE 2-4

COLLECTION OF DATA OBTAINED IN HEATED ISLAND PHENOMENA

		Variables / Data Sources	Velocity U (m/sec)	Stability S (m^{-1})	$\Gamma - \alpha$ ($^oc/m$)	Diffusivity K (m^2/sec)	Temp Excess ΔT (^oc)	Island Width 2D (m)	Charac. Length L (m)	Fr	Re	Amplitude $A = \frac{\Delta T}{\Gamma - \alpha}$ (m)	Effective Height $M = (1 - \frac{1}{e})$ (m)	Shape Parameter $X_o = \frac{U^3}{gsk}$ (m)	Symbol used in Fig. 2-7
Observation	Heated Island	Stern and Malkus (1953), Case 4	1.5	10^{-5}	2.86×10^{-3}	60	2.0	10,000	1,000	0.015	25	700	442	570	▲
		Stern and Malkus (1953) Case 3	9.0	10^{-4}	1.48×10^{-3}	10	2.0	20,000	150	0.190	135	135	85	74,000	○
		Malkus (1955) Puerto Rico	4.0	0.6×10^{-5}	1.88×10^{-3}	90 (assumed)	1.5	80,000	1,000 (assumed)	0.052	44	800	506	12,100	■
		Malkus (1963)	5.0	1.12×10^{-5}	3.3×10^{-3}	120	3.0	9,000	5,000	0.0095	208	900	575	9,500	●
	Mt. Tee Wave	Garstang et al. (1963)	5.0 9.5		4.04×10^{-3} 3.11×10^{-3}	100 (assumed)	1.5 3.5	22,000				380 1,120	239 706		⊖ ⊕
		Queney (1960)	14.0	1.5×10^{-5}		40			1,000	0.120	400				×
Numerical	Heated Island	Tanouye (1966)	1.0 3.0 5.0	1.2×10^{-5}	3.50×10^{-3}	90 (assumed)	3, 5, 10 3, 5, 10 3, 5, 10	10,000	5,000	0.0018 0.0055 0.0092	56 167 278	857 (ΔT=3) 1429 (ΔT=5) 2857 (ΔT=10)	542 (ΔT=3) 903 (ΔT=5) 1806 (ΔT=10)	90 (U=1) 850 (U=3) 2360 (U=5)	□ △ ◇
		Estoque and Bhumralker (1968)	5.0	1.5×10^{-5}	4.40×10^{-3}	90 (assumed)	10	10,000	4,314	0.095	240	2,273	1,437	9,400	▽
		Spelman (1969)	5.0	adiabatic		90 (assumed)	5	80,000	1,500		83				◎

TABLE 2-5

Maximum Vertical Velocity for Given Basic Wind and Island Temperature Excess (Tanouye 1966)

Speed of Basic Wind (m/sec)	ΔT (^{o}C)	Maximum Vertical Velocity (cm/sec)
1	3	12
	5	55
	10	250
3	3	6
	5	20
	10	180
5	3	2
	5	3
	10	10

TABLE 2-6

Classification of Literatures (Airflow over an Obstacle)

Analytical				Numerical				Experiments		Observation	General
Linear		Nonlinear		Linear		Nonlinear		Water	Wind		
Steady	Unsteady	Steady	Unsteady	Steady	Unsteady	Steady	Unsteady	Channel	Tunnel		Review
Scorer (1949, 1951, 1953) Lyra (1943) Queney (1947)	Wurtele (1953)	Long (1953, 1954, 1955) Yih (1960) Yih (1965) Drazine & Moore (1967) Miles (1968a, 1968b) Davis (1969) Pao (1969)		Pekelis (1969)			Foldvik & Wurtele (1967) Magata (1967) Spelman (1969) Orville (1965, 1968, 1969) Lin and Apelt (1970) Oobayashi (1970)	Long (1954, 1955)	Lin and Binder (1967)	Queney (1960) Fosberg (1967, 1969)	Corby (1954) Queney (1960) Krishnamurti (1964) Yih (1965) Lin & Cermak (1969)

TABLE 2-6 (Continued)

(Urban Heat Island)

Analytical				Numerical				Observations	General Review
Linear		Nonlinear		Linear		Nonlinear			
Steady	Unsteady	Steady	Unsteady	Steady	Unsteady	Steady	Unsteady		
	Olfe and Lee (1971) Vukovich (1971)					Myrup (1969) Tag (1969)		Duckworth and Sandberg (1954), Okita (1960), DeMarrais (1961), Mitchell (1961), Pooler (1963), Bornstein (1968), Ludwig and Kealoha (1968), Oke and Hannell (1968), Georgii (1968), Holmes (1969), Kopec (1970), Preston - Whyte (1970).	Landsberg (1956) Peterson (1969)

(Sea Breeze)

Analytical				Numerical				Observations
Linear		Nonlinear		Linear		Nonlinear		
Steady	Unsteady	Steady	Unsteady	Steady	Unsteady	Steady	Unsteady	
Stern and Malkus (1953)	Haurwitz (1947) Smith (1955)					Fisher (1961) Estoque (1961,1962) Magata (1965)		Wexler (1946), Fisher (1960), Moroz (1967)

TABLE 2-6 (continued)

(Heated Island)

Analytical				Numerical				Wind Tunnel Experiments	Observations
Linear		Nonlinear		Linear		Nonlinear			
Steady	Unsteady	Steady	Unsteady	Steady	Unsteady	Steady	Unsteady		
Malkus and Stern (1953) Stern and Malkus (1953)	Smith (1955)						Tanouye (1966) Estoque and Bhumralkar (1968) Spelman (1969)		Malkus and Bunker (1952) Malkus (1955, 1963)

(Heated Mountain)

Analytical				Numerical				Wind Tunnel Experiments	Observations
Linear		Nonlinear		Linear		Nonlinear			
Steady	Unsteady	Steady	Unsteady	Steady	Unsteady	Steady	Unsteady		
							Orville (1968) Spelman (1969)		Fosberg (1967, 1969)

TABLE 4-1

A Comparison of Boundary Values of Variables Obtained by the Milne Predictor Formula and $\partial^2\Psi/\partial x^2 = \partial^2\zeta/\partial x^2 = \partial^2 T/\partial x^2 = 0$ which are shown in the parentheses.

	z(cm) \ x(cm)	-96 (Boundary)	-92	-88
ψ	4	-40.46486 (-39.99815)	-39.97349	-39.94883
	8	-119.51804 (.119.93301)	-119.94967	-119.96633
	12	-200.52165 (-200.08881)	-200.00090	-199.91299
	16	-279.92819 (-280.00740)	-279.85564	-279.70390
	48	-919.99244 (-920.00461)	-919.92868	-919.85275
u	4	14.93975 (14.99163)	14.99371	14.99579
	16	19.94467 (20.0093)	19.98897	19.98244
w	4	0.12284 (-0.006165)	0.06450	0.00007
	8	-0.10791 (0.004165)	-0.05604	0.00784
	12	0.13019 (-0.021978)	0.07608	0.01957
	48	0.01594 (0.01898)	0.01746	0.01993
ζ	0	-6.33716 (-6.24965)	-6.24503	-6.24041
	4	-2.50000 (-2.50000)	-2.50000	-2.50000

TABLE 5-1

A Summary of Wind Tunnel and Numerical Studies

Variables / Case		EXPERIMENTAL										THEORETICAL (Linearized)				NUMERICAL			
		Velocity U (cm/sec)	Stability S (cm^{-1})	$\frac{\partial T}{\partial z}$ (°C/cm)	Diffusivity K (cm^2/sec)	Temp. Excess δT (°C)	Island Width 2D (cm)	Charac. Length L (cm)	$(\overline{Fr})_L$	$(Re)_L$	$(N_h)_{x=D}$	Amplitude $A=\frac{\Delta T}{T_{max}}$ (cm)	Effective Height $H=A(1-\frac{1}{e})$ (cm)	x_o (cm)	$H_{x=2D}$ (cm)	H_{max} (cm)	K (cm^2/sec)	ΔT (°C)	$(N_h)_{x=D}$
A-1 (obstacle)		12	2.90×10^{-3} * (4.04,1.76)	0.91 (1.25,0.57)	0.2 (assumed)		8 x 8 obstacle	60	0.126 (0.100,0.152)	3600									
B-1 (Heated Island)		6.0	1.5×10^{-3} (2.42,0.57)	0.45 (0.72,0.17)	0.2 (assumed)	48	8	60	0.100 (0.065,0.134)	1800	5.40	66	42	735	1.15	14	2.7	26	0.99
B-2 (Heated Island)		6.0	1.5×10^{-3} (2.42,0.57)	0.45 (0.72,0.17)	0.2 (assumed)	84	8	60	0.100 (0.065,0.134)	1800	7.40	116	73	735	2.02	28	6.5	57	0.88
B-3 (Heated Island)	B-3	6.0	3.03×10^{-3} (4.46,1.59)	0.95 (1.40,0.52)	0.2 (assumed)	107	8	60	0.064 (0.048,0.080)	1800	5.55	76	48	364	2.42	24	2.3	55	0.71
	Equivalent Mt in B-3	6.0	3.03×10^{-3} (4.46,1.59)	0.95 (1.40,0.52)	0.2 (assumed)		4cm high Plateau	60	0.064 (0.048,0.080)	1800									
	B-3 in Neutral Situation	6.0	Neutral			107	8	60	0.064 (0.048,0.080)	1800									
C-1	Unheated Obstacle	6.0	1.5×10^{-3} (2.42,0.57)				8 x 8 obstacle	60	0.100 (0.065,0.134)	1800									
	Heated Obstacle	6.0	1.5×10^{-3} (2.42,0.57)			20	8 x 8 obstacle	60	0.100 (0.065,0.134)	1800									
3-dim.	Heated Island	6.0	1.5×10^{-3} (2.42,0.57)			64	8 x 30	60	0.100 (0.065,0.134)	1800	10.08								

* The first number shows the value in the lower layer and the second one indicates the value in the upper layer

TABLE 5-2

Case A-1 : Experimental Temperature Distribution Data

z(cm) \ x(cm)	-60	-48	-40	-32	-20	-12	-4	8	12	16	20	24	28	32
0.64	307.2	306.7	306.5	306.2	304.3	302.6	301.4	307.5	307.7	301.9	302.9	305.5	304.8	306.5
1.27	309.2	308.9	308.6	308.7	306.7	305.3	304.1	308.9	308.2	307.0	307.9	310.1	309.9	308.9
2.54	311.0	310.8	310.8	310.6	309.4	308.2	306.8	311.3	310.3	310.8	312.0	311.7	311.3	310.3
5.08	311.3	311.0	311.0	310.8	310.3	309.6	308.4	313.1	313.1	313.4	311.5	310.3	311.0	311.0
7.62	313.1	312.7	312.4	312.0	311.3	310.6	309.7	317.6	313.4	310.3	312.7	315.3	316.0	314.8
12.70	316.2	315.7	315.5	315.3	314.8	314.5	313.9	314.8	316.7	318.8	319.7	320.6	320.9	321.1
17.78	320.2	319.7	319.9	319.5	319.0	319.0	319.4	320.6	321.1	322.5	322.3	322.8	322.5	323.0
22.86	323.5	323.2	323.5	323.5	331.7	323.0	323.3	323.9	323.7	324.2	323.9	323.9	323.7	324.2
38.10	332.6	332.6	332.4	332.1	332.7	331.2	330.8	331.2	331.0	331.0	330.7	330.7	330.3	330.0

TABLE 5-2 (Continued)

Case A-1 : Experimental Temperature Distribution Data

z(cm) \ x(cm)	36	40	44	48	52	56	60	64	72	80	100	120	140
0.64	305.8	306.7	305.8	306.2	306.2	306.2	307.5	305.5	306.5	307.2	306.5	307.0	305.8
1.27	307.9	308.4	308.7	308.7	308.7	309.2	308.9	308.7	307.7	308.2	308.2	307.7	306.7
2.54	310.1	309.9	309.6	309.4	309.9	310.3	310.3	309.9	309.6	310.1	308.9	309.4	308.9
5.08	310.8	310.3	310.1	309.9	309.9	309.6	310.3	310.3	310.8	311.0	309.9	310.3	310.3
7.62	315.3	313.8	312.2	311.7	311.7	311.7	312.4	312.4	312.9	313.6	312.4	313.1	313.8
12.70	320.6	319.5	318.3	317.4	316.9	316.7	316.4	315.7	318.1	319.7	318.8	319.0	319.2
17.78	322.3	322.0	321.1	320.6	320.2	219.9	320.2	320.2	321.8	322.8	321.6	322.0	321.8
22.86	323.5	323.5	322.5	322.8	322.0	329.3	322.8	322.3	323.5	323.9	323.9	324.4	324.2
38.10	329.8	329.8	329.8	329.5	329.3	323.0	329.3	329.1	329.1	329.3	329.5	329.1	328.1

TABLE 5-3

Case B-1 : Experimental Temperature Distribution Data

z(cm) \ x(cm)	-20	-16	-12	-8	-4	0	2	4	6	8	10	12	14	16	18	20
0	290.0	290.0	290.0	290.0	290.0	341	341	341	341	341	290.0	290.0	290.0	290.0	290.0	290.0
0.64	292.8	292.5	291.8	291.8	293.0	303.0	315.7	320.6	319.2	300.9	297.3	296.0	294.5	292.8	292.5	292.3
1.27	294.3	294.0	293.8	293.8	294.8	297.0	299.9	308.7	306.7	303.6	297.8	296.8	296.0	295.3	295.0	294.8
2.54	296.0	295.8	295.8	295.8	296.5	297.8	298.2	299.2	308.7	306.5	299.2	298.2	298.0	297.5	297.3	297.3
2.08	298.7	298.5	298.2	298.5	299.0	299.7	299.7	299.7	299.9	305.0	305.3	300.7	300.2	300.2	300.2	299.9
7.62	300.4	300.2	300.2	300.4	300.9	300.9	300.9	300.9	300.7	301.6	303.3	302.4	301.2	301.2	301.2	301.2
12.70	302.1	302.1	302.1	302.1	302.4	302.6	302.9	302.6	302.6	302.6	302.4	302.4	302.4	302.1	301.9	301.9
17.78	303.1	303.1	303.1	303.1	303.1	303.1	303.1	303.1	303.1	303.1	303.1	302.9	302.6	302.4	302.4	302.1
22.86	303.6	303.6	303.6	303.6	303.6	303.6	303.6	303.6	303.6	303.6	303.3	303.5	303.1	302.9	302.6	302.6
38.10	306.0	306.0	306.0	306.0	306.0	306.0	306.0	306.0	306.0	306.0	306.0	306.0	306.0	306.0	306.2	306.2

TABLE 5-3 (Continued)

Case B-1 : Experimental Temperature Distribution Data

z(cm) \ x(cm)	22	24	26	28	30	32	34	36	38	40	44	48	52	56	60
0	290.0	290.0	290.0	290.0	290.0	290.0	290.0	290.0	290.0	290.0	290.0	290.0	290.0	290.0	290.0
0.64	292.1	292.1	292.1	292.5	292.5	292.8	292.8	293.3	293.5	293.5	293.8	293.8	294.0	294.0	294.0
1.27	294.8	294.8	294.8	295.0	295.0	295.0	295.0	295.3	295.5	295.5	295.8	295.8	296.0	296.0	296.0
2.54	297.0	297.0	297.0	297.3	297.0	297.0	297.0	297.3	297.3	297.3	297.3	297.5	297.5	297.5	297.5
2.08	299.9	299.7	299.7	299.7	299.5	299.5	299.5	299.5	299.5	299.5	299.7	299.7	299.7	299.7	299.9
7.62	301.2	301.2	300.9	301.2	301.4	301.2	301.4	301.2	301.2	301.2	301.2	300.9	300.9	301.2	301.2
12.70	302.1	302.1	302.1	302.1	302.1	302.1	302.1	302.1	302.4	302.4	302.4	302.4	302.4	302.4	302.4
17.78	302.1	302.4	302.4	302.4	302.6	302.4	302.6	302.6	302.9	302.9	302.9	302.9	302.6	302.6	302.6
22.86	302.4	302.4	302.6	302.9	302.9	303.1	303.3	303.1	303.1	303.3	303.3	303.1	303.1	303.1	303.3
38.10	306.2	306.0	306.0	306.0	306.0	306.0	306.0	306.0	306.0	306.0	306.0	306.0	306.0	306.0	306.0

TABLE 5-4

Case B-2 : Experimental Temperature Distribution Data

z(cm) \ x(cm)	-20	-16	-12	-8	-4	0	4	6	8	10	12	16	18
0	290.0	290.0	290.0	290.0	290.0	377.3	377.3	377.3	377.3	290.0	290.0	290.0	290.0
0.64	293.5	293.3	292.8	292.8	294.0	305.0	327.7	329.5	318.1	300.7	298.5	294.3	293.5
1.27	294.8	294.8	299.5	299.5	295.8	298.7	313.8	316.7	312.2	300.2	298.2	296.8	296.3
2.54	296.8	296.5	296.5	296.8	298.0	300.0	303.8	316.4	316.7	302.1	300.4	299.2	298.5
5.08	299.5	299.2	299.2	299.5	300.2	301.4	302.1	303.8	309.9	307.5	302.6	301.9	301.6
7.62	304.3	304.3	304.3	304.3	304.6	304.6	304.6	304.8	304.8	305.5	306.0	305.0	304.6
12.70	303.3	303.3	303.6	303.6	303.8	304.1	304.1	304.6	304.6	307.0	307.2	304.6	304.3
17.78	304.3	304.3	304.3	304.3	304.6	304.6	304.6	304.8	304.8	305.5	306.0	305.0	304.6
22.86	305.0	305.0	305.0	305.0	305.3	305.3	305.3	305.3	305.5	305.8	306.2	305.3	305.0
38.10	306.7	306.7	306.7	306.7	307.0	306.7	306.2	306.5	306.2	306.0	306.2	306.2	306.2

TABLE 5-4 (Continued)

Case B-2 : Experimental Temperature Distribution Data

z(cm) \ x(cm)	20	22	24	26	28	30	32	34	38	40	42	44
0	290.0	290.0	290.0	290.0	290.0	290.0	290.0	290.0	290.0	290.0	290.0	290.0
0.64	293.3	293.3	293.5	293.5	293.5	294.3	294.3	294.5	294.8	294.8	295.0	295.5
1.27	296.0	295.8	296.0	296.0	296.3	296.3	296.5	296.5	296.8	296.8	297.0	297.0
2.54	298.2	298.2	298.2	298.2	298.5	298.5	298.5	298.7	298.5	298.7	299.0	299.0
5.08	301.4	301.2	301.2	301.4	301.4	301.4	301.4	301.4	301.4	301.4	301.6	301.6
7.62	302.6	302.9	302.6	302.6	302.9	302.9	302.9	302.9	302.9	303.1	303.1	303.1
1.27	304.3	304.3	304.3	304.3	304.3	304.3	304.6	304.6	304.3	304.6	304.6	304.6
17.78	304.8	304.8	304.8	304.8	304.8	304.8	305.0	305.0	305.0	305.0	305.3	305.0
22.86	305.0	305.3	305.5	305.3	305.5	305.5	305.8	305.8	306.0	306.0	305.8	305.5
38.10	306.2	306.2	306.2	306.2	306.2	306.5	306.5	306.7	307.0	307.2	307.5	307.5

TABLE 5-5

Case B-3 : Experimental Temperature Distribution Data

z(cm) \ x(cm)	-20	-16	-12	-8	-4	0	4	8	10	12	16	18	20
0	298.0	298.0	298.0	298.0	298.0	411.9	411.9	411.9	298.0	298.0	298.0	298.0	298.0
0.64	304.6	300.9	300.2	301.9	301.6	328.4	364.8	326.7	314.3	312.7	307.0	304.3	302.9
1.27	307.9	306.5	306.0	306.2	306.0	311.7	332.1	324.4	313.8	312.7	311.3	309.9	309.2
2.54	312.7	312.0	311.5	312.0	312.2	315.5	317.8	328.8	318.1	318.1	317.1	316.4	315.7
5.08	318.3	317.6	317.4	317.8	318.3	319.7	319.9	326.7	325.1	321.1	321.6	321.3	321.1
7.62	323.2	322.8	322.8	323.0	323.2	323.5	323.7	324.9	325.8	323.5	324.2	324.2	324.2
12.70	326.7	327.0	326.7	327.0	327.2	327.7	327.9	327.0	326.3	326.3	326.0	326.0	326.3
17.78	328.4	328.6	328.6	328.6	328.8	328.8	337.1	327.9	327.4	327.4	327.2	327.7	327.7
22.86	329.8	330.0	330.0	330.0	330.3	330.0	330.2	329.8	329.1	329.1	328.1	328.6	328.6
38.10	336.7	336.7	336.7	336.9	336.9	336.9	330.3	337.1	337.3	337.3	337.6	337.6	337.6

TABLE 5-5 (Continued)

Case B-3 : Experimental Temperature Distribution Data

z(cm) \ x(cm)	22	24	26	28	30	32	34	36	38	40	42	44
0	298.0	298.0	298.0	298.0	298.0	298.0	298.0	298.0	298.0	298.0	298.0	298.0
0.64	301.6	302.6	303.8	305.3	305.8	306.7	306.o	307.7	307.2	307.7	307.5	307.7
1.27	308.4	308.7	309.6	310.3	310.8	311.3	311.0	312.0	311.7	312.0	312.0	312.2
2.54	315.3	315.5	315.7	316.2	316.2	316.4	316.0	316.7	316.4	316.4	316.7	316.7
5.08	320.6	320.4	320.6	320.9	321.1	321.3	321.1	321.6	321.6	321.6	321.3	321.6
7.62	324.2	323.9	324.2	324.2	324.4	324.4	324.4	324.6	324.9	324.6	324.6	324.6
12.70	326.7	327.0	327.0	327.0	327.0	327.0	327.0	327.2	327.2	327.2	327.4	327.2
17.78	328.4	328.8	329.1	329.1	329.1	328.8	328.8	329.1	329.1	329.1	329.1	329.1
22.86	329.8	330.3	330.7	331.0	331.0	331.0	330.7	331.0	331.0	331.2	331.0	331.0
38.10	337.6	337.8	337.8	338.0	338.0	338.2	338.2	338.2	338.2	338.3	338.2	338.2

TABLE 5-6

Case B-3 Neutral : Experimental Temperature Distribution Data

r(cm) \ x(cm)	-12	-8	-4	0	4	8	12	16	20	24	28	36	44	52
0	290.0	290.0	290.0	412.0	412.0	412.0	290.0	290.0	290.0	290.0	290.0	290.0	290.0	290.0
0.64	290.6	290.8	292.1	298.0	311.5	322.5	300.4	291.6	290.6	290.6	290.3	290.8	290.8	290.8
1.27	290.8	291.1	292.3	295.0	314.8	318.5	296.5	292.0	291.3	291.3	291.1	291.6	291.3	291.3
2.54	291.1	291.6	292.8	294.3	305.0	321.3	298.2	293.3	292.3	292.3	292.1	292.1	292.1	292.1
5.08	292.5	292.8	293.0	293.8	294.8	305.0	301.4	294.8	293.8	293.5	293.3	293.3	293.3	293.0
7.62	293.3	293.8	294.3	294.5	294.5	296.3	301.6	295.8	294.5	294.3	294.0	293.8	293.8	293.5
12.70	294.5	294.8	295.3	295.0	295.0	294.8	297.0	299.0	295.8	295.0	294.5	294.5	294.3	294.3
17.78	295.3	295.3	295.3	295.0	295.0	295.0	295.3	297.3	297.o	295.8	295.0	294.8	299.8	299.5
22.86	295.3	295.5	295.8	295.3	295.0	295.0	295.0	295.8	297.3	296.5	295.8	295.3	295.0	295.0
38.10	296.5	296.3	296.5	296.5	296.5	296.5	296.5	296.5	296.5	296.5	296.3	295.8	295.8	295.8

TABLE 5-7

Case C-1 (Unheated Mountain) : Experimental Temperature Distribution Data

z(cm) \ x(cm)	-20	-16	-12	-8	-4	10	12	14	16	18	20	22	24	26	28	30
0	290.0	290.0	290.0	290.0	290.0	290.0	290.0	290.0	290.0	290.0	290.0	290.0	290.0	290.0	290.0	290.0
0.64	292.3	292.1	291.6	291.3	290.8	294.8	294.5	293.5	291.8	291.3	291.3	291.3	291.3	291.3	291.6	291.8
1.27	293.8	293.8	293.3	293.0	292.8	295.5	295.3	294.8	294.0	294.0	293.8	293.8	293.8	293.8	293.8	294.0
2.54	295.8	295.8	295.3	295.0	294.8	297.0	296.8	296.8	296.5	296.3	296.3	296.3	296.5	296.5	296.5	296.5
5.08	297.5	297.3	297.0	296.8	296.8	298.5	299.0	299.2	299.2	299.2	299.0	298.2	298.2	298.5	298.7	298.7
7.62	299.0	299.0	298.7	298.2	298.2	299.5	300.2	300.4	300.7	300.4	300.2	300.0	297.7	299.9	299.9	299.9
12.70	301.6	301.6	301.6	301.6	301.4	301.6	301.9	301.6	301.6	301.6	301.6	301.6	301.6	301.6	301.9	301.9
17.78	303.3	303.3	303.1	303.1	303.1	302.6	302.9	302.9	303.1	303.1	302.9	302.9	303.1	303.1	303.1	303.1
22.86	304.1	304.1	304.1	304.1	304.1	303.3	303.6	303.6	303.8	303.8	303.8	303.8	303.8	303.8	303.8	303.8
38.10	306.7	306.7	306.7	306.7	306.7	306.2	306.5	306.5	306.5	306.7	306.7	306.7	306.5	306.7	306.7	306.7

TABLE 5-7 (Continued)

Case C-1 (Unheated Mountain) : Experimental Temperature Distribution Data ution Data

z(cm) \ x(cm)	32	34	36	38	40	42	44	46	48	50	54	58
0	290.0	290.0	290.0	290.0	290.0	290.0	290.0	290.0	290.0	290.0	290.0	290.0
0.64	292.1	292.1	292.5	292.5	292.8	292.8	293.0	293.0	293.0	293.3	293.5	293.8
1.27	294.0	294.3	294.5	294.5	294.5	294.8	294.8	295.0	295.0	295.0	295.3	295.3
2.54	296.5	296.8	296.8	296.8	297.0	297.0	297.0	297.3	297.0	297.0	297.3	297.5
5.08	299.2	299.2	299.2	299.2	299.2	299.2	299.2	299.5	299.5	299.2	299.5	299.5
7.62	300.2	300.2	300.2	300.2	300.2	300.2	300.4	300.4	300.2	300.4	300.4	300.7
12.70	301.9	301.9	301.9	301.9	301.9	301.9	302.1	302.1	302.1	302.1	302.4	302.4
17.78	303.1	302.9	303.1	302.9	302.9	303.1	303.1	303.1	303.1	303.1	303.1	303.1
22.86	304.1	303.8	303.8	303.8	303.8	303.8	304.1	304.1	304.1	304.1	304.1	304.1
38.10	306.7	306.7	306.7	306.7	306.7	306.7	306.7	306.7	306.7	306.7	306.7	307.0

TABLE 5-7

Case C-1 (Unheated Mountain) : Experimental Temperature Distribution Data

z(cm) \ x(cm)	0	4	8
8	300.0	300.0	300.0
9.27	303.6	303.6	303.6
24.51	298.9	299.2	299.9
29.59	304.4	304.6	304.6
34.67	305.5	305.5	305.8
39.75	306.7	306.7	307.0
42.29	308.0	308.0	308.0
44.83	308.7	308.9	309.2
46.10	309.2	309.2	309.4
46.74	310.0	310.0	310.4

TABLE 5-8

Case C-1 (Heated Mountain) : Experimental Temperature Distribution Data

z(cm) \ x(cm)	-20	-16	-12	-8	-4	10	12	14	16	18	21	23	25	27	29
0	290.0	290.0	290.0	290.0	290.0	290.0	290.0	290.0	290.0	290.0	290.0	290.0	290.0	290.0	290.0
0.64	291.6	291.3	289.8	289.8	289.3	297.3	296.8	295.3	292.5	290.6	290.1	290.1	290.1	290.3	290.3
1.27	293.3	293.3	292.1	292.1	291.6	296.5	296.5	296.0	294.5	293.8	293.0	293.0	293.0	293.0	293.0
2.54	295.8	295.5	294.8	294.8	294.5	298.7	298.7	298.7	298.7	297.3	296.8	296.8	296.8	296.8	296.8
5.08	297.5	297.3	296.8	296.5	296.5	300.4	300.2	300.2	299.7	299.2	299.2	299.2	299.0	299.0	299.2
7.62	299.5	299.5	299.2	299.2	299.2	302.1	301.9	301.9	301.6	301.6	301.4	301.4	301.4	301.6	301.6
12.70	301.9	301.4	301.6	301.4	301.6	301.6	302.4	303.3	302.9	302.6	302.1	302.1	302.1	302.1	302.1
17.78	303.6	303.6	303.3	303.6	303.1	303.1	303.1	303.1	303.1	303.1	303.1	303.1	303.1	303.1	303.1
22.86	304.6	304.6	304.6	304.6	304.3	304.1	304.1	304.1	304.1	304.1	304.1	304.1	303.8	303.8	303.8
38.10	306.7	306.7	306.7	306.7	306.7	306.0	306.2	306.2	306.2	306.2	306.2	306.2	306.2	306.5	306.5

TABLE 5-8 (Continued)

Case C-1 (Heated Mountain) : Experimental Temperature Distribution Data

z(cm) \ x(cm)	31	33	35	37	39	41	43	45	47	49	51	53	55	57
0	290.0	290.0	290.0	290.0	290.0	290.0	290.0	290.0	290.0	290.0	290.0	290.0	290.0	290.0
0.64	290.8	291.1	291.3	291.8	292.1	292.1	292.3	292.3	292.3	292.3	292.5	292.5	292.5	293.0
1.27	293.3	293.3	293.5	293.5	293.8	293.8	294.0	294.0	294.0	294.0	294.3	294.3	294.3	294.5
2.54	296.8	296.8	296.8	297.0	297.0	297.0	297.0	297.3	297.0	297.3	297.3	297.3	297.3	297.5
5.08	299.2	299.2	299.5	299.5	299.5	299.5	299.5	299.7	299.5	299.7	299.7	299.7	299.7	299.7
7.62	301.4	301.6	301.6	301.6	301.6	301.6	301.9	301.9	301.9	301.9	301.9	301.9	301.9	301.9
12.70	302.1	302.1	302.1	302.1	302.4	302.4	302.4	302.4	302.4	302.4	302.4	302.4	302.4	302.4
17.78	303.1	303.1	303.3	303.1	303.1	303.1	303.1	303.3	303.1	303.1	303.1	303.1	303.1	303.3
22.86	303.8	304.1	304.1	304.1	304.1	303.8	304.1	304.1	304.1	304.1	304.1	304.1	304.1	304.3
38.10	306.5	306.5	306.5	306.5	306.5	306.5	306.5	306.5	306.5	306.7	306.5	306.7	306.5	306.7

TABLE 5-8 (Continued)

Case C-1 (Heated Mountain) : Experimental Temperature Distribution Data

z(cm) \ x(cm)	0	2	4	6	8
8	310.0	310.0	310.0	310.0	310.0
8.64	305.1	306.8	307.0	308.3	307.5
9.27	301.9	303.2	303.6	304.1	304.1
10.54	301.4	301.9	302.7	302.9	303.2
13.08	301.4	301.9	302.2	302.2	302.2
15.62	303.2	303.2	303.4	303.4	303.4
20.70	303.4	303.4	303.4	303.6	303.8
25.78	304.4	304.4	304.4	304.4	304.4
46.10	305.5	305.5	305.5	305.5	305.5
30.86	309.3	309.3	309.3	309.7	309.7

FIGURES

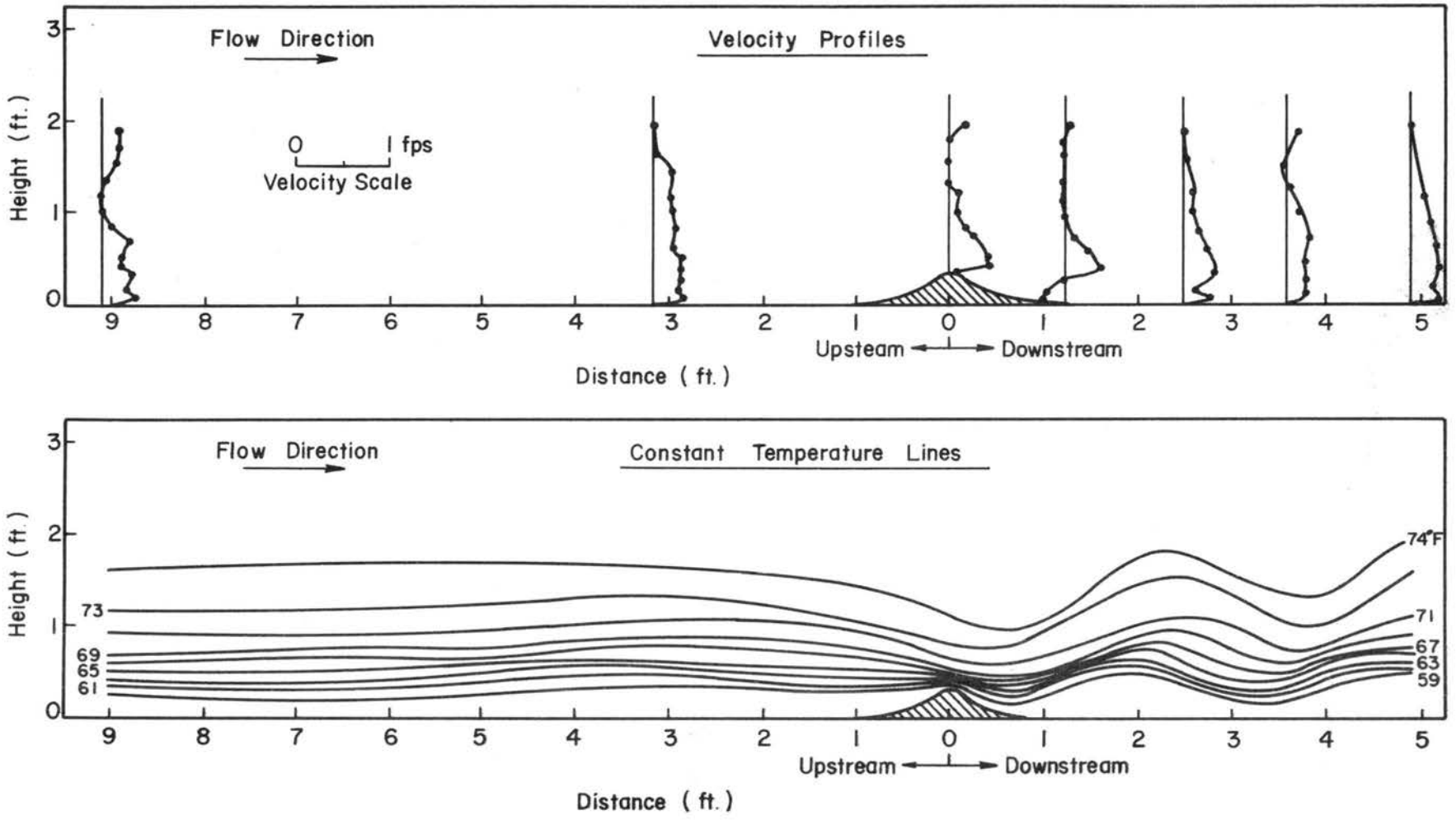

Fig. 1-1 Typical constant temperature lines and velocity profiles from a mountain lee-wave simulation in a wind tunnel. $(Fr)_L = 0.238$, $U = 7.25$ cm/sec, $L = 18$ cm, $s = 3.83 \times 10^{-3}$ cm^{-1} (Lin and Binder, 1967).

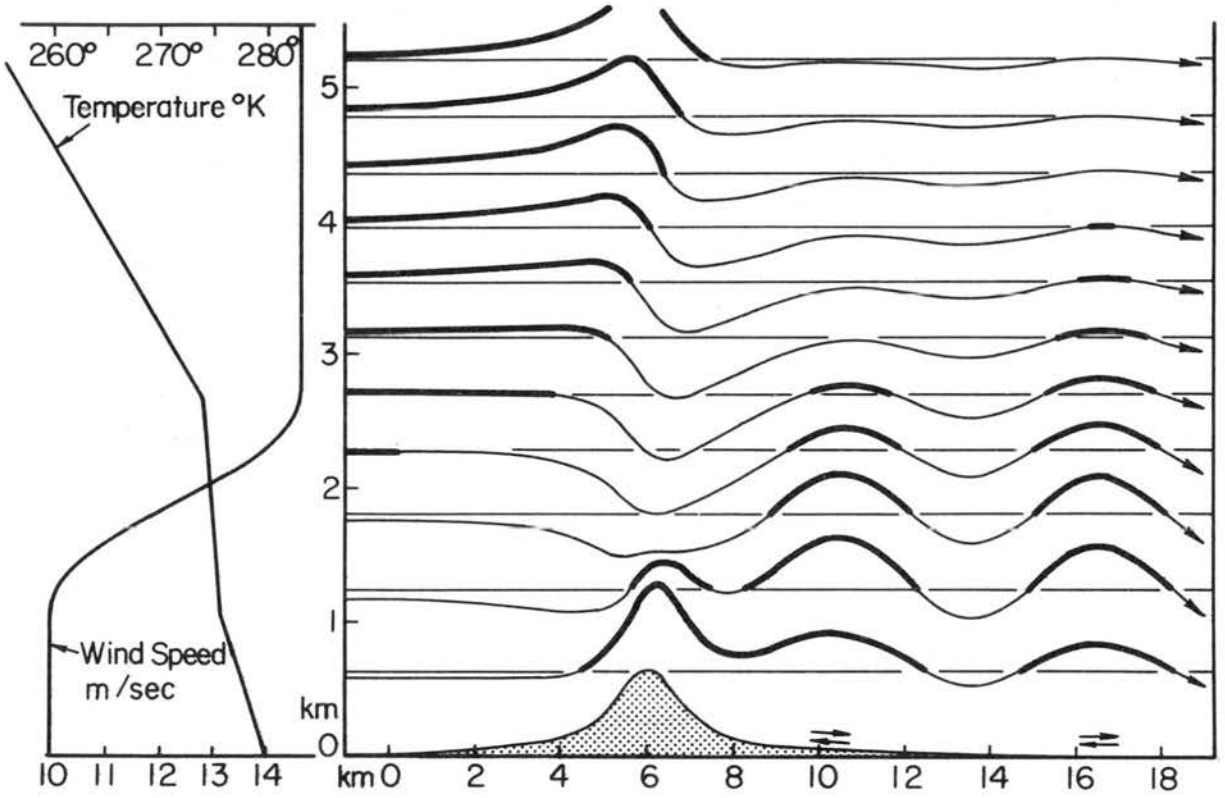

Fig. 2-1 Scorer's two-layer model of airflow over a mountain (1949).

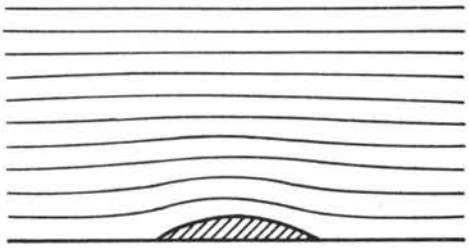

$(\overline{Fr})_H = 0.50, \beta = 0.10, b = 0.40$

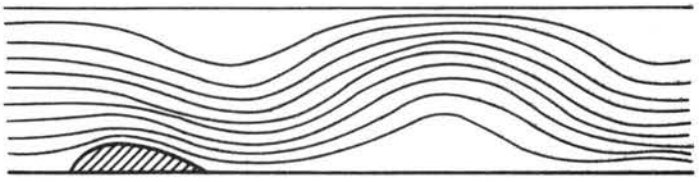

$(\overline{Fr})_H = 0.25, \beta = 0.15, b = 0.40$

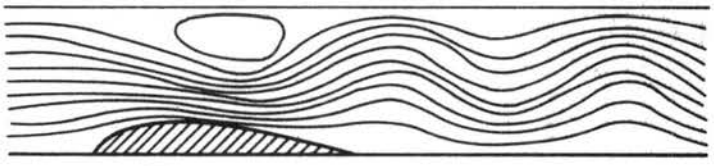

$(\overline{Fr})_H = 0.20, \beta = 0.20, b = 1.0$

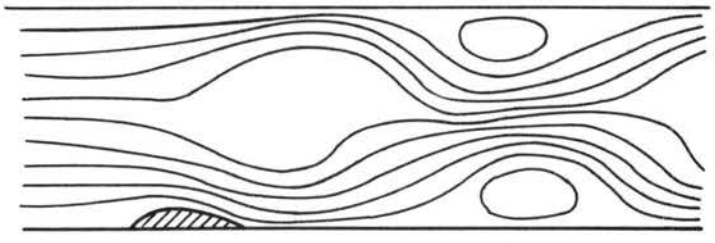

$(\overline{Fr})_H = 0.083, \beta = 0.124, b = 0.4$

Fig. 2-2 Some of Long's (1955) theoretically computed streamlines of fluid flow over an obstacle.

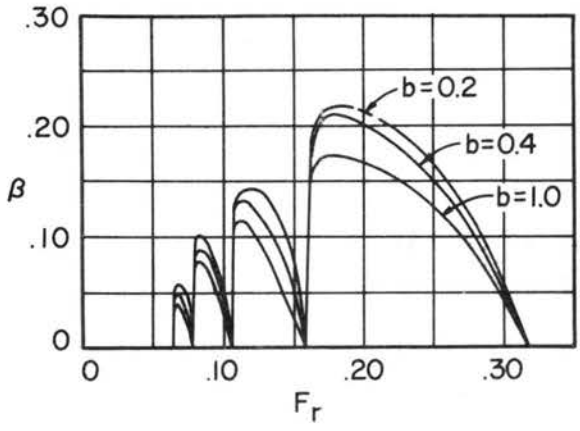

Fig. 2-3 Criteria of overturning instability (Long, 1955). β is a dimensionless obstacle height; obstacle height/channel height. b is a dimensionless half width of the obstacle and Fr is the Froude number. Overturning instability is observed if an obstacle exceeds the critical height given by the solid lines.

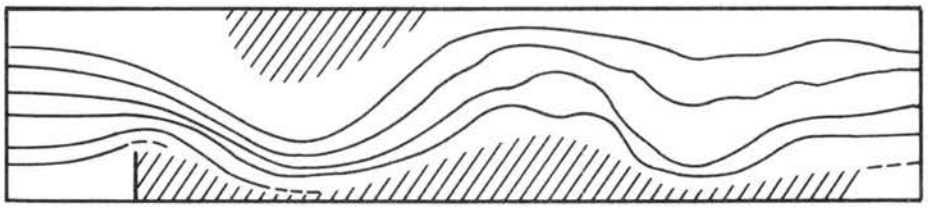

Observed Flow over Thin Barrier for k = 1.50

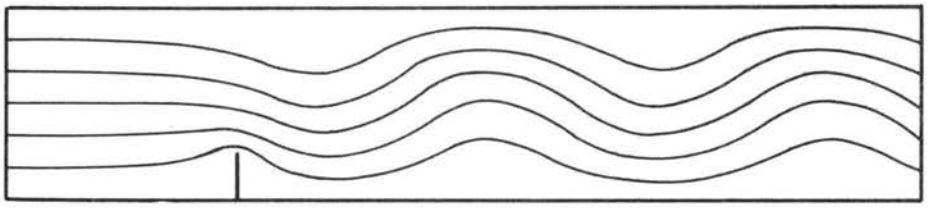

Calculated Flow over Thin Barrier for k = 1.50

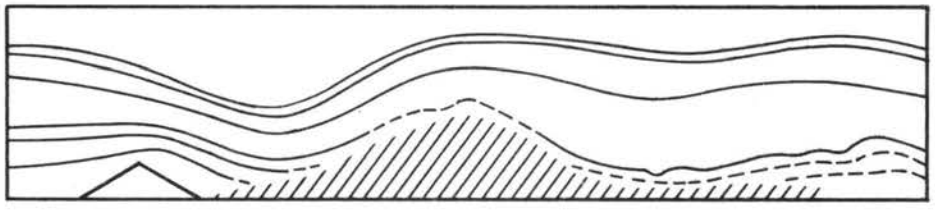

Observed Flow over Triangular Obstacle for k = 2.70

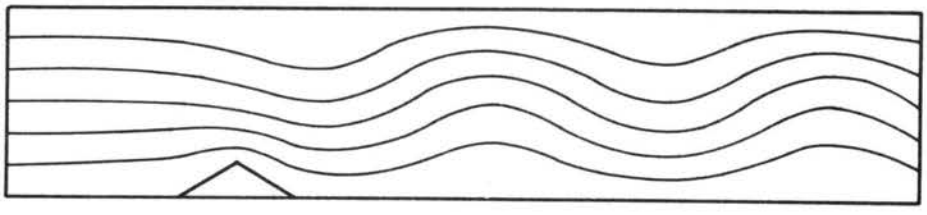

Calculated Flow over Triangular Obstacle for k = 2.70

Fig. 2-4 Some of Davis' results (1969). In each case the upper figure was obtained from a water channel experiment and the lower one was computed from Long's model. Hatched region indicates the area where turbulent motion was observed.

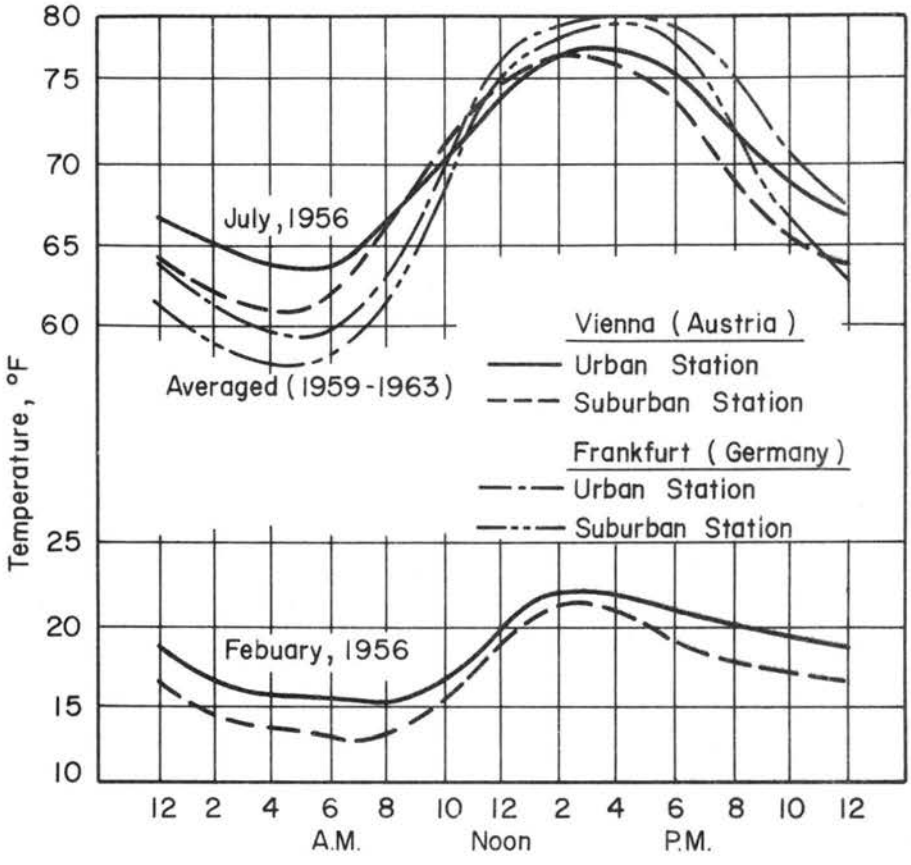

Fig. 2-5 Diurnal temperature variation in Vienna, Austria (Mitchell, 1961) for February and July, and Frankfurt, Germany, (Georgii, 1968) in summer for both an urban and a suburban stations.

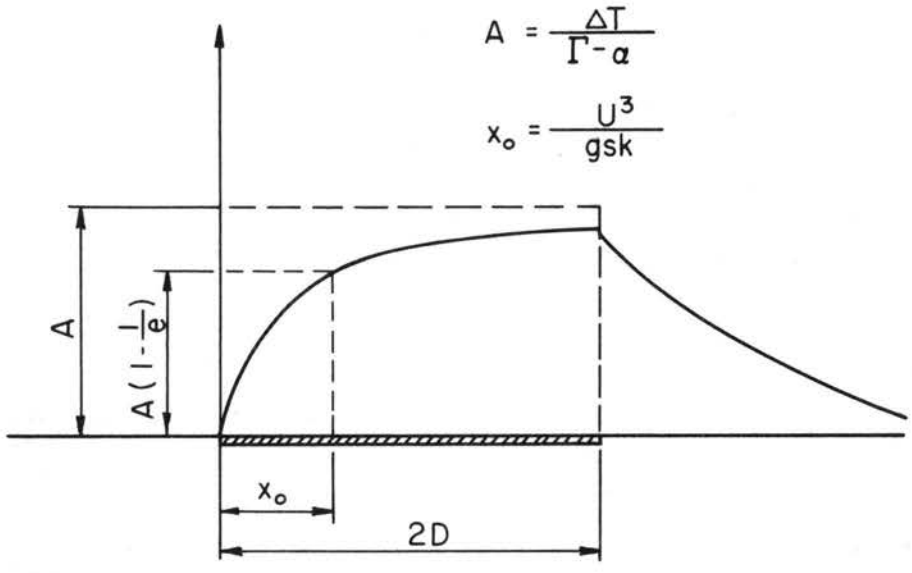

ΔT : Temperature Excess over an Island

Γ : Adiabatic Lapse Rate

α : $-\frac{\partial T}{\partial z}$

x : Shape Parameter

s : Stability, $\frac{\Gamma - \alpha}{T}$

Fig. 2-6 Sketch of an equivalent thermal mountain (Stern and Malkus, 1953).

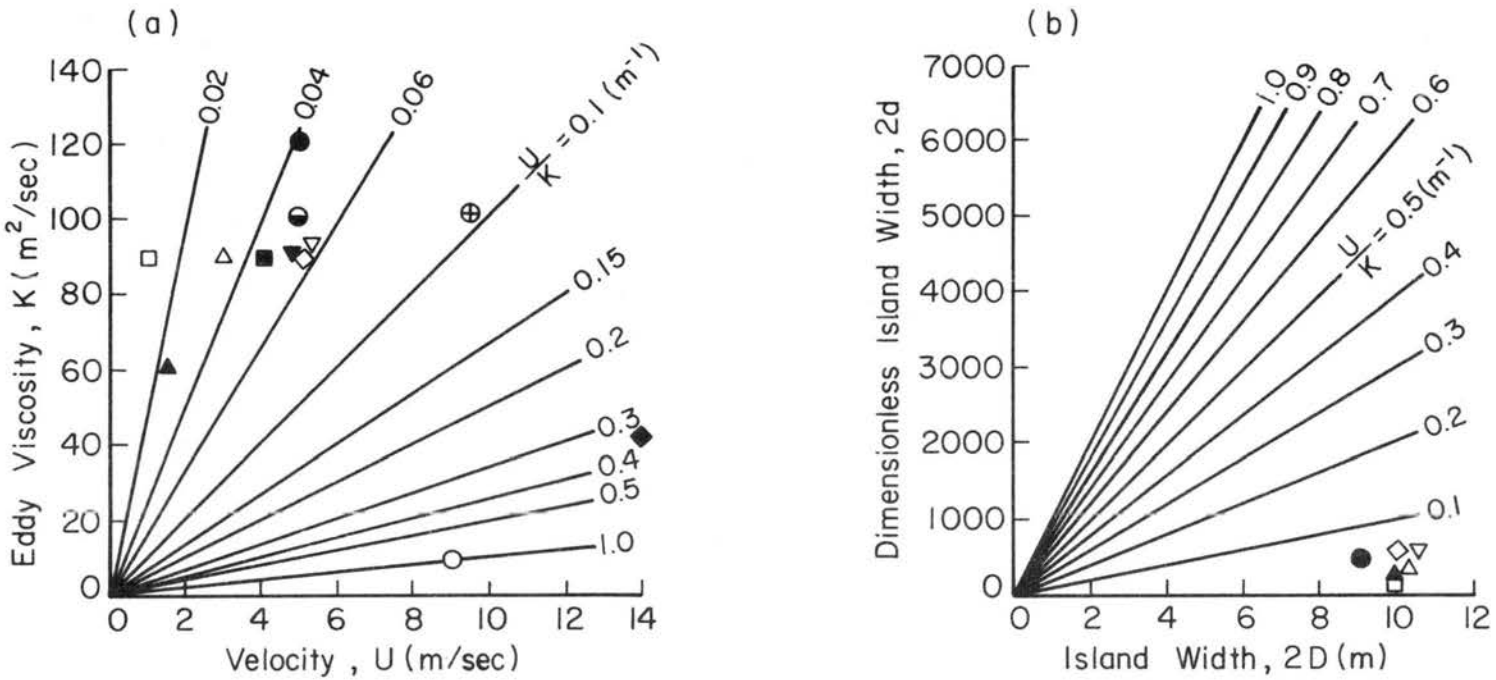

Fig. 2-7 Meteorological factors observed and assumed in numerical simulations. ▲ Stern and Malkus (1953), Case 4; ■ Malkus (1955), Puerto Rico; ● Malkus (1963), ○ Stern and Malkus (1953), Case 3; x A typical mountain lee-wave (Queney, 1960); □ Tanouye (1966), u = 1 m/sec; △ Tanouye (1966), u = 3 m/sec; ◇ Tanouye (1966), u = 5 m/sec; ▽ Estoque (1968); ◎ Spelman (1968); ⊖ , ⊕ Garstang et al. (1965).

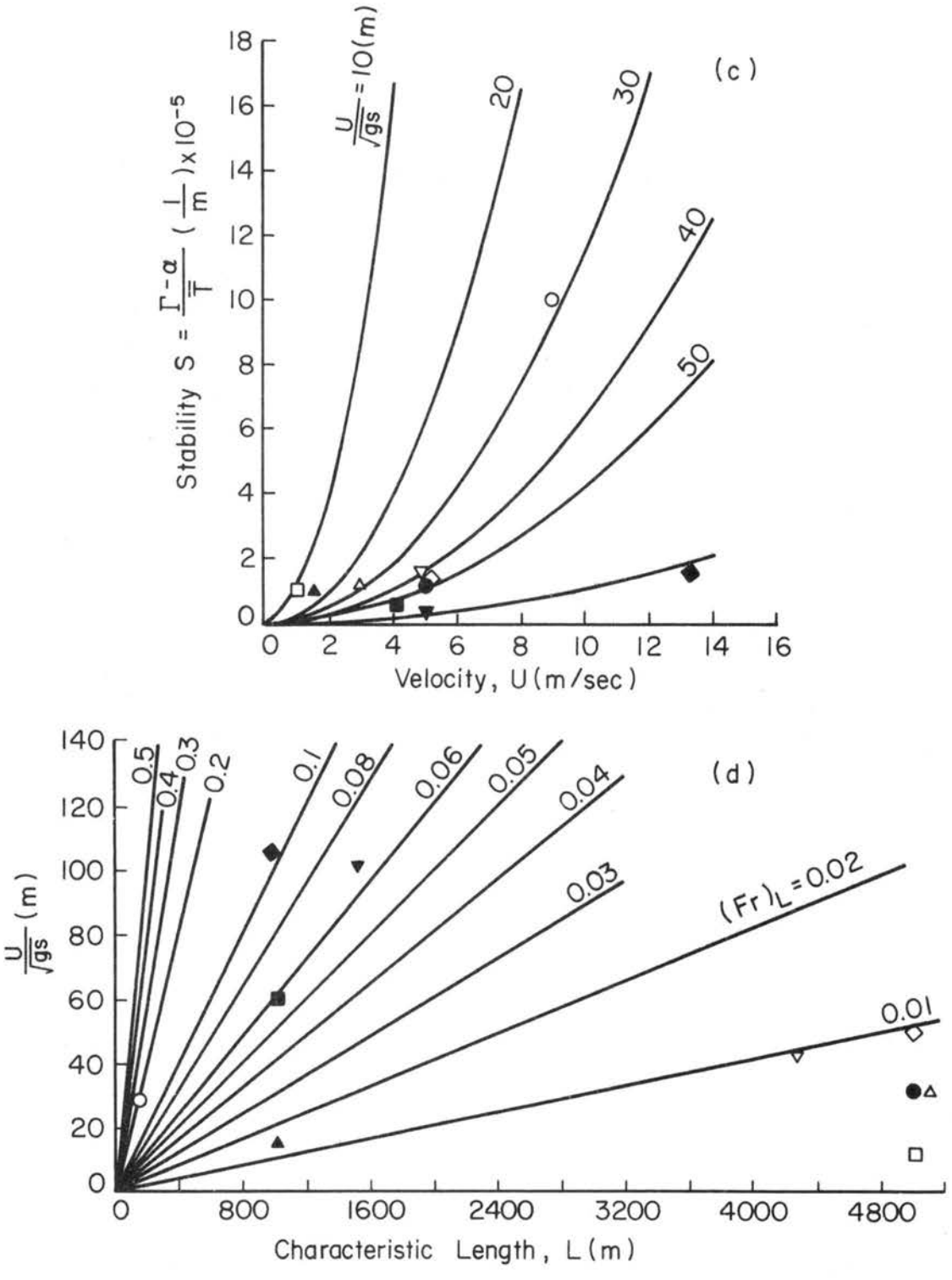

Fig. 2-7 (continued)

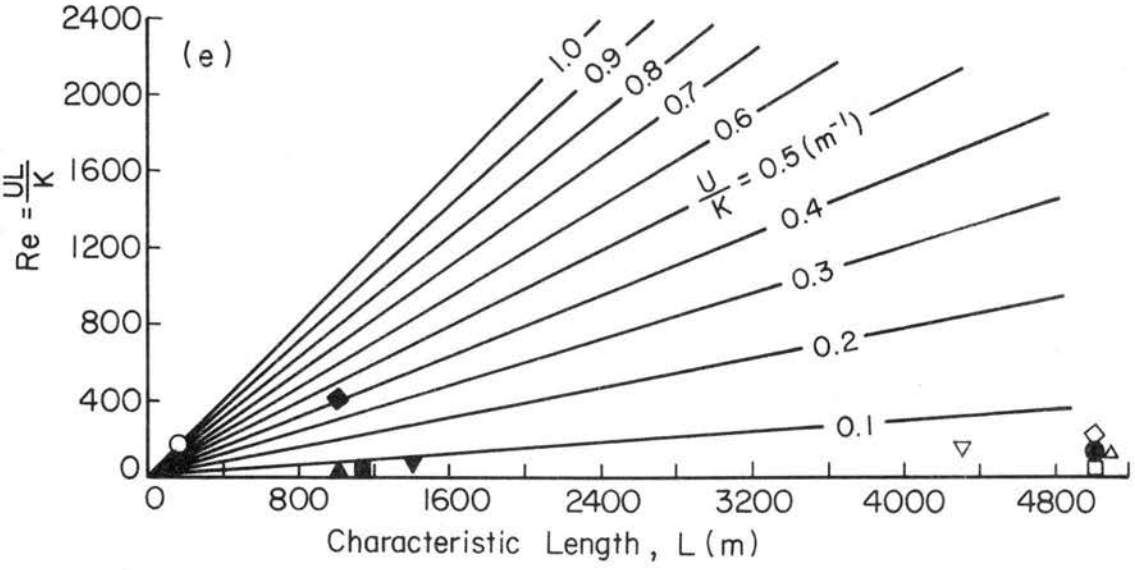

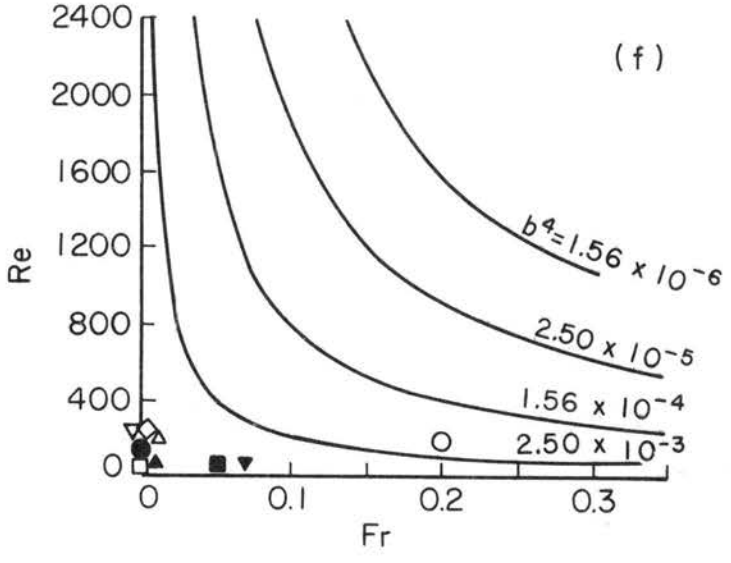

Fig. 2-7 (continued)

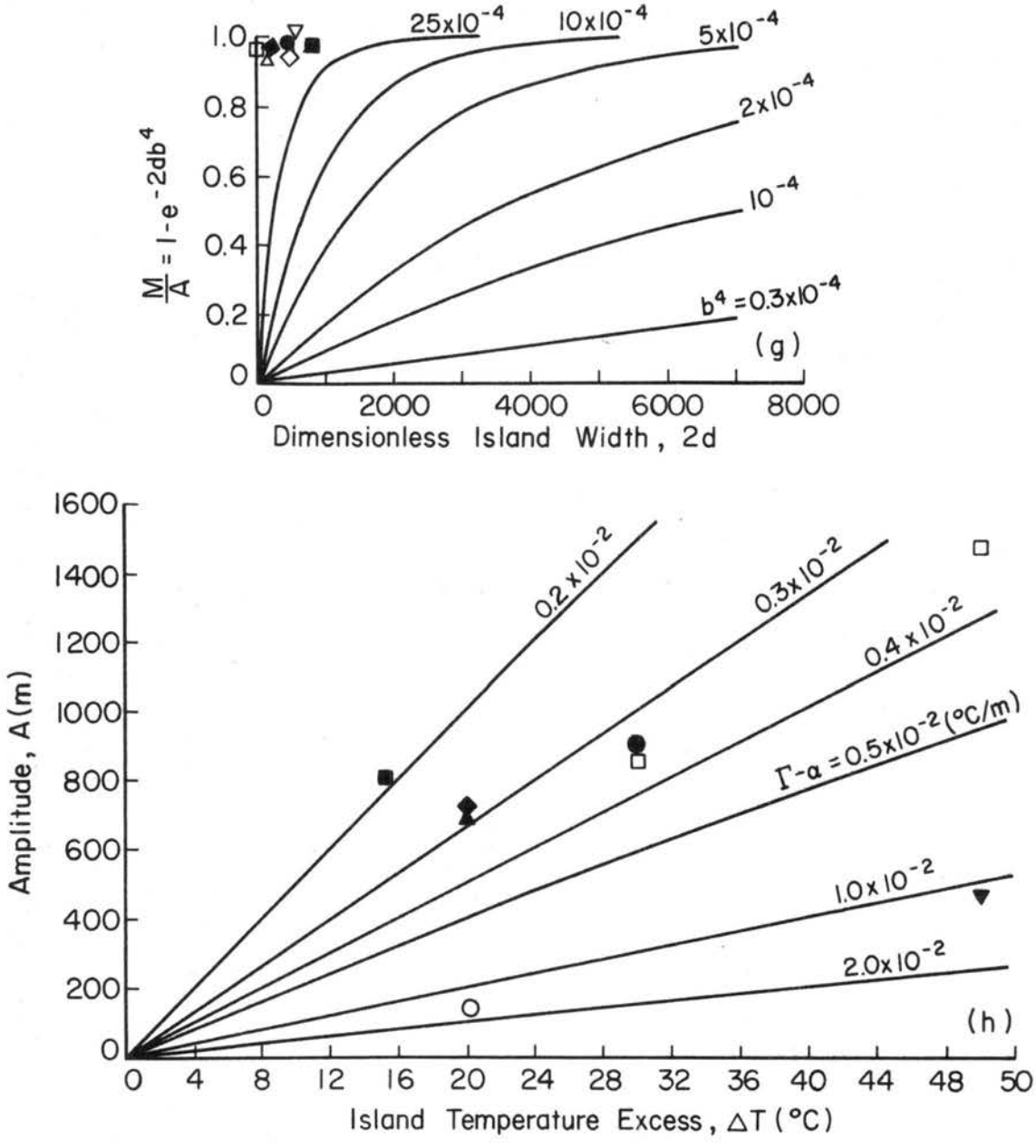

Fig. 2-7 (continued)

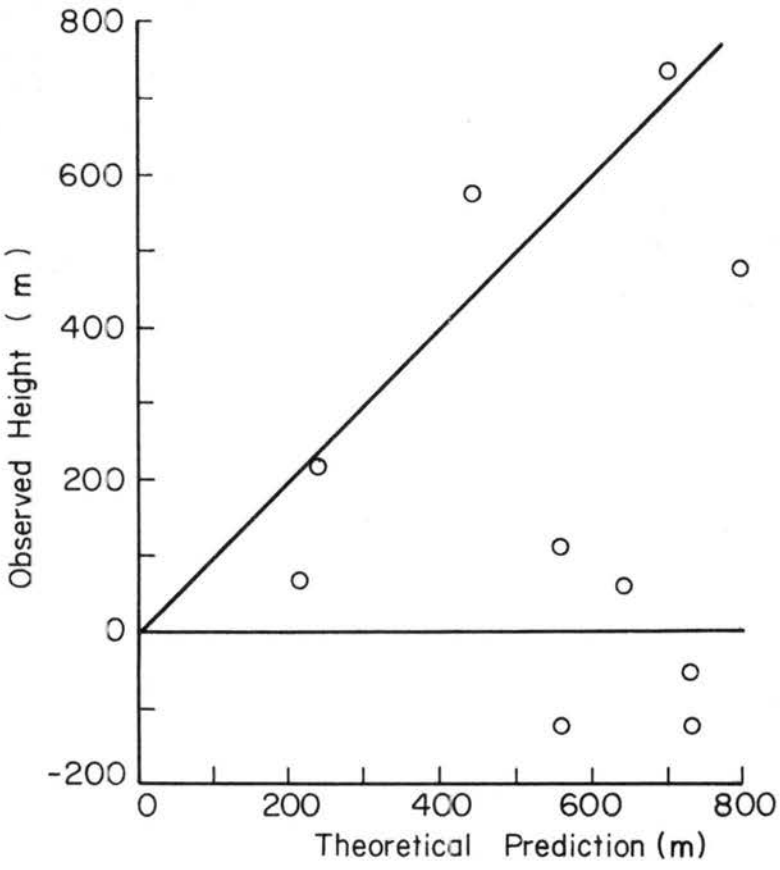

Fig. 2-8 Correlation of observed and predicted height of equivalent thermal mountains (Garstang et al., 1965).

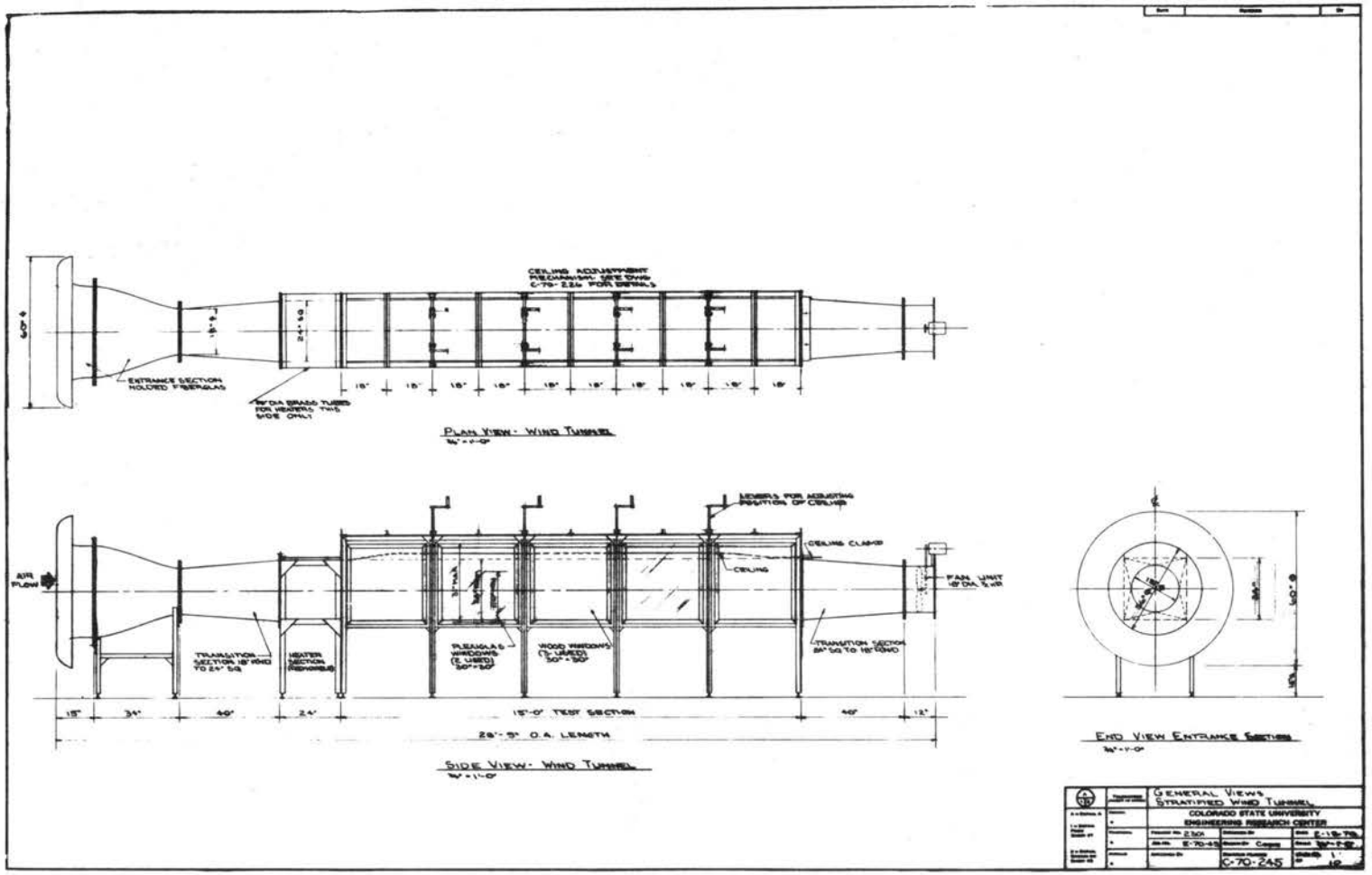

Fig. 3-1 General views of the stratified wind tunnel.

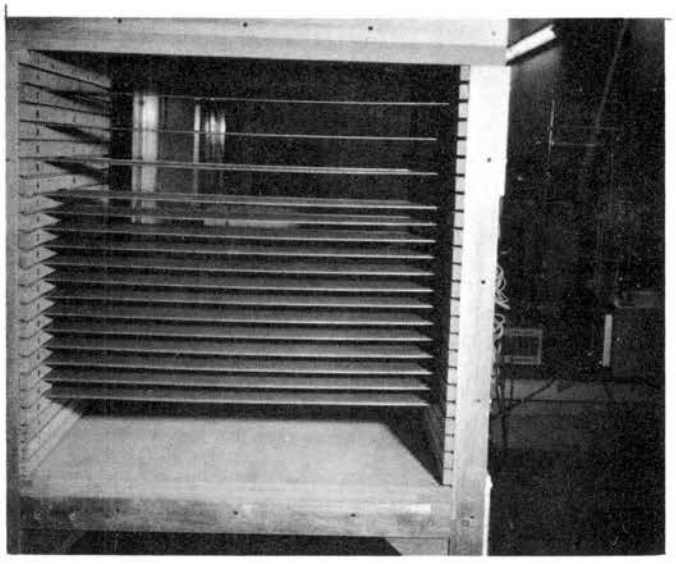

Fig. 3-2 Final arrangements of the entrance heaters. Sixteen heaters of 2' x 6" were used.

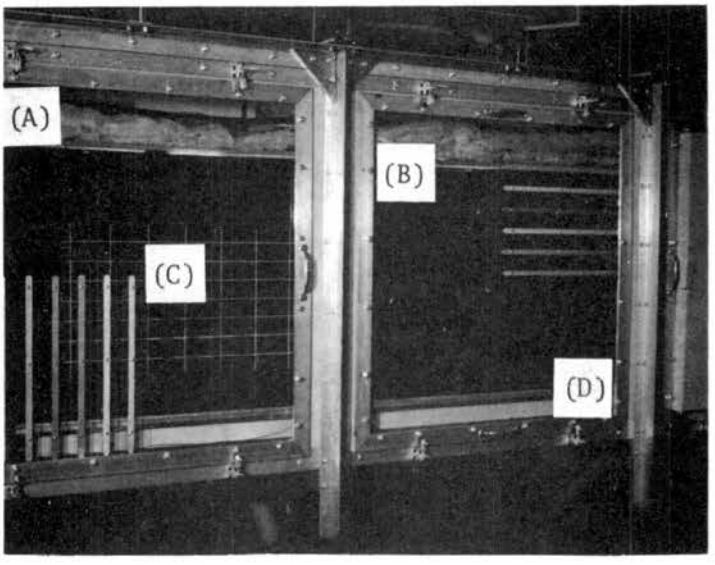

(A) Ceiling Insulation

(B) Ceiling Heater (2' x 3')

(C) Slots for Instrumentation

(D) Cooling Panel

Fig. 3-3 Removable plexiglas windows with slots for instrumentation. Ceiling heaters, insulation, and cooling panels are also included.

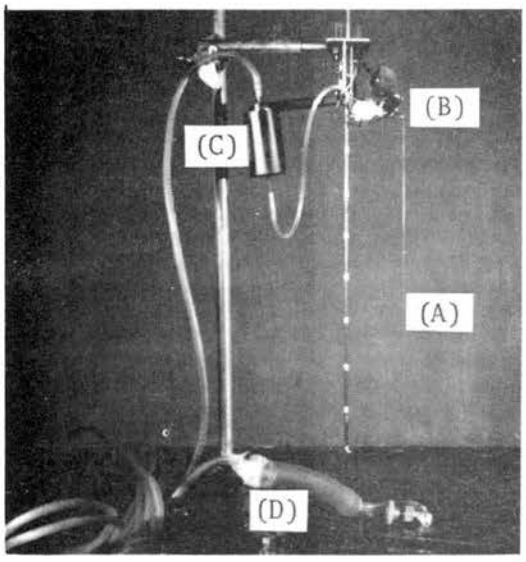

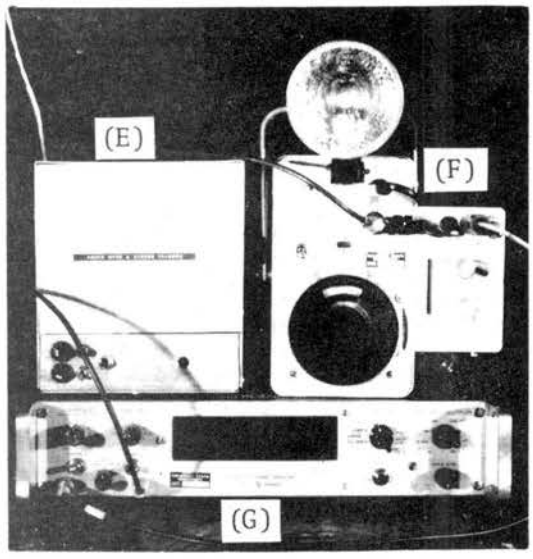

(A) Nichrome Wire

(B) Oil Outlet

(C) Oil Reservoir

(D) Air Bag

(E) Trigger Circuit

(F) Strobe System

(G) Electronic Counter

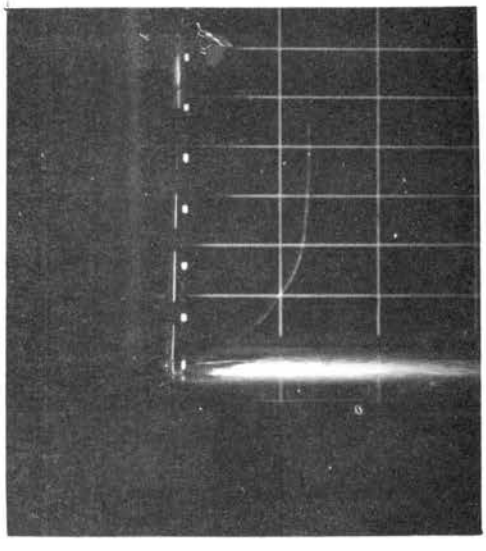

A Typical Velocity Profile (Neutral Case)

Fig. 3-4 Smoke wire and attached instruments for velocity measurements. A typical velocity profile is included.

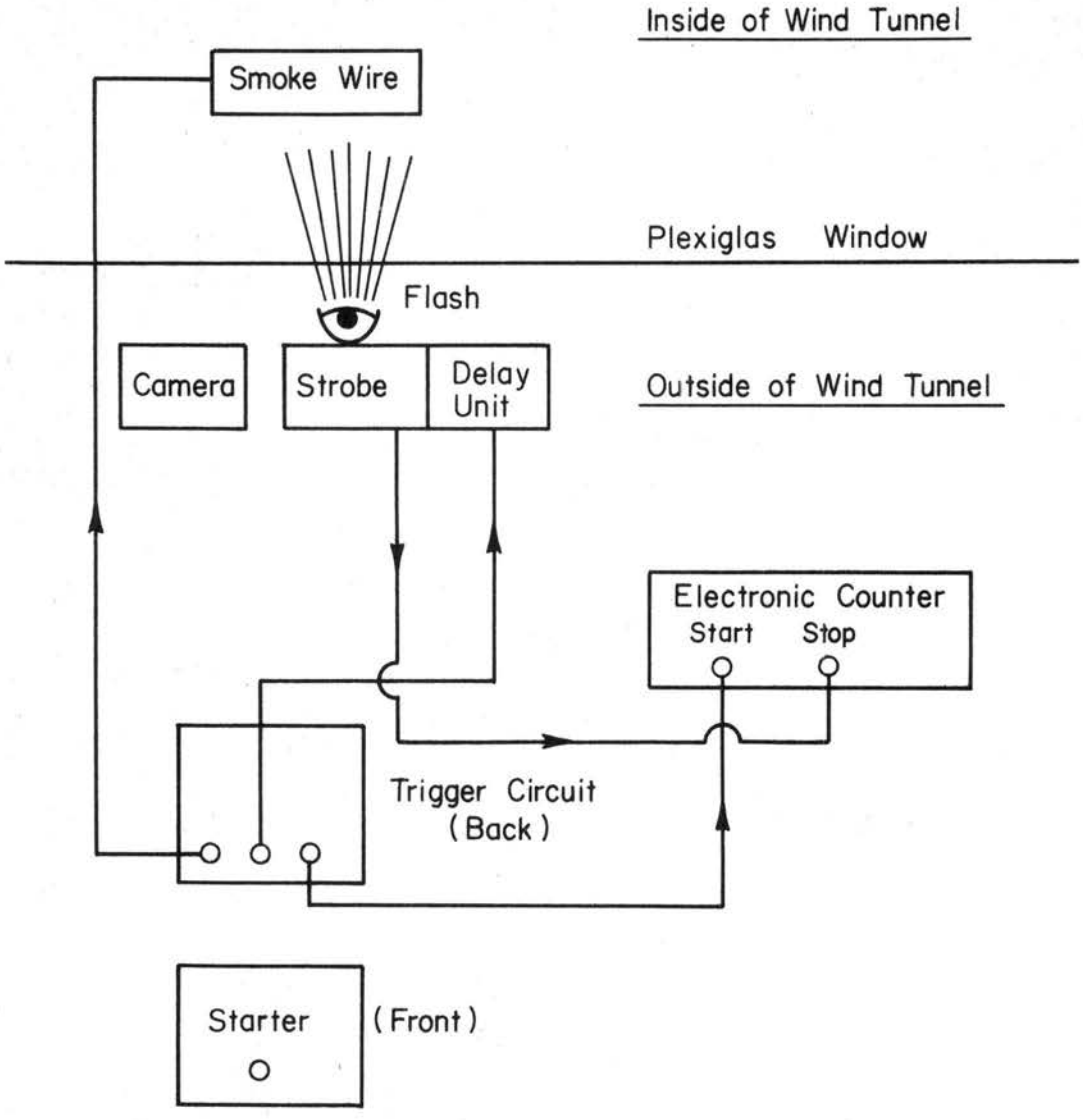

Fig. 3-5 A schematic diagram of a smoke wire arrangement.

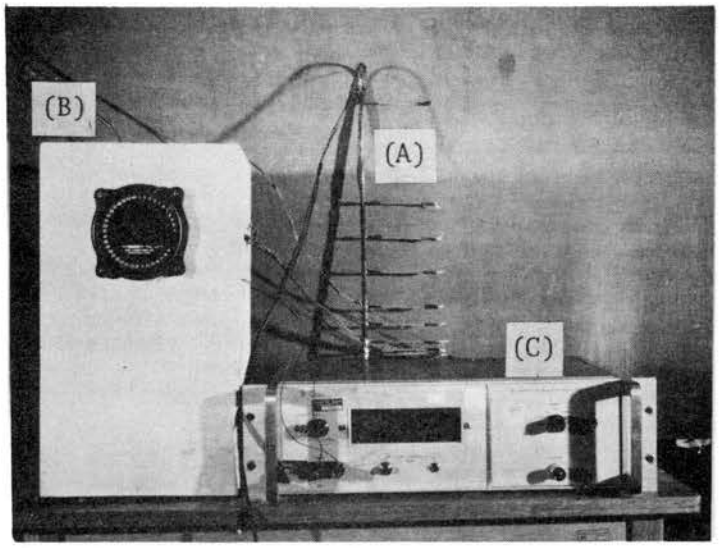

(A) Thermocouple Rake

(B) Thermocouple Rotary Switch

(C) Digital Voltage Meter

Fig. 3-6 Instruments used in the temperature measurements.

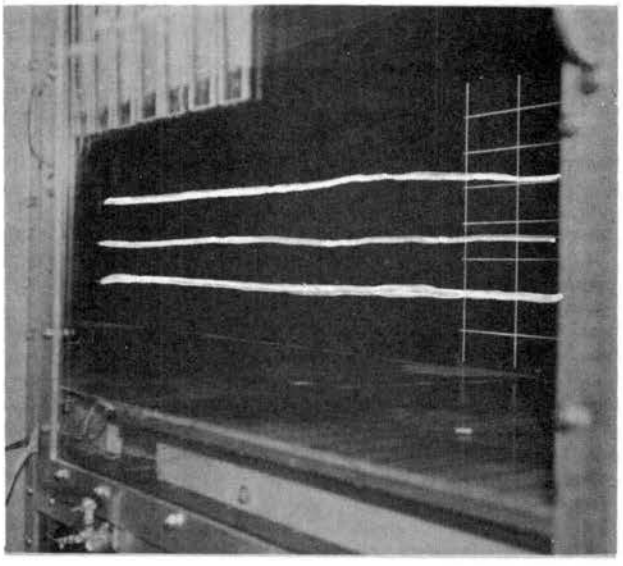

Fig. 3-7 Flow visualization by $TiCl_4$ smoke when no obstacle was placed on the floor. $\left(\overline{Fr} \right)_H = 0.0824$.

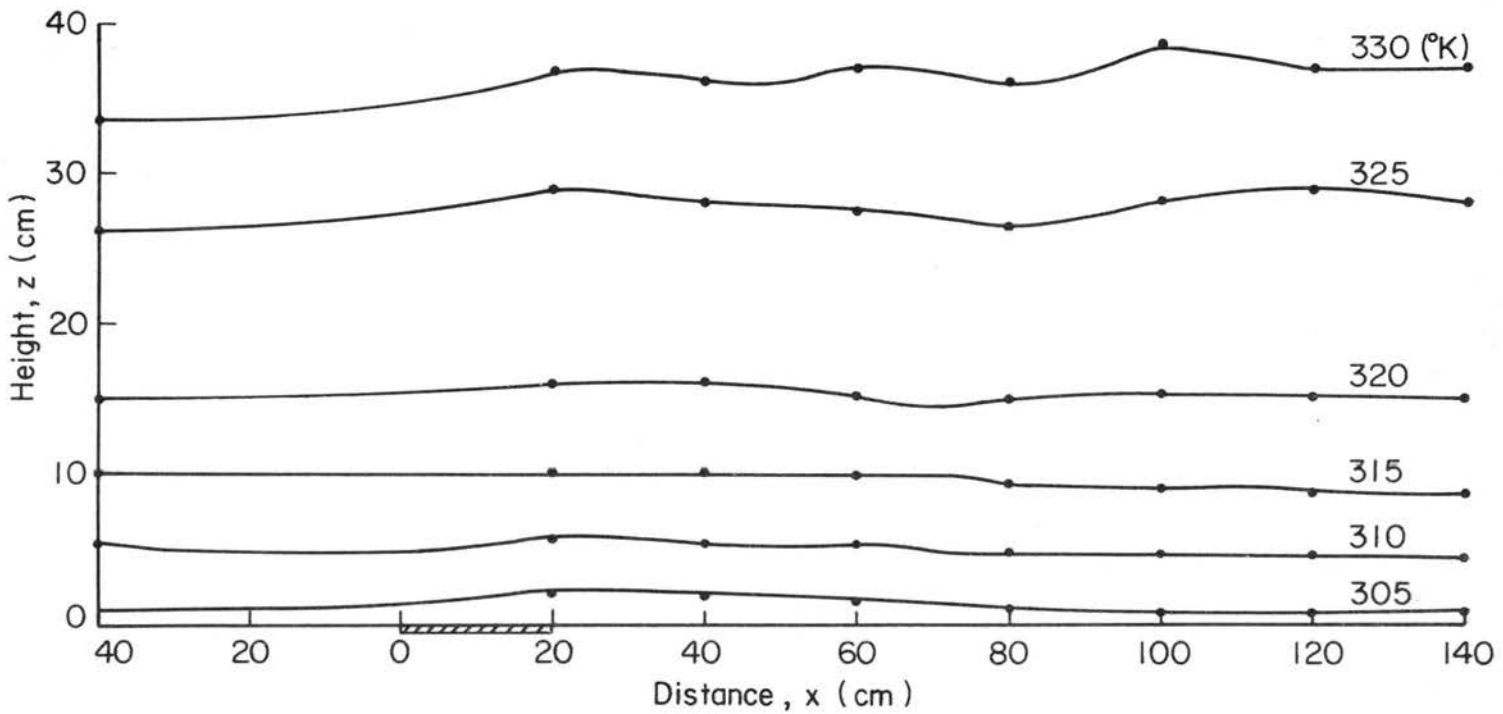

Fig. 3-8 Temperature contour lines when no obstacle was placed on the floor. $(\overline{Fr})_H = 0.168$.

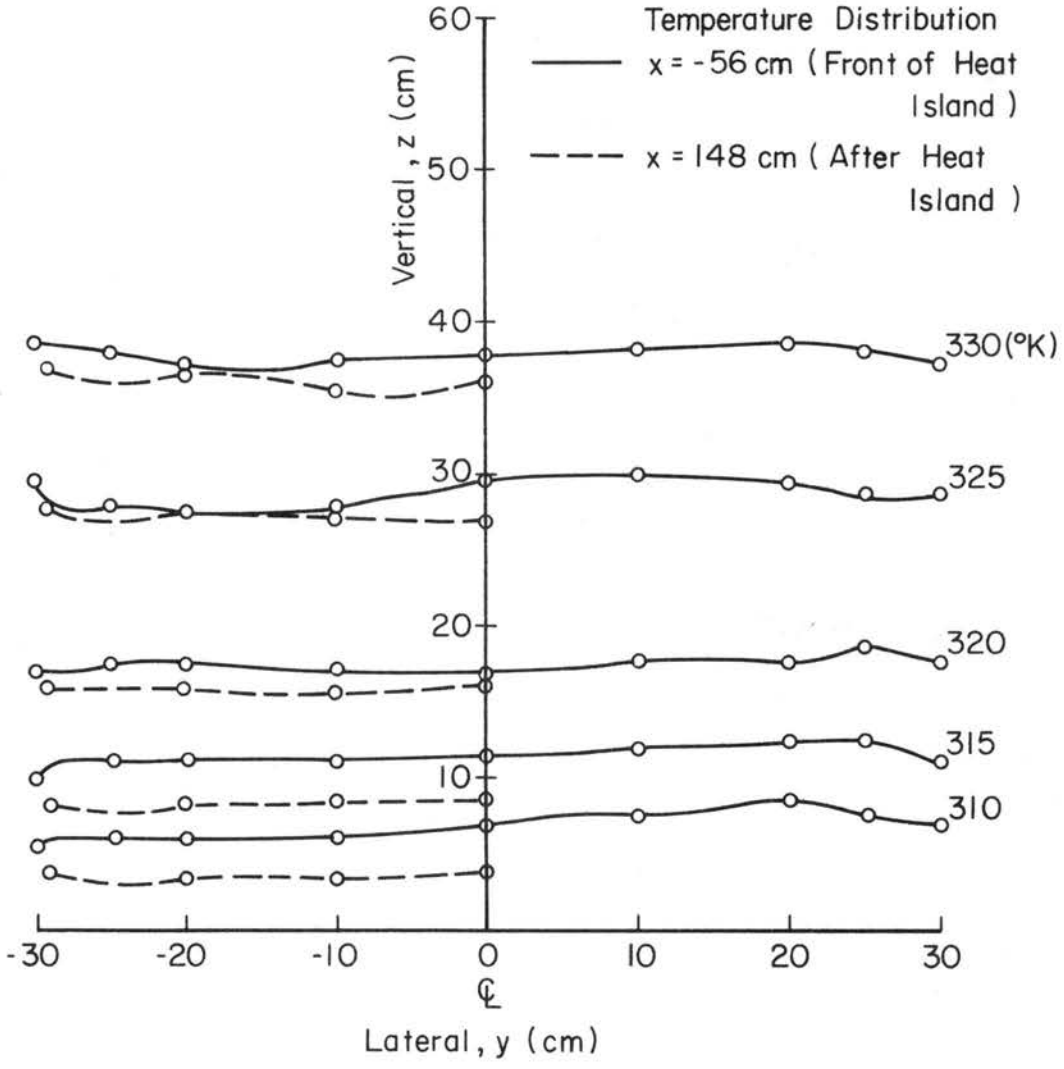

Fig. 3-9 Temperature distributions in the cross sections upstream (x = -56 cm) and downstream (x = 148 cm) of the heated island. (Fr) = 0.163.

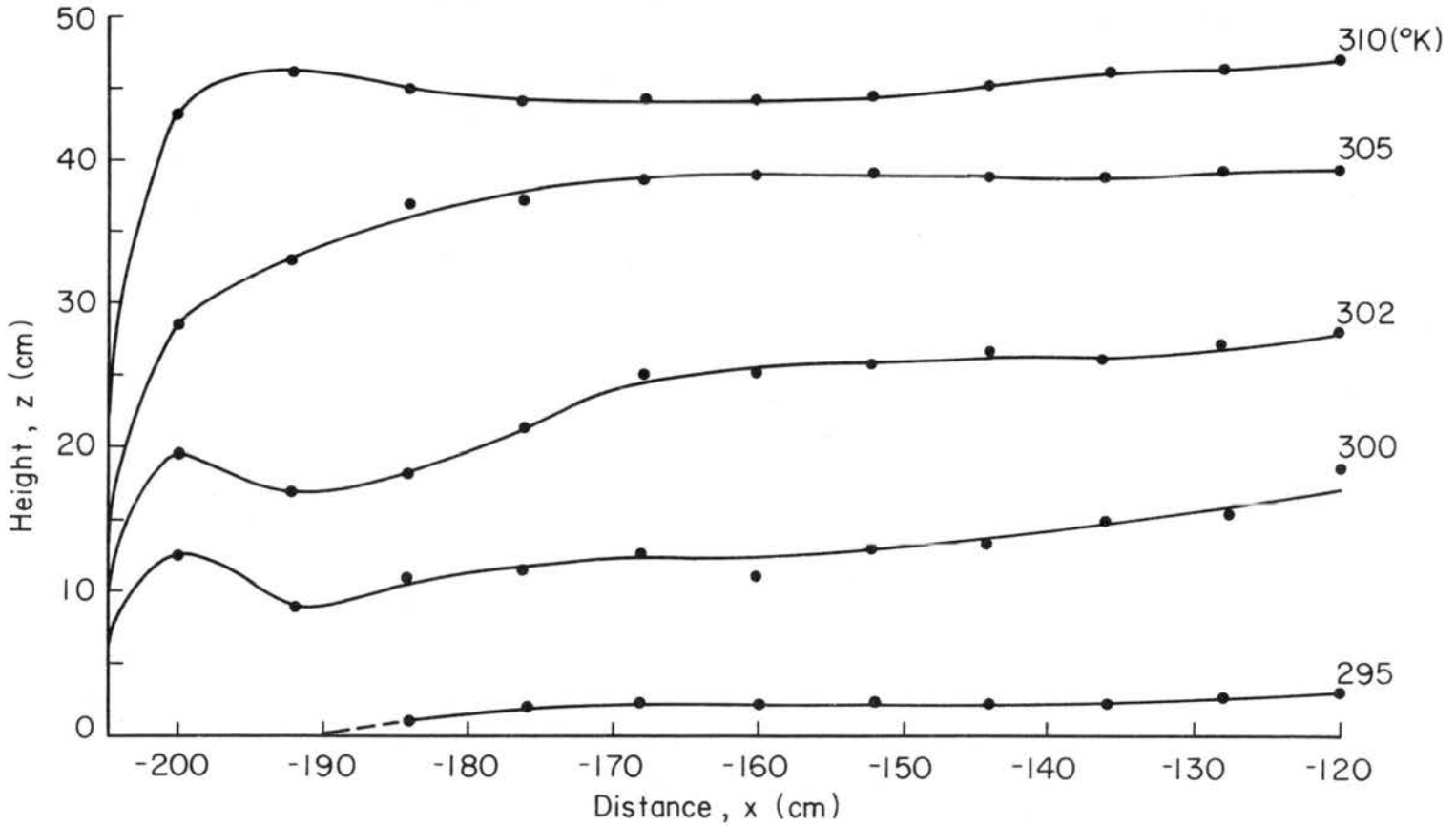

Fig. 3 10 Temperature contour lines downstream of the entrance heaters.
(Fr) = 0.159.

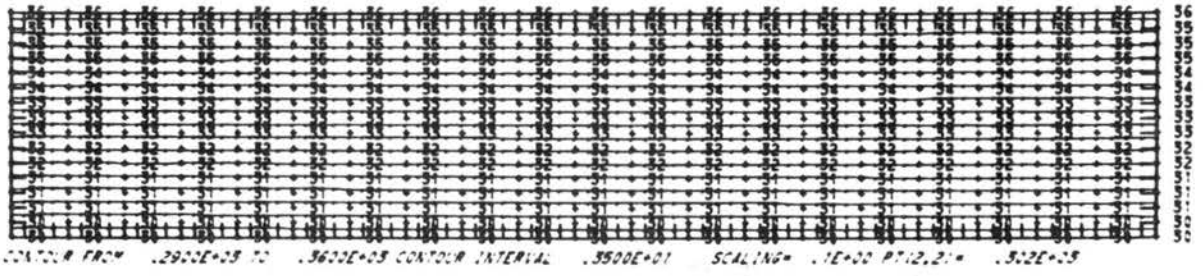

t = 23.19 sec

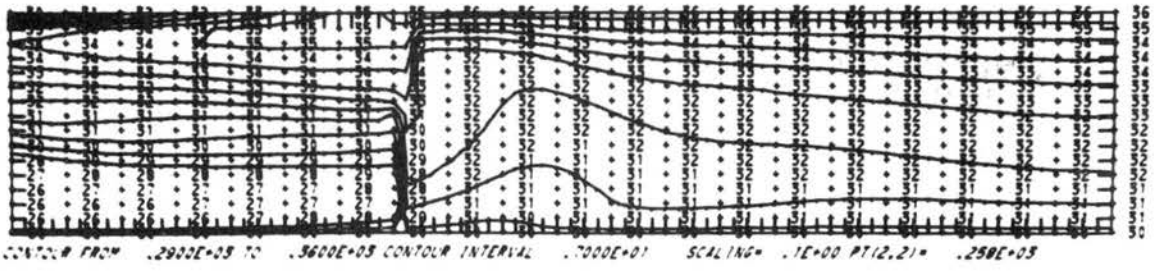

t = 6.29 sec

Fig. 3-11 Numerically computed isotherms with and without entrance heaters. a) without and b) with heaters.

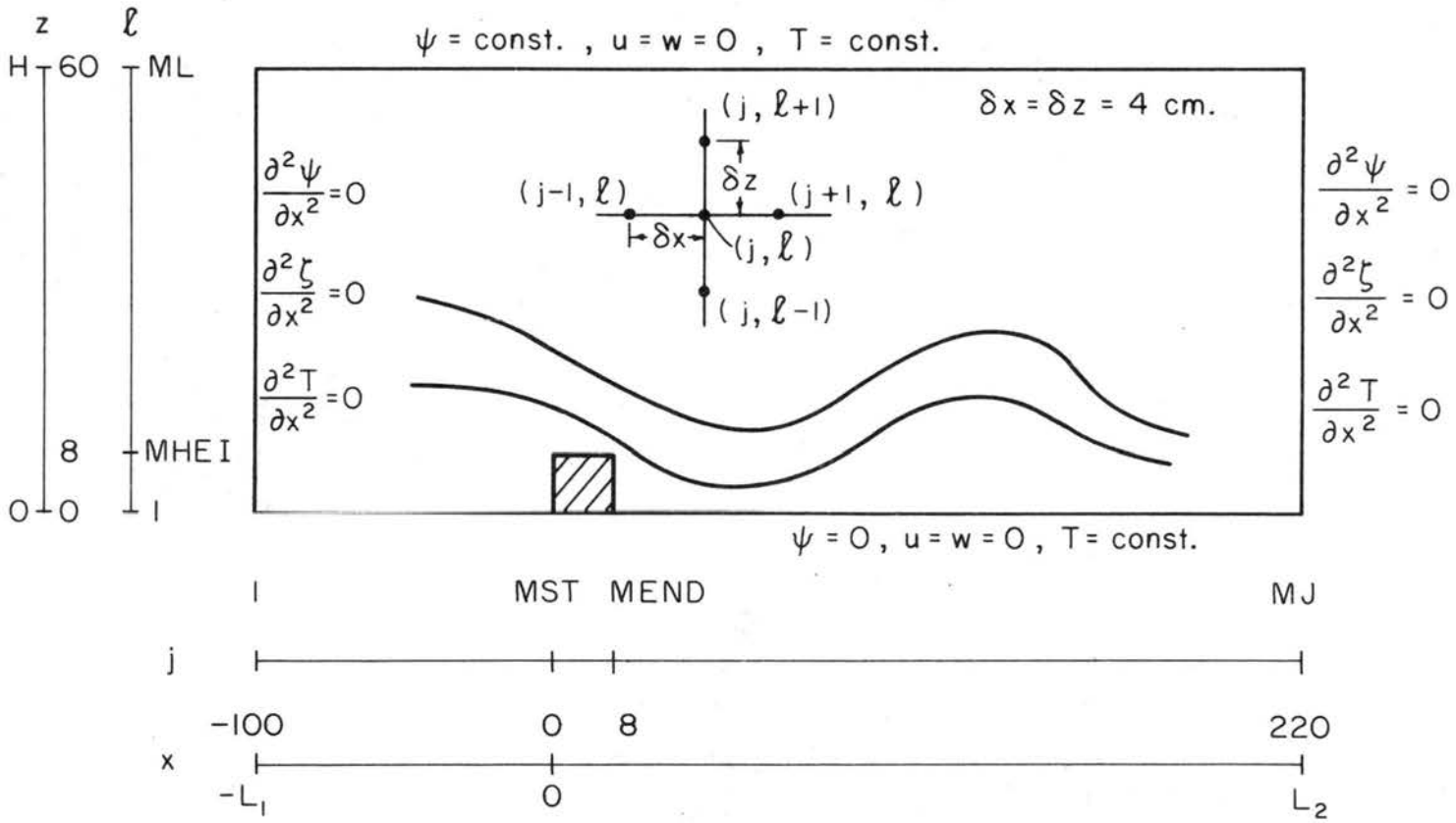

Fig. 4-1 Schematic diagram of the numerical computational region, the grid system, and boundary conditions.

Stream Function

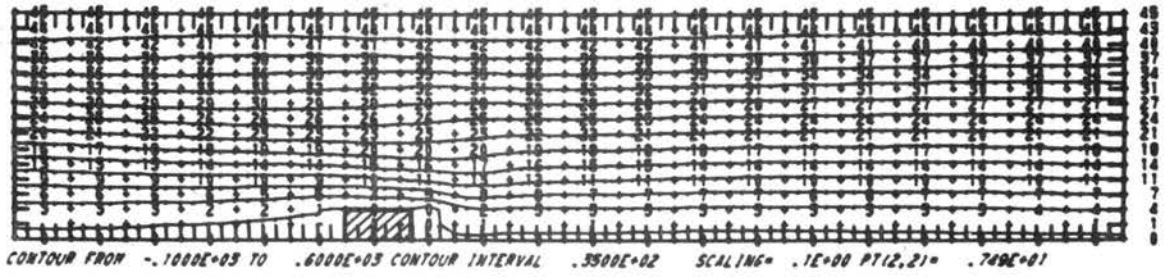

Vorticity

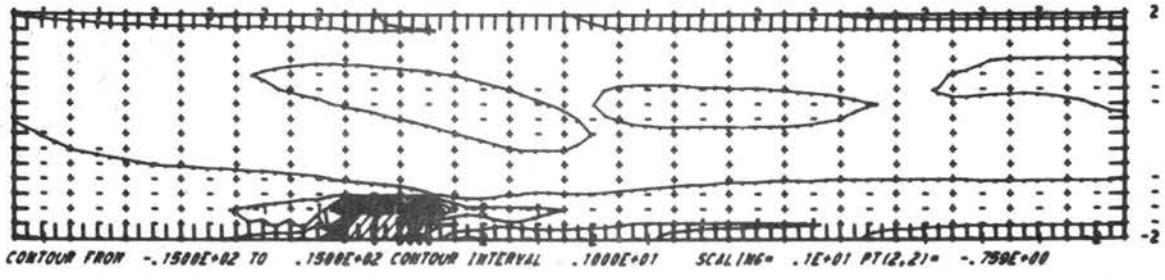

Temperature

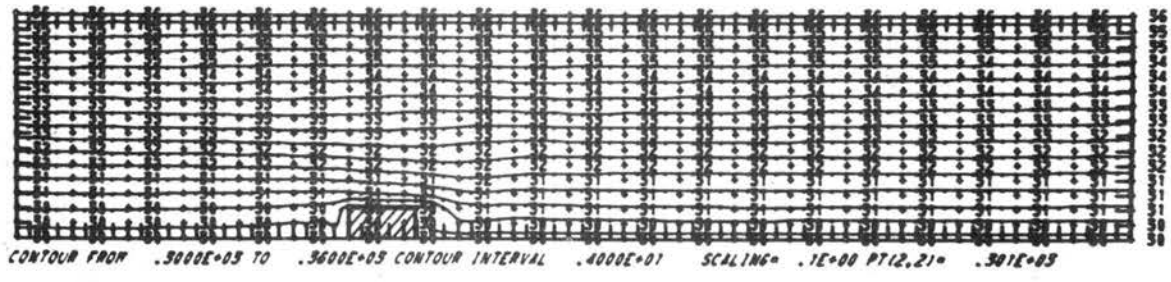

Stream Function in Neutral Situation

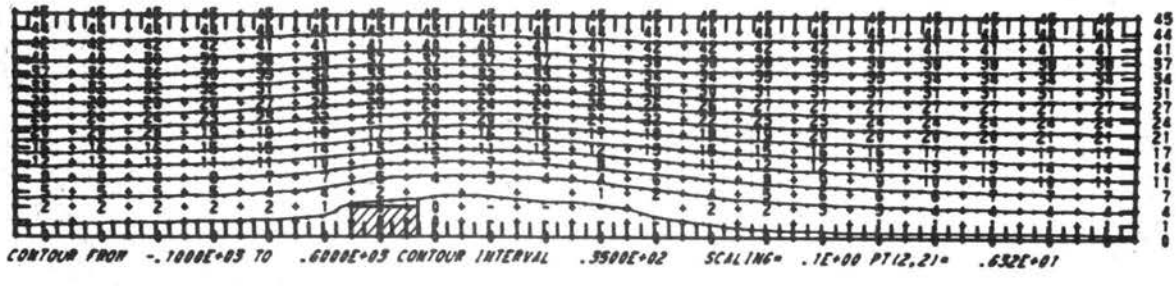

Fig. 4-2 Numerical (upstream difference scheme); contour lines of stream function, vorticity, and temperature at $t = 16.15$ sec when $(\overline{Fr})_H = 0.077$.

The bottom one is the streamlines in a neutral situation at $t = 23.33$ sec.

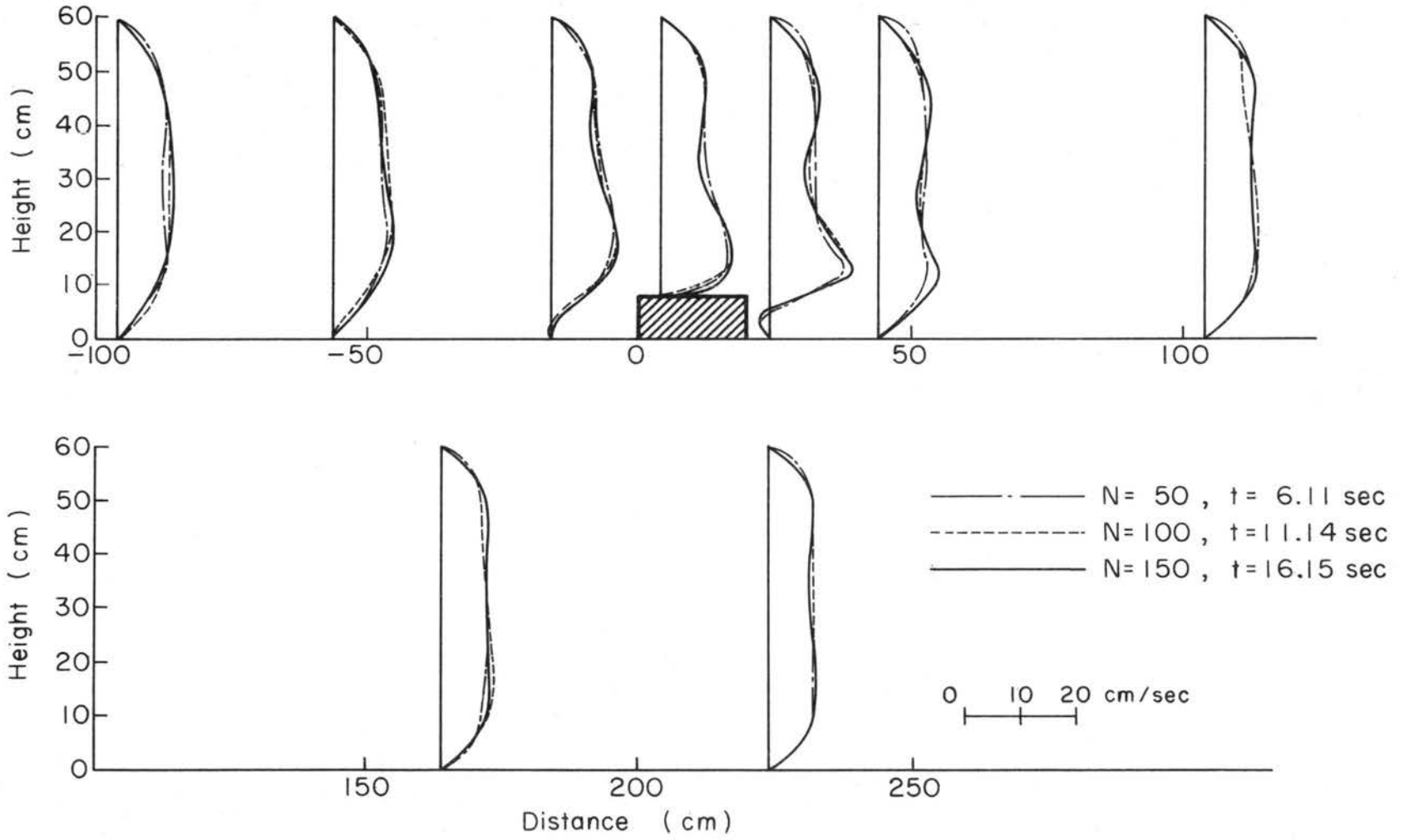

Fig. 4-3 Time variations of u in the same flow situation as in Fig. 4-2.

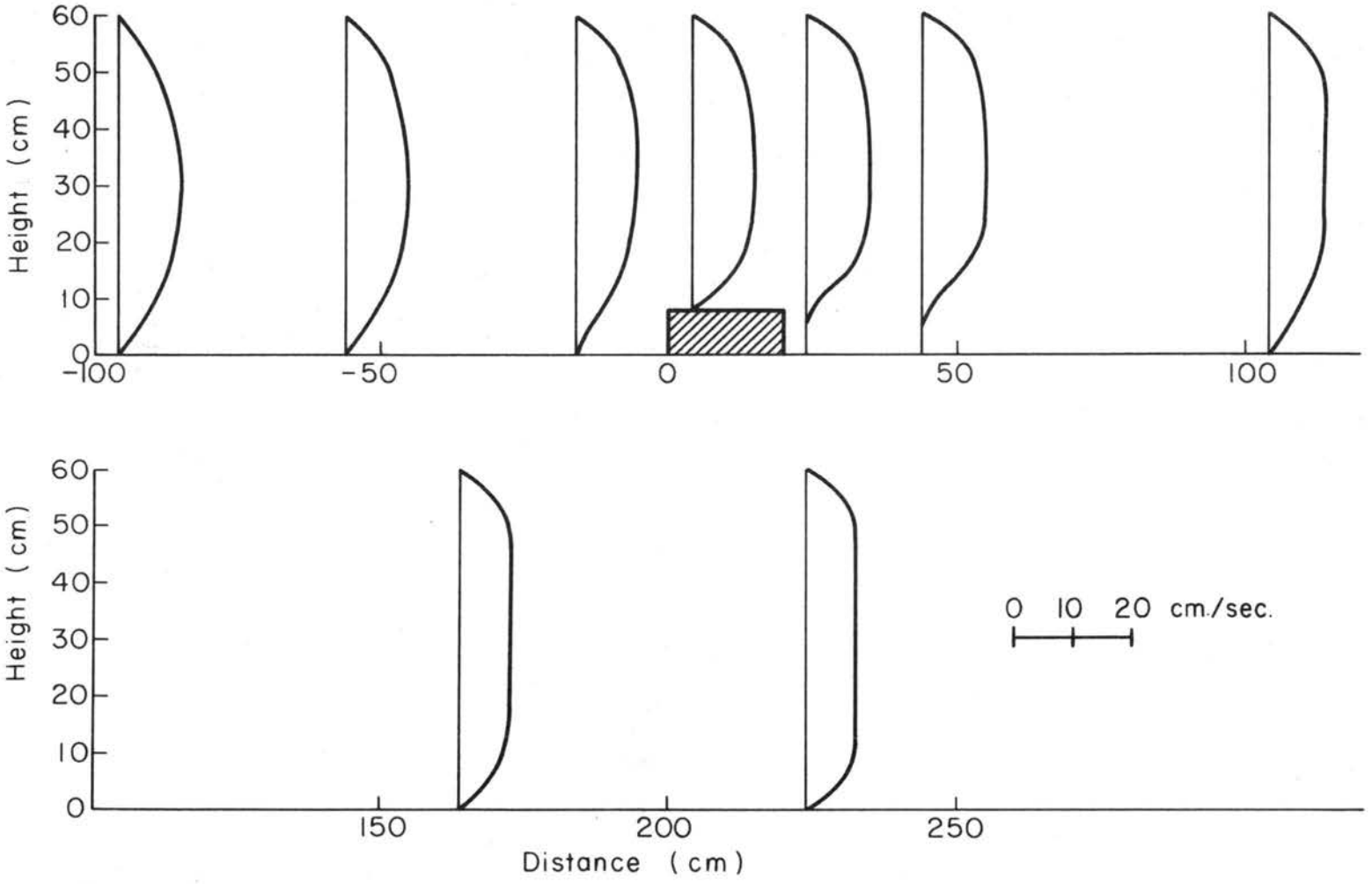

Fig. 4-4 Horizontal velocity profiles in the neutral situation corresponding to the last picture in Fig. 4-2.

Stream Function

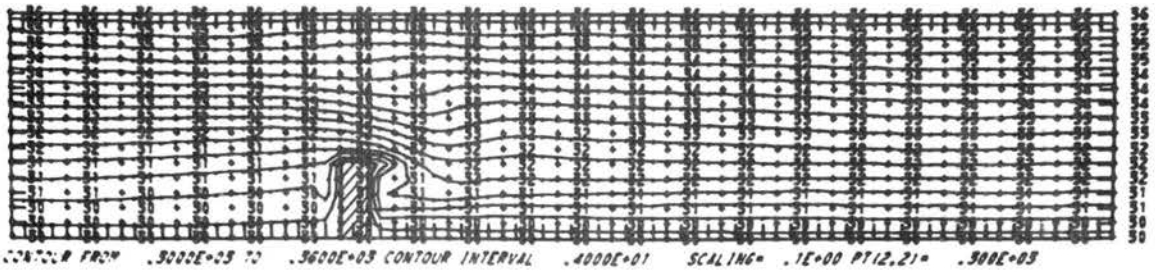

Vorticity

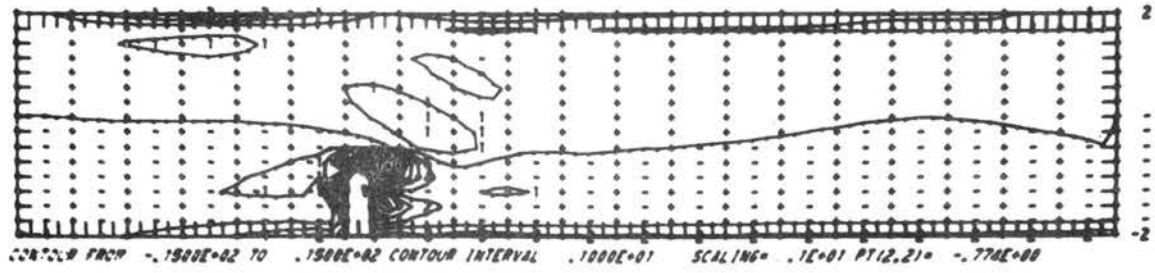

Temperature

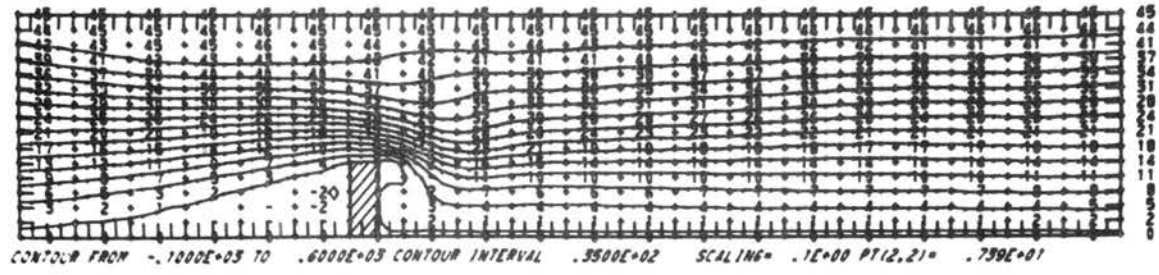

Fig. 4-5 Numerical (upstream difference scheme); contour lines of stream function, vorticity, and temperature at t = 9.45 sec in the same flow situation as in Fig. 4-2 but the obstacle height was increased to 20 cm from 8 cm.

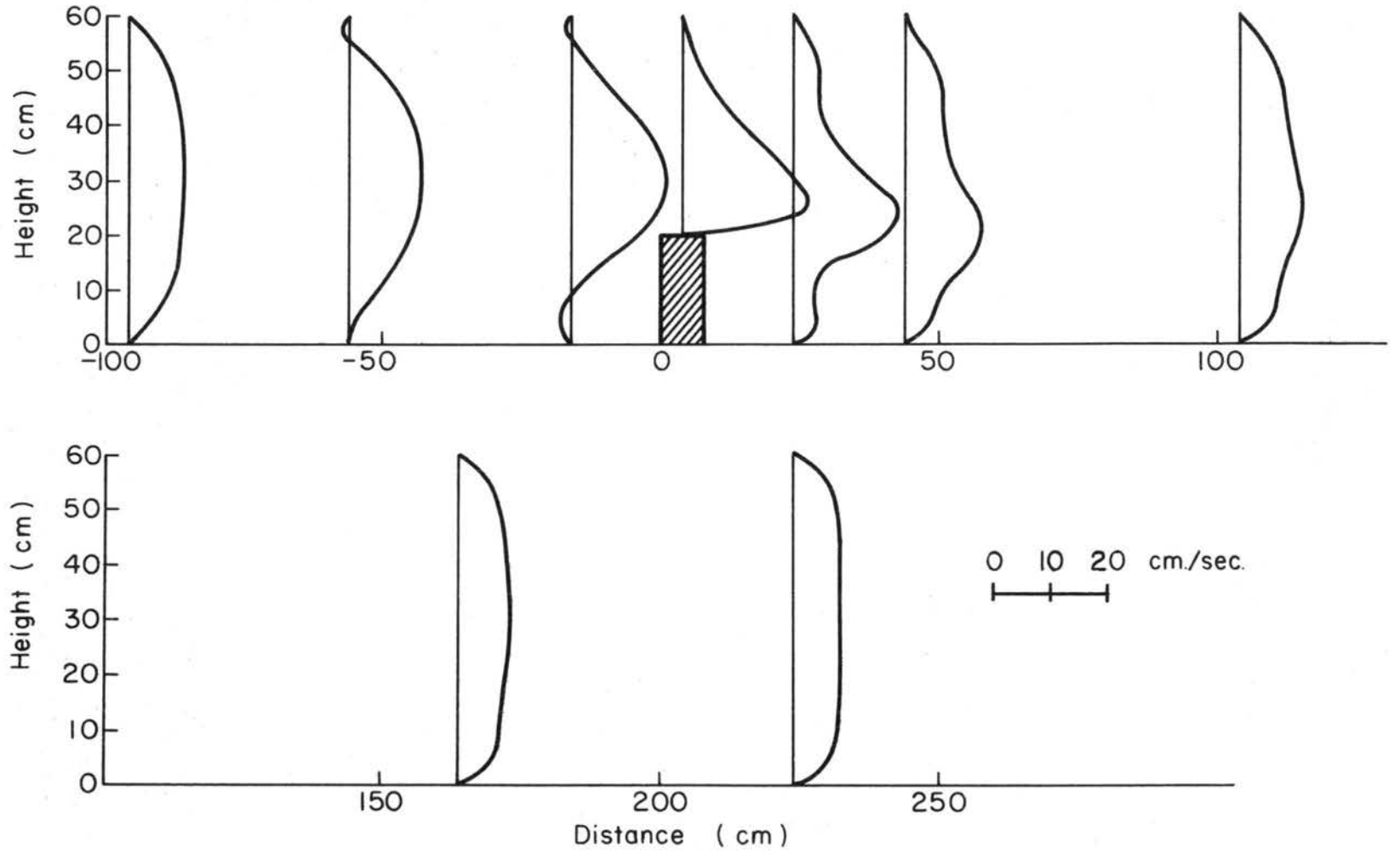

Fig. 4-6 Horizontal velocity profiles corresponding to Fig. 4-5.

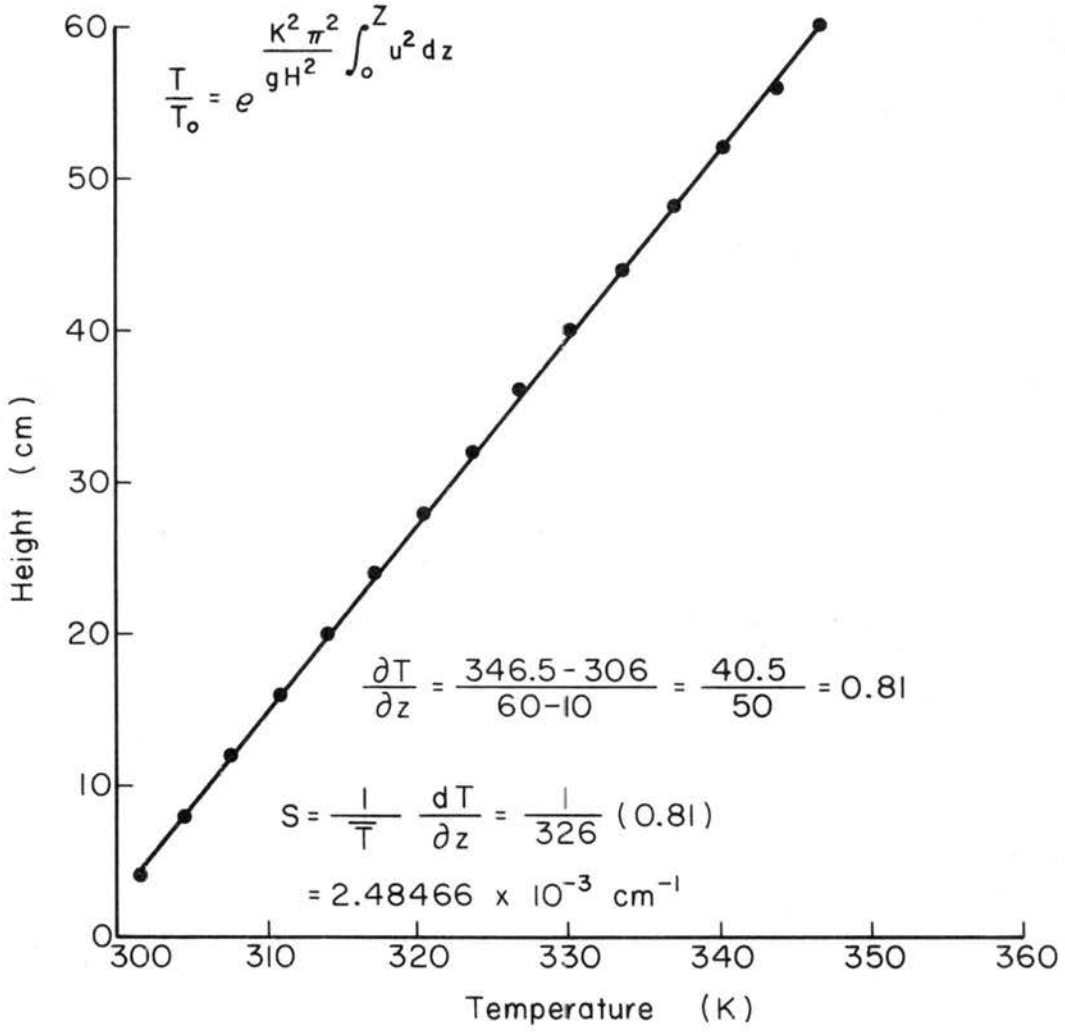

Fig. 4-7 A temperature distribution to satisfy upstream boundary condition of Long's model.

Stream Function

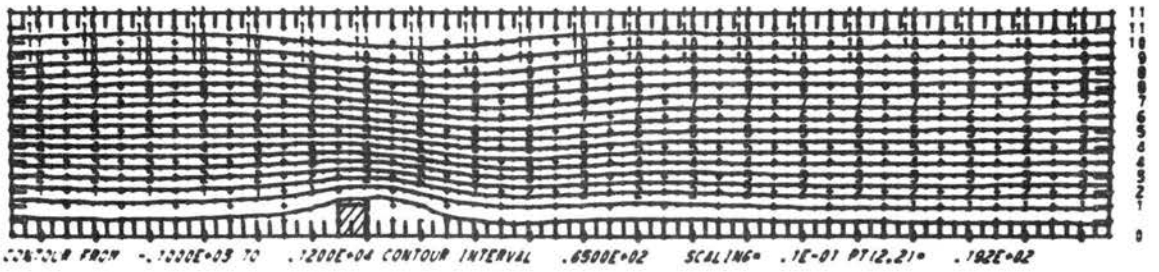

Vorticity

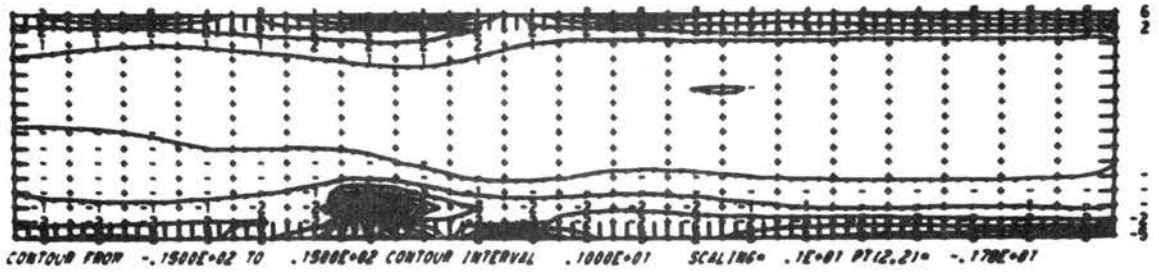

Temperature

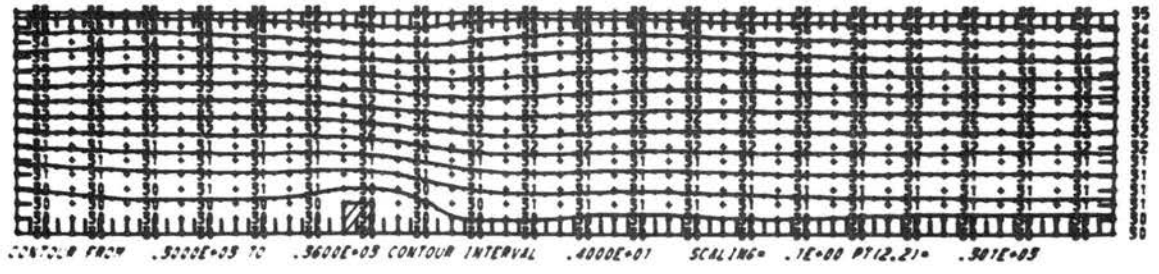

Fig. 4-8 Numerical (upstream difference scheme); contour lines of stream function, vorticity and temperature at t = 8.96 sec when upstream boundary condition in Fig. 4-7 was used. $(\overline{Fr})_H$ = 0.2122.

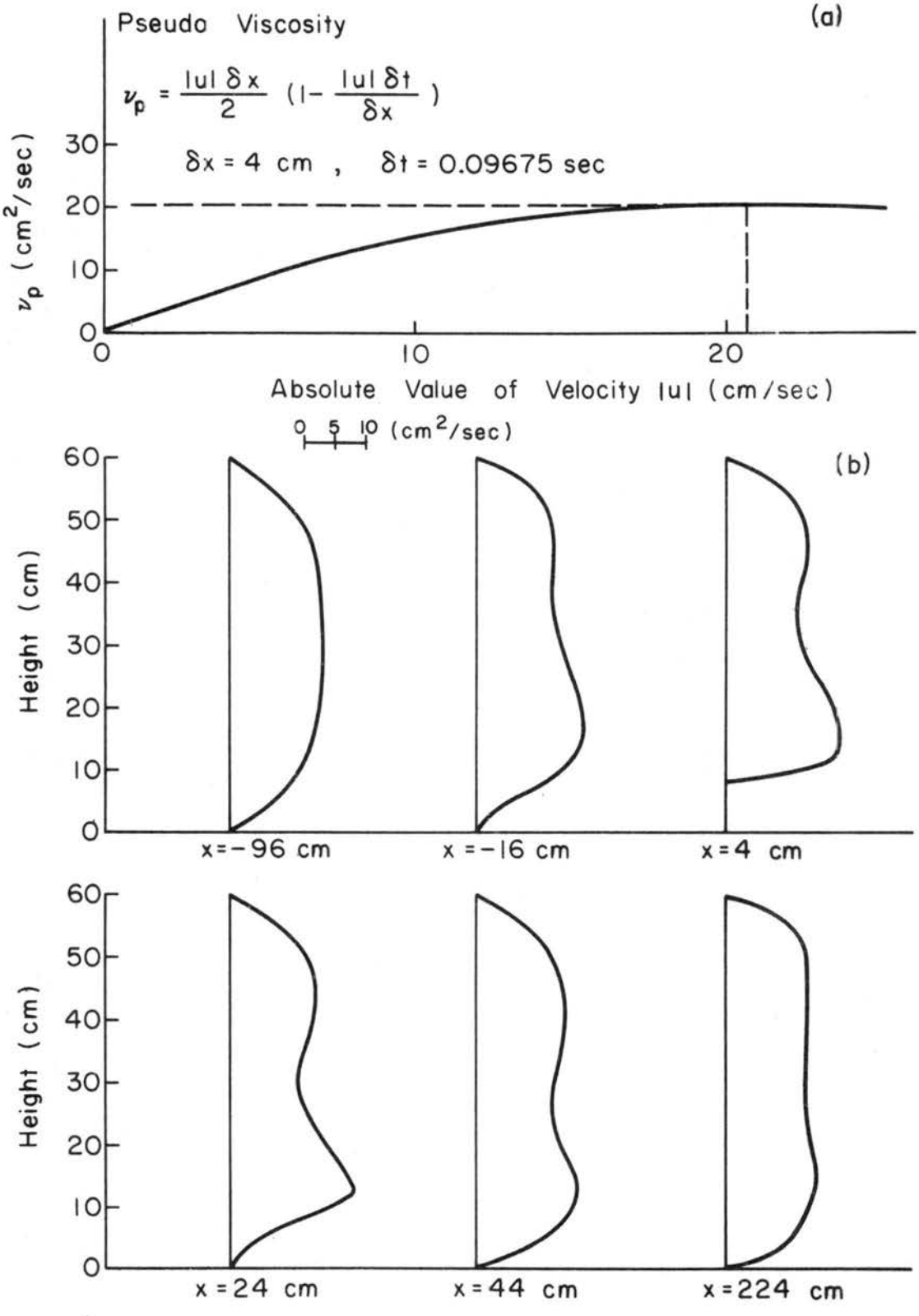

Fig. 4-9 Numerical pseudo viscosity in the flow situation described in Fig. 4-8; a) ν_p vs. $|u|$ when $\delta x = 4$ cm and $\delta t = 0.09675$ sec, b) computed pseudo viscosity profiles at several locations.

Stream Function

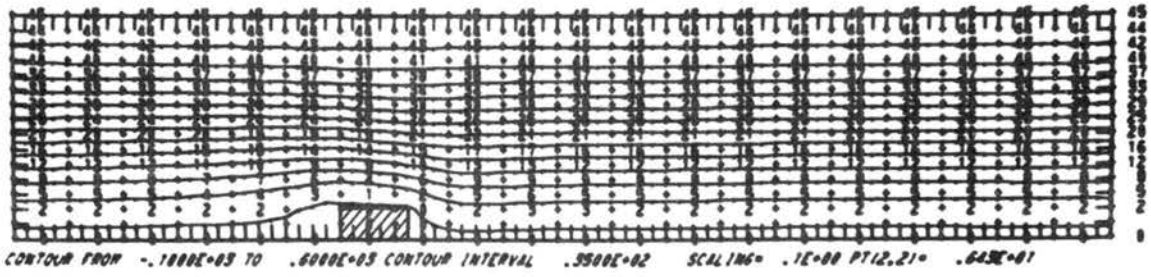

Vorticity

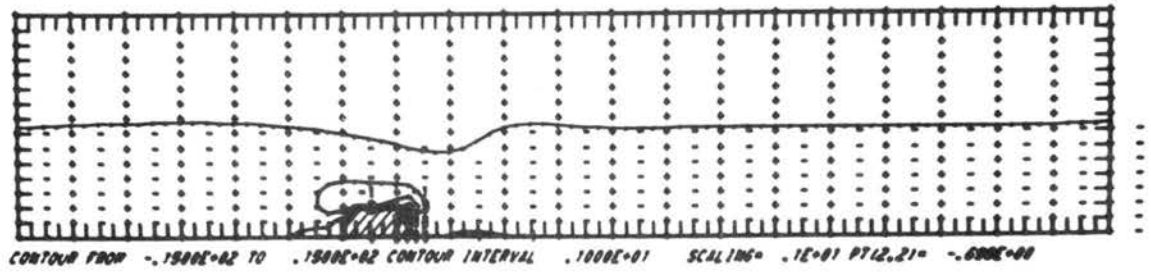

Temperature

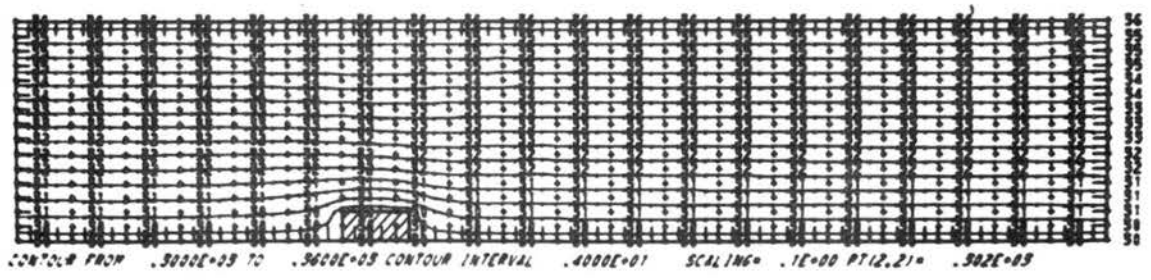

Fig. 4-10 Numerical (upstream difference scheme); contour lines of stream function, vorticity, and temperature at $t = 8.52$ sec when $\nu = 20$ cm^2/sec (cf. Fig. 4-2 where $\nu = 0.18$ cm^2/sec).

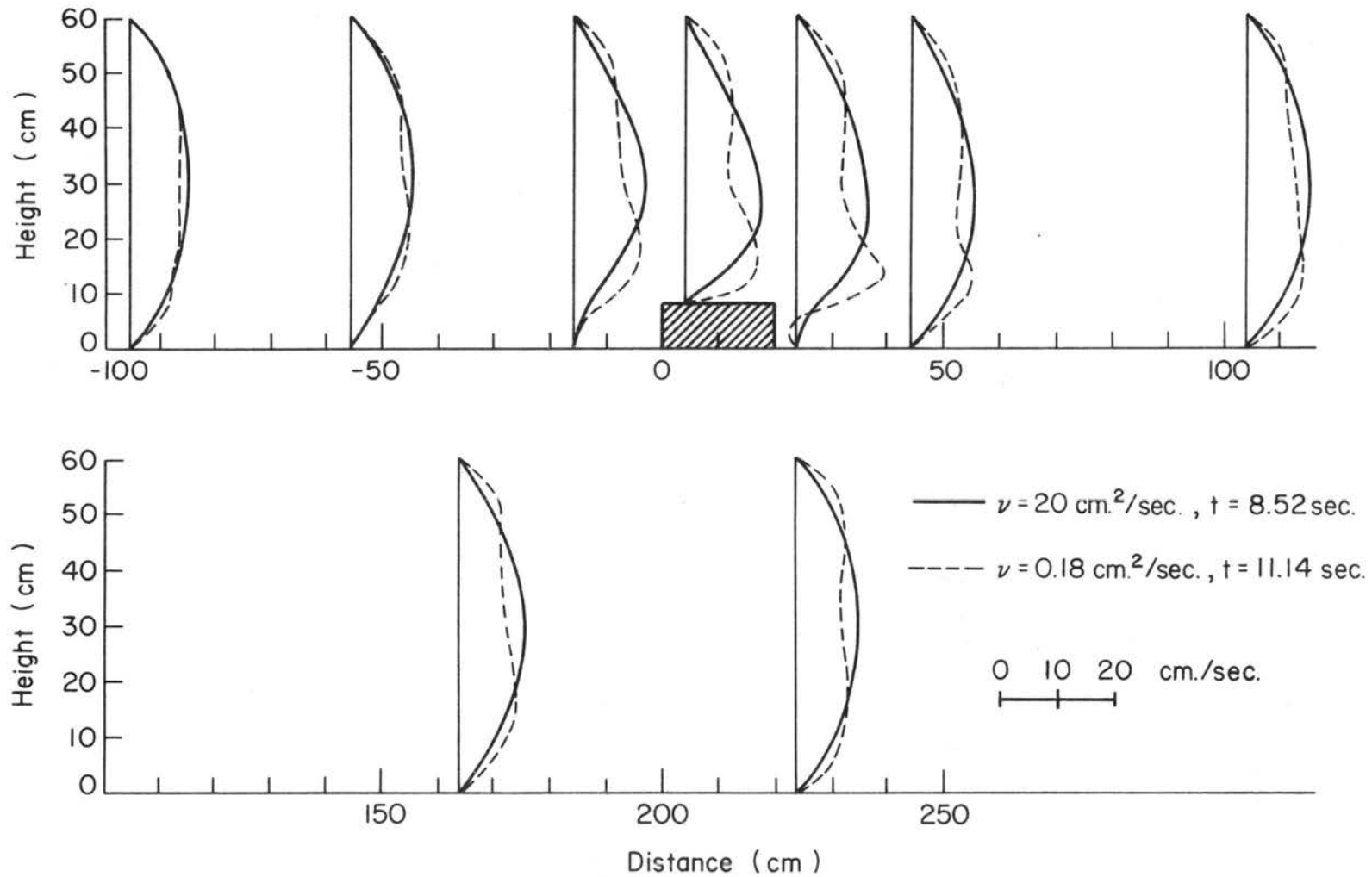

Fig. 4-11 Horizontal velocity profiles corresponding to Fig. 4-10. Dashed lines are those of Fig. 4-2.

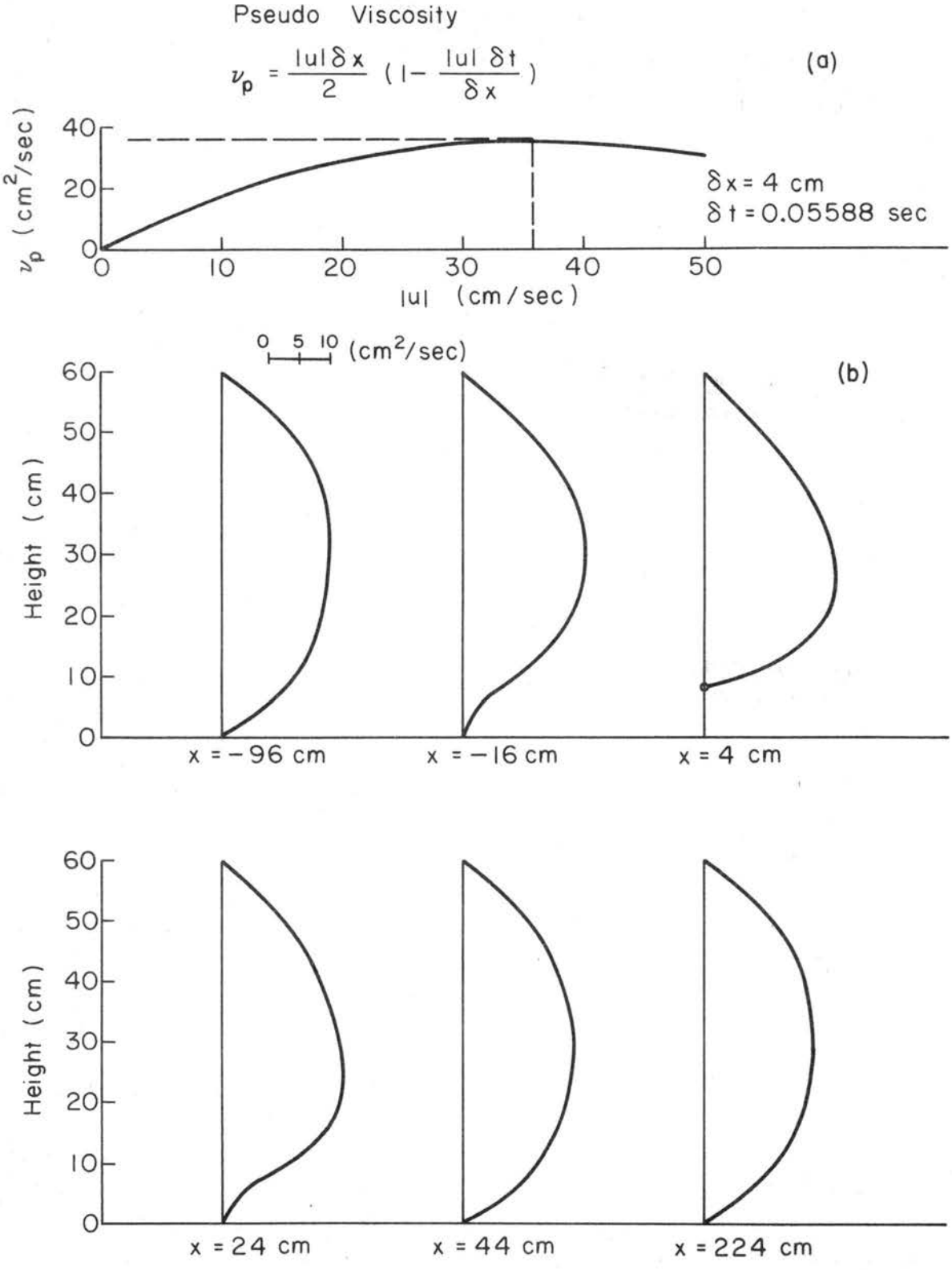

Fig. 4-12 Numerical pseudo viscosity in the flow situation described in Fig. 4-10; a) ν_p vs. $|u|$ when $\delta x = 4$ cm and $\delta t = 0.0558$ sec, b) computed pseudo viscosity profiles at several locations.

(a)

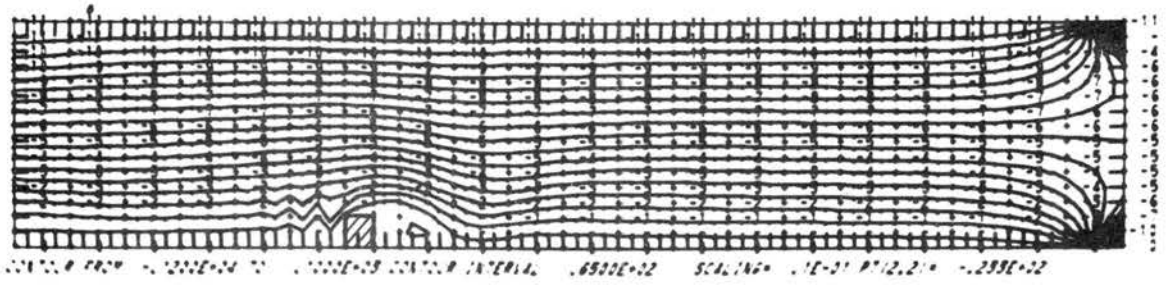

(b)

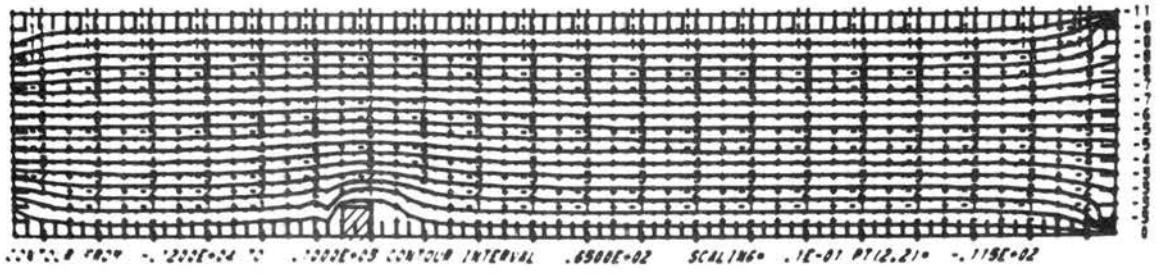

(c)

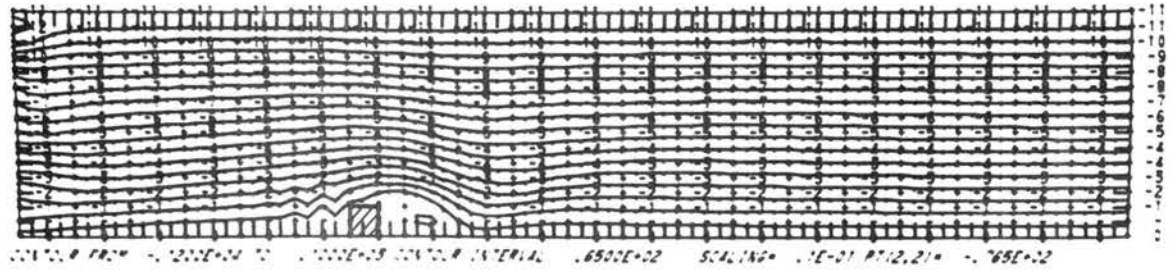

(d)

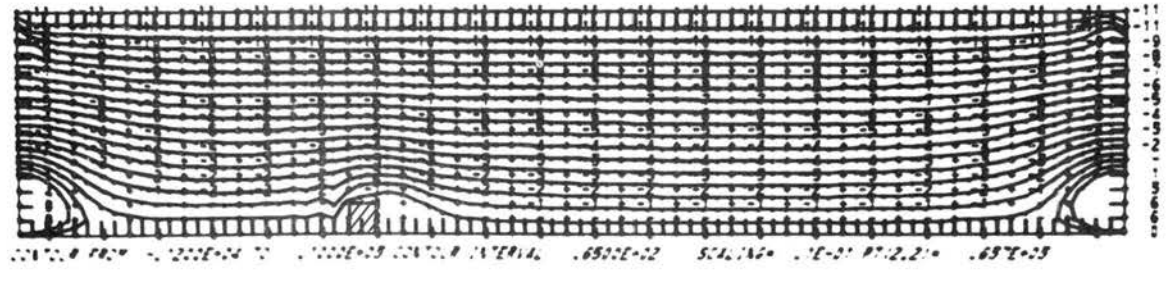

Fig. 4-13 Trials of different lateral boundary conditions; a) $\zeta = \frac{\partial w}{\partial x} - \frac{\partial u}{\partial z}$ in Arakawa's scheme with upstream difference every other step, b) $\zeta = \frac{\partial w}{\partial x} - \frac{\partial u}{\partial z}$ in Arakawa's scheme with upstream difference every 30 time steps, c) Milne prediction, and d) periodic boundary condition.

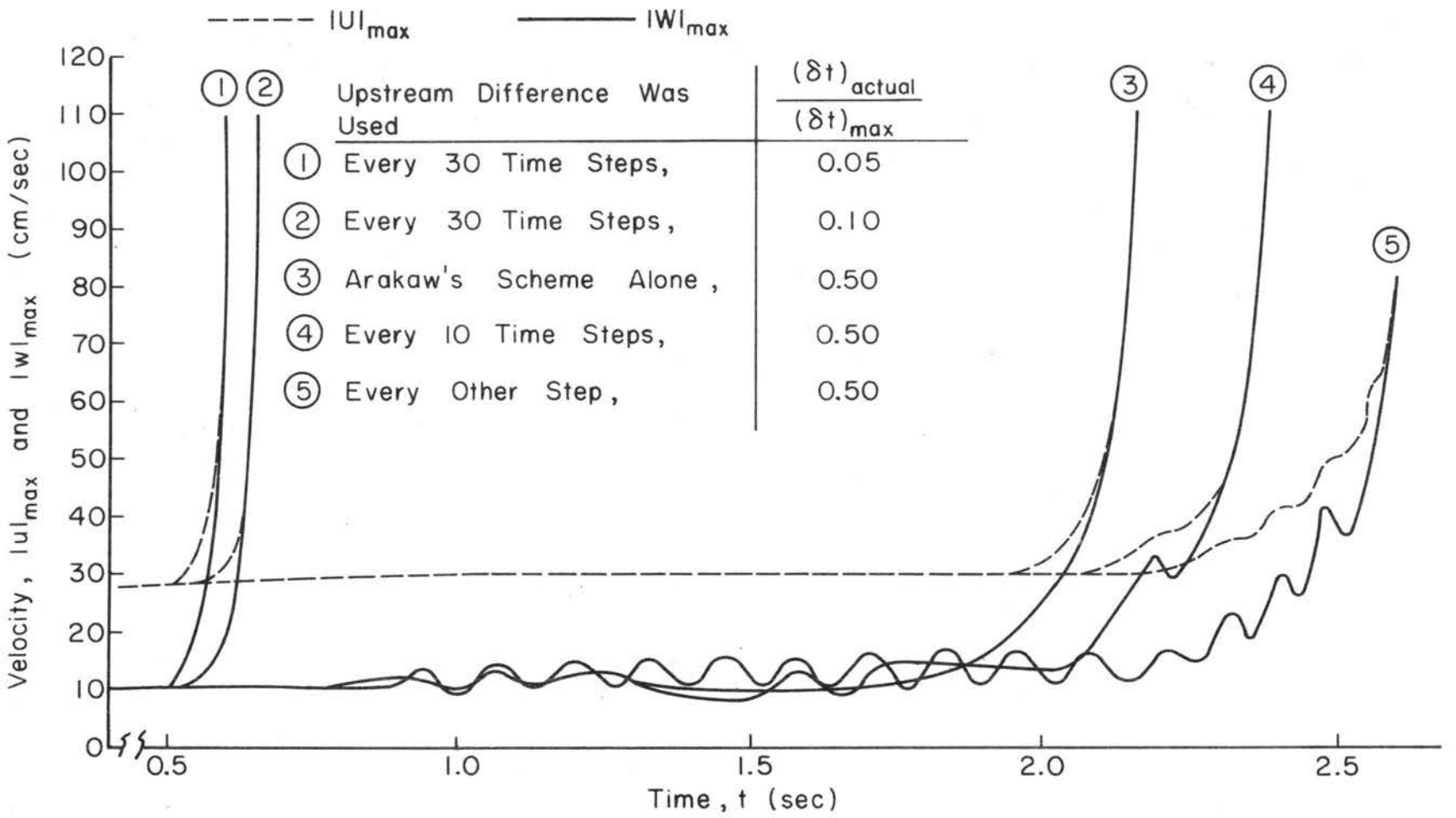

Fig. 4-14 Maximum velocity components $|u|_{max}$ and $|w|_{max}$ vs. integrated time in different finite difference schemes.

(a)

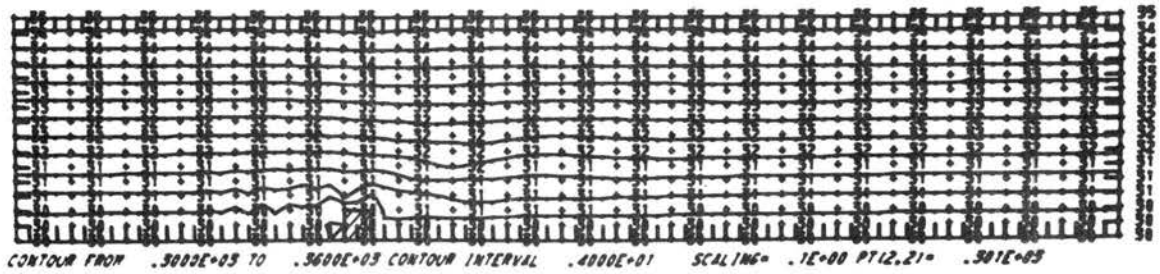

(b)

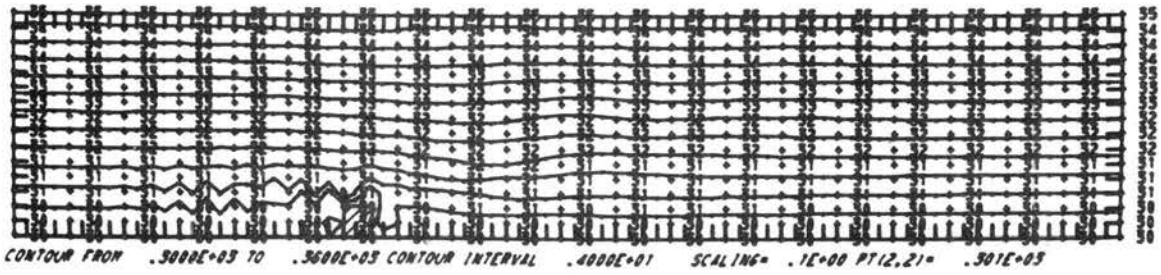

(c)

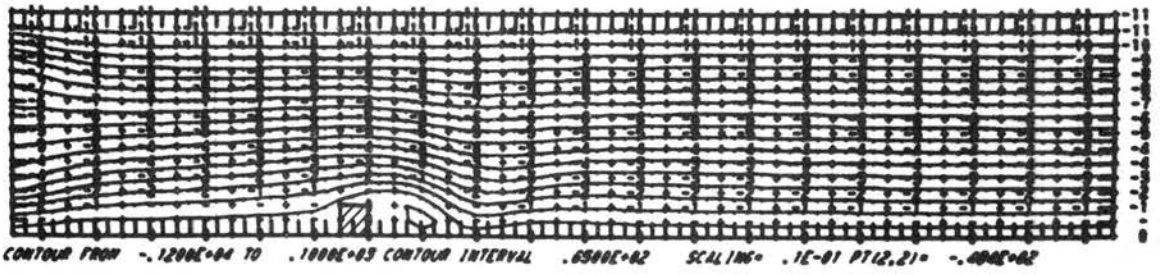

Fig. 4-15 Further investigations of lateral boundary conditions; a) and b) are isotherms respectively at $t = 2.84$ and 4.38 sec when $\frac{\partial^2 T}{\partial x^2} = 0$ were used, c) averaging procedures were added to $\frac{\partial^2 \psi}{\partial x^2} = 0$.

Stream Function

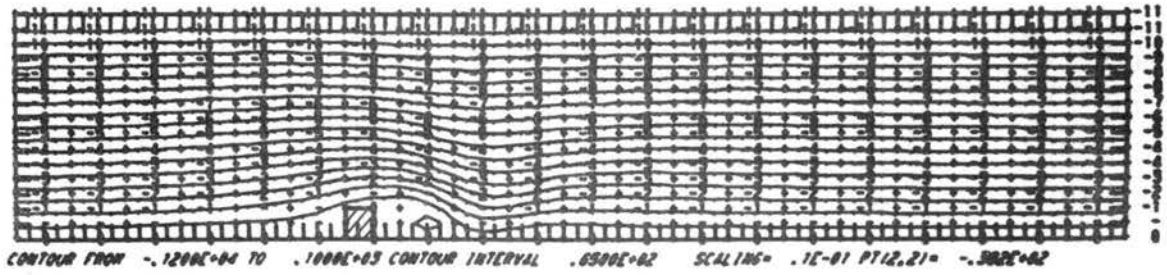

Vorticity

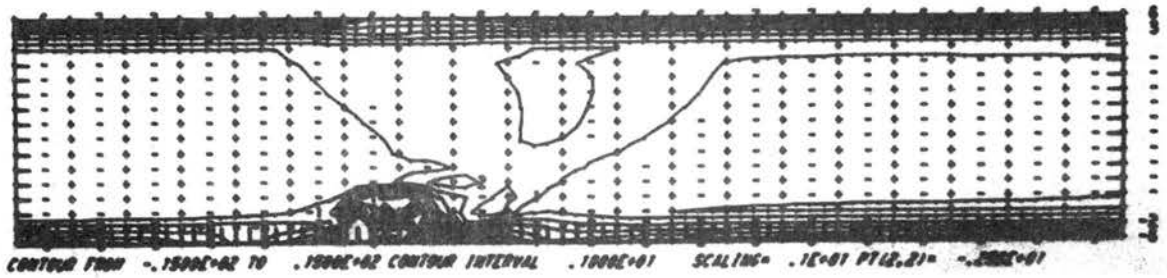

Temperature

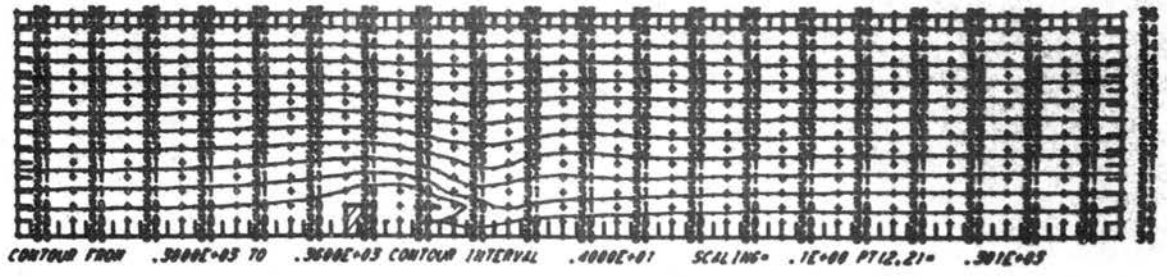

Fig. 4-16 A mixed scheme; upstream difference scheme in the upstream and Arakawa's one in the downstream of the obstacle.

$\frac{\partial^2 \psi}{\partial x^2} = \frac{\partial^2 \zeta}{\partial x^2} = \frac{\partial^2 T}{\partial x^2} = 0$ were used at lateral boundaries.

Stream Function at t = 5.74 sec

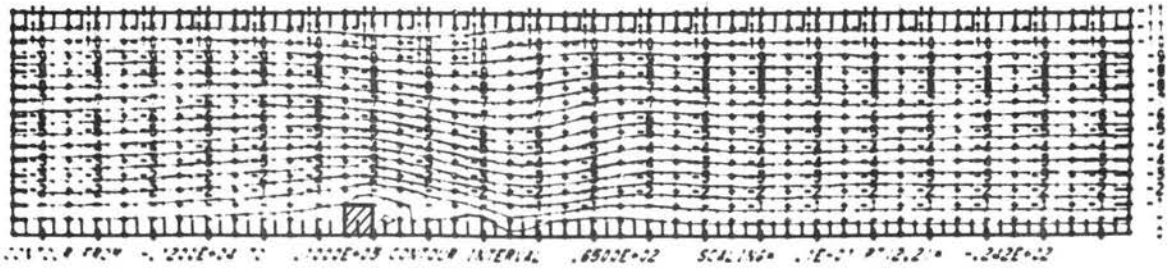

at t = 12.11 sec

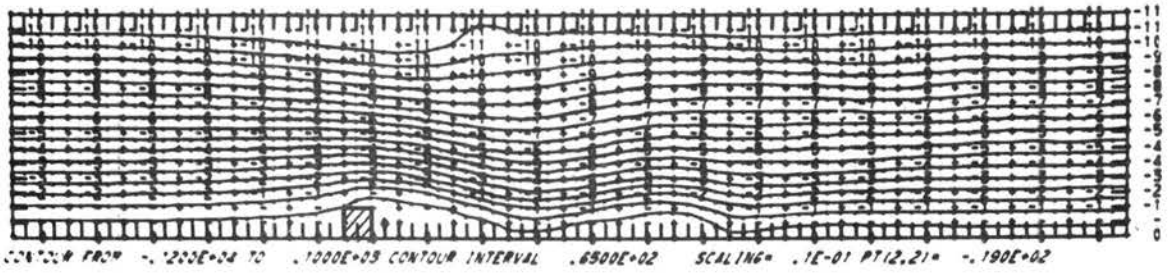

at t = 17.82 sec

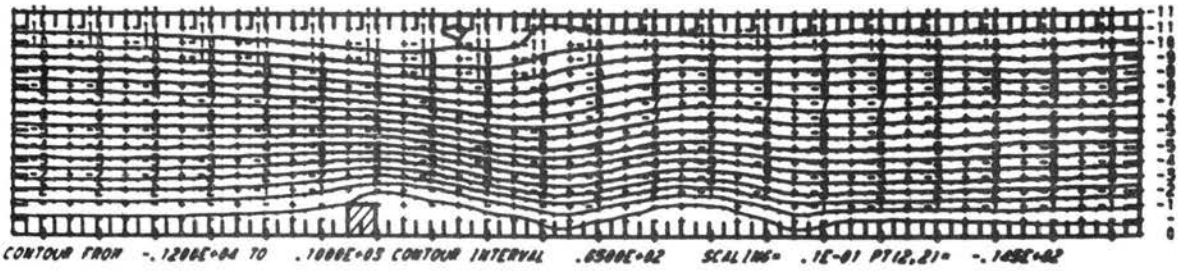

at t = 20.84 sec

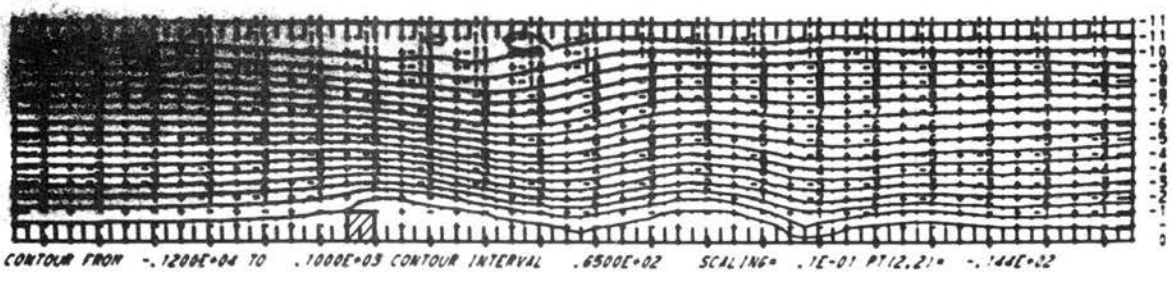

Fig. 4-17 Streamlines at t = 5.74, 12.11, 17.82, and 20.84 sec obtained by further integration of the scheme described in Fig. 4-16.

Vorticity at t = 5.74 sec

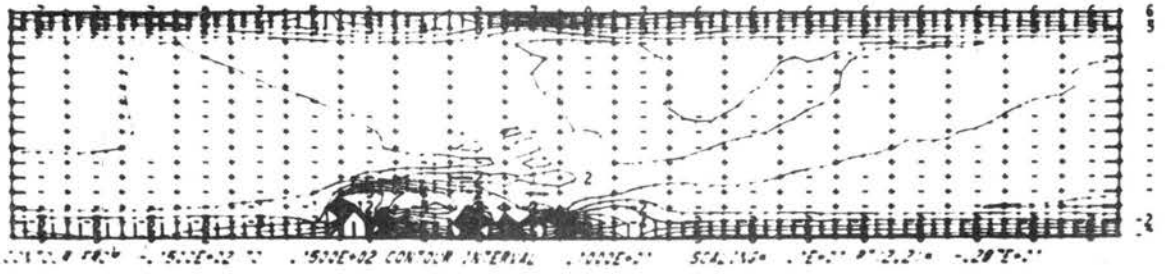

at t = 12.11 sec

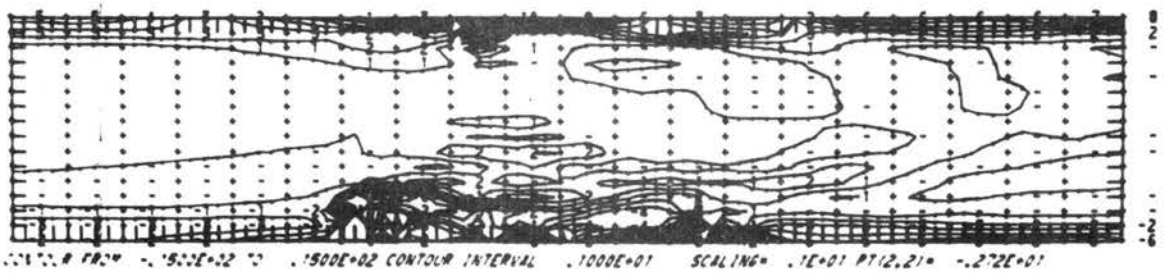

at t = 17.82 sec

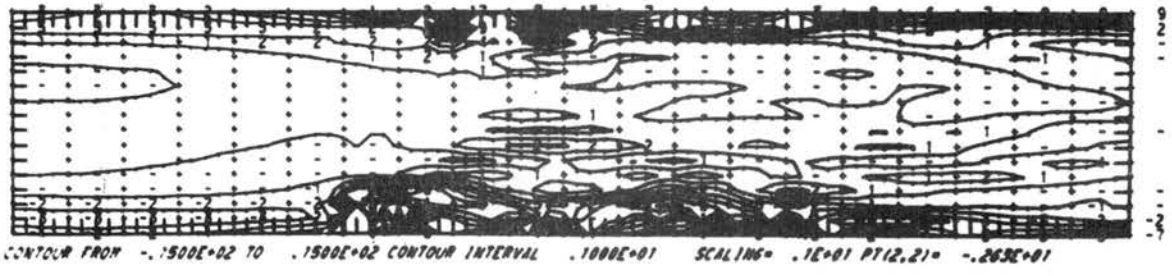

at t = 20.84 sec

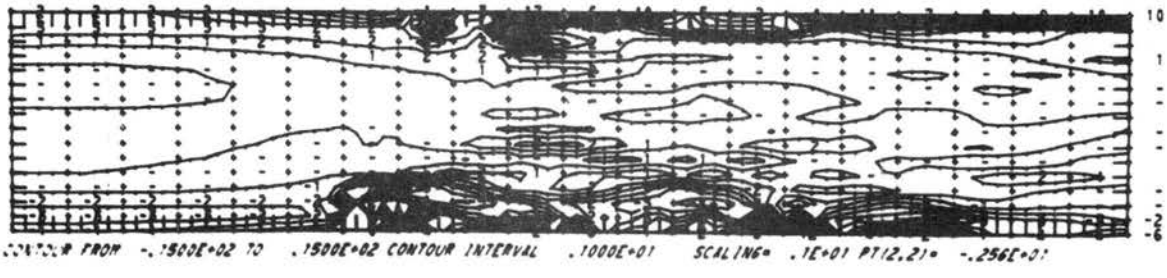

Fig. 4-18 Vorticity contour lines corresponding to Fig. 4-17.

Temperature at t = 5.74 sec

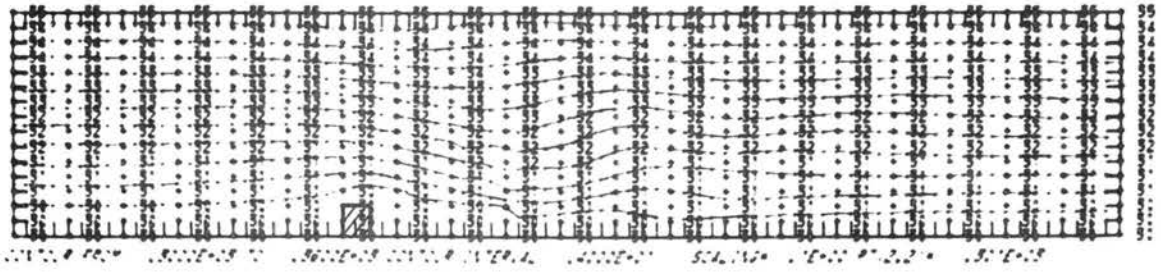

at t = 12.11 sec

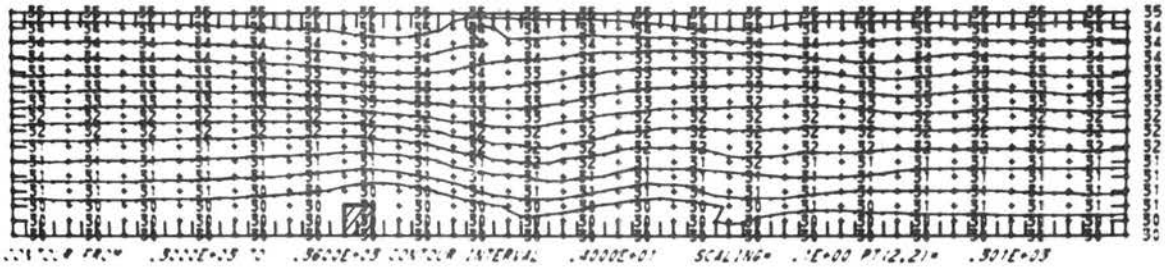

at t = 17.82 sec

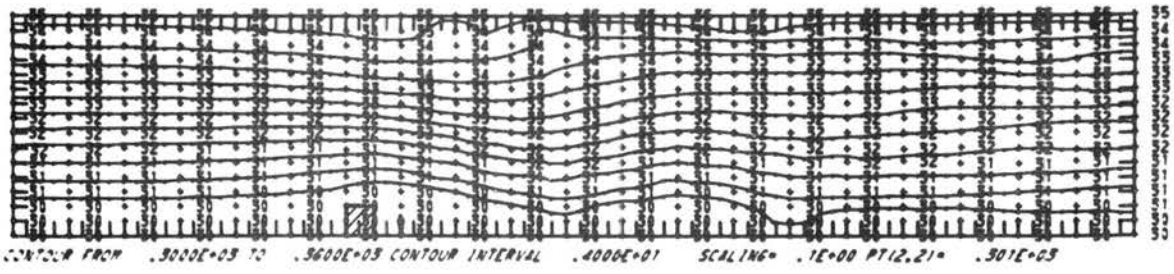

at t = 20.84 sec

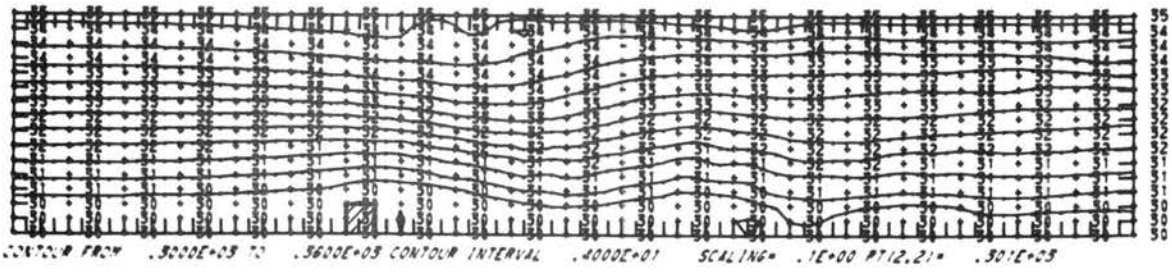

Fig. 4-19 Temperature contour lines corresponding to Fig. 4-17.

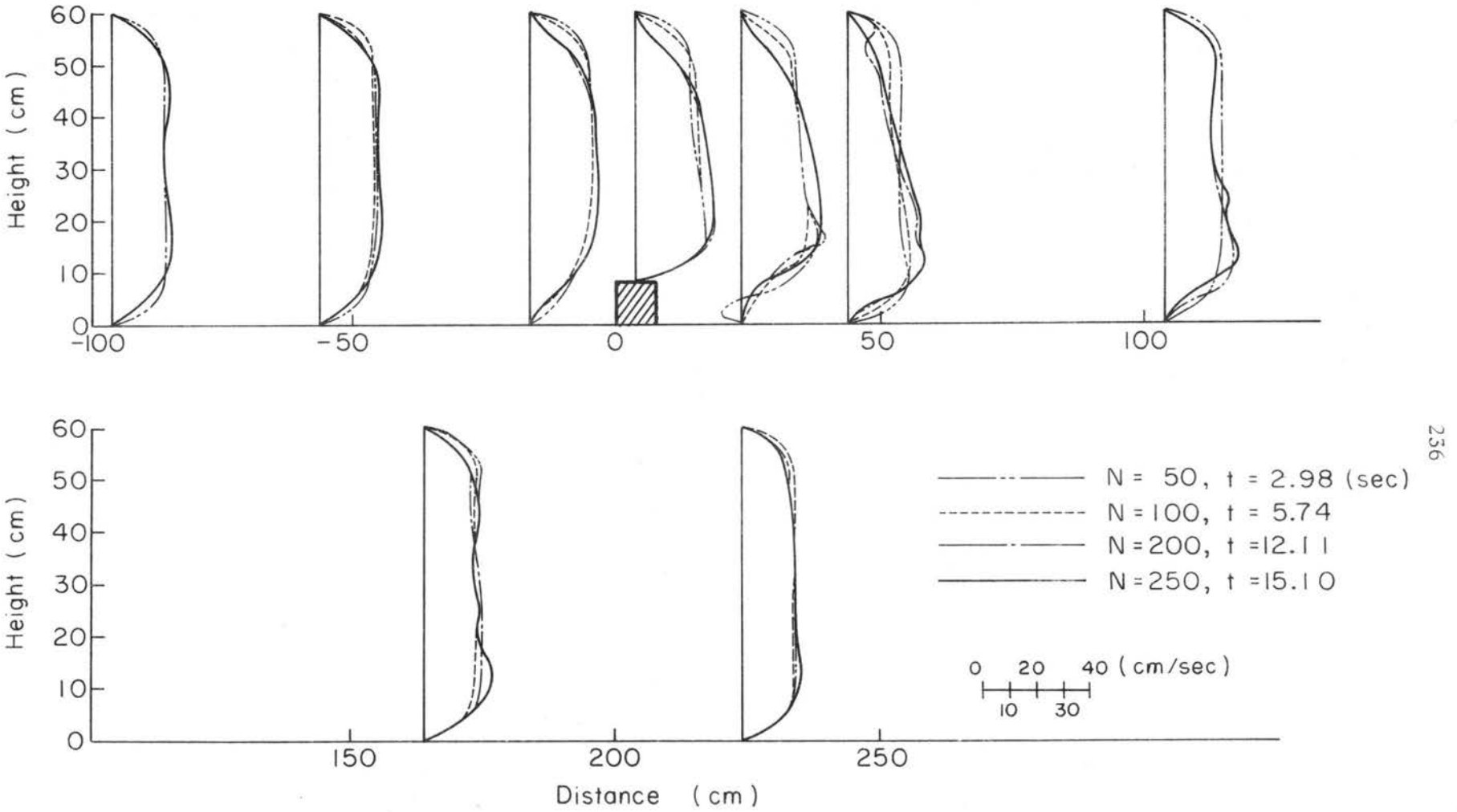

Fig. 4-20 Time variations of horizontal velocity profiles in a mixed scheme described in Fig. 4-16.

Stream Function

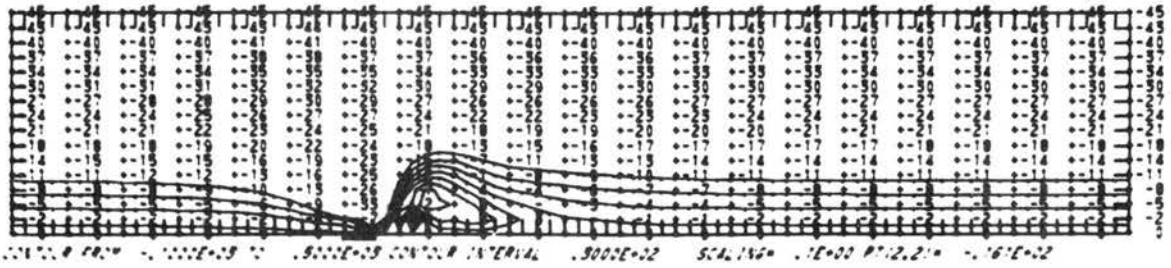

Vorticity

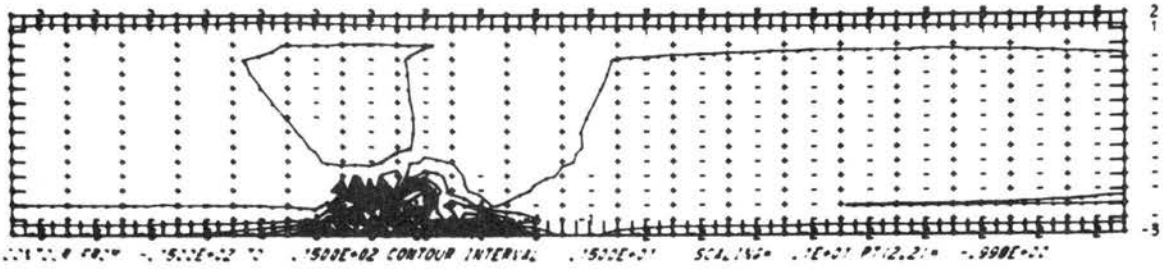

Temperature

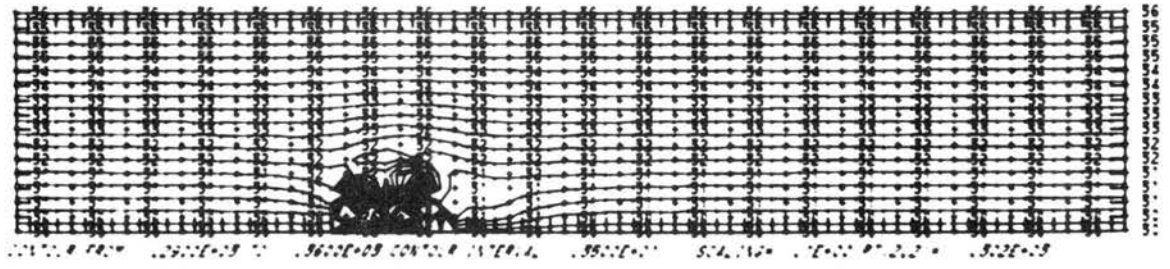

Fig. 4-21 Airflow over a heated island; contour lines of stream function, vortex, and temperature obtained by a mixed scheme. $(\overline{Fr})_H = 0.077$, $\Delta T = 62^{o}C$.

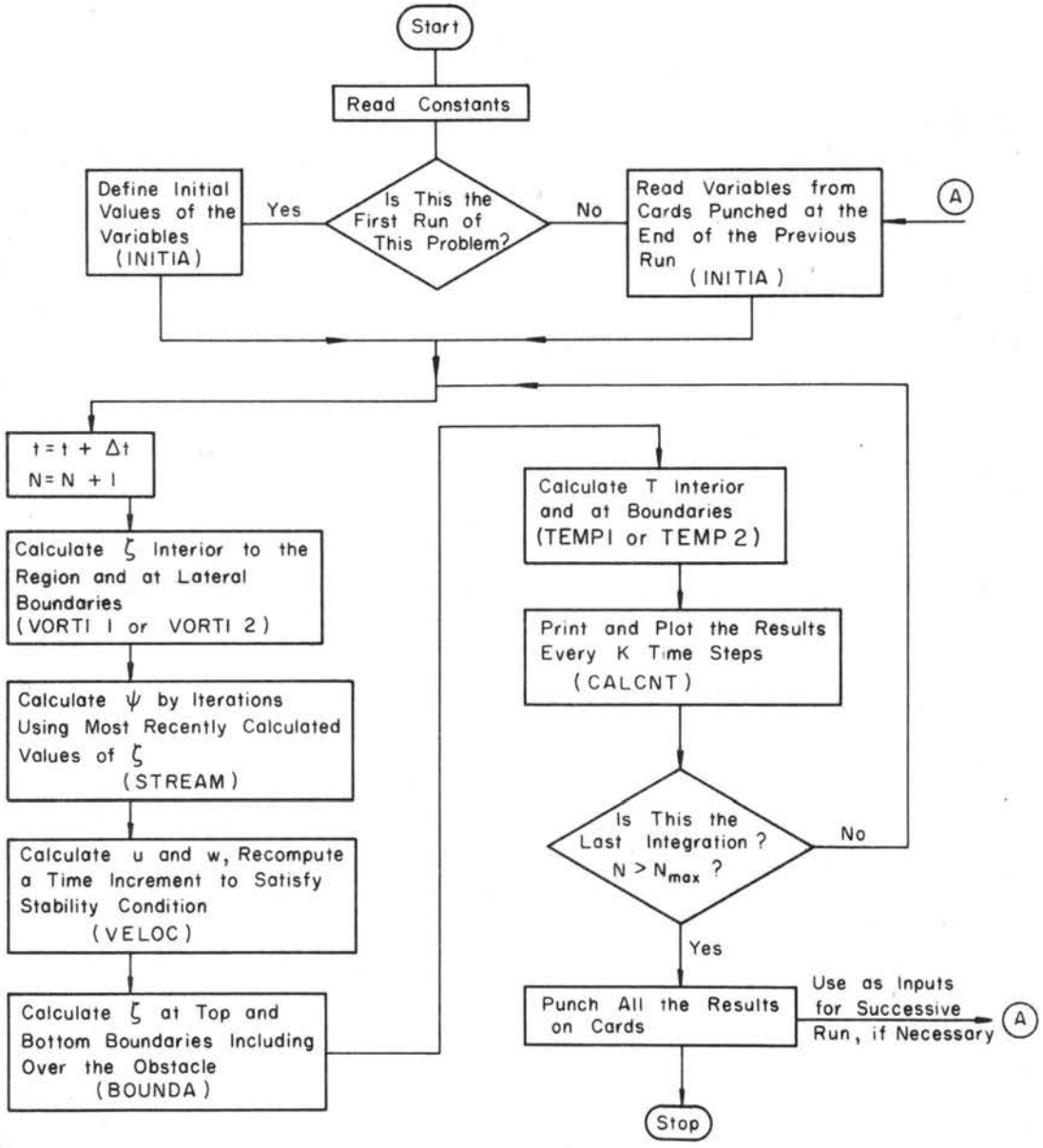

Fig. 4-22 Schematic diagram of the flow chart of the program.

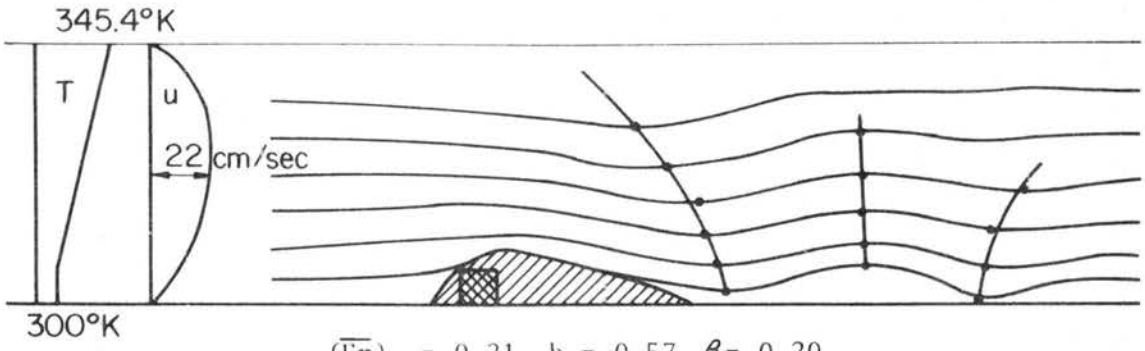

$(\overline{Fr})_H$ = 0.21, b = 0.57, β = 0.20

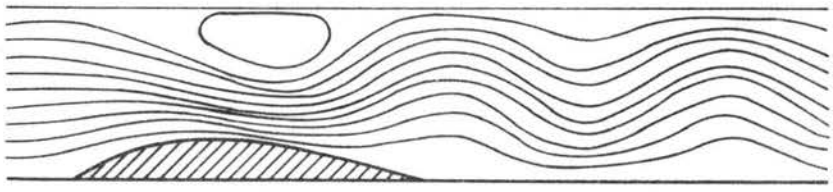

$(\overline{Fr})_H$ = 0.20, b = 1.0, β = 0.20

Fig. 5-1 A test calculation of airflow over a square obstacle by the present numerical model and comparison with Long's results (1955). b: half width of the obstacle, β: obstacle height/channel height.

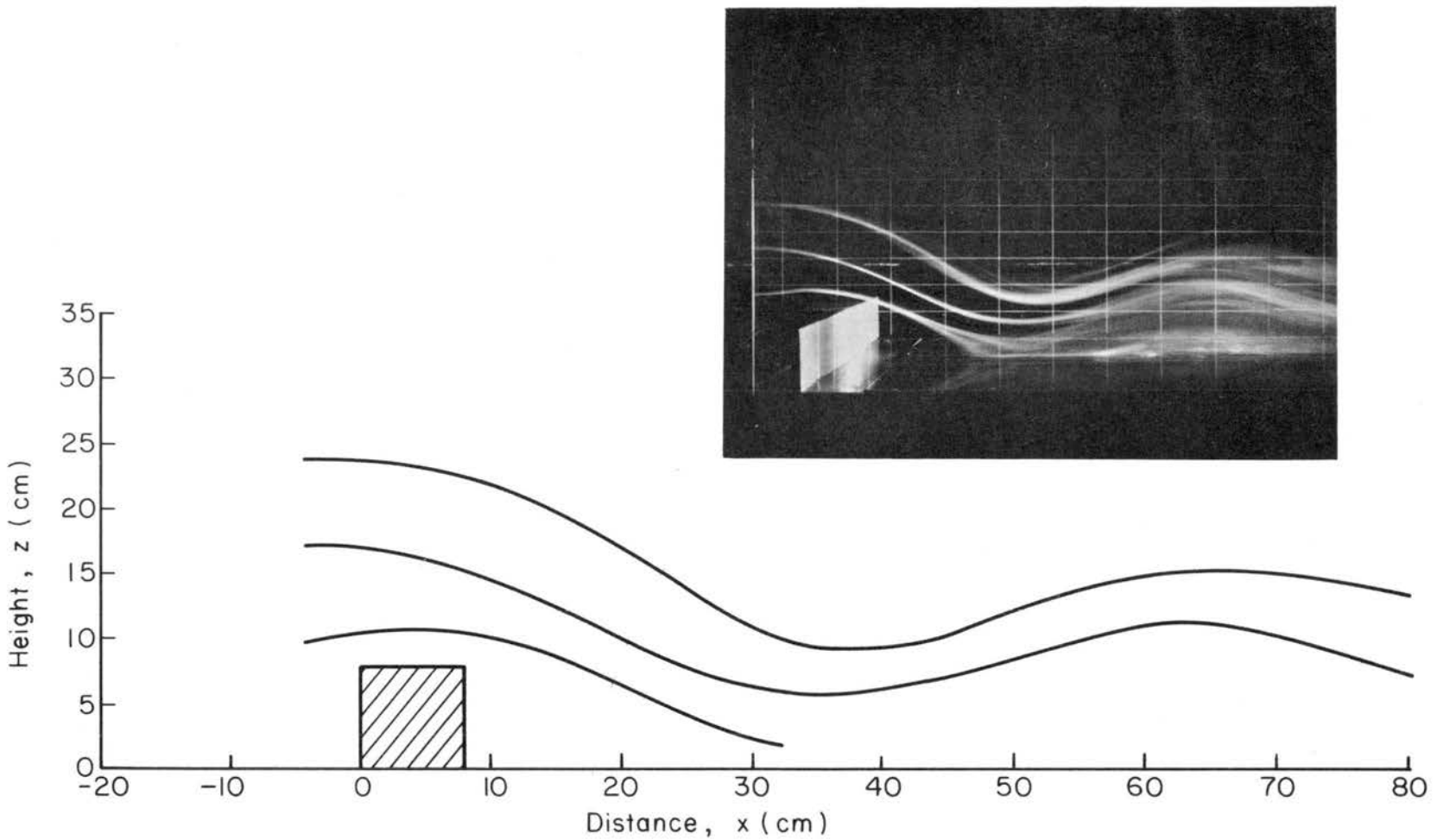

Fig. 5-2 Streamlines obtained from a smoke visualization picture when $(\overline{Fr})_H = 0.144$, (October 7, 1970).

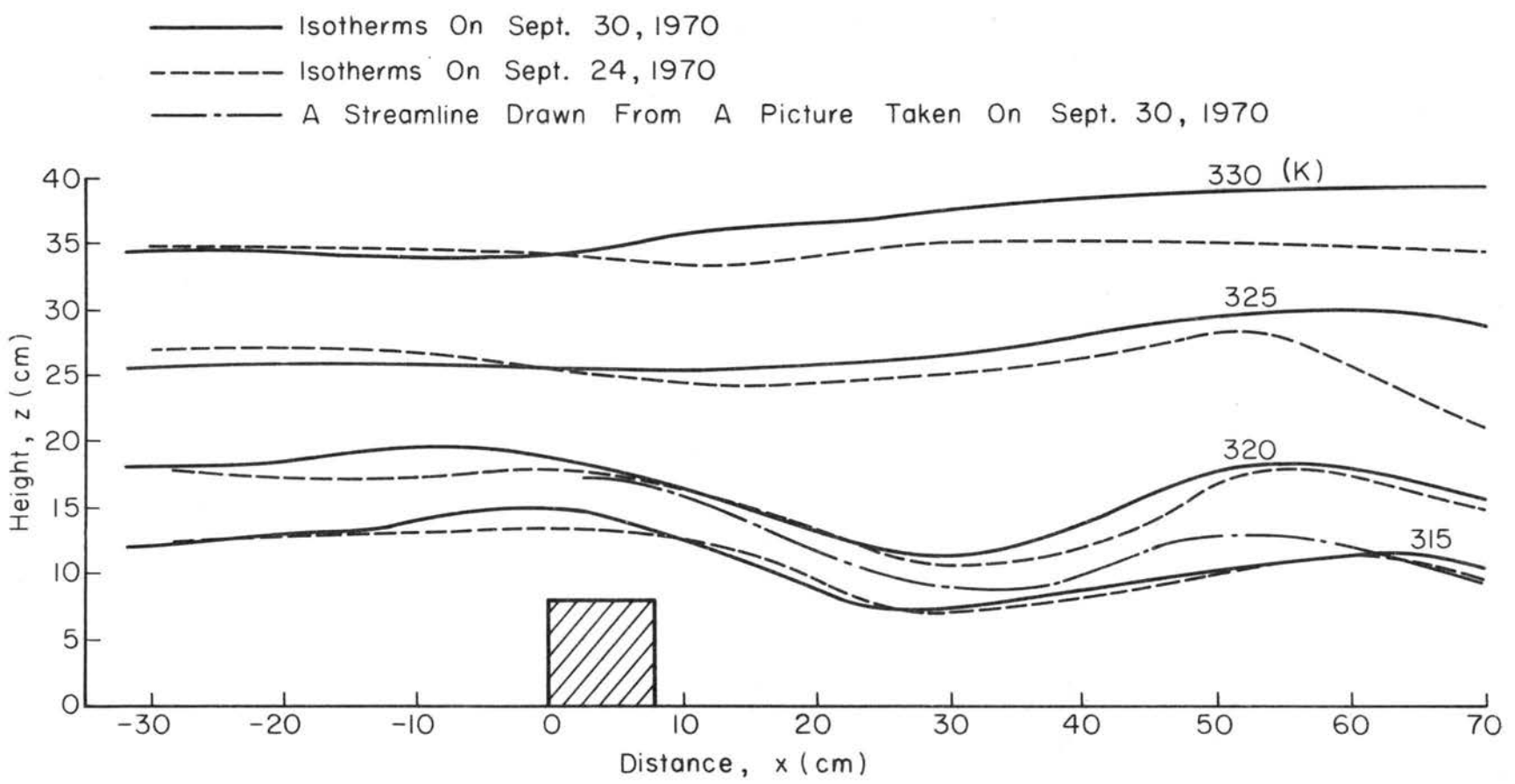

Fig. 5-3 Case A-1 (Experimental): Isotherms over square obstacle. $\overline{(Fr)}_H = 0.126$.

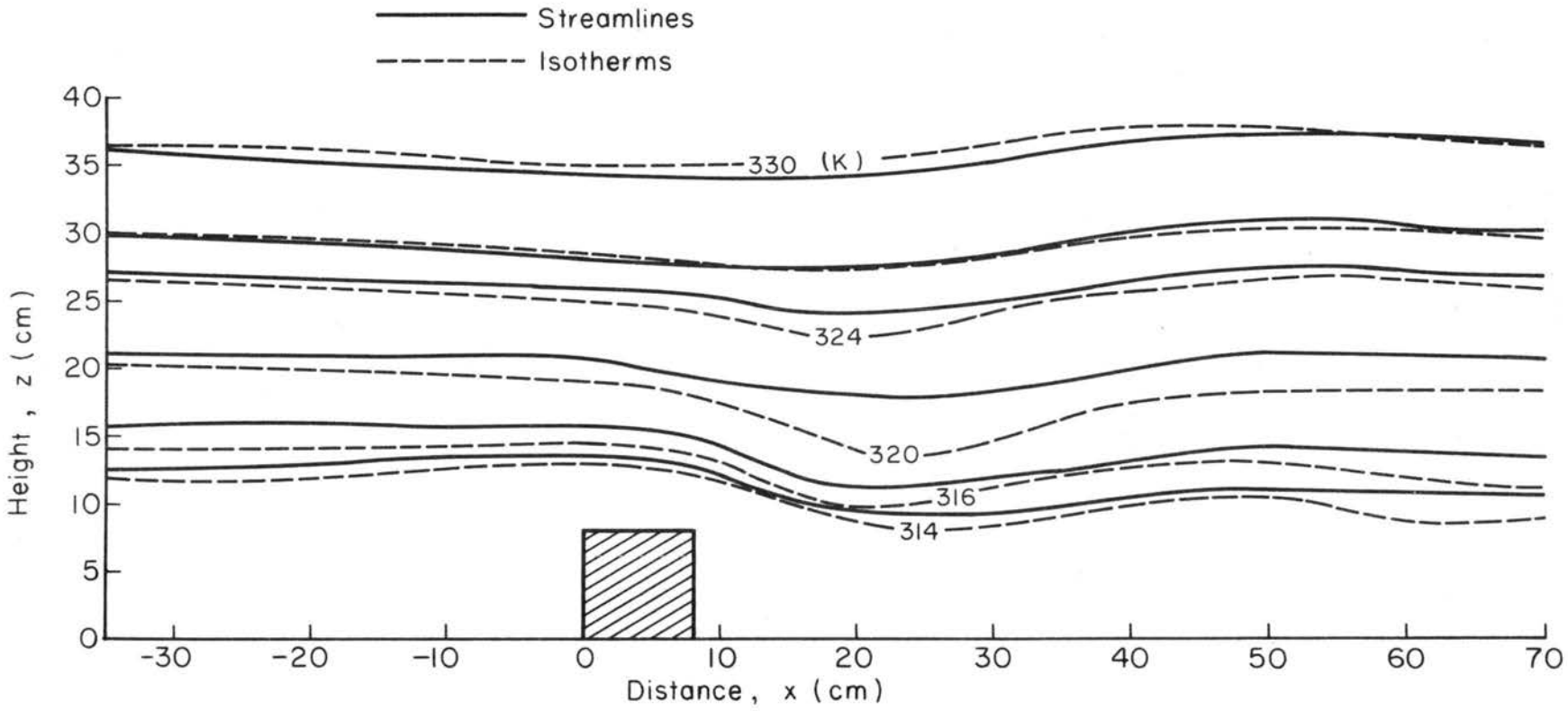

Fig. 5-4 Case A-1 (Numerical): Streamlines and isotherms obtained by the present numerical model under the same boundary conditions as the wind tunnel experiment. $(\overline{Fr})_H = 0.126$.

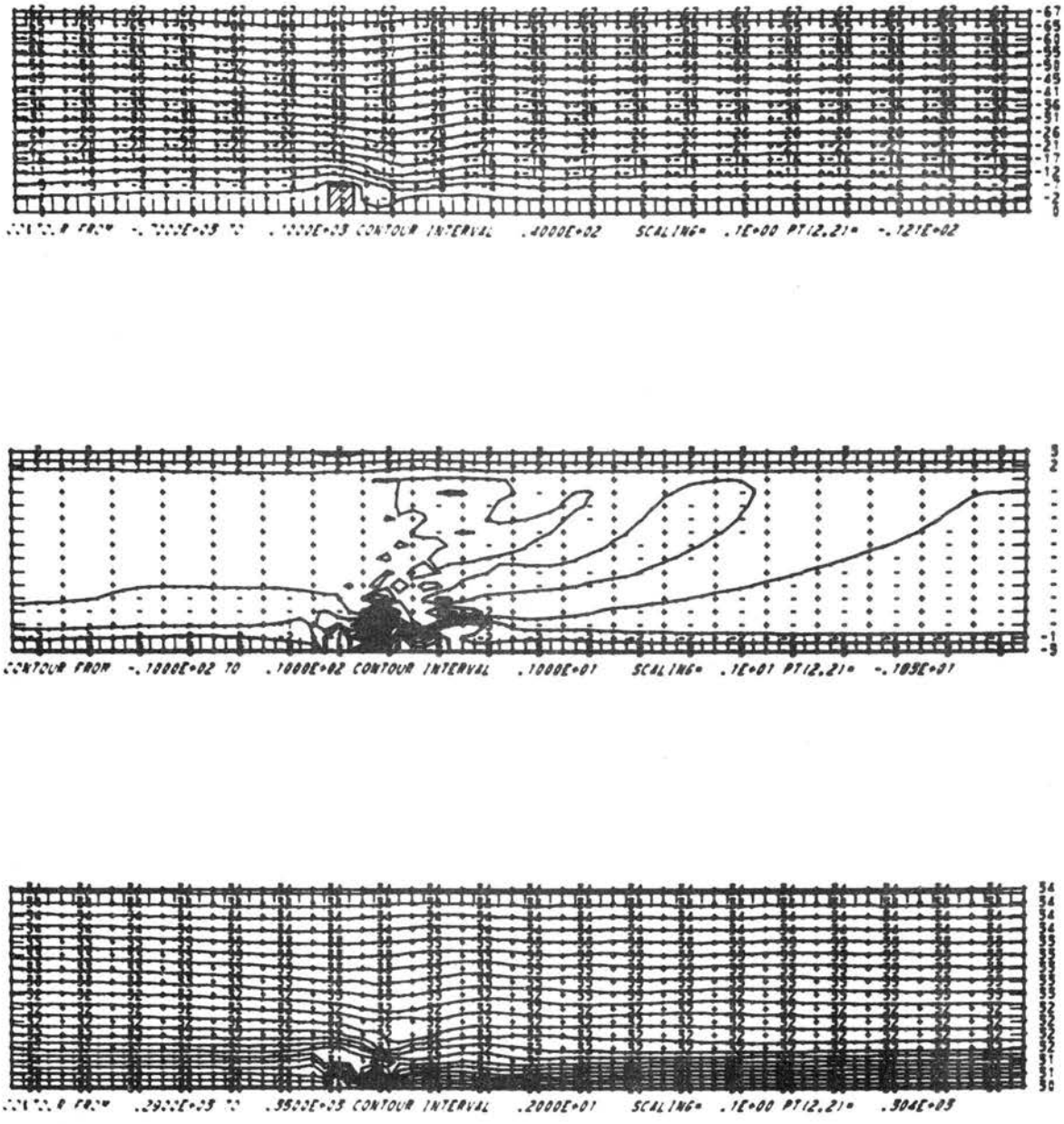

Fig. 5-5 Case A-1 (Numerical): Computed stream function, vorticity, and temperature contour lines at t = 7.21 sec. under the same flow conditions as in Fig. 5-3.

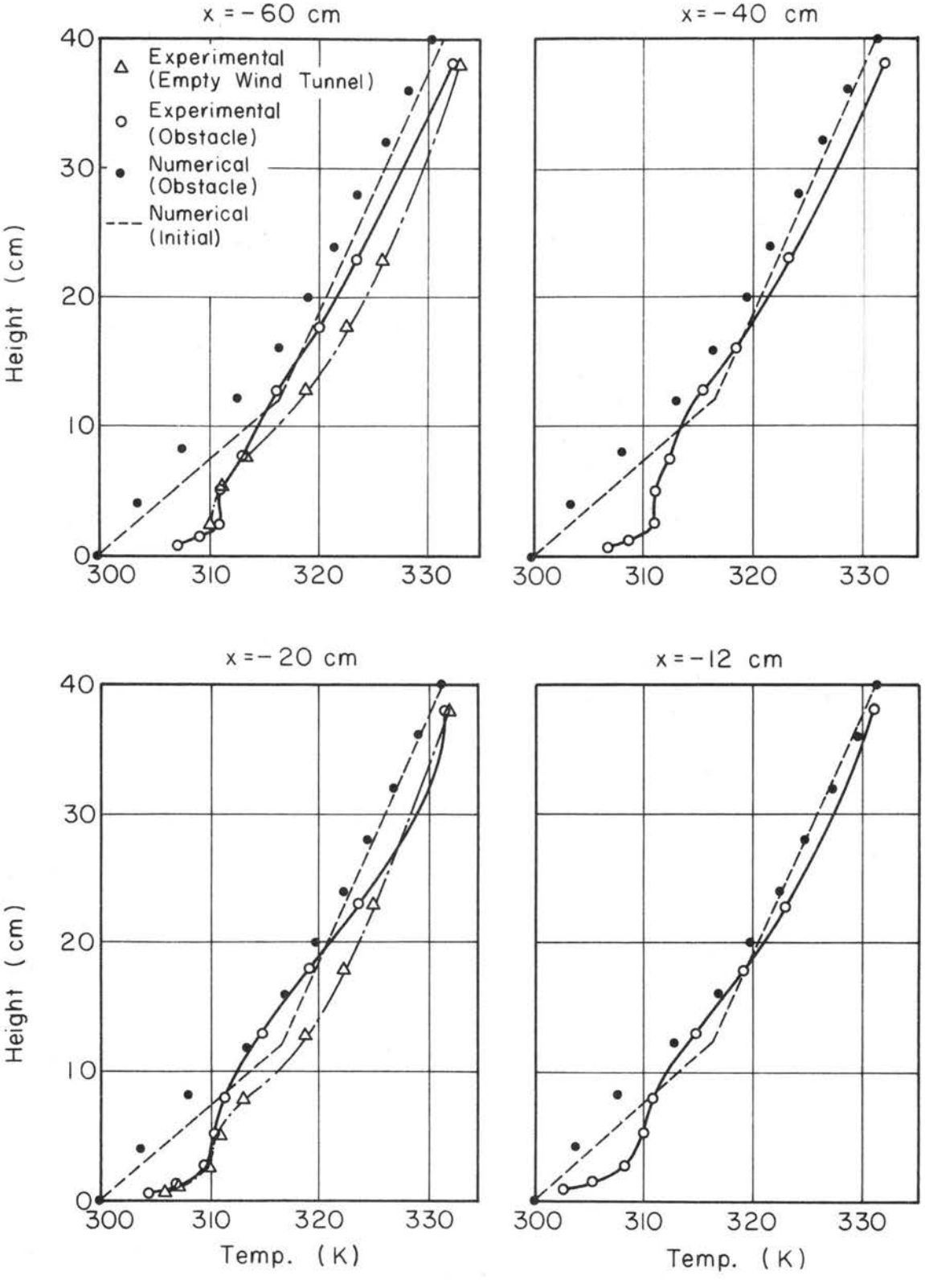

Fig. 5-6 Case A-1: Temperature profiles at various locations obtained by wind tunnel and numerical experiments.

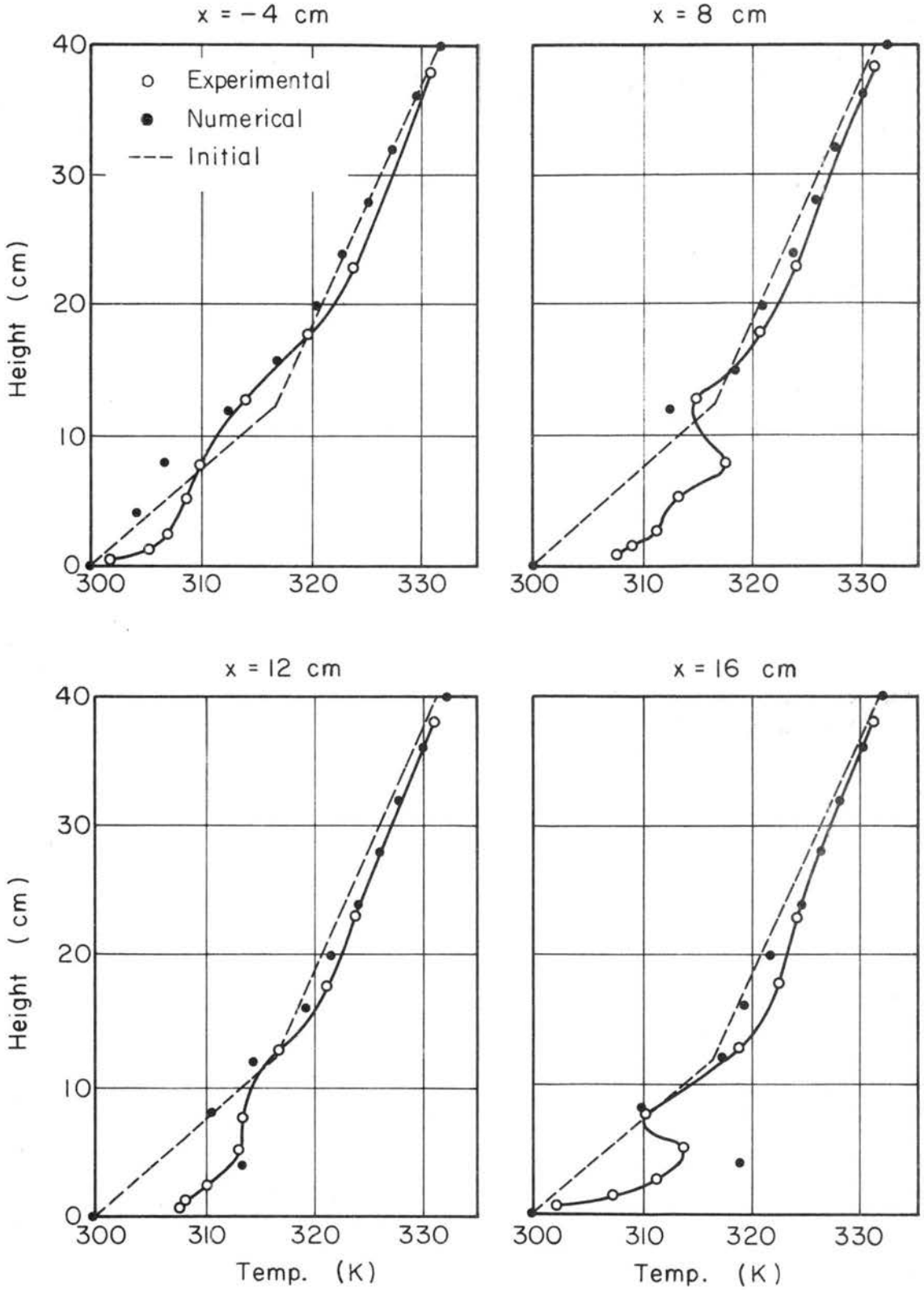

Fig. 5-6 (continued) Case A-1: Temperature profiles at various locations obtained by wind tunnel and numerical experiments.

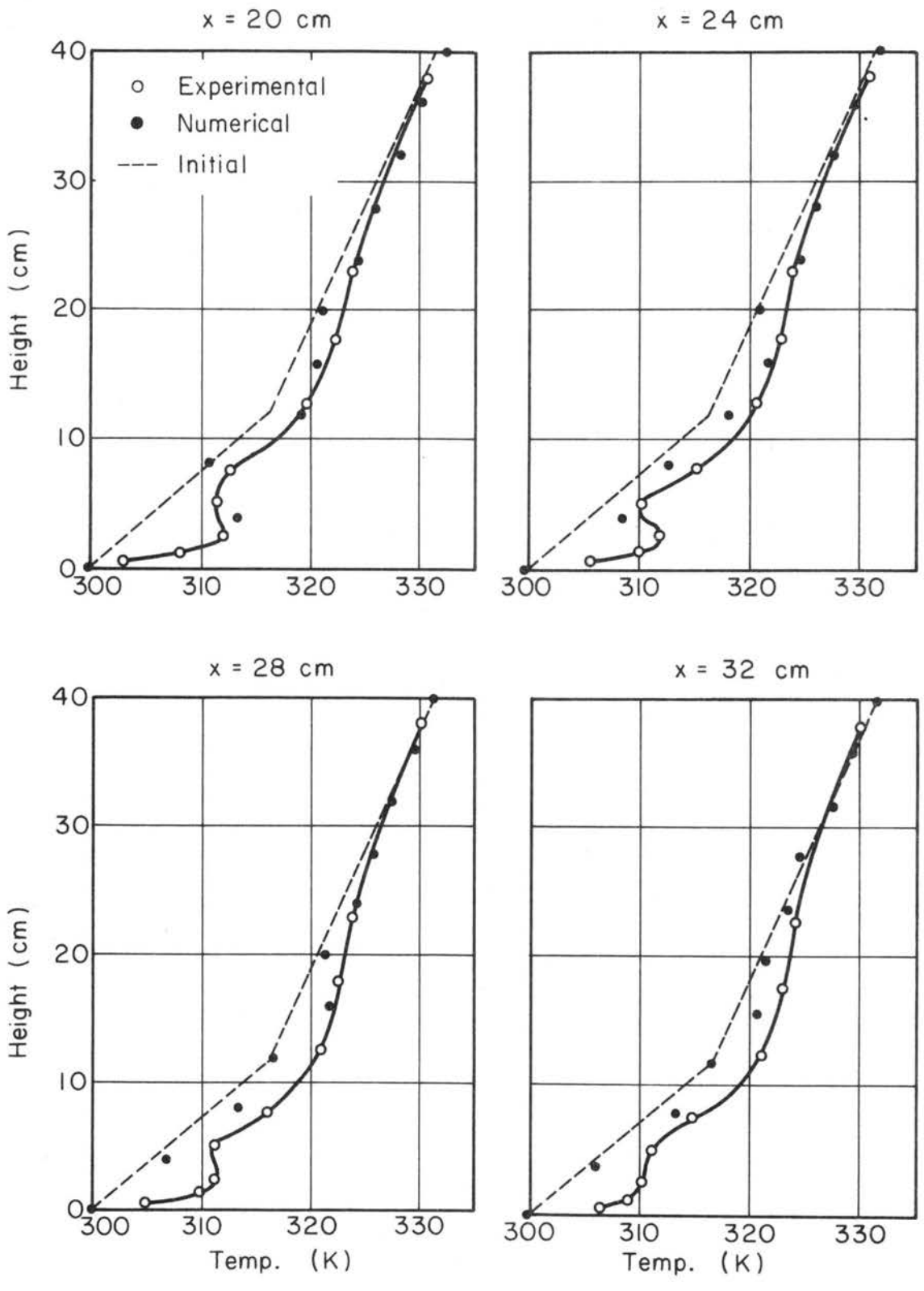

Fig. 5-6 (continued) Case A-1: Temperature profiles at various locations obtained by wind tunnel and numerical experiments.

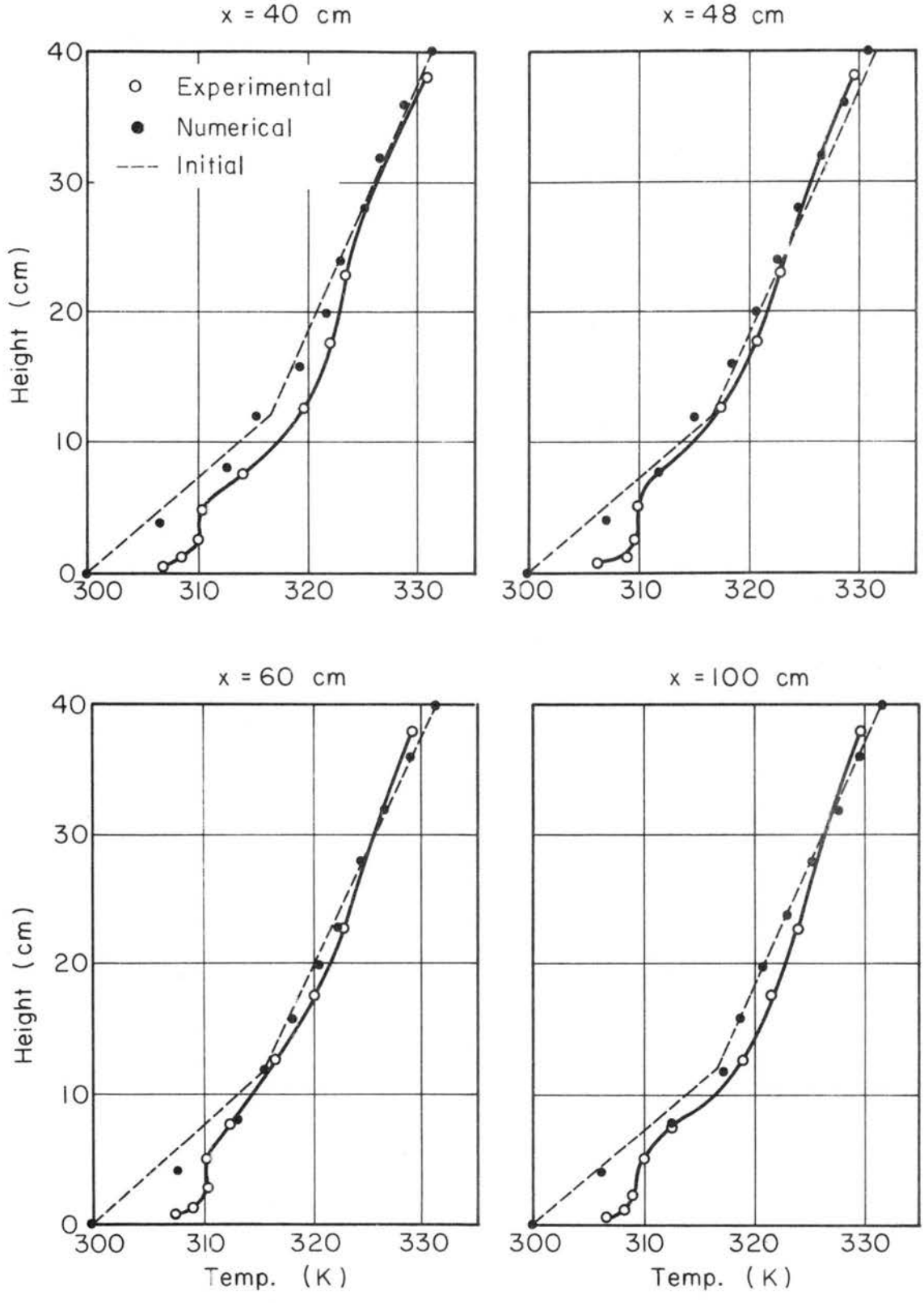

Fig. 5-6 (continued) Case A-1: Temperature profiles at various locations obtained by wind tunnel and numerical experiments.

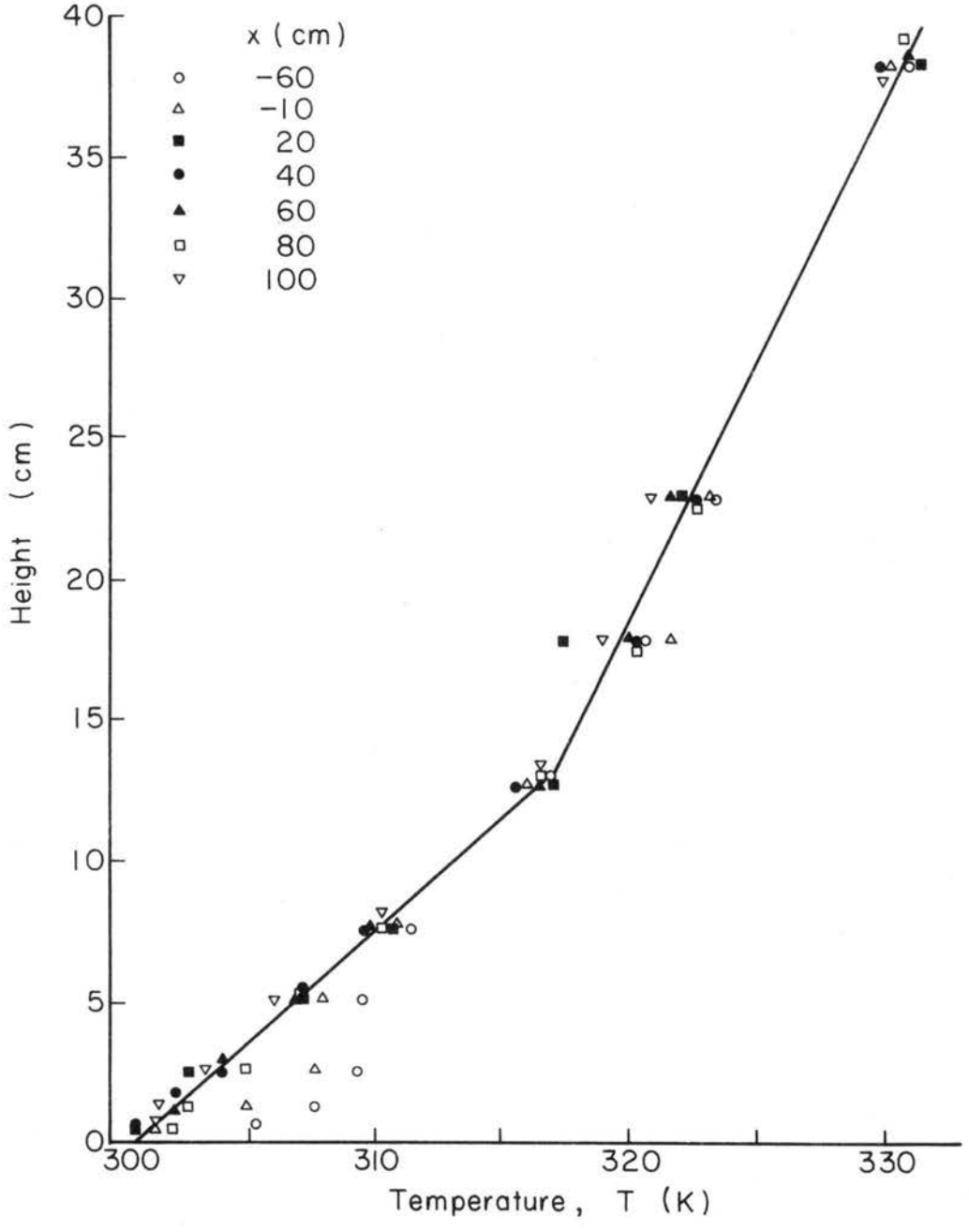

Fig. 5-7 Case A-1: Temperature profiles at various locations obtained by wind tunnel experiments without an obstacle. Distribution shown by a solid line was used as an initial value of the numerical model.

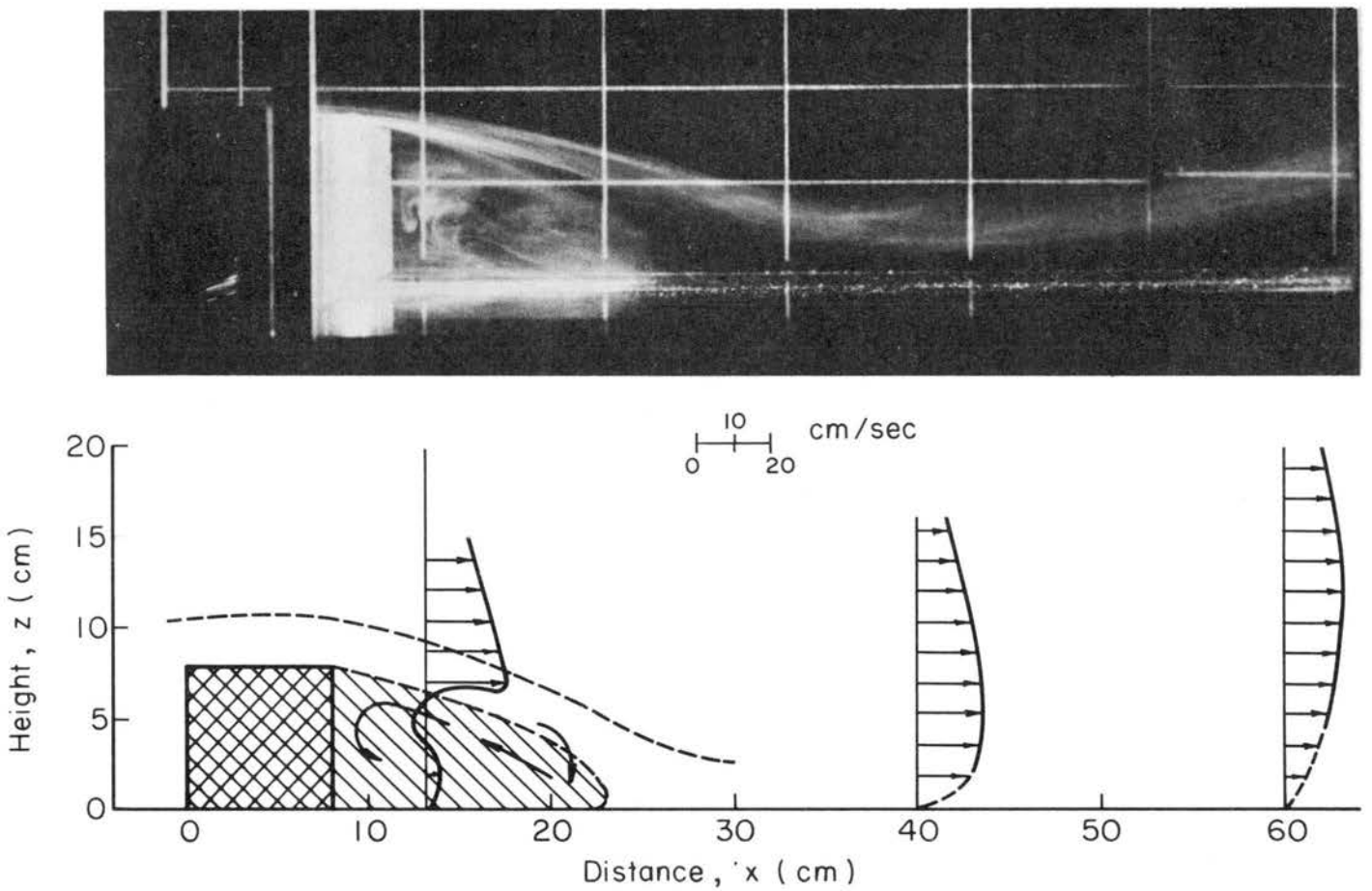

Fig. 5-8 Case A-1 (Experimental): Flow behind the obstacle; $(\overline{Fr})_H = 0.126$, b = 0.567, $\beta = 0.15$.

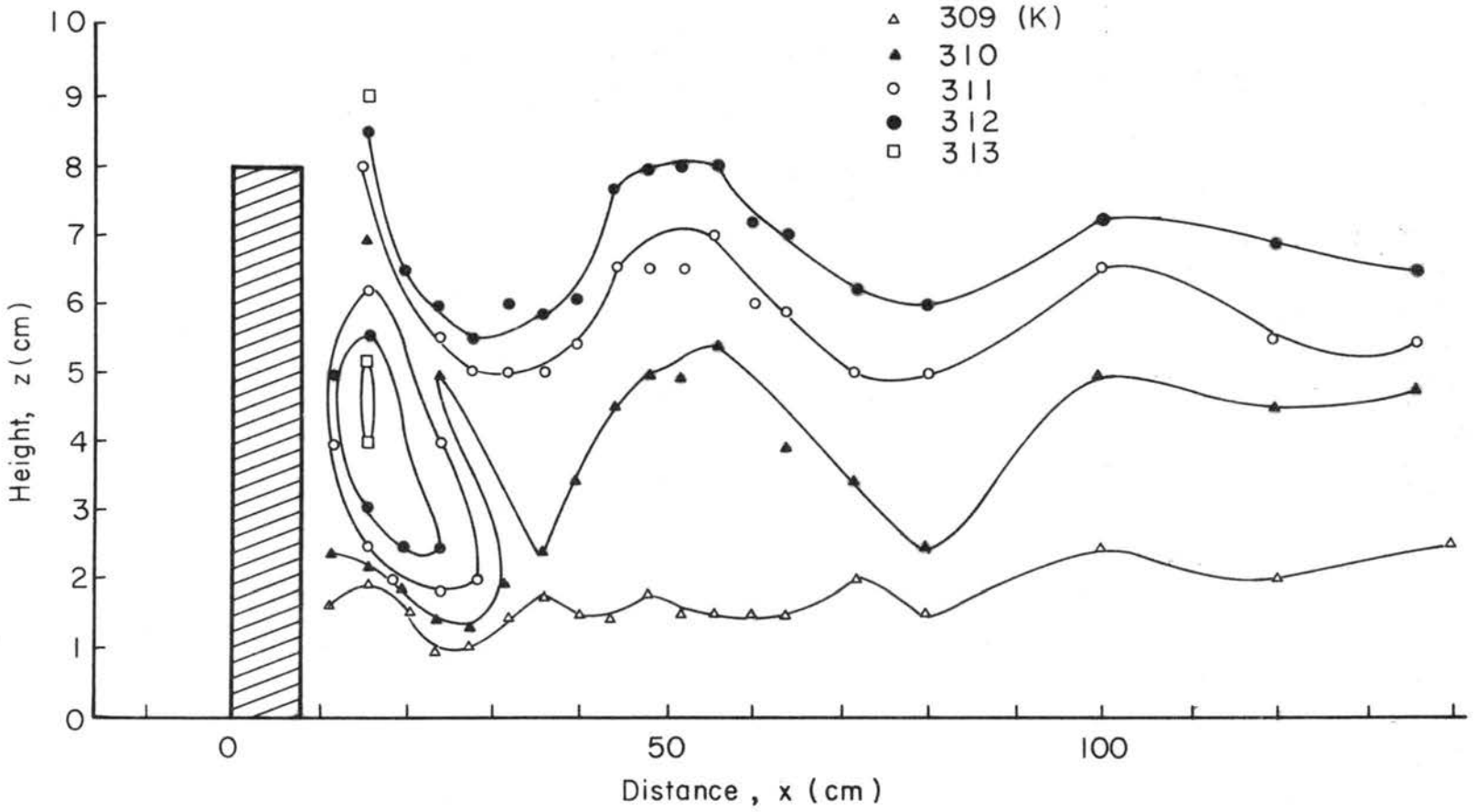

Fig. 5-9 Case A-1 (Experimental): Temperature field behind the obstacle; $(\overline{Fr})_H = 0.126$.

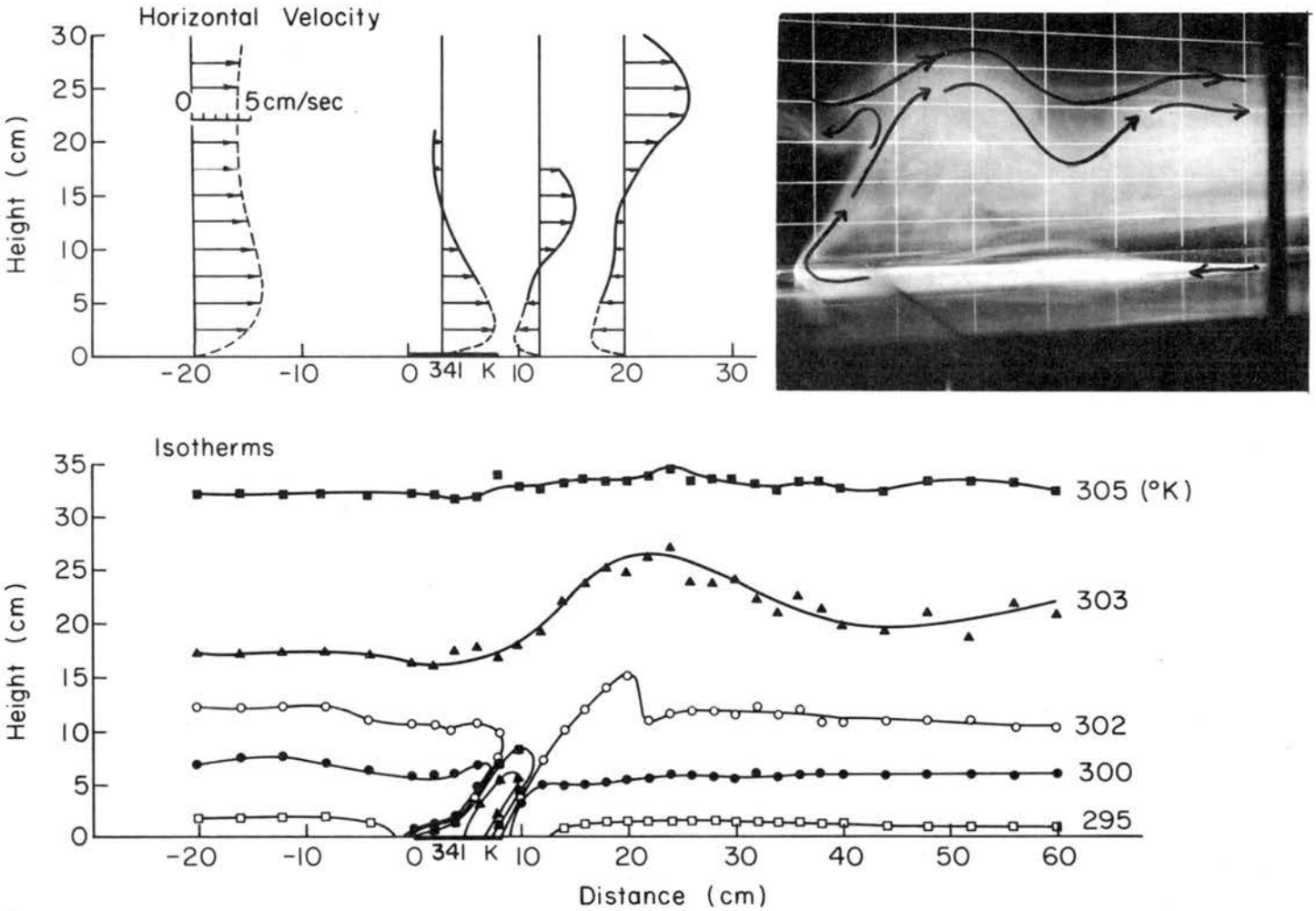

Fig. 5-10 Case B-1 (Experimental): Measured horizontal velocity profiles and isotherms when $(\overline{Fr})_H = 0.100$, and $N_h = 5.40$. Photograph shows a flow visualization by $TiCl_4$ smoke introduced at the right bottom corner of the picture.

Stream Function

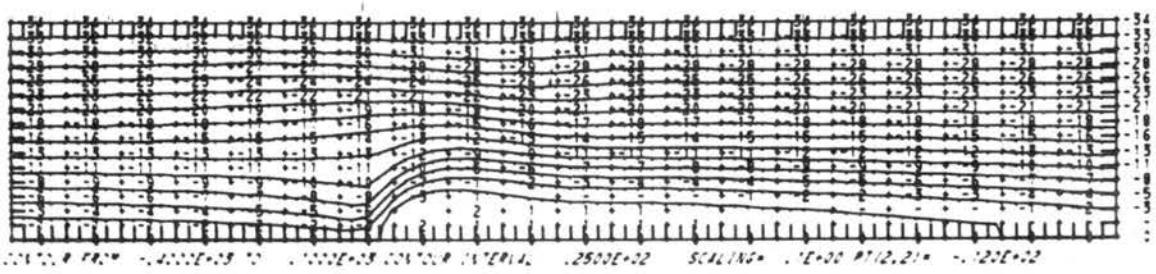

Vorticity

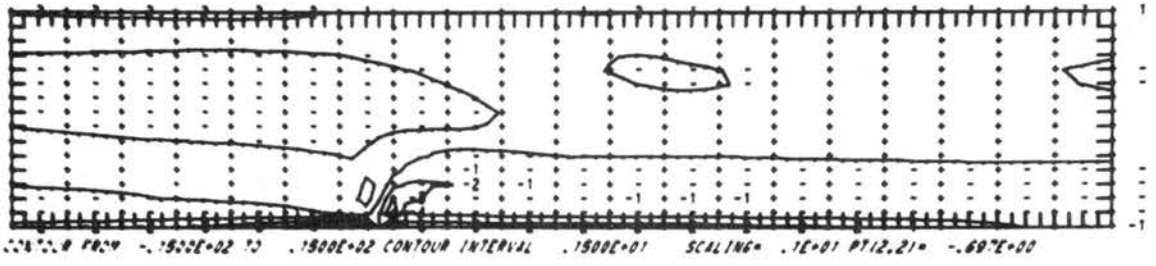

Temperature

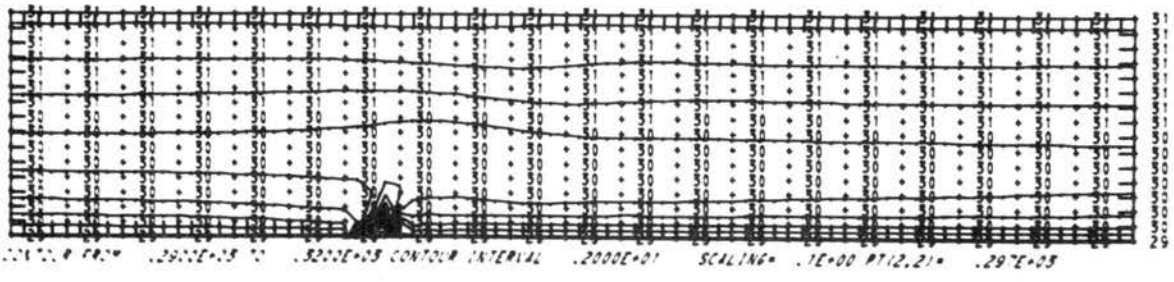

Fig. 5-11 Case B-1 (Numerical): Computed stream function, vorticity, and temperature contour lines at t = 27.11 sec. under the same flow conditions as in Fig. 5-10.

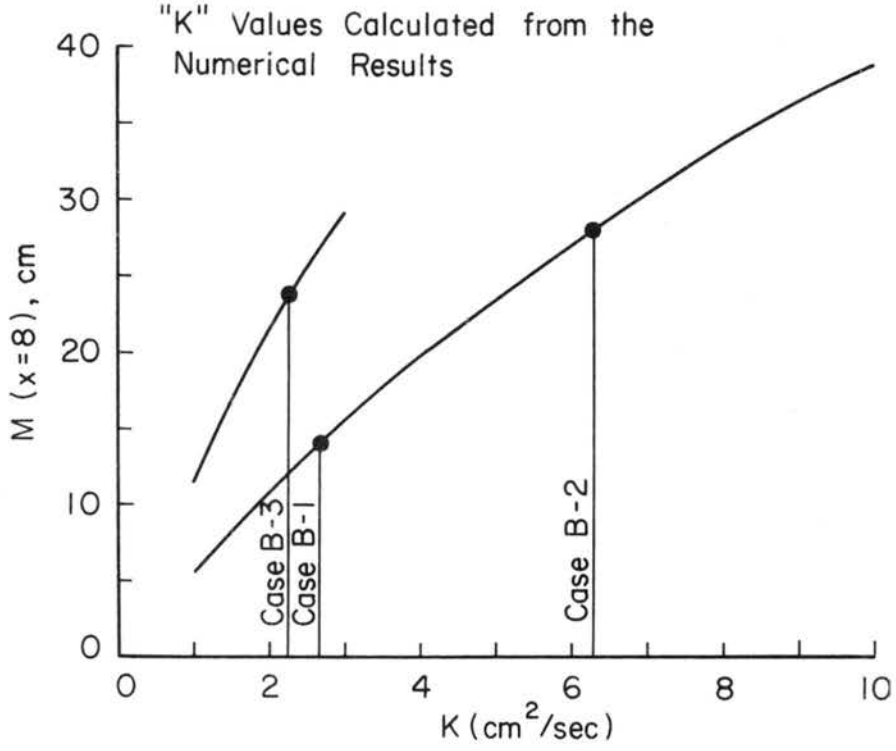

Fig. 5-12 Relation between an equivalent thermal mountain height at x =8 cm and viscosity K from Eq. 2.2.2.7-2.

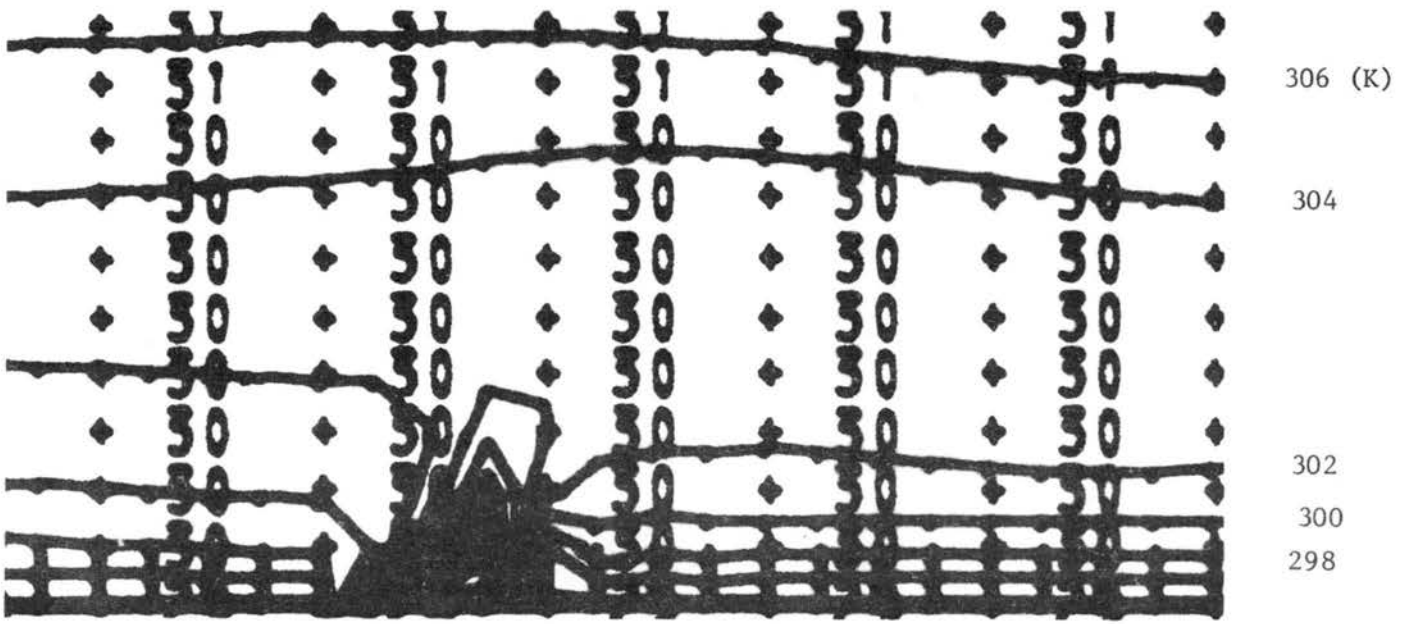

Fig. 5-13 Case B-1 (Numerical): Isotherms in the vicinity of the heated island (enlarged from the bottom figure in Fig. 5-11).

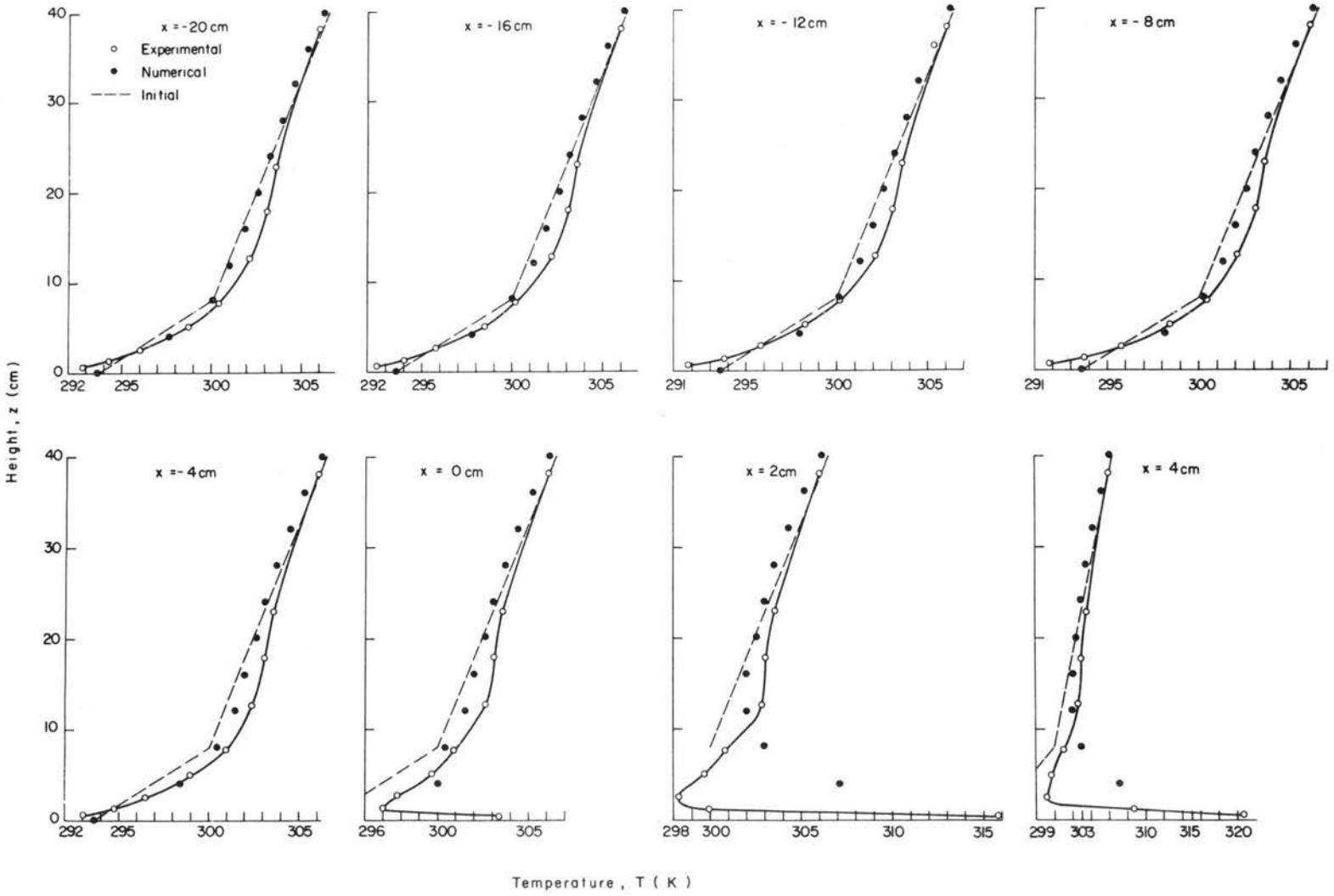

Fig. 5-14 Case B-1 (Experimental and Numerical): Comparison of experimental and numerical vertical temperature distributions at various locations

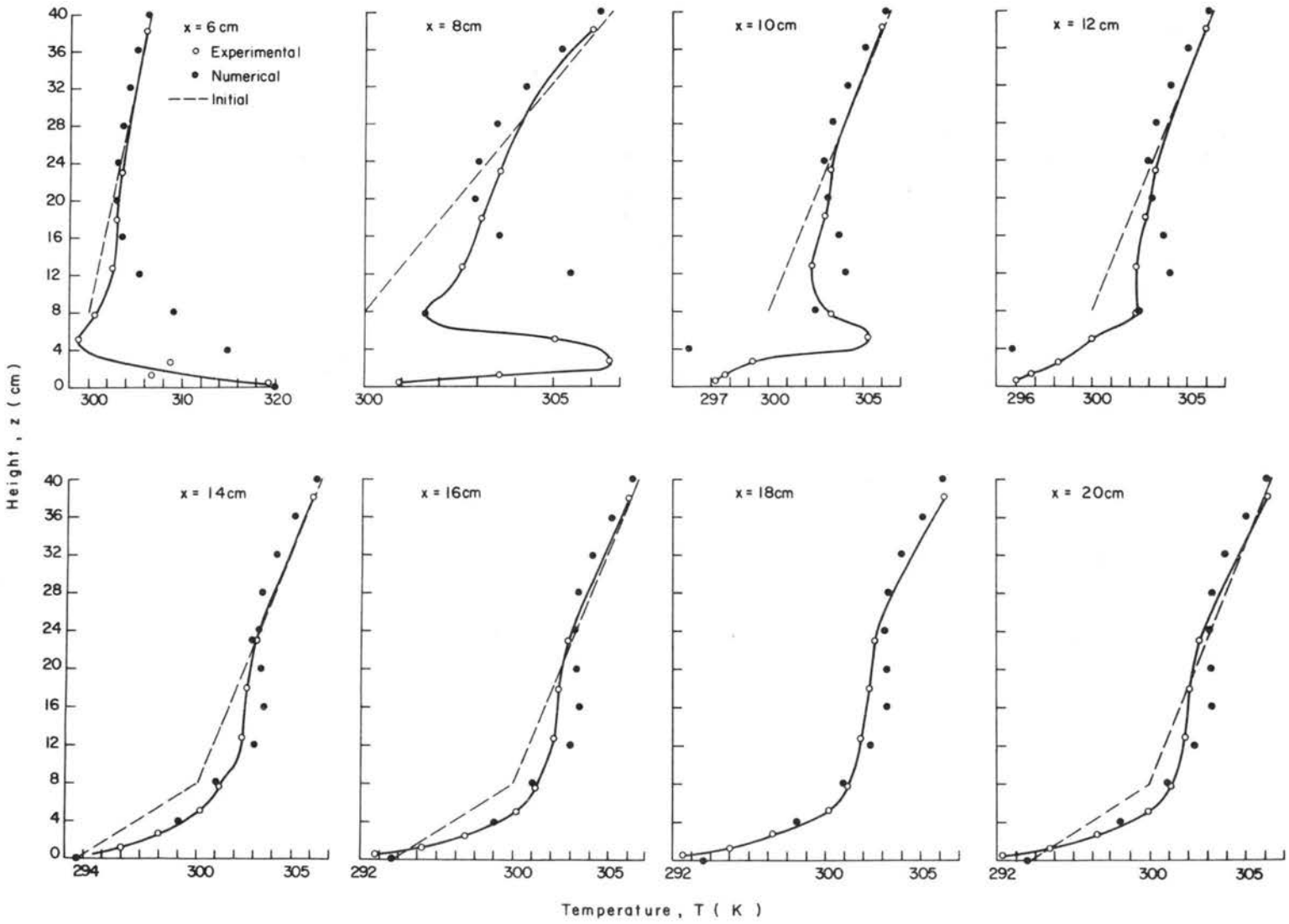

Fig.5-14 (continued)

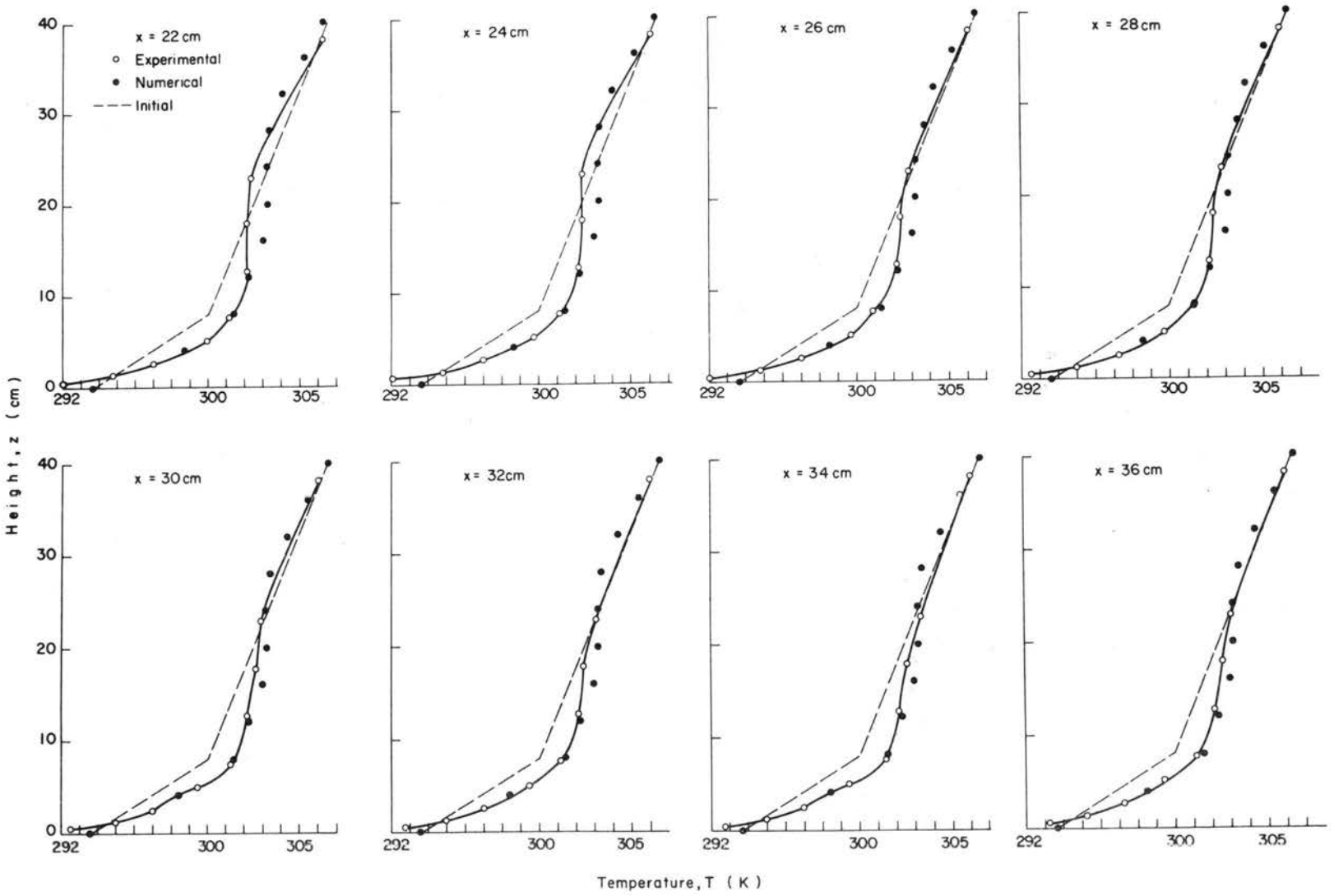

Fig. 5-14 (continued)

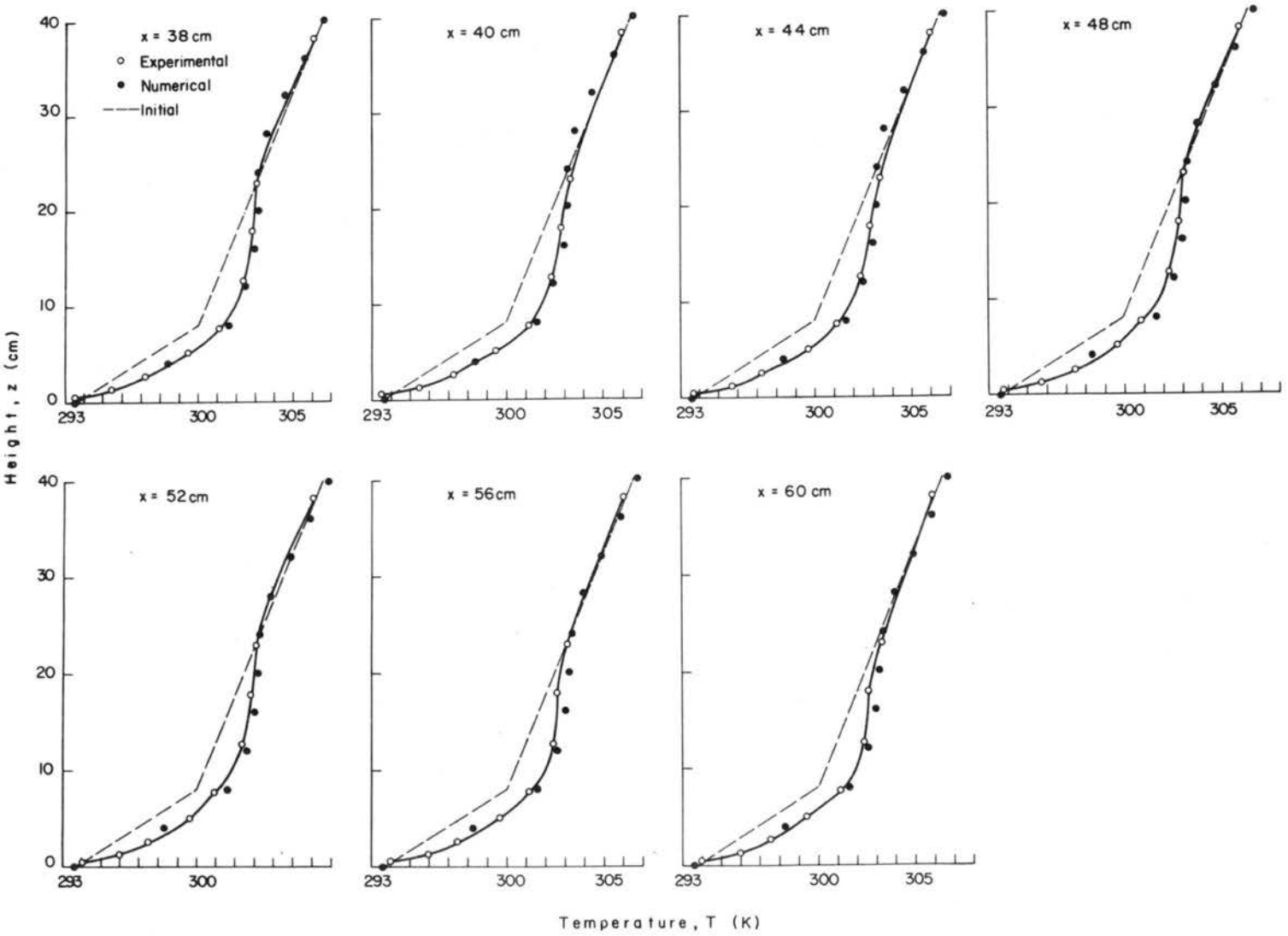

Fig. 5-14 (continued)

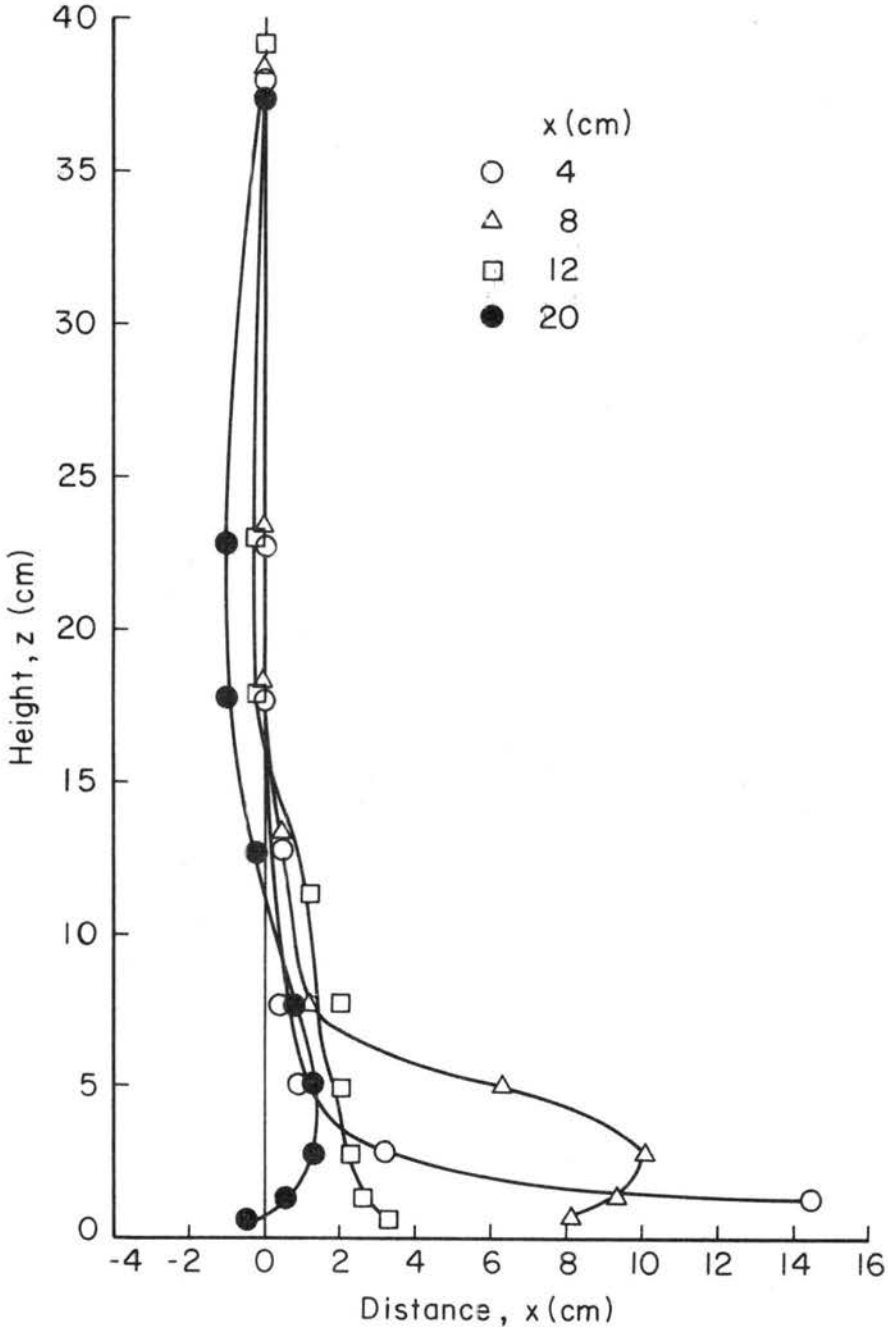

Fig. 5-15 Case B-1 (Experimental): Measured vertical profiles of temperature defect, $T_x - T_{x=-20}$.

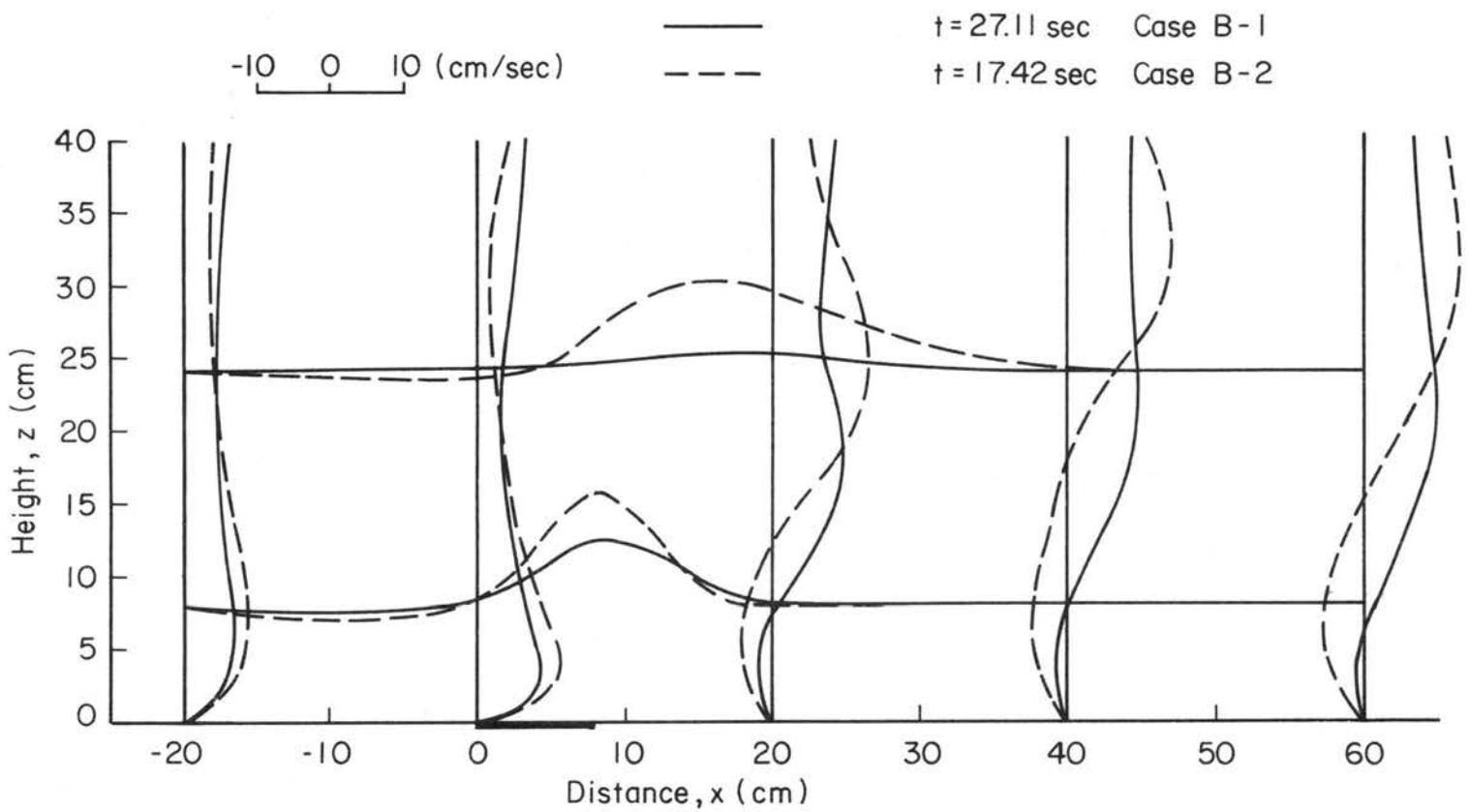

Fig. 5-16 Case B-1 and Case B-2 (Numerical): Computed horizontal and vertical velocity profiles; ——— Case B-1, ------ Case B-2.

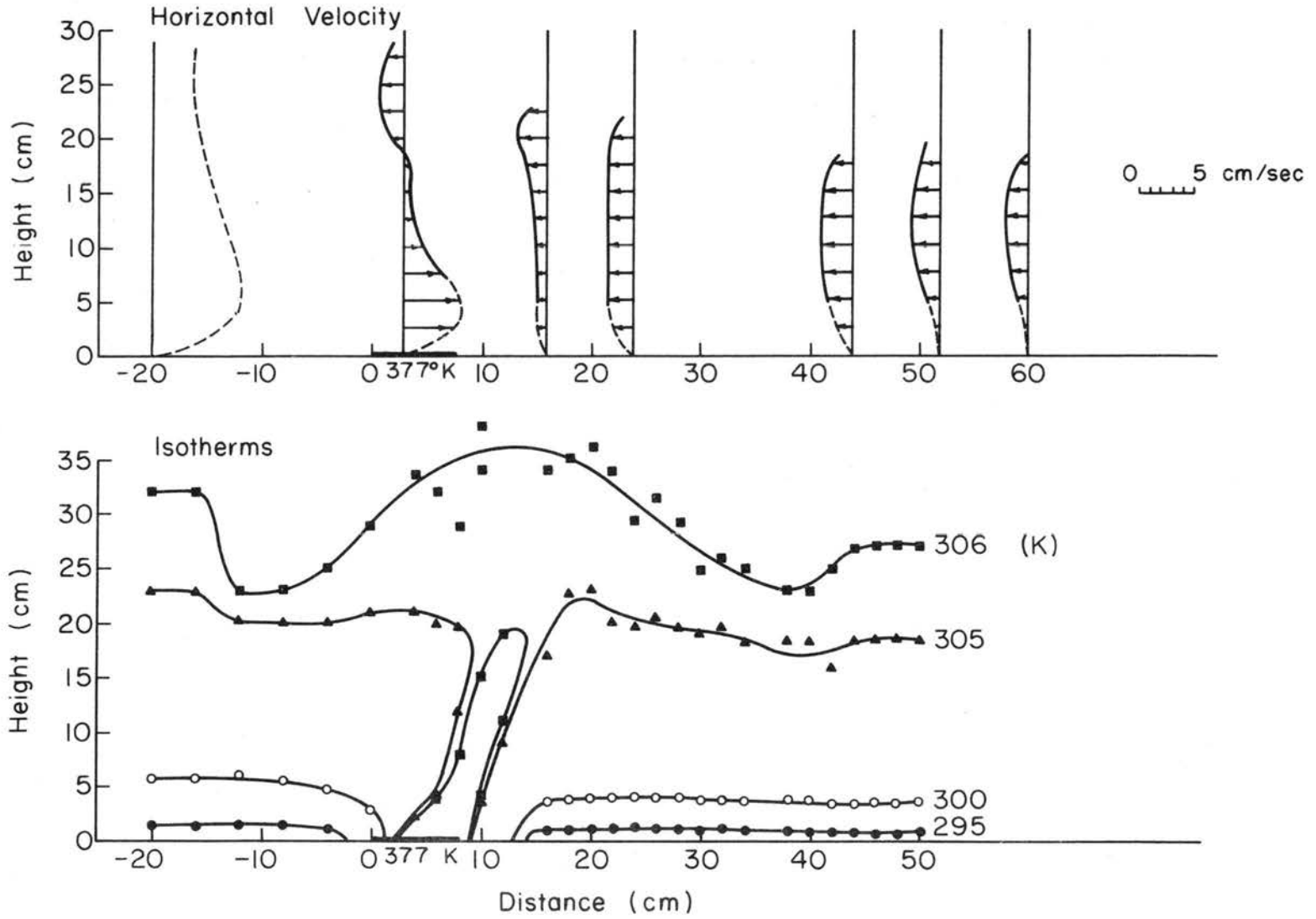

Fig. 5-17 Case B-2 (Experimental): Measured horizontal velocity profiles and isotherms when $(\overline{Fr})_H = 0.100$, and $N_h = 7.40$.

Stream Function

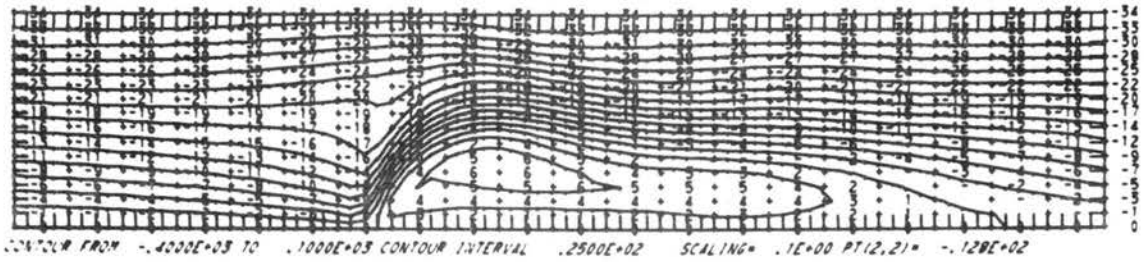

Vorticity

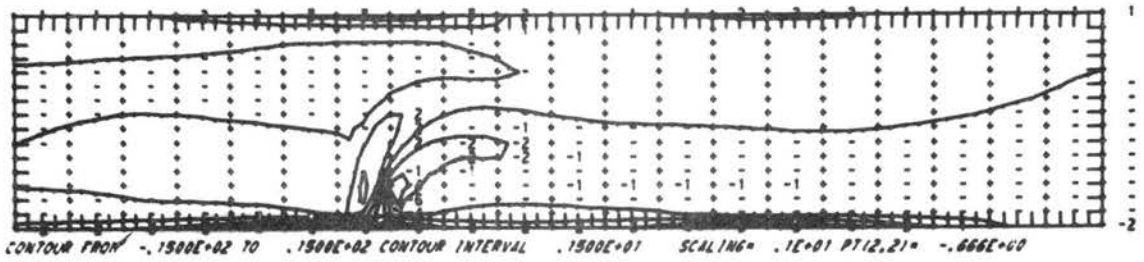

Temperature

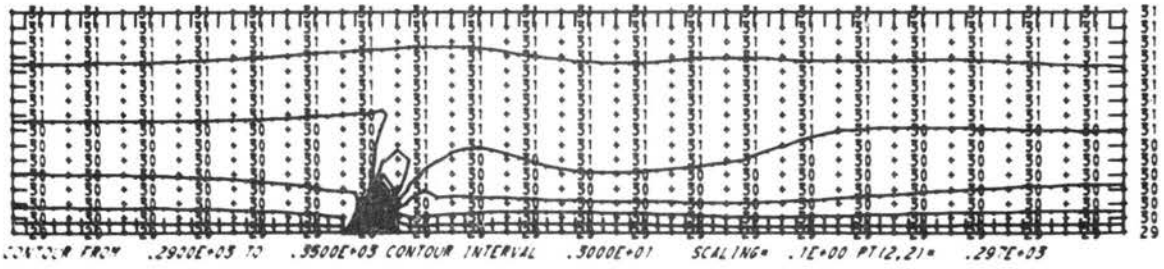

Fig. 5-18 Case B-2 (Numerical): Computed stream function, vorticity and temperature contour lines at t = 17.42sec under the same flow conditions in Fig. 5-17.

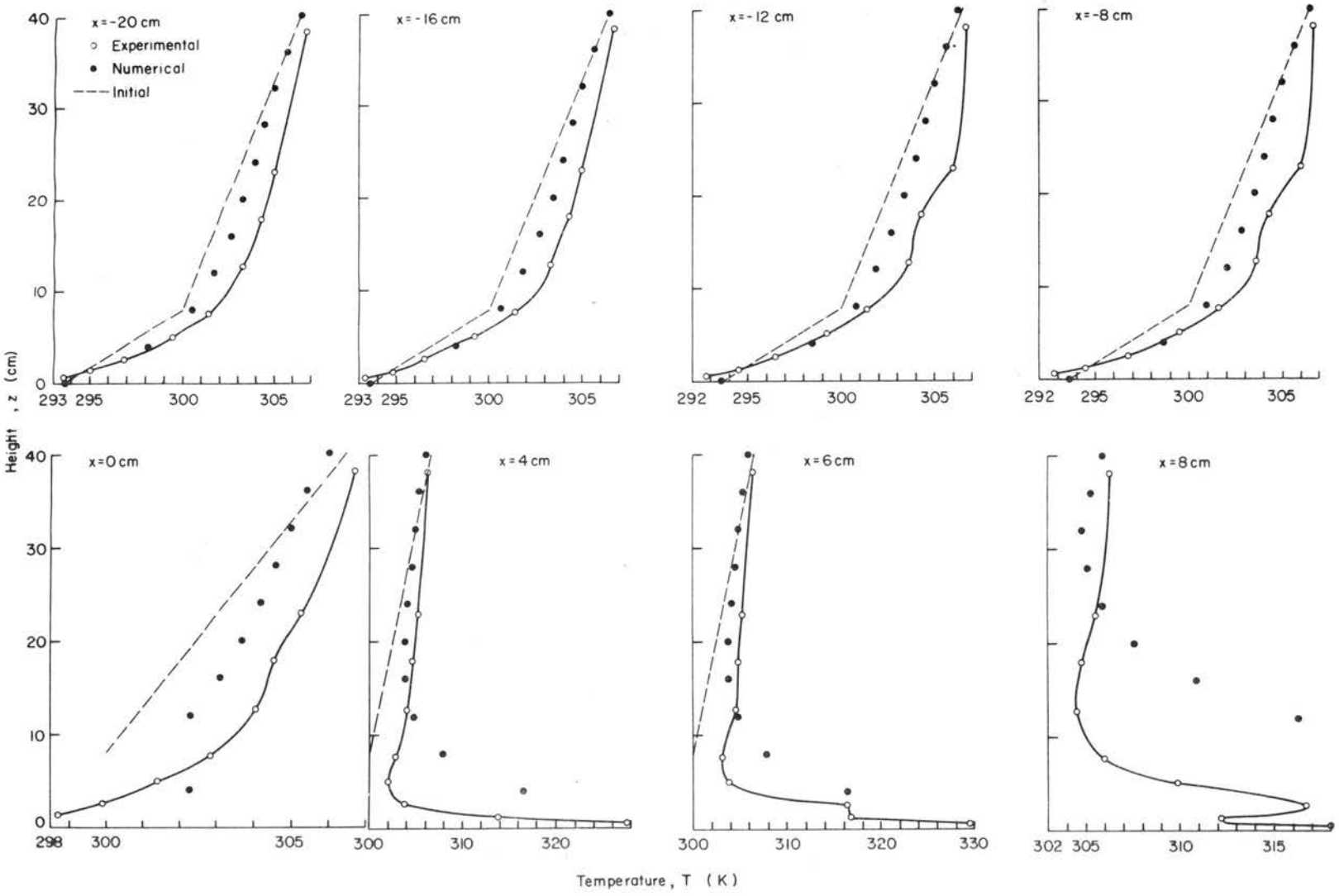

Fig. 5-19 Case B-2 (Experimental and Numerical): Comparison of experimental and numerical vertical temperature distributions at various locations.

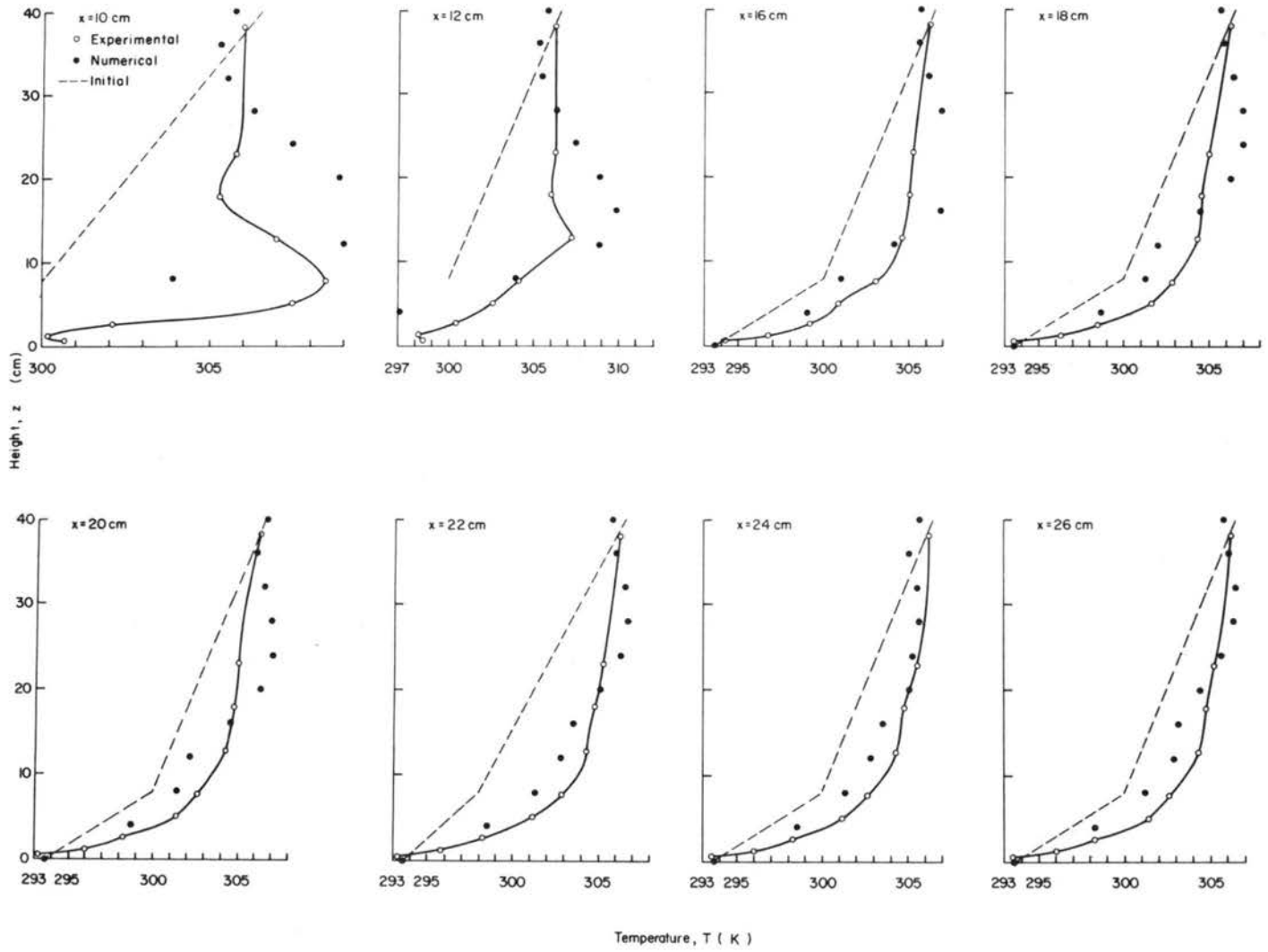

Fig. 5-19 (continued)

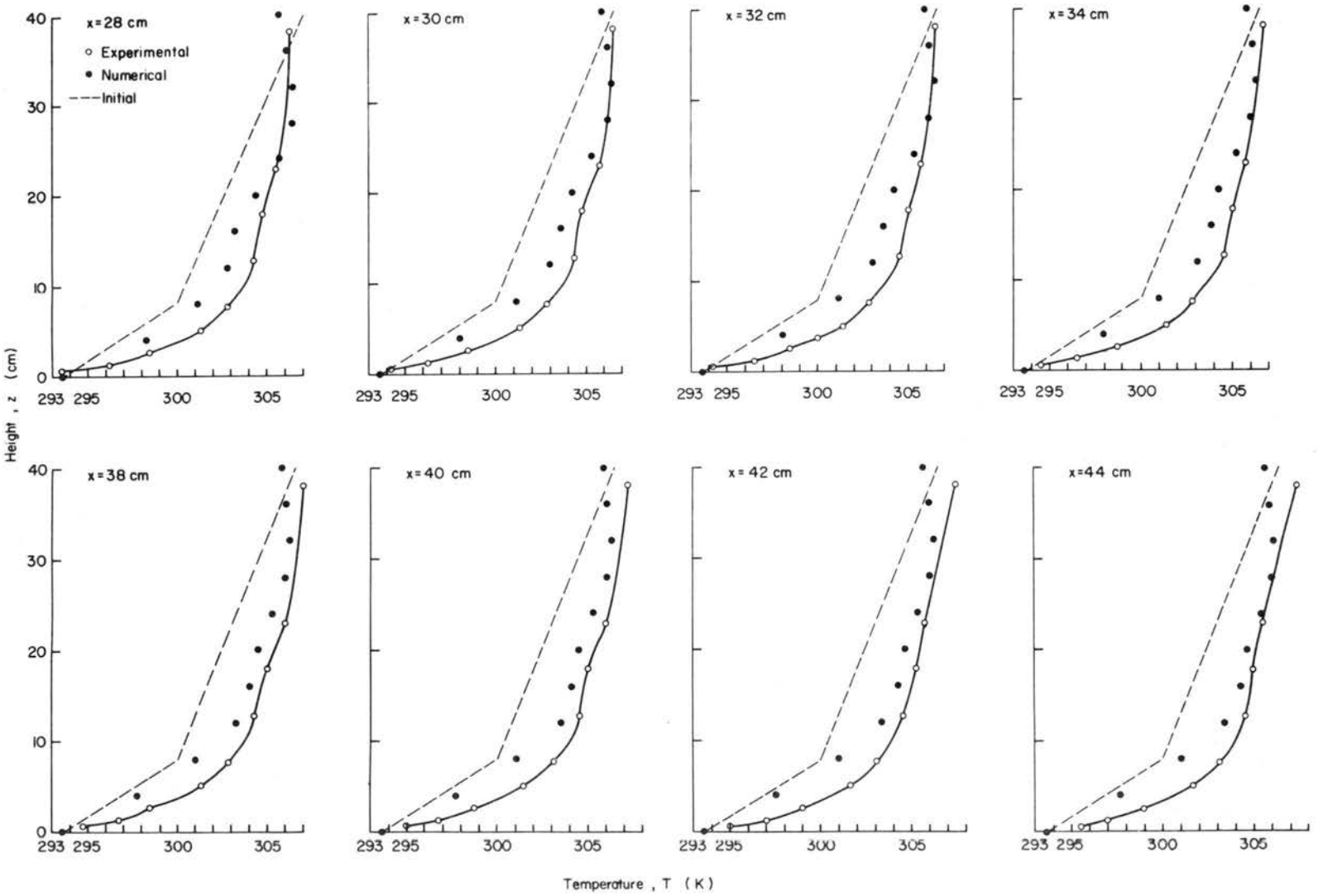

Fig. 5-19 (continued)

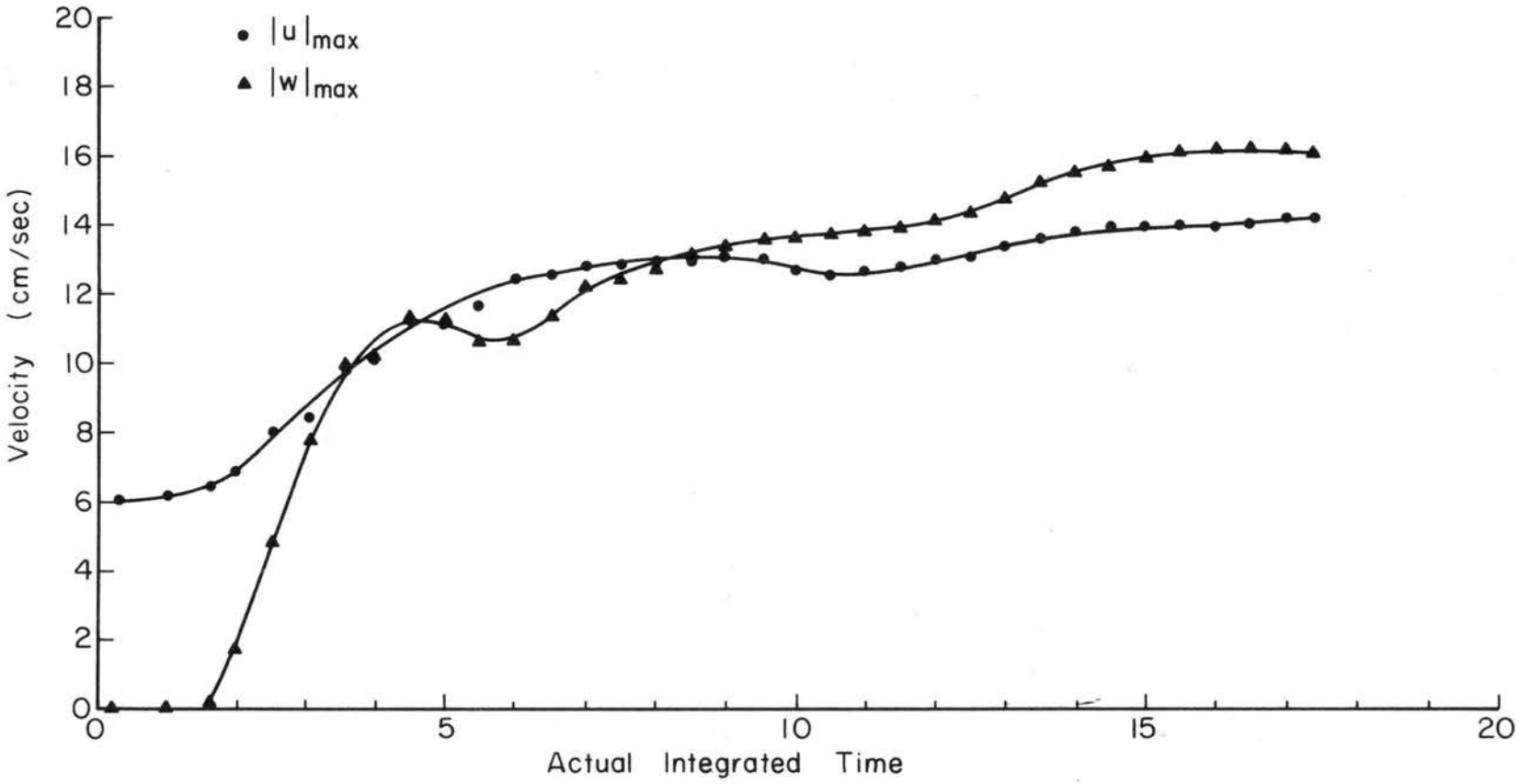

Fig. 5-20 Case B-2 (Numerical): Variation of $/u/_{max}$ and $/w/_{max}$ with integrated time in the computational region.

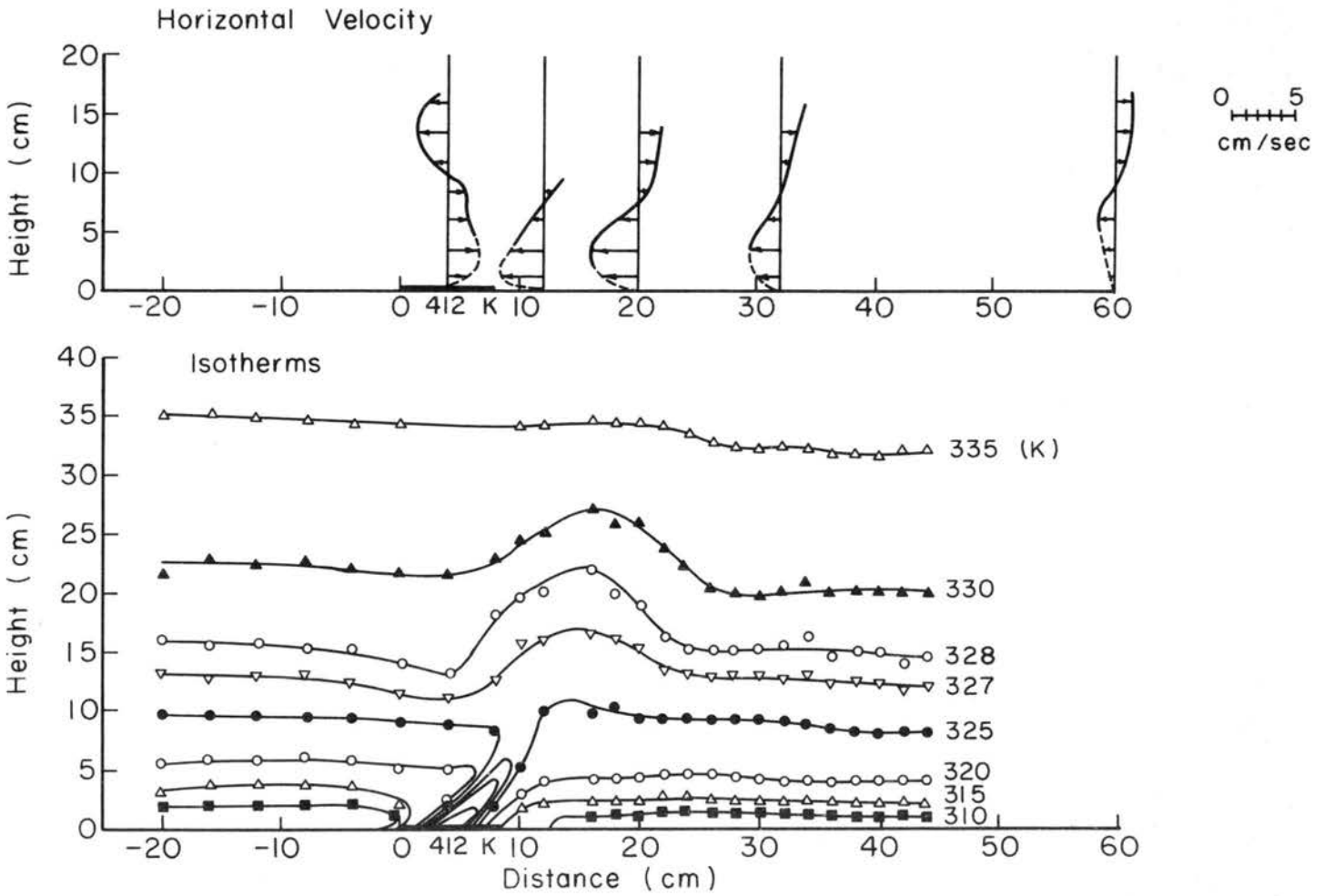

Fig. 5-21 Case B-3 (Experimental): Measured horizontal velocity profiles and isotherms when $(\overline{Fr})_H = 0.064$, and $N_h = 5.55$.

Stream Function

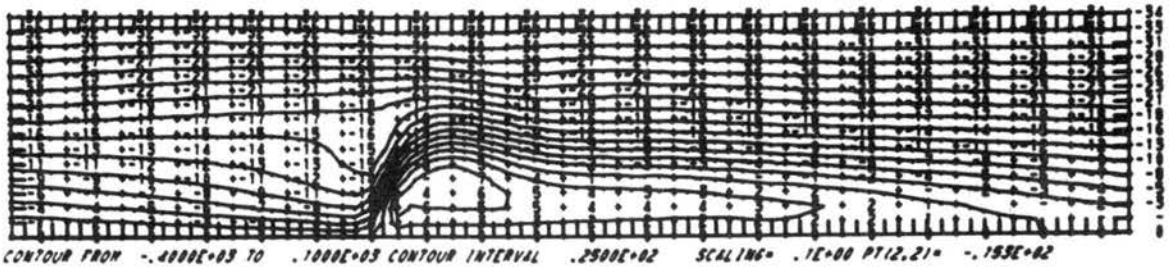

Vorticity

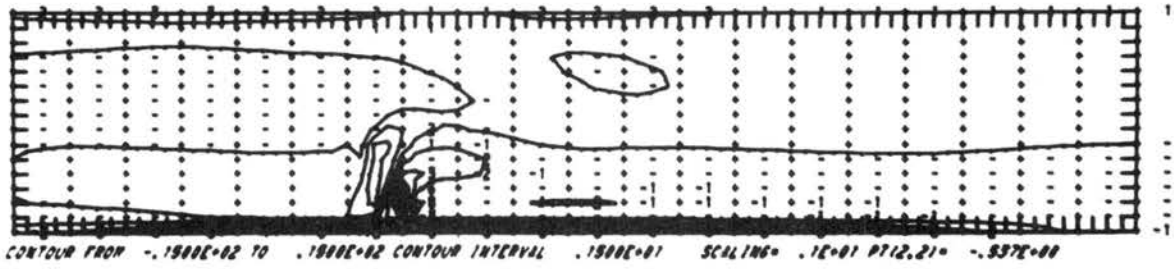

Temperature

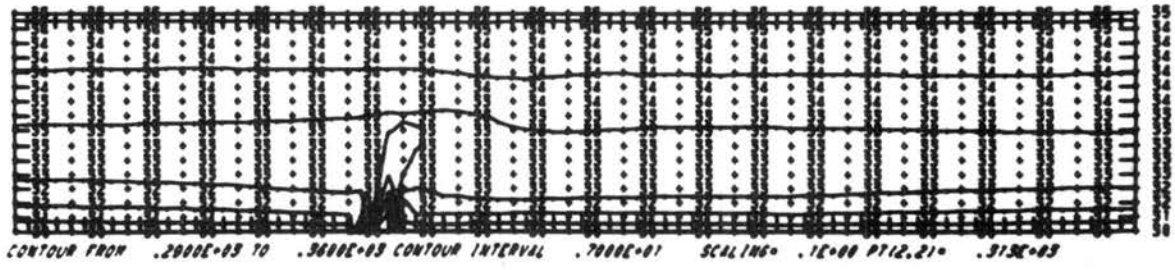

Fig. 5-22 Case B-3 (Numerical): Computed stream function, vorticity and temperature contour lines at t = 16.94 sec under the same flow condition in Fig. 5-21.

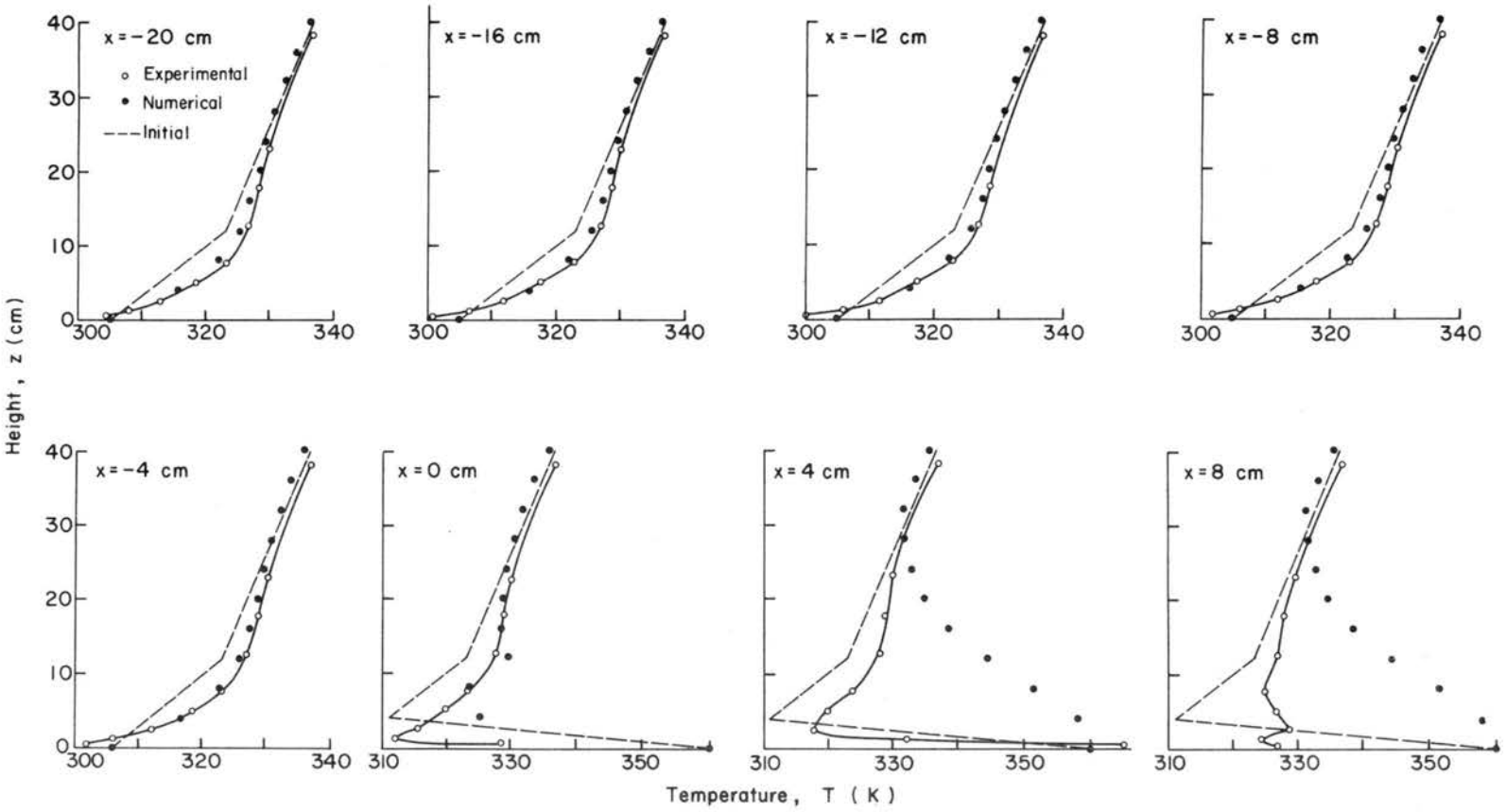

Fig. 5-23 Case B-3 (Experimental and Numerical): Comparison of experimental and numerical vertical temperature distributions at various locations.

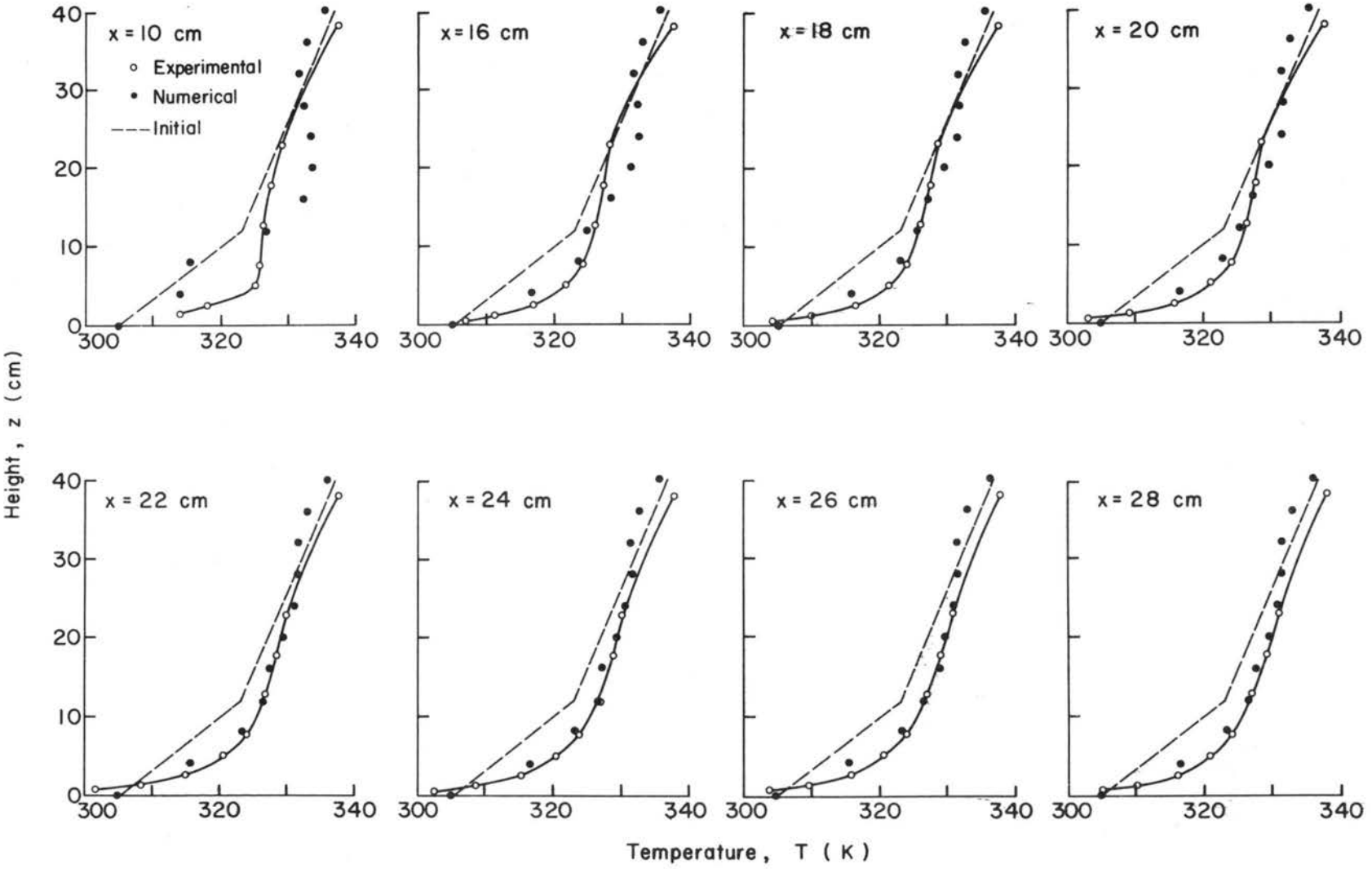

Fig. 5-23 (continued)

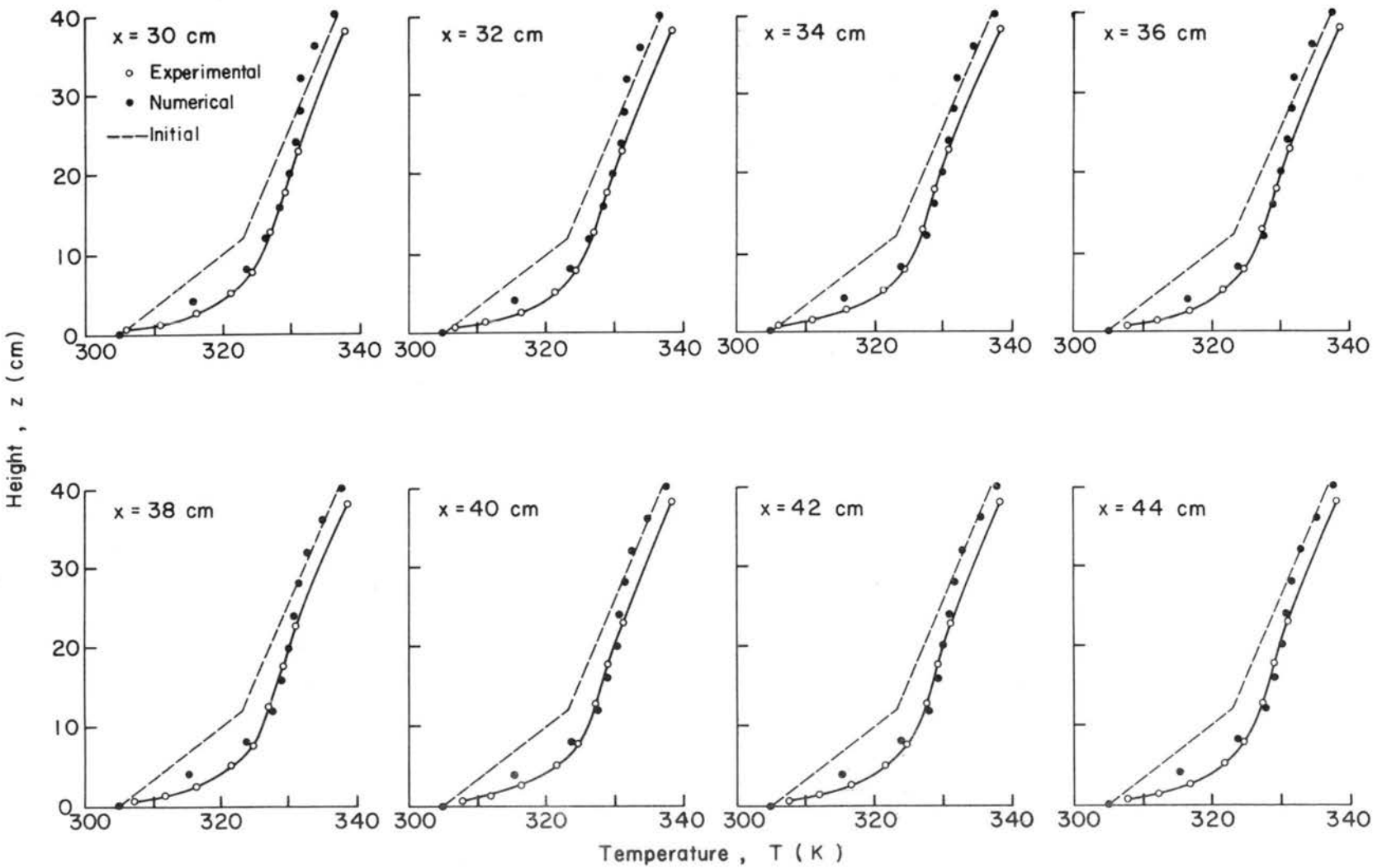

Fig. 5-23 (continued)

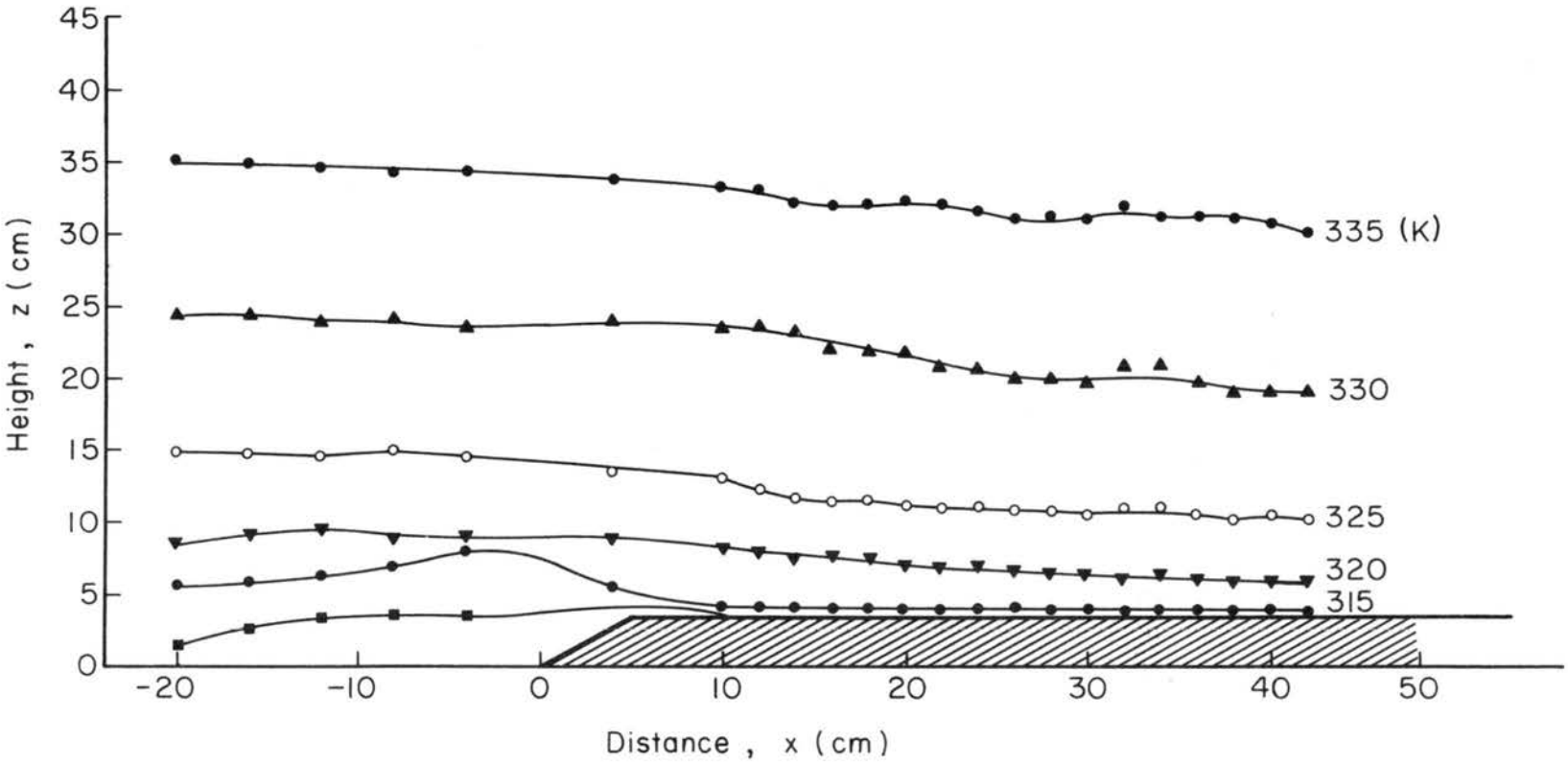

Fig. 5-24 The first application of Case B-3 (Experimental): Measured isotherms over the equivalent mountain given by the flow conditions in Case B-3.

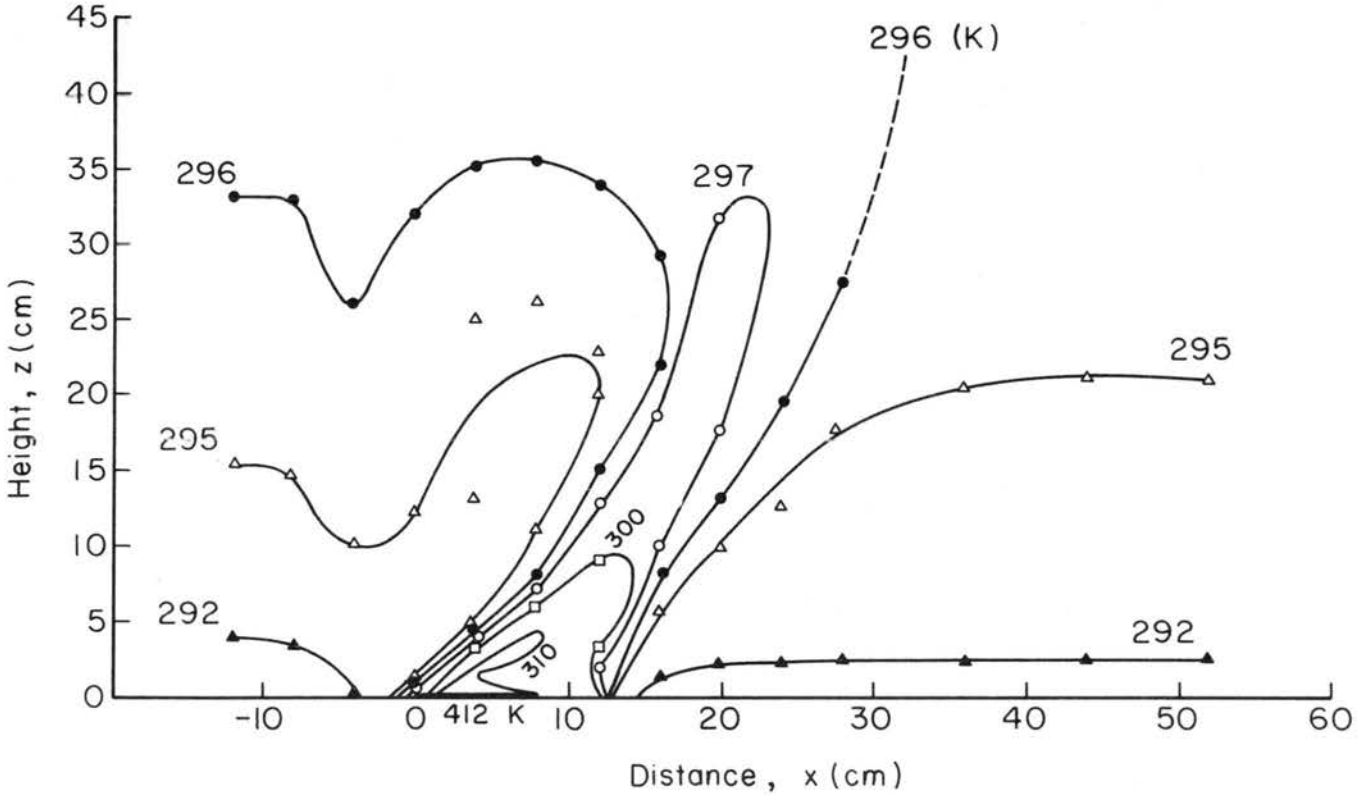

Fig. 5-25 The second application of Case B-3 (Experimental): Measured isotherms in Case B-3 in a neutral stratification.

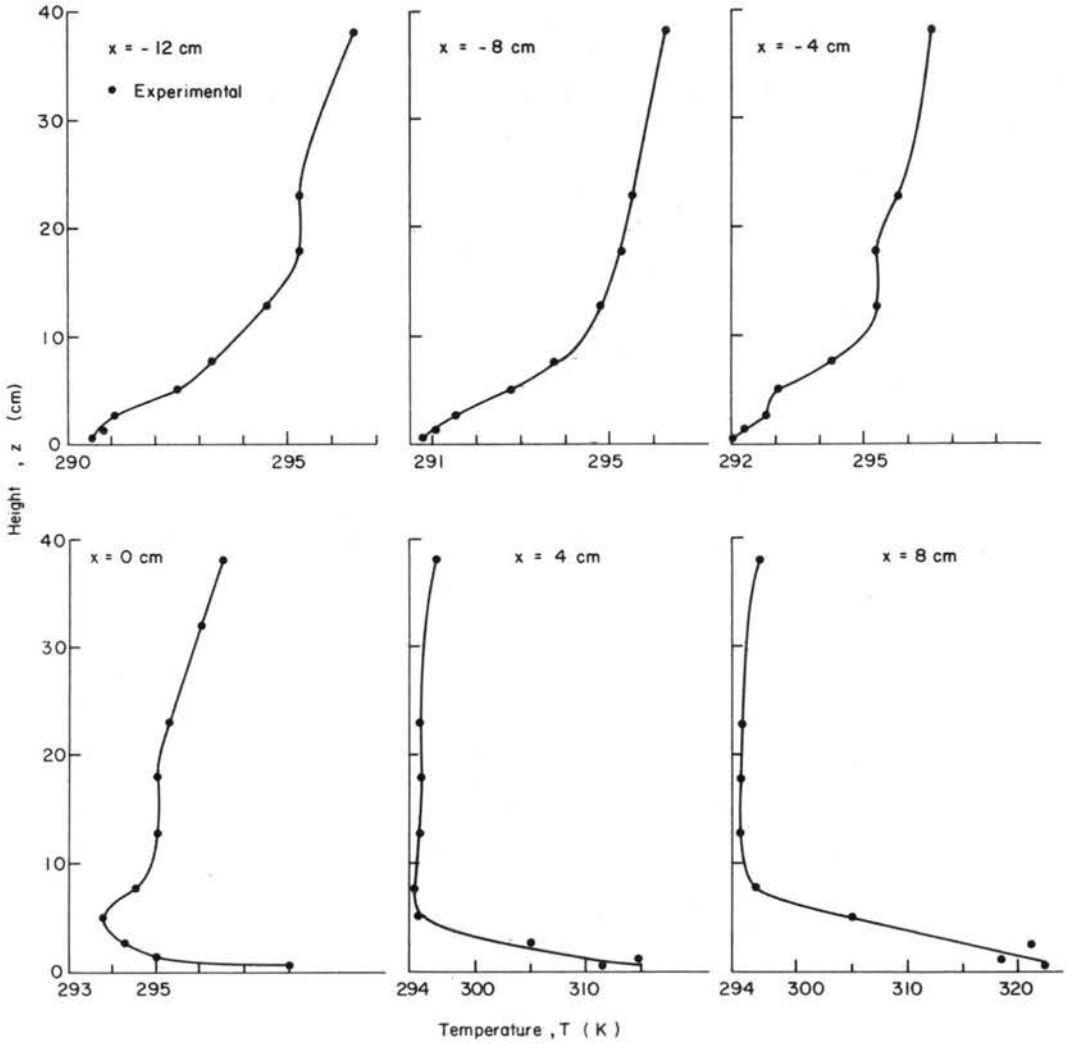

Fig. 5-26 The second application of Case B-3 (Experimental): Measured vertical temperature distributions of Case B-3 in a neutral stratification.

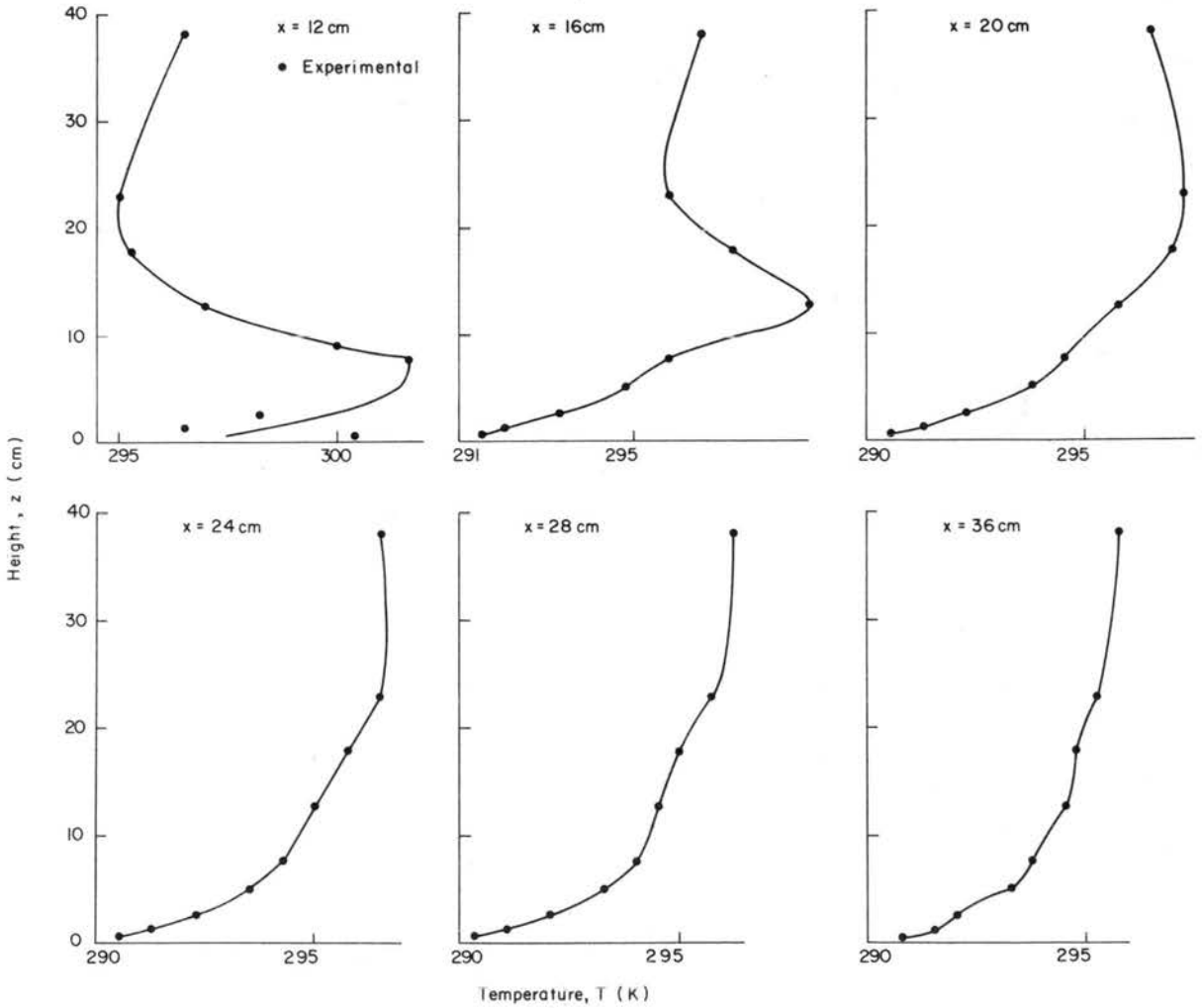

Fig. 5-26 (continued)

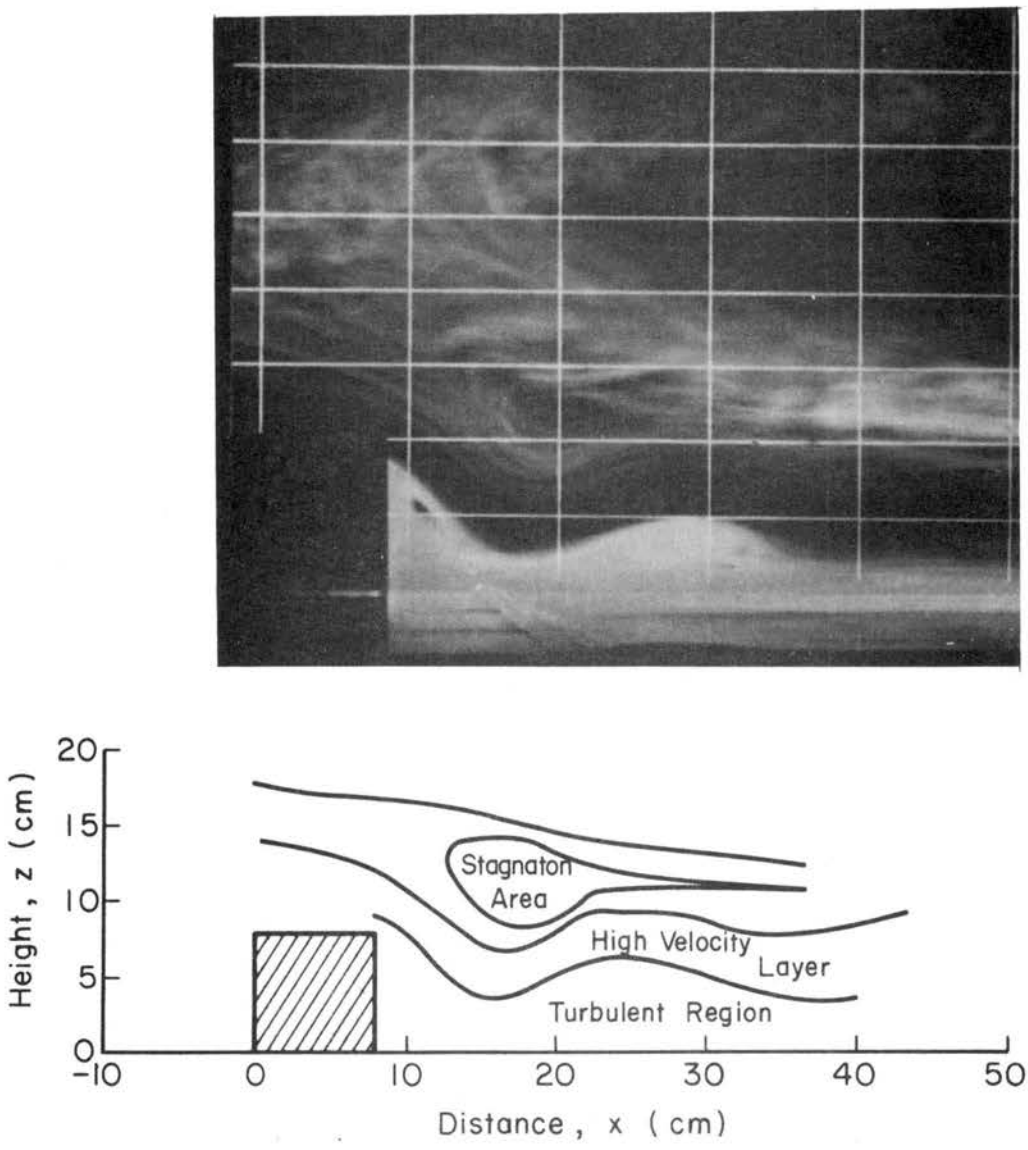

Fig. 5-27 Case C-1 (Experimental): A flow visualization by Ti Cl_4 smoke when the obstacle was not heated. $(\overline{Fr})_H = 0.100$.

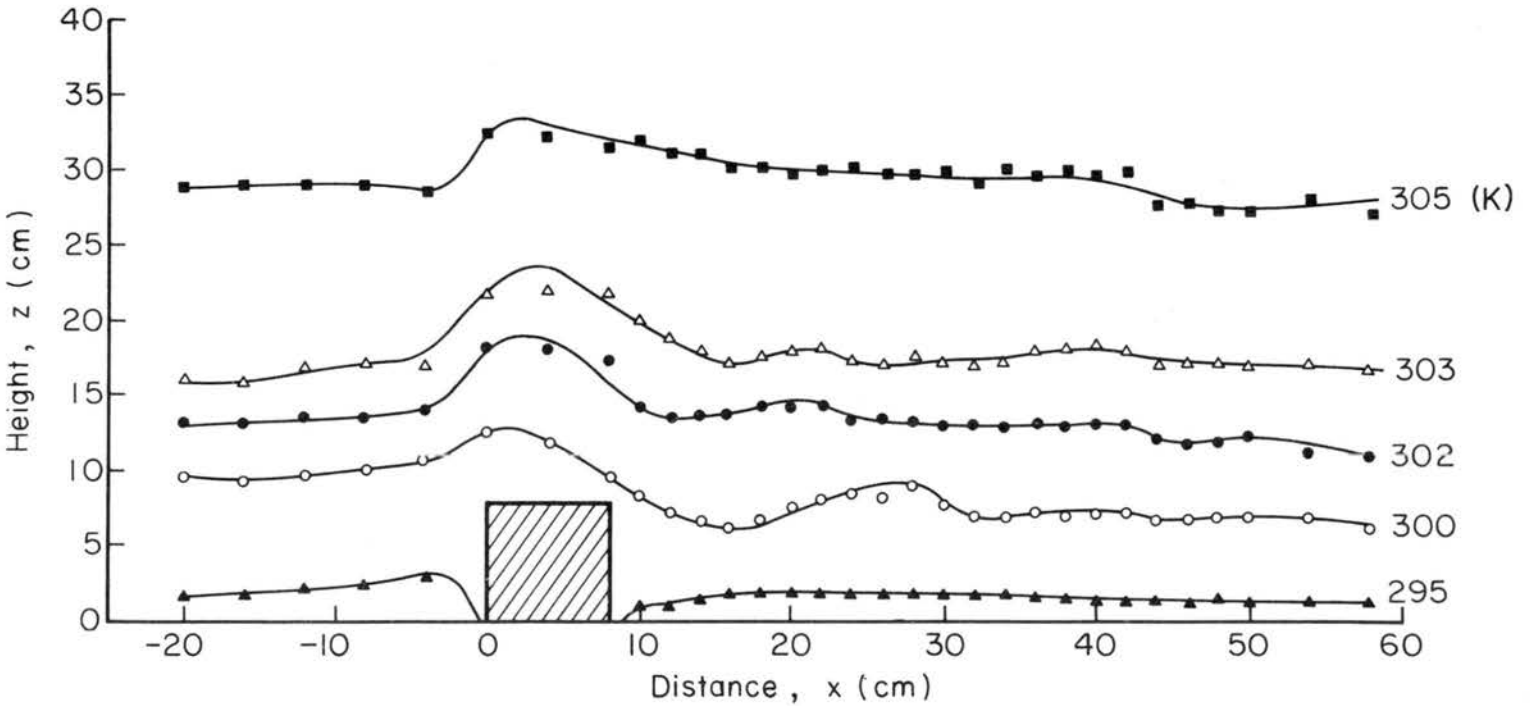

Fig. 5-28 Case C-1 (Experimental): Isotherms under the same flow conditions in Fig. 5-27.

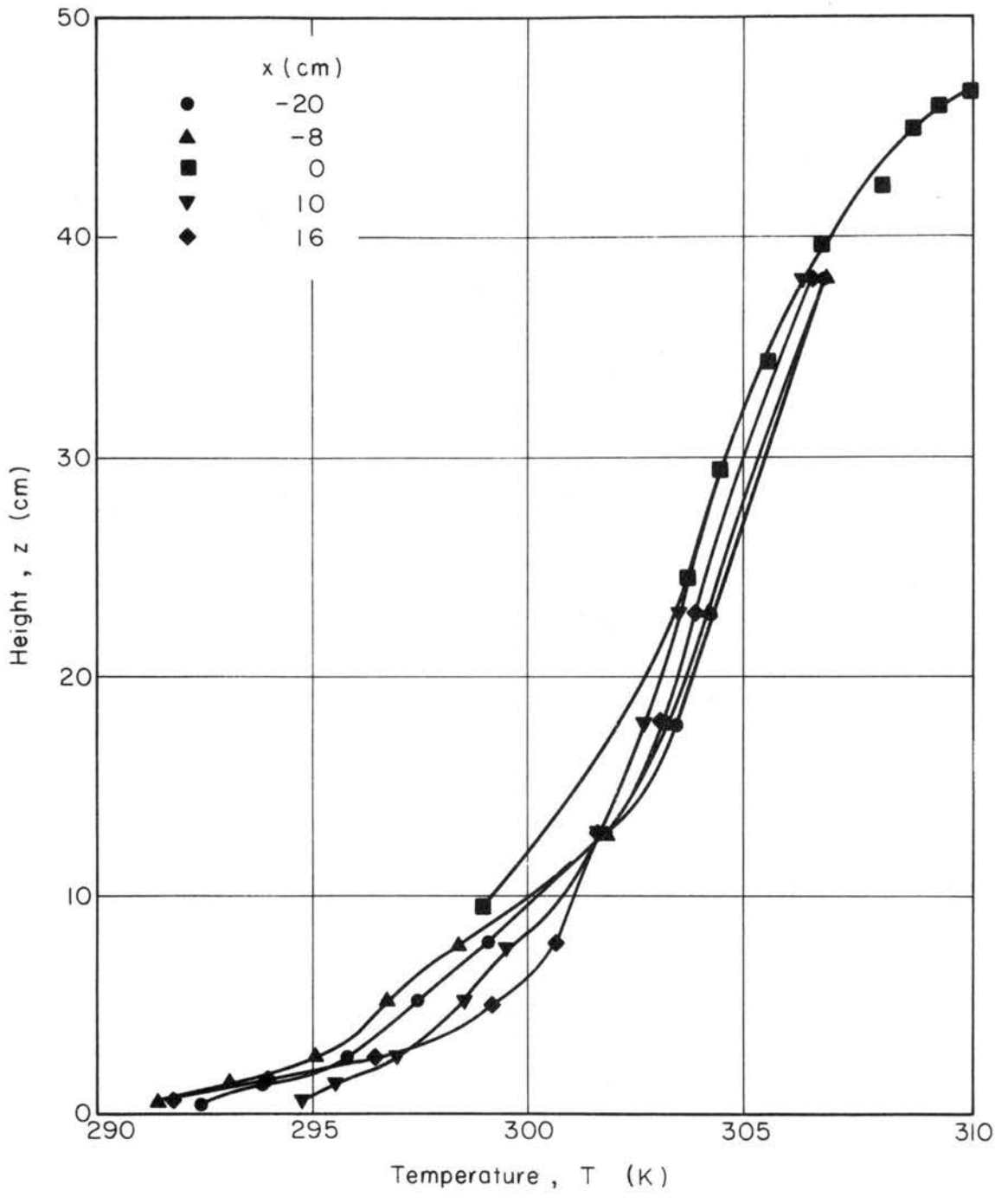

Fig. 5-29 Case C-1 (Experimental): Vertical temperature distributions under the same condition in the previous figures.

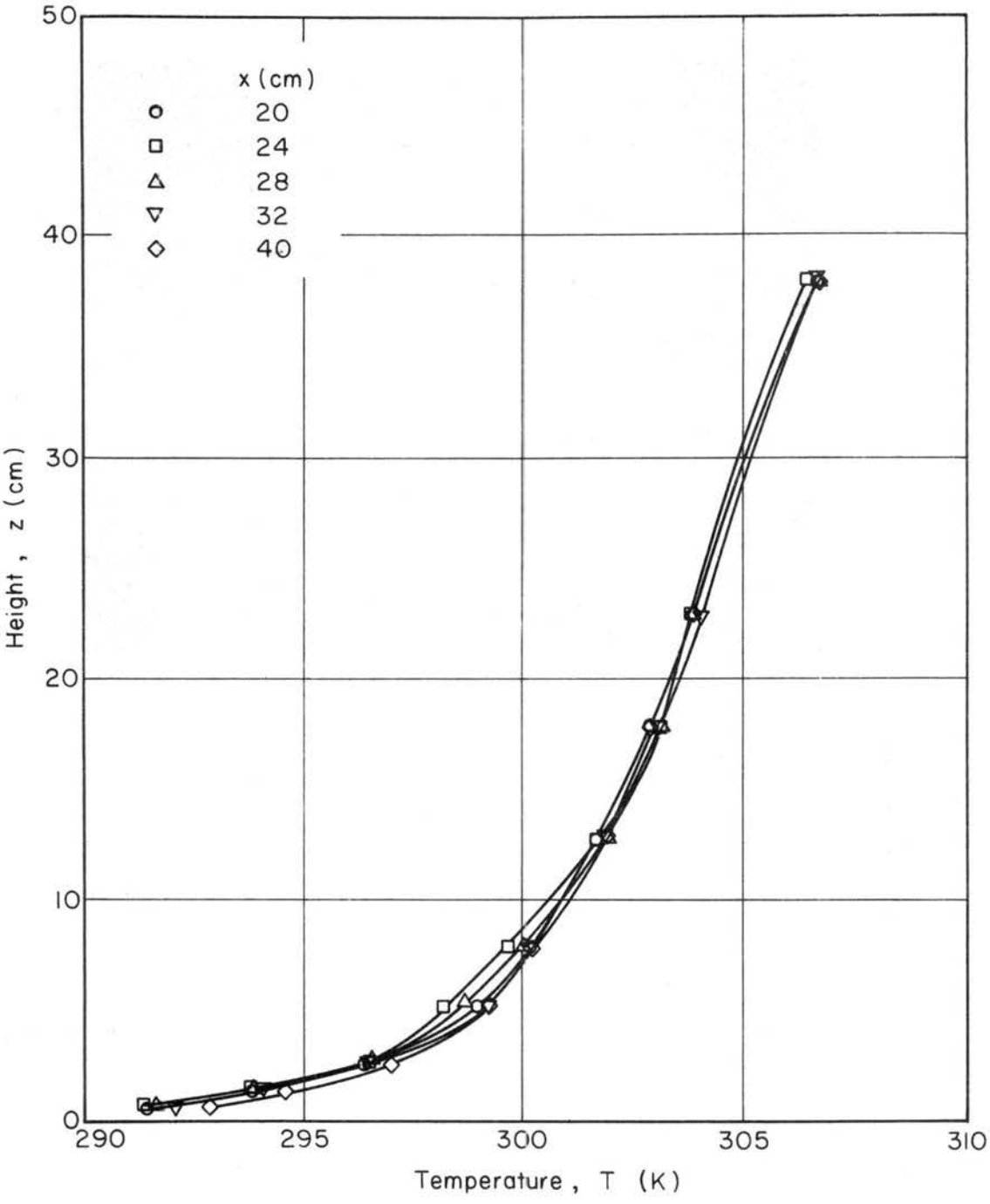

Fig. 5-29 (continued) Case C-1 (Experimental): Vertical temperature distributions under the same condition in the previous figures.

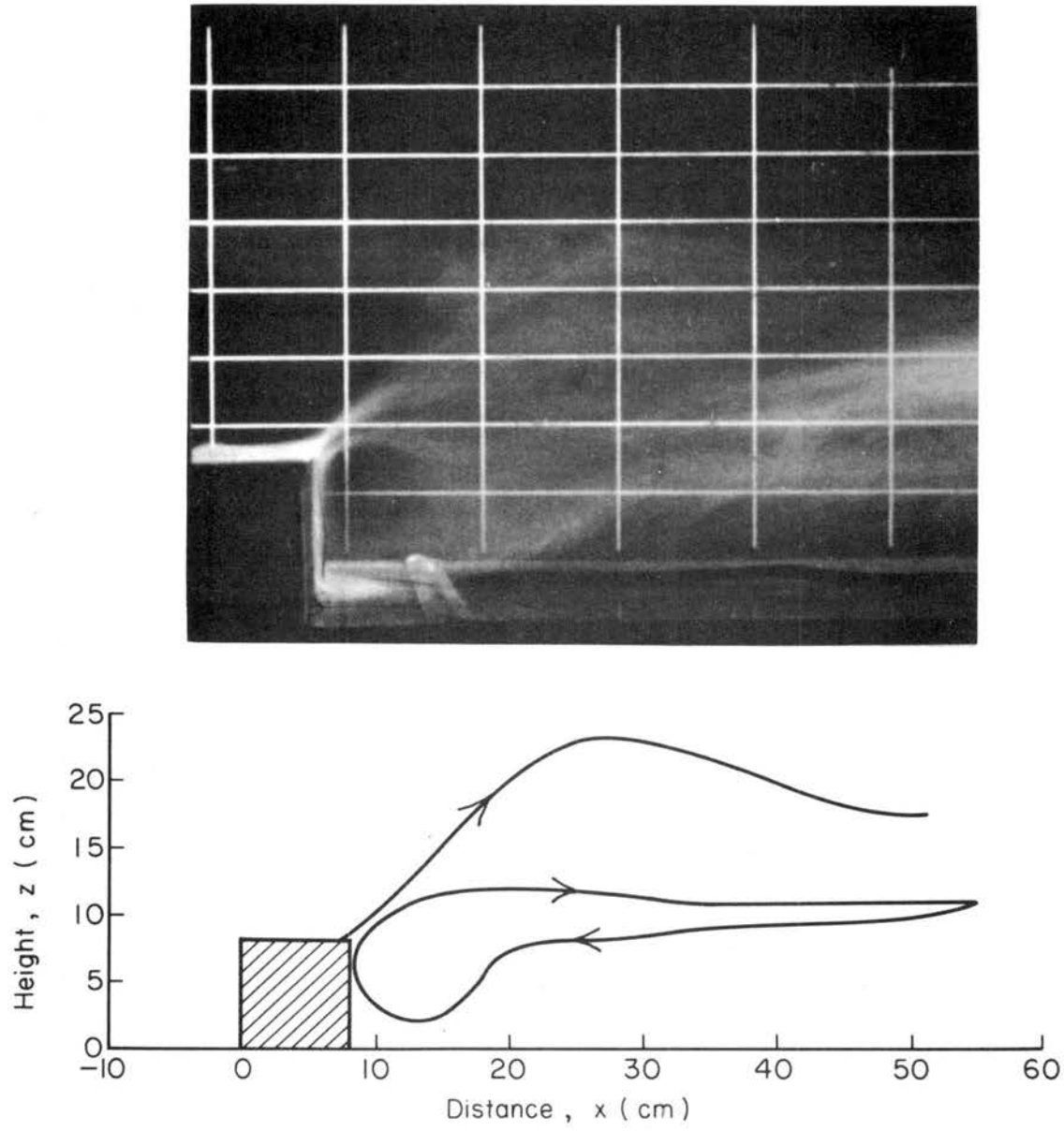

Fig. 5-30 Case C-1 (Experimental): A flow visualization by $TiCl_4$ smoke when the obstacle was heated at 310°K while floor temperature was 290°K. $(\overline{Fr})_H = 0.100$.

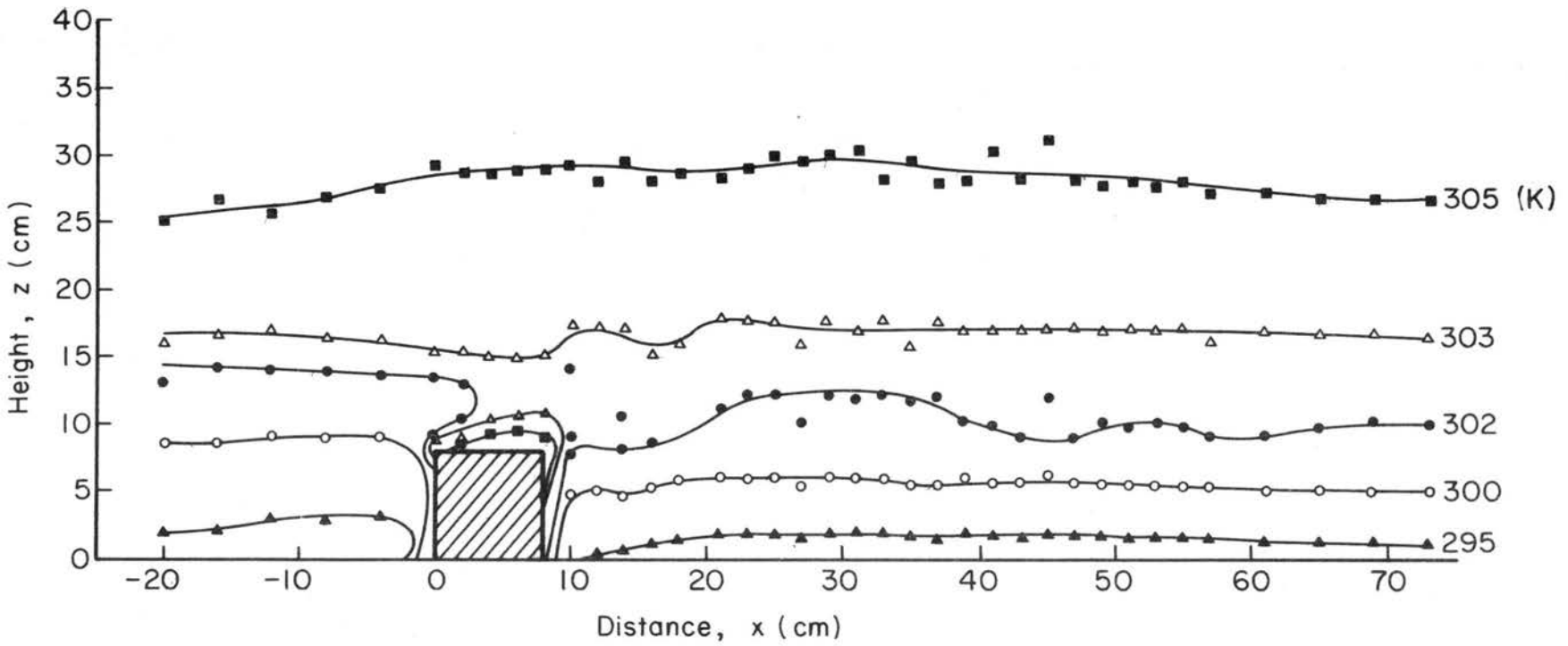

Fig. 5-31 Case C-1 (Experimental): Isotherms under the same flow conditions in Fig. 5-30.

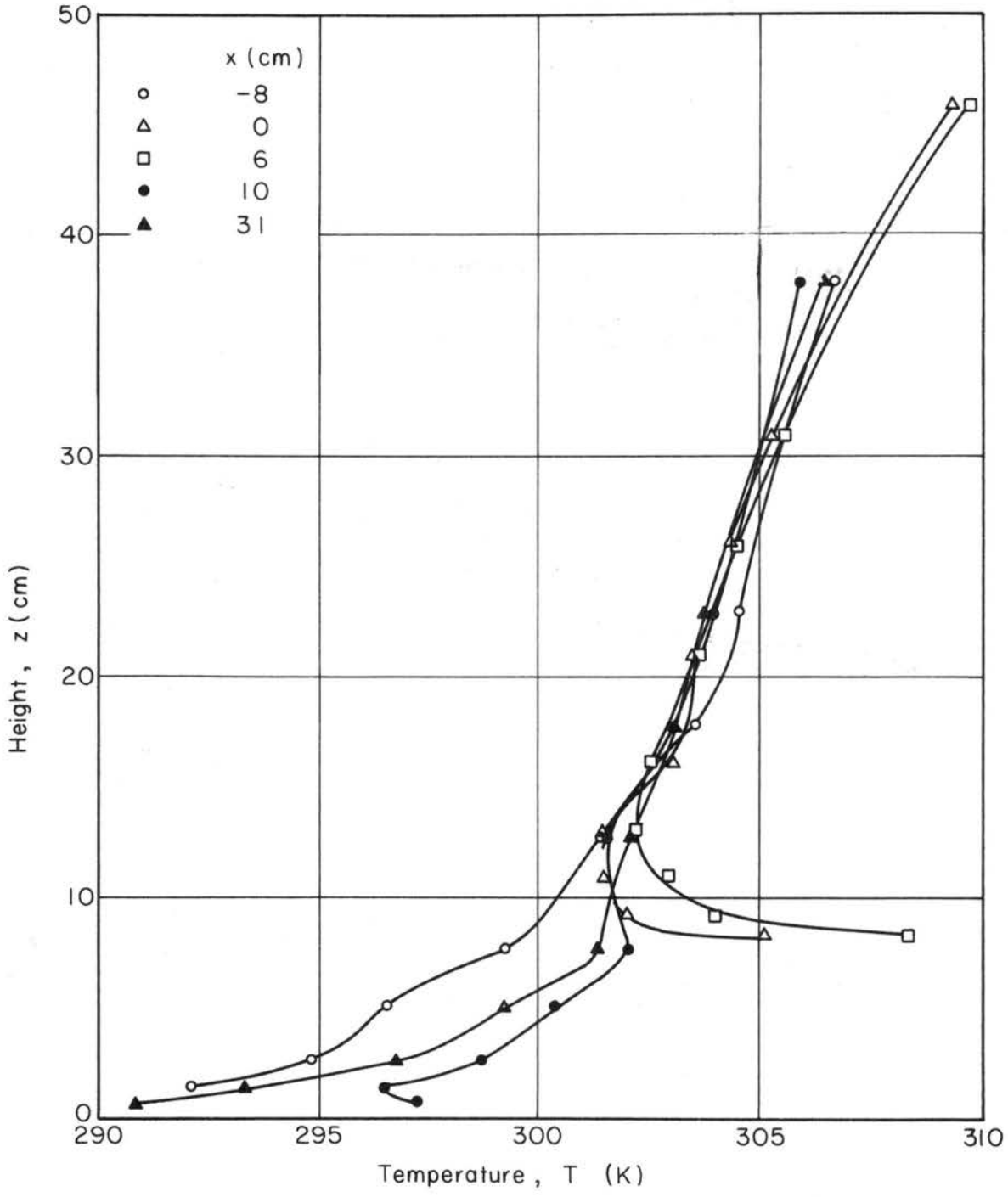

Fig. 5-32 Case C-1 (Experimental): Vertical Temperature distributions under the same flow situations in the previous figures.

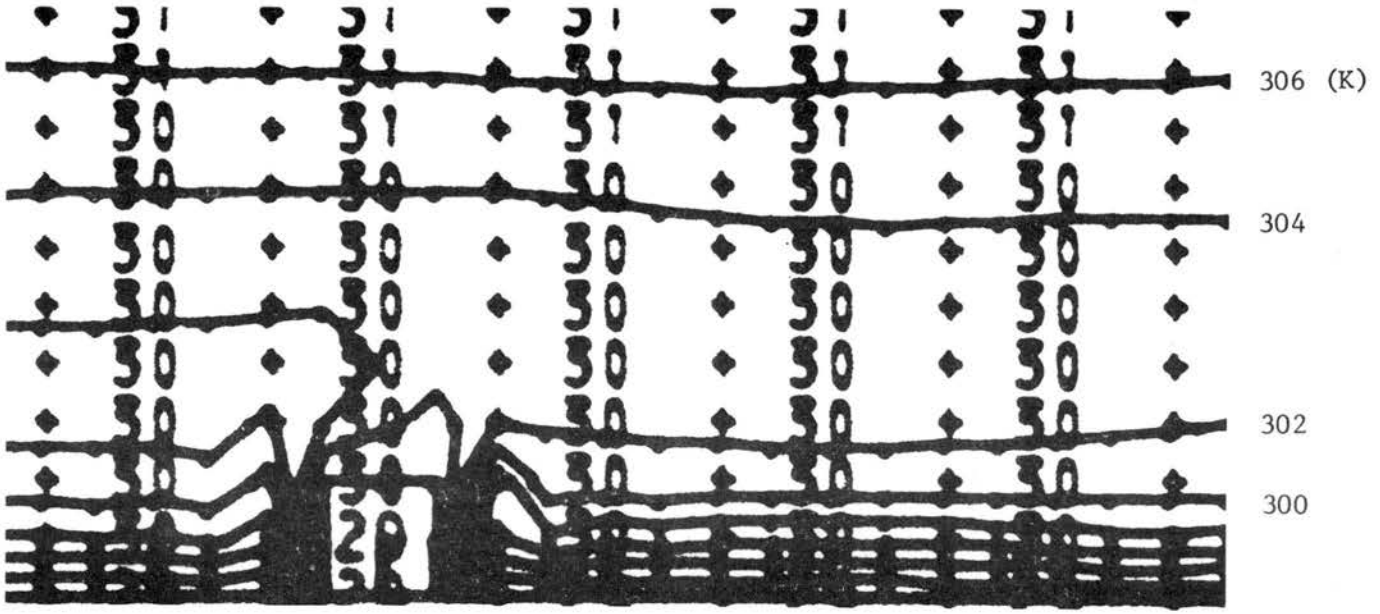

Fig. 5-33 Case C-1 (Numerical): Isotherms computed numerically under the same flow situations of the experiment.

Stream Function

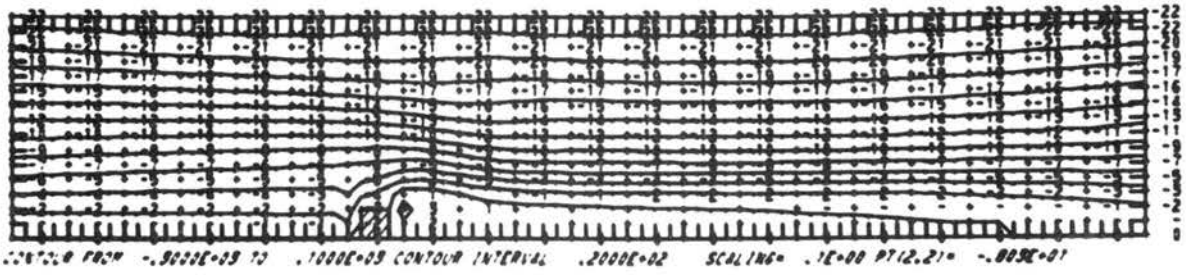

Vorticity

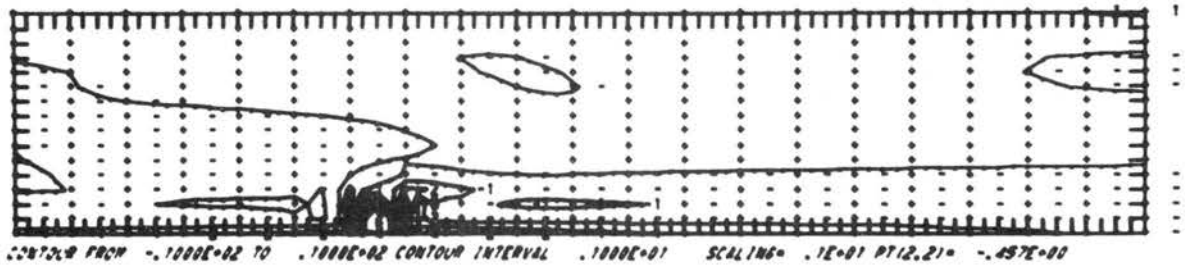

Horizontal Velocity u

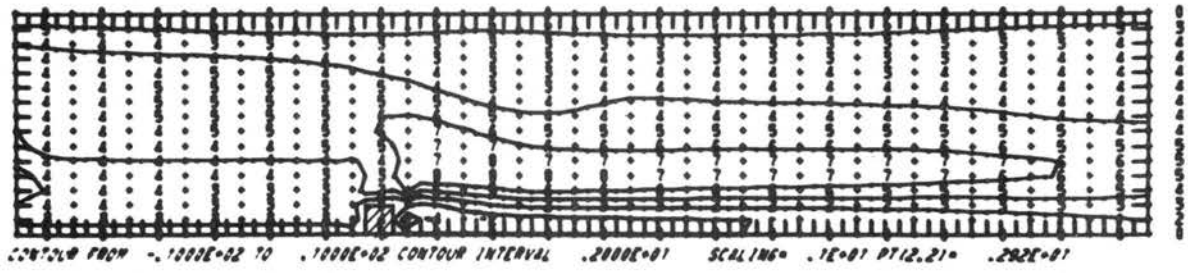

Vertical Velocity w

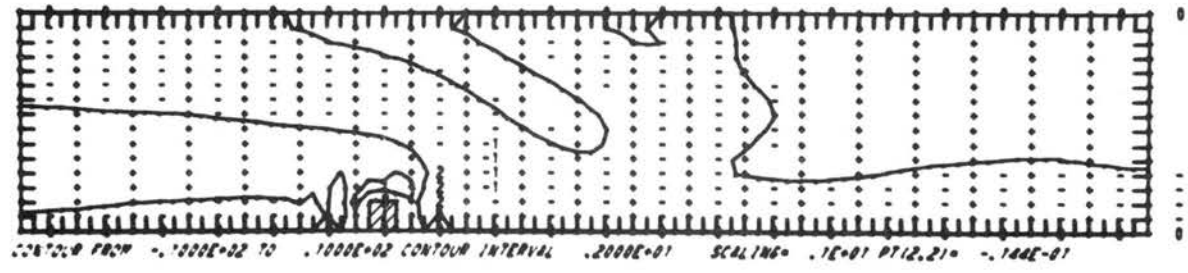

Fig. 5-34 Case C-1 (Numerical): Computed stream function vorticity, and velocity components u and w at t = 27.84 sec.

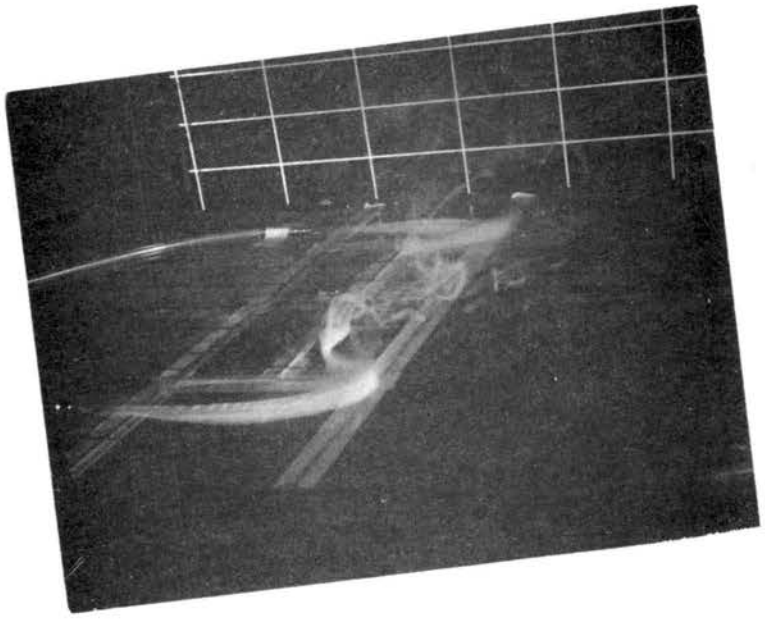

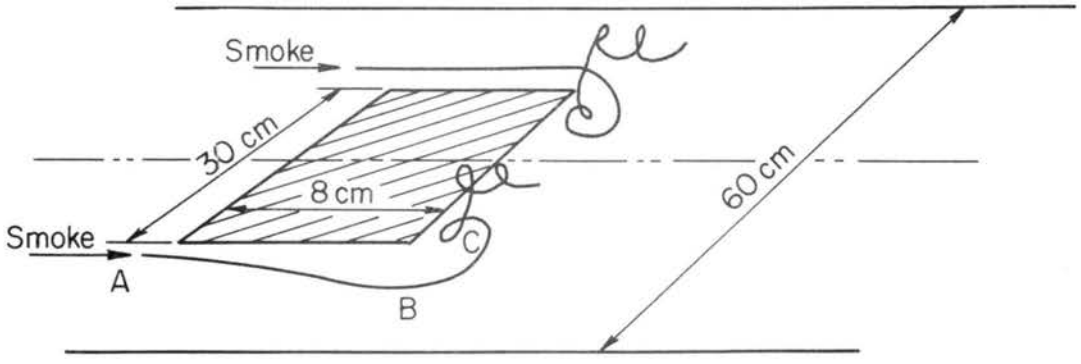

Fig. 5-35 Airflow over a rectangular heated island: $(\overline{Fr})_H = 0.100$, $N_h = 10.08$. The heated ares is 30 x 8 cm rectangular.

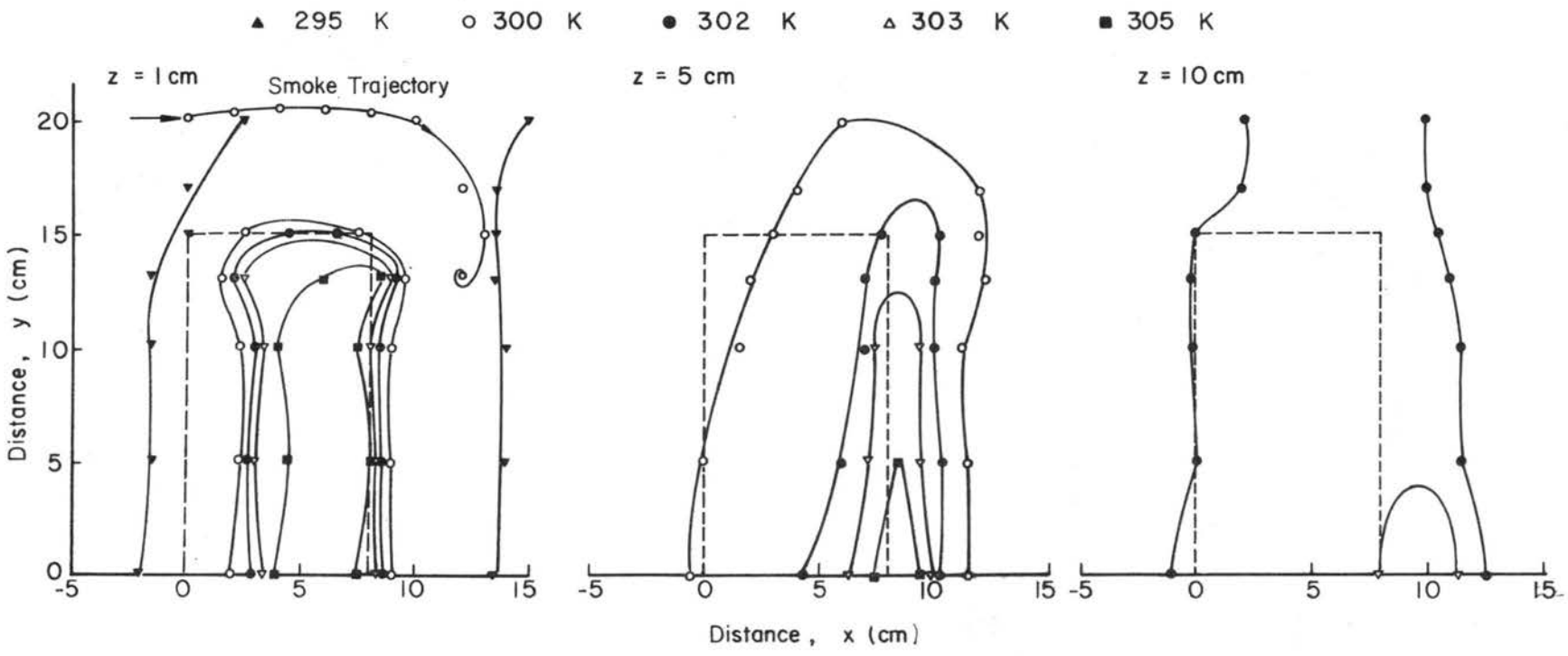

Fig. 5-36 Isotherms in the horizontal planes in the flow described in Fig. 5-35. A heated area is shown by a dashed line.

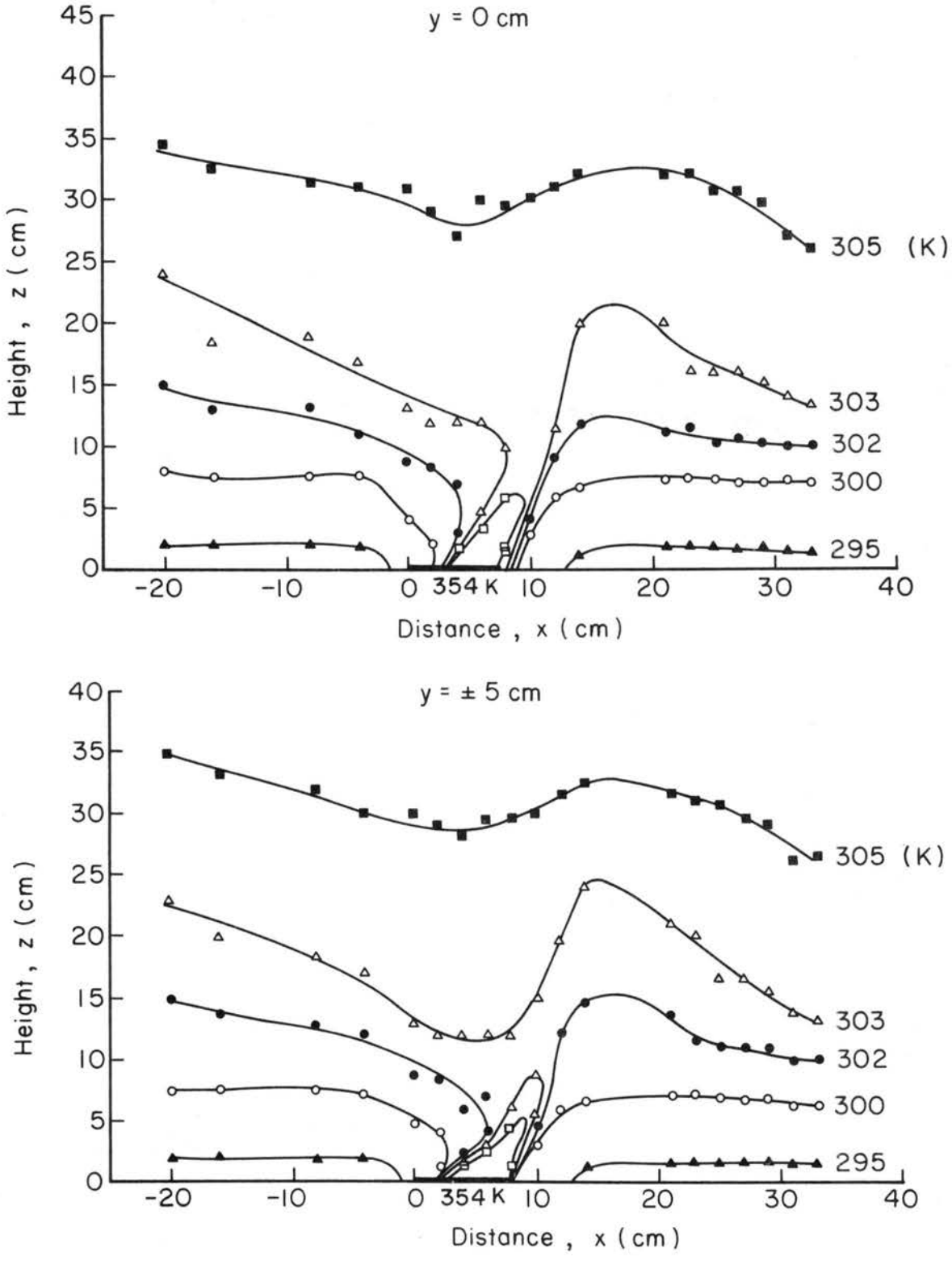

Fig. 5-37 Isotherms in the vertical planes parallel to the flow direction. Flow situation is the same as in Fig. 5-35.

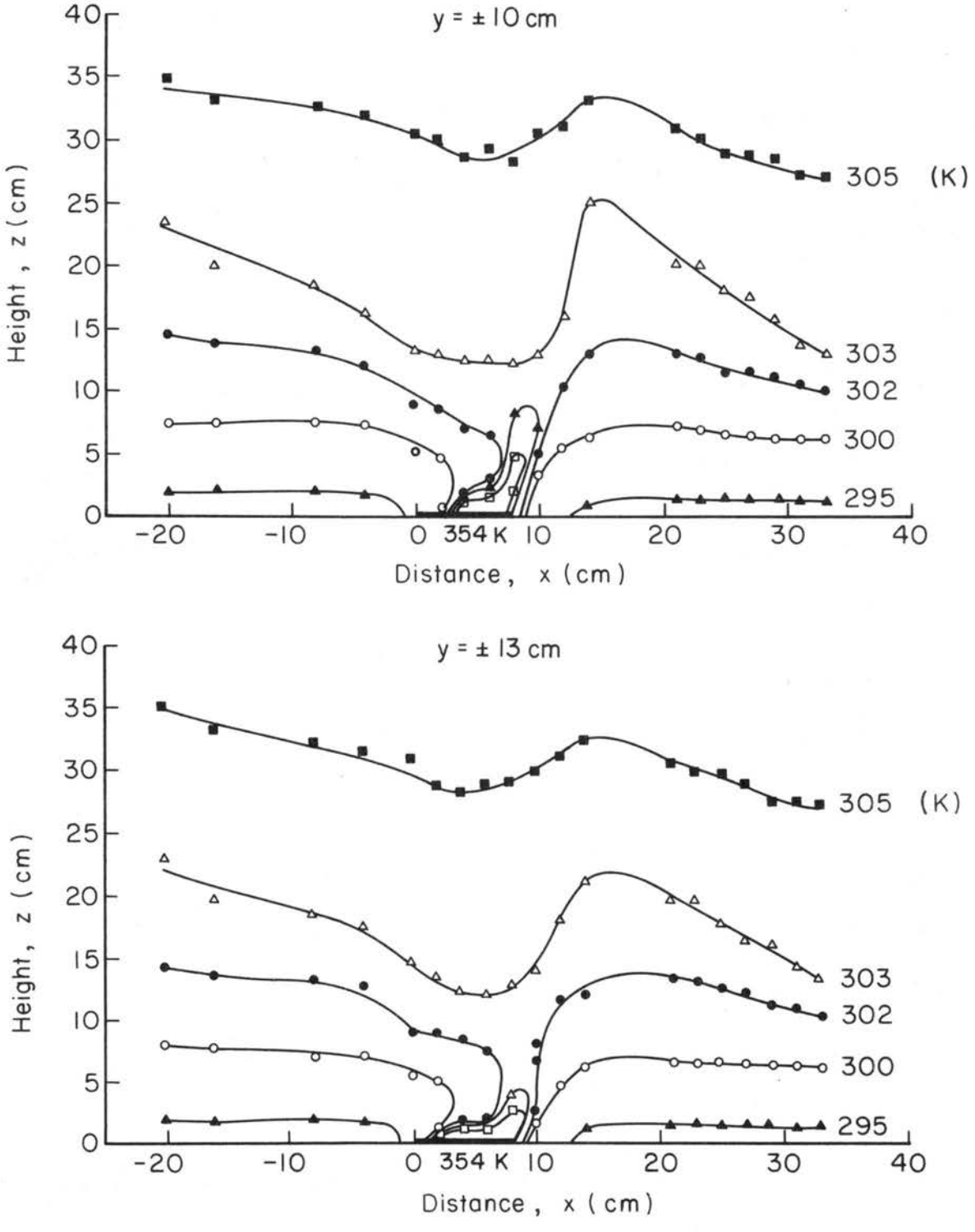

Fig. 5-37 (continued) Isotherms in the vertical planes parallel to the flow direction. Flow situation is the same as in Fig. 5-35.

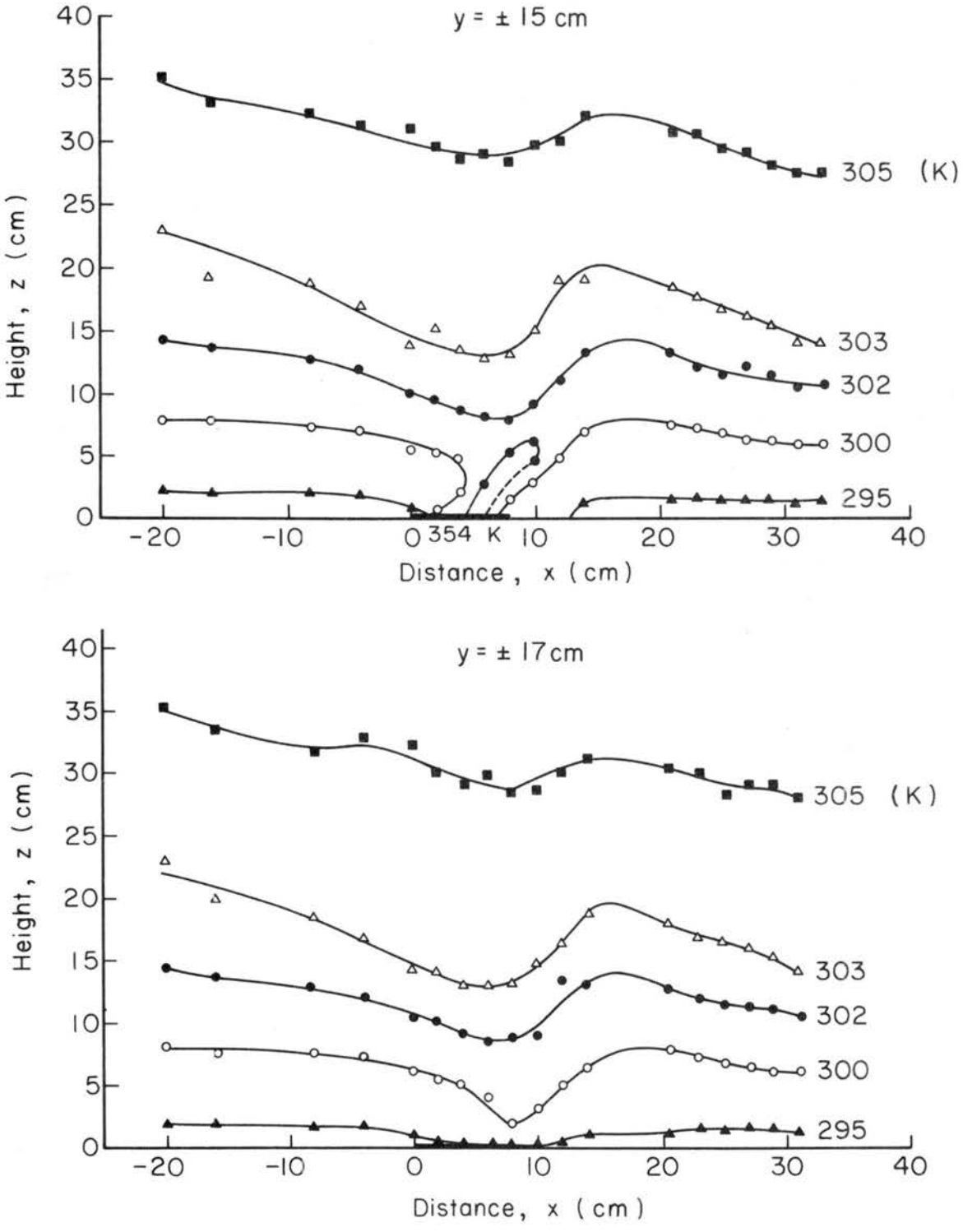

Fig. 5-37 (continued) Isotherms in the vertical planes parallel to the flow direction. Flow situation is the same as in Fig. 5-35.

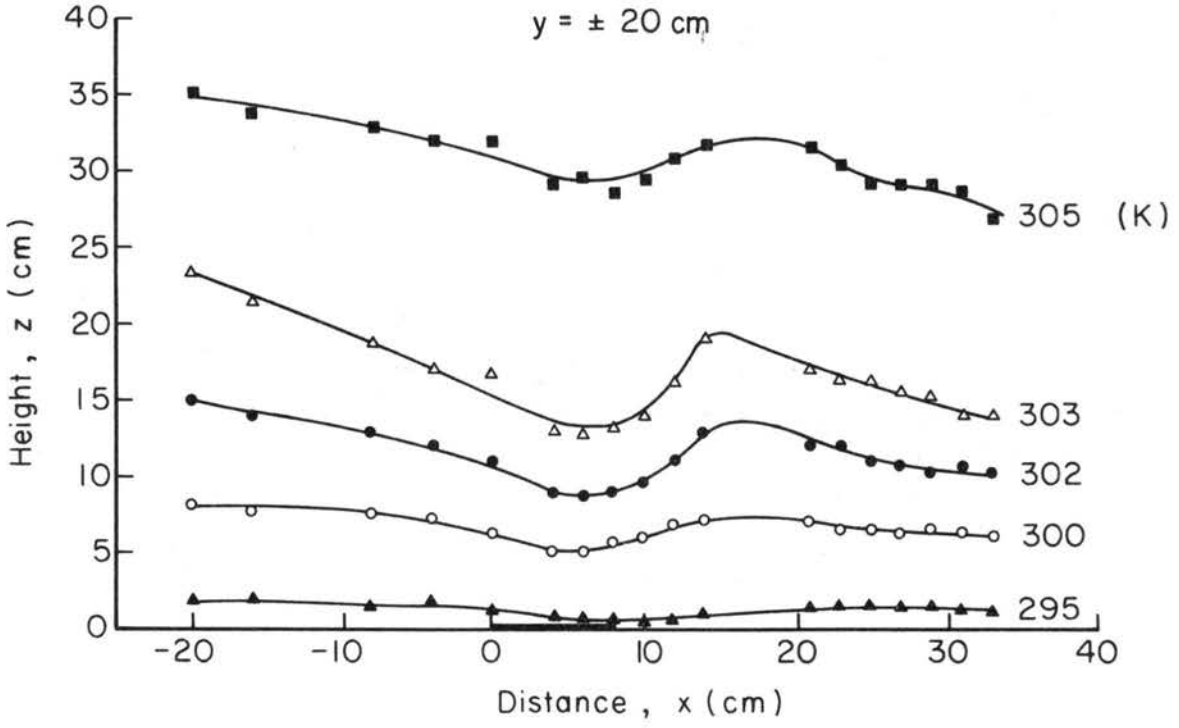

Fig. 5-37 (continued) Isotherms in the vertical planes parallel to the flow direction. Flow situation is the same as in Fig. 5-35.

Unclassified

Security Classification

DOCUMENT CONTROL DATA - R&D

(Security classification of title, body of abstract and indexing annotation must be entered when the overall report is classified)

1. ORIGINATING ACTIVITY *(Corporate author)*
Fluid Dynamics and Diffusion Laboratory
College of Engineering, Colorado State University
Fort Collins, Colorado 80521

2a. REPORT SECURITY CLASSIFICATION
unclassified

2b. GROUP

3. REPORT TITLE
Numerical and Wind Tunnel Simulation of Response of Stratified Shear Layers to Nonhomogeneous Surface Features

4. DESCRIPTIVE NOTES *(Type of report and inclusive dates)*
Technical Report

5. AUTHOR(S) *(Last name, first name, initial)*
Yamada, T., and Meroney, R.N.

6. REPORT DATE	7a. TOTAL NO. OF PAGES	7b. NO. OF REFS
June 1971	290	143

8a. CONTRACT OR GRANT NO.	9a. ORIGINATOR'S REPORT NUMBER(S)
N00014-68-A-0493	CER70-71TY-RNM62
b. PROJECT NO. NR 062-414/6-6-68 (code 438)	
c.	9b. OTHER REPORT NO(S) *(Any other numbers that may be assigned this report)*
d.	

10. AVAILABILITY/LIMITATION NOTICES
Distribution of this report is unlimited

11. SUPPLEMENTARY NOTES	12. SPONSORING MILITARY ACTIVITY
	Office of Naval Research U.S. Dept. of Defense, Washington, D.C.

13. ABSTRACT In this report four different categories of flow are investigated in a thermal wind tunnel:

1) Airflow over an infinitely wide obstacle,
2) Airflow over an infinitely wide heated island,
3) Airflow over an infinitely wide heated obstacle, and
4) Airflow over a heated island with a finite width.

The first three categories are two dimensional aspects of prototype phenomena: a mountain lee-wave, an urban heat island, and a heated mountain, respectively. The last displays a three dimensional feature of a corresponding urban heat island phenomenon. Numerical models were constructed for the first three cases. However, for the three dimensional problem, only the wind tunnel experiment was conducted since a numerical integration for such a three dimensional problem is not practical yet.

Both laboratory and numerical results showed close agreement. They indicated strong nonlinearity; perturbation quantities could not be neglected compared with their mean values especially in the vicinity of the disturbing source (obstacle, heated area), and a linear super-position rule could not be applied to predict the solution of combined effects of heating and topography.

DD FORM 1 JAN 64 1473

Unclassified

Security Classification

14. KEY WORDS	LINK A		LINK B		LINK C	
	ROLE	WT	ROLE	WT	ROLE	WT
Mountain lee-wave						
Heat island						
Heated mountain						
Stratification						
Numerical simulation						
Thermal wind tunnel						

INSTRUCTIONS

1. ORIGINATING ACTIVITY: Enter the name and address of the contractor, subcontractor, grantee, Department of Defense activity or other organization *(corporate author)* issuing the report.

2*a*. REPORT SECURITY CLASSIFICATION: Enter the overall security classification of the report. Indicate whether "Restricted Data" is included. Marking is to be in accordance with appropriate security regulations.

2*b*. GROUP: Automatic downgrading is specified in DoD Directive 5200.10 and Armed Forces Industrial Manual. Enter the group number. Also, when applicable, show that optional markings have been used for Group 3 and Group 4 as authorized.

3. REPORT TITLE: Enter the complete report title in all capital letters. Titles in all cases should be unclassified. If a meaningful title cannot be selected without classification, show title classification in all capitals in parenthesis immediately following the title.

4. DESCRIPTIVE NOTES: If appropriate, enter the type of report, e.g., interim, progress, summary, annual, or final. Give the inclusive dates when a specific reporting period is covered.

5. AUTHOR(S): Enter the name(s) of author(s) as shown on or in the report. Enter last name, first name, middle initial. If military, show rank and branch of service. The name of the principal author is an absolute minimum requirement.

6. REPORT DATE: Enter the date of the report as day, month, year; or month, year. If more than one date appears on the report, use date of publication.

7*a*. TOTAL NUMBER OF PAGES: The total page count should follow normal pagination procedures, i.e., enter the number of pages containing information.

7*b*. NUMBER OF REFERENCES: Enter the total number of references cited in the report.

8*a*. CONTRACT OR GRANT NUMBER: If appropriate, enter the applicable number of the contract or grant under which the report was written.

8*b*, 8*c*, & 8*d*. PROJECT NUMBER: Enter the appropriate military department identification, such as project number, subproject number, system numbers, task number, etc.

9*a*. ORIGINATOR'S REPORT NUMBER(S): Enter the official report number by which the document will be identified and controlled by the originating activity. This number must be unique to this report.

9*b*. OTHER REPORT NUMBER(S): If the report has been assigned any other report numbers *(either by the originator or by the sponsor)*, also enter this number(s).

10. AVAILABILITY/LIMITATION NOTICES: Enter any limitations on further dissemination of the report, other than those imposed by security classification, using standard statements such as:

(1) "Qualified requesters may obtain copies of this report from DDC."

(2) "Foreign announcement and dissemination of this report by DDC is not authorized."

(3) "U. S. Government agencies may obtain copies of this report directly from DDC. Other qualified DDC users shall request through _____."

(4) "U. S. military agencies may obtain copies of this report directly from DDC. Other qualified users shall request through _____."

(5) "All distribution of this report is controlled. Qualified DDC users shall request through _____."

If the report has been furnished to the Office of Technical Services, Department of Commerce, for sale to the public, indicate this fact and enter the price, if known.

11. SUPPLEMENTARY NOTES: Use for additional explanatory notes.

12. SPONSORING MILITARY ACTIVITY: Enter the name of the departmental project office or laboratory sponsoring *(paying for)* the research and development. Include address.

13. ABSTRACT: Enter an abstract giving a brief and factual summary of the document indicative of the report, even though it may also appear elsewhere in the body of the technical report. If additional space is required, a continuation sheet shall be attached.

It is highly desirable that the abstract of classified reports be unclassified. Each paragraph of the abstract shall end with an indication of the military security classification of the information in the paragraph, represented as *(TS)*, *(S)*, *(C)*, *or (U)*.

There is no limitation on the length of the abstract. However, the suggested length is from 150 to 225 words.

14. KEY WORDS: Key words are technically meaningful terms or short phrases that characterize a report and may be used as index entries for cataloging the report. Key words must be selected so that no security classification is required. Idenfiers, such as equipment model designation, trade name, military project code name, geographic location, may be used as key words but will be followed by an indication of technical context. The assignment of links, rules, and weights is optional.

April 1971

DISTRIBUTION LIST FOR UNCLASSIFIED
TECHNICAL REPORTS ISSUED UNDER
CONTRACT N00014-68-A TASK 000-414
0493-0001

Defense Documentation Center
Cameron Station
Alexandria, Virginia 22314 (12)

Technical Library
Naval Ship Research and Development Laboratory
Annapolis, Maryland 21402

Professor Bruce Johnson
Engineering Department
Naval Academy
Annapolis, Maryland 21402

Library
Naval Academy
Annapolis, Maryland 21402

Professor W.R. Debler
Department of Engineering Mechanics
University of Michigan
Ann Arbor, Michigan 48108

Professor W.P. Graebel
Department of Engineering Mechanics
University of Michigan
College of Engineering
Ann Arbor, Michigan 48108

Professor Finn C. Michelsen
Naval Architecture and Marine Engineering
445 West Engineering Building
University of Michigan
Ann Arbor, Michigan 48108

Dr. Francis Ogilvie
Department of Naval Architecture and Marine Engineering
University of Michigan
Ann Arbor, Michigan 48108

Professor W.W. Willmarth
Department of Aerospace Engineering
University of Michigan
Ann Arbor, Michigan 48108

Dr. S.A. Piacsek
Argonne National Laboratory
Applied Mathematics Division
9700 S. Cass Avenue
Argonne, Illinois 60439

AFOSR (REM)
1400 Wilson Boulevard
Arlington, Virginia 22204

Professor S. Corrsin
Mechanics Department
The Johns Hopkins University
Baltimore, Maryland 20910

Professor L.S.G. Kovasznay
The Johns Hopkins University
Baltimore, Maryland 20910

Professor O.M. Phillips
The Johns Hopkins University
Baltimore, Maryland 20910

Librarian
Department of Naval Architecture
University of California
Berkeley, California 94720

Professor Israel Cornet
Department of Mechanical Engineering
University of California
Berkeley, California 94720

Professor M. Holt
Division of Aeronautical Sciences
University of California
Berkeley, California 94720

Professor E.V. Laitone
Department of Mechanical Engineering
University of California
Berkeley, California 94720

Professor P. Lieber
Department of Mechanical Engineering
University of California
Institute of Engineering Research
Berkeley, California 94720

Professor J.R. Paulling
Department of Naval Architecture
University of California
Berkeley, California 94720

Professor J.V. Wehausen
Department of Naval Architecture
University of California
Berkeley, California 94720

Professor E.R. van Driest
Virginia Polytechnic Institute and University
Department of Aerospace Engineering
Blacksburg, Virginia 24061

Commander
Boston Naval Shipyard
Boston, Massachusetts 02129

Director
Office of Naval Research Branch Office
495 Summer Street
Boston, Massachusetts 02210

Commander
Puget Sound Naval Shipyard
Bremerton, Washington 98314

Professor J.J. Foody
Chairman, Engineering Department
State University of New York
Maritime College
Bronx, New York 10465

Dr. Alfred Ritter
Assistant Head, Applied Mechanics Department
Cornell Aeronautical Laboratory, Inc.
Buffalo, New York 14221

Dr. J.W. Morris
Manager, Material Sciences Section
Advanced Materials Research
Bell Aerospace Company
P.O. Box 1
Buffalo, New York 14240

Professor G.H. Carrier
Department of Engineering and Applied Physics
Harvard University
Cambridge, Massachusetts 02138

Commanding Officer
NROTC Naval Administrative Unit
Massachusetts Institute of Technology
Cambridge, Massachusetts 02139

Professor M.A. Abkowitz
Department of Naval Architecture and Marine Engineering
Massachusetts Institute of Technology
Cambridge, Massachusetts 02139

Professor A.T. Ippen
Department of Civil Engineering
Massachusetts Institute of Technology
Cambridge, Massachusetts 02139

Professor L.N. Howard
Department of Mathematics
Massachusetts Institute of Technology
Cambridge, Massachusetts 02139

Professor E.W. Merrill
Department of Mathematics
Massachusetts Institute of Technology
Cambridge, Massachusetts 02139

Professor E. Mollo-Christensen
Room 54-1722
Massachusetts Institute of Technology
Cambridge, Massachusetts 02139

Professor N. Newman
Department of Naval Architecture and Marine Engineering
Massachusetts Institute of Technology
Cambridge, Massachusetts 02139

Professor A.H. Shapiro
Department of Mechanical Engineering
Massachusetts Institute of Technology
Cambridge, Massachusetts 02139

Commander
Charleston Naval Shipyard
U.S. Naval Base
Charleston, South Carolina 29408

A.R. Kuhlthau, Director
Research Laboratories for the Engineering Sciences
Thorton Hall, University of Virginia
Charlottesville, Virginia 22903

Director
Office of Naval Research Branch Office
536 South Clark Street
Chicago, Illinois 60605

Library
Naval Weapons Center
China Lake, California 93555

Professor J.M. Burgers
Institute of Fluid Dynamics and Applied Mathematics
University of Maryland
College Park, Maryland 20742

Professor Pai
Institute for Fluid Dynamics and Applied Mathematics
University of Maryland
College Park, Maryland 20740

Acquisition Director
NASA Scientific & Technical Information
P.O. Box 33
College Park, Maryland 20740

Technical Library
Naval Weapons Laboratory
Dahlgren, Virginia 22448

Computation & Analyses Laboratory
Naval Weapons Laboratory
Dahlgren, Virginia 22448

Dr. C.S. Wells, Jr.
Manager - Fluid Mechanics
Advanced Technology Center, Inc.
P.O. Box 6144
Dallas, Texas 75222

Dr. R.H. Kraichnan
Dublin, New Hampshire 03444

Commanding Officer
Army Research Office
Box CM, Duke Station
Durham, North Carolina 27706

Professor A. Charnes
The Technological Institute
Northwestern University
Evanston, Illinois 60201

Dr. Martin H. Bloom
Polytechnic Institute of Brooklyn
Graduate Center, Dept. of Aerospace
Engineering and Applied Mechanics
Farmingdale, New York 11735

Technical Documents Center
Building 315
U.S. Army Mobility Equipment
Research and Development Center
Fort Belvoir, Virginia 22060

Professor J.E. Cermak
College of Engineering
Colorado State University
Ft. Collins, Colorado 80521

Technical Library
Webb Institute of Naval Architecture
Glen Cove, Long Island, New York 11542

Professor E.V. Lewis
Webb Institute of Naval Architecture
Glen Cove, Long Island, New York 11542

Dr. B.N. Pridmore Brown
Northrop Corporation
NORAIR-Div.
Hawthorne, California 90250

Dr. J.P. Breslin
Stevens Institute of Technology
Davidson Laboratory
Hoboken, New Jersey 07030

Dr. D. Savitsky
Stevens Institute of Technology
Davidson Laboratory
Hoboken, New Jersey 07030

Mr. C.H. Henry
Stevens Institute of Technology
Davidson Laboratory
Hoboken, New Jersey 07030

Dr. J.P. Craven
University of Hawaii
1801 University Avenue
Honolulu, Hawaii 96822

Professor E.L. Resler
Graduate School of Aeronautical Engineering
Cornell University
Ithaca, New York 14851

Professor John Miles
c/o I.G.P.P.
University of California, San Diego
La Jolla, California 92038

Director
Scrippe Institution of Oceanography
University of California
La Jolla, California 92037

Professor A. Ellis
University of California, San Diego
Department of Aerospace & Mechanical Engineering
La Jolla, California 92037

Dr. B. Sternlicht
Mechanical Technology Incorporated
968 Albany-Shaker Road
Latham, New York 12110

Dr. Coda Pan
Mechanical Technology Incorporated
968 Albany-Shaker Road
Latham, New York 12110

Mr. P. Eisenberg, President
Hydronautics, Inc.
Pindell School Road
Howard County
Laurel, Maryland 20810

Mr. M.P. Tulin
Hydronautics, Inc.
Pindell School Road
Howard County
Laurel, Maryland 20810

Mr. Alfonso Alcedan L.,Director
Laboratorio Nacional De Hydraulics
Antigui Cameno A. Ancon
Casilla Jostal 682
Lima, Peru

Commander
Long Beach Naval Shipyard
Long Beach, California 90802

Professor John Laufer
Department of Aerospace Engineering
University Park
Los Angeles, California 90007

Professor J.M. Killen
St. Anthony Falls Hydraulic Lab.
University of Minnesota
Minneapolis, Minnesota 55414

Lorenz G. Straub Library
St. Anthony Falls Hydraulic Lab.
Mississippi River at 3rd Avenue S.E.
Minneapolis, Minnesota 55414

Professor J. Ripkin
St. Anthony Falls Hydraulic Lab.
University of Minnesota
Minneapolis, Minnesota 55414

Dr. W. Silberman
St. Anthony Falls Hydraulic Lab.
Mississippi River at 3rd Avenue S.E.
Minneapolis, Minnesota 55414

Superintendent
Naval Postgraduate School
Library Code 0212
Monterey, California 93940

Professor A.B. Metzner
University of Delaware
Newark, New Jersey 19711

Technical Library
Naval Underwater Systems Center
Newport, Rhode Island 02840

Professor Dudley D. Fuller
Department of Mechanical Engineering
Columbia University
New York, New York 10027

Professor V. Castelli
Department of Mechanical Engineering
Columbia University
New York, New York 10027

Professor H. Elrod
Department of Mechanical Engineering
Columbia University
New York, New York 10027

Professor J.J. Stoker
Institute of Mathematical Sciences
New York University
251 Mercer Street
New York, New York 10003

Society of Naval Architects and Marine Engineering
74 Trinity Place
New York, New York 10006

Engineering Societies Library
345 East 47th Street
New York, New York 10017

Office of Naval Research
New York Area Office
207 W. 24th Street
New York, New York 10011

Miss O.M. Leach, Librarian
National Research Council
Aeronautical Library
Montreal Road
Ottawa 7, Canada

Technical Library
Naval Ship Research and Development Center
Panama City, Florida 32401

Technical Library
Naval Undersea R & D Center
Pasadena Laboratory
3202 E. Foothill Boulevard
Pasadena, California 91107

Dr. Andrew Fabula
Naval Undersea Research & Development Center
Pasadena Laboratory
3202 E. Foothill Boulevard
Pasadena, California 91107

Dr. J.W. Hoyt
Naval Undersea R & D Center
Pasadena Laboratory
3202 E. Foothill Boulevard
Pasadena, California 91107

Professor A. Acosta
Department of Mechanical Engineering
California Institute of Technology
Pasadena, California 91109

Professor H. Liepmann
Department of Aeronautics
California Institute of Technology
Pasadena, California 91109

Professor M.S. Plesset
Engineering Division
California Institute of Technology
Pasadena, California 91109

Professor A. Roshko
California Institute of Technology
Pasadena, California 91109

Professor T.Y. Wu
Department of Engineering
California Institute of Technology
Pasadena, California 91109

Director
Office of Naval Research Branch Office
1030 E. Green Street
Pasadena, California 91101

Naval Ship Engineering Center
Philadelphia Division
Technical Library
Philadelphia, Pennsylvania 19112

Technical Library
Philadelphia Naval Shipyard
Philadelphia, Pennsylvania 19112

Professor R.C. Mac Camy
Department of Mathematics
Carnegie Institute of Technology
Pittsburgh, Pennsylvania 15213

Dr. Paul Kaplan
Oceanics, Inc.
Plainview, Long Island, New York 11803

Technical Library
Naval Missile Center
Point Mugu, California 93441

Technical Library
Naval Civil Engineering Laboratory
Port Hueneme, California 93041

Commander
Portsmouth Naval Shipyard
Portsmouth, New Hampshire 03801

Commander
Norfolk Naval Shipyard
Portsmouth, Virginia 23709

Professor F.E. Bisshopp
Division of Engineering
Brown University
Providence, Rhode Island 02912

Dr. William A. Gross, Vice President
Ampex Corporation
401 Broadway
Redwood City, California 94063

Dr. H.N. Abramson
Southwest Research Institute
8500 Culebra Road
San Antonio, Texas 78228

Editor
Applied Mechanics Review
Southwest Research Institute
8500 Culebra Road
San Antonio, Texas 78206

Office of Naval Research
San Francisco Area Office
50 Fell Street
San Francisco, California 94102

Library
Pearl Harbor Naval Shipyard
Box 400
FPO San Francisco, California 96610

Technical Library
Hunters Point Naval Shipyard
San Francisco, California 94135

Librarian
Naval Ordnance Laboratory
White Oak
Silver Spring, Maryland 20910

Fenton Kennedy Document Library
The Johns Hopkins University
Applied Physics Laboratory
8621 Georgia Avenue
Silver Spring, Maryland 20910

Professor E.Y. Hsu
Department of Civil Engineering
Stanford University
Stanford, California 94305

Dr. Byrne Perry
Department of Civil Engineering
Stanford University
Stanford, California 94305

Dr. R.L. Street
Department of Civil Engineering
Stanford University
Stanford, California 94305

Professor Milton Van Dyke
Department of Aeronautical Engineering
Stanford University
Stanford, California 94305

Professor R.C. Di Prima
Department of Mathematics
Rensselaer Polytechnic Institute
Troy, New York 12180

Professor J. Lumley
Ordnance Research Laboratory
Pennsylvania State University
University Park, Pennsylvania 16801

Dr. M. Sevik
Ordnance Research Laboratory
Pennsylvania State University
University Park, Pennsylvania 16801

Dr. J.M. Robertson
Department of Theoretical and Applied Mechanics
University of Illinois
Urbana, Illinois 61803

Technical Library
Mare Island Naval Shipyard
Vallejo, California 94592

Code 438
Office of Naval Research
Department of the Navy
Arlington, Virginia 22217 (3)

Code 461
Office of Naval Research
Department of the Navy
Arlington, Virginia 22217

Code 463
Office of Naval Research
Department of the Navy
Arlington, Virginia 22217

Code 472
Office of Naval Research
Department of the Navy
Arlington, Virginia 22217

Code 468
Office of Naval Research
Department of the Navy
Arlington, Virginia 22217

Code 473
Office of Naval Research
Department of the Navy
Arlington, Virginia 22217

Code 481
Office of Naval Research
Department of the Navy
Arlington, Virginia 22217

Code 2627
Naval Research Laboratory
Washington, D.C. 20390 (6)

Library, Code 2620 (ONRL)
Naval Research Laboratory
Washington, D.C. 20390 (6)

Code 6170
Naval Research Laboratory
Washington, D.C. 20390

Code 4000
Director of Research
Naval Research Laboratory
Washington, D.C. 20390

Code 8030 (Maury Center)
Naval Research Laboratory
Washington, D.C. 20390

Code 8040
Naval Research Laboratory
Washington, D.C. 20390

Code 031
Naval Ship Systems Command
Washington, D.C. 20390

Code 0341
Naval Ship Systems Command
Washington, D.C. 20390

Code 03412B (L. Benen)
Naval Ship Systems Command
Washington, D.C. 20390

Code 03412 (J. Schuler)
Naval Ship Systems Command
Washington, D.C. 20390

Code 2052
Naval Ship Systems Command
Washington, D. C. 20390

Code 6034
Naval Ship Engineering Center
Center Building
Prince George's Center
Hyattsville, Maryland 20782

Code 6110
Naval Ship Engineering Center
Center Building
Prince George's Center
Hyattsville, Maryland 20782

Code 6113
Naval Ship Engineering Center
Center Building
Prince George's Center
Hyattsville, Maryland 20782

Code 6114
Naval Ship Engineering Center
Center Building
Prince George's Center
Hyattsville, Maryland 20782

Code 6120E
Naval Ship Engineering Center
Center Building
Prince George's Center
Hyattsville, Maryland 20782

Code 6136
Naval Ship Engineering Center
Center Building
Prince George's Center
Hyattsville, Maryland 20782

Dr. A. Powell
Code 01
Naval Ship Research and Development Center
Washington, D.C. 20034

Mr. W.M. Ellsworth
Code 0H50
Naval Ship Research and Development Center
Washington, D.C. 20034

Central Library
Code L42
Naval Ship Research and Development Center
Washington, D.C. 20034

Dr. W.E. Cummins
Code 500
Naval Ship Research and Development Center
Washington, D.C. 20034

Mr. S.F. Crump
Code 513
Naval Ship Research and Development Center
Washington, D.C. 20034

Mr. R. Wermter
Code 520
Naval Ship Research and Development Center
Washington, D.C. 20034

Dr. P. Pien
Code 521
Naval Ship Research and Development Center
Washington, D.C. 20034

Dr. W.B. Morgan
Code 540
Naval Ship Research and Development Center
Washington, D.C. 20034

Mr. P. Granville
Code 541
Naval Ship Research and Development Center
Washington, D.C. 20034

Mr. J.B. Hadler
Code 560
Naval Ship Research and Development Center
Washington, D.C. 20034

Dr. H.R. Chaplin
Code 600
Naval Ship Research and Development Center
Washington, D.C. 20034

Mr. G.H. Gleissner
Code 800
Naval Ship Research and Development Center
Washington, D.C. 20034

Dr. M. Strasberg
Code 901
Naval Ship Research and Development Center
Washington, D.C. 20034

Mr. J. McCarthy
Code 552
Naval Ship Research and Development Center
Washington, D.C. 20034

Code 03
Naval Air Systems Command
Washington, D.C. 20360

AIR 5301
Naval Air Systems Command
Department of the Navy
Washington, D.C. 20360

Code ORD 03
Naval Ordnance Systems Command
Washington, D.C. 20360

Code ORD 035
Naval Ordnance Systems Command
Washington, D.C. 20360

Code ORD 05413
Naval Ordnance Systems Command
Washington, D.C. 20360

Code ORD 9132
Naval Ordnance Systems Command
Washington, D.C. 20360

Oceanographer of the Navy
Washington, D.C. 20390

Commander
Naval Oceanographic Office
Washington, D.C. 20390

Chief Scientist (CNM PM-1)
Strategic Systems Project Office
Department of the Navy
Washington, D.C. 20360

Technical Division (CNM PM 11-20)
Deep Submergence Systems Project Office
Department of the Navy
Washington, D.C. 20360

Dr. A.L. Slafkosky
Scientific Advisor
Commandant of the Marine Corps (Code AX)
Washington, D.C. 20380

Librarian Station 5-2
Coast Guard Headquarters
NASSIF Building
400 7th Street, S.W.
Washington, D.C. 20591

Office of Research and Development
Maritime Administration
441 G. Street, N.W.
Washington, D.C. 20235

Division of Ship Design
Maritime Administration
441 G. Street, N.W.
Washington, D.C. 20235

National Science Foundation
Engineering Division
1800 G. Street, N.W.
Washington, D.C. 20550

Dr. G. Kulin
National Bureau of Standards
Washington, D.C. 20234

Science & Technology Division
Library of Congress
Washington, D.C. 20540

Chief of Research & Development
Office of Chief of Staff
Department of the Army
The Pentagon, Washington, D.C. 20310

Professor A. Thiruvengadam
Department of Mechanical Engineering
The Catholic University of America
Washington, D.C. 20017

Professor G. Birkhoff
Department of Mathematics
Harvard University
Cambridge, Massachusetts 02138

AIR 604
Naval Air Systems Command
Department of the Navy
Washington, D.C. 20360

Dr. A.S. Iberall, President
General Technical Services, Inc.
451 Penn Street
Yeadon, Pennsylvania 19050

Professor J.F. Kennedy, Director
Iowa Institute of Hydraulic Research
State University of Iowa
Iowa City, Iowa 52240

Professor L. Landweber
Iowa Institute of Hydraulic Research
State University of Iowa
Iowa City, Iowa 52240

Dr. Lee Segel
Department of Mathematics
Rensselaer Polytechnic Institute
Troy, New York 12180

Code 6101E
Naval Ship Engineering Center
Center Building
Prince George's Center
Hyattsville, Maryland 20782

109°

108°

107°

38°

37°

COLORADO
NEW MEXICO

UPPER COLORADO RIVER BASIN

DEPARTMENT OF CIVIL ENGINEERING

Hydrology Program Colorado State University

Research Sponsor U.S. Bureau of Reclamation

Division of Atmospheric Water Resources Management

December 1970

LINEAR HYDROGRAPHS OF SPECIFIC YIELD IN CFS/SQ.ML.

Map I

- ■ Active (as of 1968) Stream gage station with more than 20 years of Record.
- ○ Active (as of 1968) Stream gage station with more than 10 years and less than 20 years of Record.
- ● Active (as of 1968) Stream gage station with less than 10 years of Record or discontinued station.

Disappointment Creek
1274800
1274830
1274860
1272420
1272440
GROUND HOG RES.
Dolores
Beaver Cr.
West Dolores River
1275600
1278000
Dolores River
1278050
1279000
1279600
Fall Cr.
1272460
1272455
1272465
TROUT LAKE
1278800
1073452
1371565
1371570
1371575
1073472
1073480
1073476
1073468
1073464
CASCADE RES.
1073460
1073456
1073448
1073444
1073440
1073424
1073420
1073436
1073432
1073428
1073418
1073416
1073412
1073408
1073404
1073400
1073396
1073080
1073060
1073040
1073020
1073000
1073200
1073800
1074400
1074600
1075200
1075850
1075840
1075830
1075820
1075810
1075800
1376050
1075870
1075860
1076450
1076430
1076440
1076460
1076420
1076410
1076400
1076600
1076800
1076200
1077800
1078200
1077600
1078000
1077400
1077250
1072200
1077090
1077030
1077045
1077075
1077060
1077015
Rio Blanco
RIVER
Piedra
Los Pinos
Florida
JUAN
Animas River
SAN JUAN RIVER
Lost Canyon Cr
River
1277200
1276400
Mc Elmo Cr.
1071860
1072075
1072045
1072060
1072030
1072015
1073080
1073060
Aztec River
Mancos
1072000
1072400
SAN
Canyon
Companero
HORSE LAKE
BOULDER LAKE

UPPER COLORADO RIVER BASIN

DEPARTMENT OF CIVIL ENGINEERING

Hydrology Program Colorado State University

Research Sponsor U.S. Bureau of Reclamation

Division of Atmospheric Water Resources Management

December 1970

LINEAR GRAPHS OF MEAN MONTHLY COEFFICIENTS OF VARIATION

Map 2

- ■ Active (as of 1968) Stream gage station with more than 20 years of Record.
- ○ Active (as of 1968) Stream gage station with more than 10 years and less than 20 years of Record.
- ● Active (as of 1968) Stream gage station with less than 10 years of Record or discontinued station.

109°
108°
107°
38°
37°

GROUND HOG RES.
TROUT LAKE
CASCADE RES.
COLORADO
NEW MEXICO
HORSE LAKE
BOULDER LAKE

Dolores River
Fall Cr.
West Dolores River
Beaver Cr.
Lost Canyon Cr
Mc Elmo Cr.
Aztec Mancos River
SAN JUAN RIVER
Los Pinos River
Piedra River
Rio Blanco
Canyon Companero

1274800 1274830 1274860 1272420 1272440 1272460 1272455 1272465 1371565 1371570 1371575 1376050 1073472 1073480 1073476 1073468 1278050 1279000 1279600 1278000 1278800 1073452 1073464 1275600 1277200 1276400 1073460 1073456 1073448 1075870 1075860 1076450 1075850 1076430 1076440 1076460 1077860 1078200 1077800 1078000 1077600 1072075 1072045 1072060 1072030 1072015 1071860 1073080 1073432 1073436 1073428 1073420 1073424 1073444 1073440 1075840 1075830 1076420 1077400 1072200 1077250 1077090 1077030 1077045 1077075 1077060 1077015 1073060 1073416 1073412 1073408 1073040 1073020 1072000 1075820 1075810 1075800 1076410 1076400 1076600 1076800 1076200 1072400 1073000 1073400 1073200 1073404 1073800 1075200 1074400 1074600

UPPER COLORADO RIVER BASIN
DEPARTMENT OF CIVIL ENGINEERING
Hydrology Program Colorado State University

Research Sponsor U.S. Bureau of Reclamation
Division of Atmospheric Water Resources
Management

December 1970
DURATION CURVES OF MONTHLY
FLOW DATA

Map 3

- ■ Active (as of 1968) Stream gage station with more than 20 years of Record.
- ○ Active (as of 1968) Stream gage station with more than 10 years and less than 20 years of Record.
- ● Active (as of 1968) Stream gage station with less than 10 years of Record or discontinued station.